

BPS Boojums in $\mathcal{N} = 2$ supersymmetric gauge theories

Masato Arai¹, Filip Blaschke² and Minoru Eto³

*Department of Physics, Yamagata University, Kojirakawa-machi 1-4-12,
Yamagata, Yamagata 990-8560, Japan*

E-mail: ¹ meto@sci.kj.yamagata-u.ac.jp

E-mail: ² arai@sci.kj.yamagata-u.ac.jp

E-mail: ³ fblasch@sci.kj.yamagata-u.ac.jp

ABSTRACT: We study 1/4 Bogomol'nyi-Prasad-Sommerfield (BPS) composite solitons of vortex strings, domain walls and boojums in $\mathcal{N} = 2$ supersymmetric Abelian gauge theories in four dimensions. We obtain solutions to the 1/4 BPS equations with the finite gauge coupling constant. To obtain numerical solutions for generic coupling constants, we construct globally correct approximate functions which allow us to easily find fixed points of a gradient flow equations. We analytically/numerically confirm that the negative mass of a single boojum appearing at the end point of the vortex string on the logarithmically bent domain wall is equal to the half-mass of the 't Hooft-Polyakov monopole. We examine various configurations and clarify how the shape of the boojum depends on the coupling constants and moduli parameters. We find a semi-local boojum with a size moduli which appears when the semi-local string ends on the domain wall. We introduce a “magnetic” scalar potential which offers an intuitive understanding that the end point of vortex string is the source of magnetic field. It can explain that “height” of the domain wall corresponds to the magnetic scalar potential, but also it gives a physical meaning to the scalar function appearing in the Taubes' equation for BPS Abrikosov-Nilsen-Olesen vortex. Dyonic solutions are also obtained. When the configuration is extended to the dyonic case, the domain wall becomes an electric capacitor storing electric charges on its skin and the boojum charge density becomes proportional to $\vec{E} \cdot \vec{B}$. We also find analytic solutions to the 1/4 BPS equations for specific values of the coupling constants. We study the composite solitons from the view points of the Nambu-Goto and Dirac-Born-Infeld actions, and find the semi-local BIon as the counterpart of the semi-local Boojum.

Contents

1. Introduction and summary	2
2. The Model	10
2.1 Abelian vortex-wall system	10
2.2 1/4 BPS state	12
2.3 The moduli matrix formalism	13
3. Axially symmetric solutions	15
3.1 Gradient flow	16
3.2 1/4 BPS solutions	19
3.3 Weak coupling regime	31
3.4 Strong coupling regime	44
3.5 The magnetic scalar potential	45
4. Non-axially symmetric solutions	50
4.1 $N_F = 2$	50
4.2 $N_F \geq 3$	59
5. A magnetic capacitor	69
5.1 Linearly aligned vortex strings ending on a domain wall from one side	69
5.2 Linearly aligned vortex strings ending on a domain wall from two sides	74
5.3 Vortex strings ending on a slanting domain wall	78
6. Dyonic extension	87
6.1 Basic formulae	87
6.2 The dyonic domain wall as an electric capacitor	91
6.3 1/4 BPS dyonic configurations	93
7. Approximate solutions to Abelian master equations	99
7.1 Approximations to ANO vortex	102
7.2 Approximations to domain wall	105
8. Exact solutions to 1/4 BPS solitons	108
8.1 $M = \text{diag}(m, 0, -m, -m)$	109
8.2 $M = \text{diag}(2m, m, 0, 0, -m, -2m)/2$	111
8.3 Other exact solutions	114

9. Low energy effective theory and Nambu-Goto/DBI action	115
9.1 Nambu-Goto action and Hamiltonian	115
9.2 Domain wall, its dyonic extension and the NG action	116
9.3 Dyonic extension of spike domain wall and NG action	118
9.4 Relation between solutions of NG action and DBI action	120
9.5 The semi-local BIon: Round spike configuration and DBI action	125
10. Outlook	129

1. Introduction and summary

Topological solitons have long been appreciated in various fields in modern physics such as string theory, field theory, cosmology, nuclear physics and condensed matter physics. They often appear with spontaneously broken symmetries which support stability of the solutions with conserved topological charges. Typical examples are Nielsen-Olesen vortex string in the Abelian-Higgs model [1] and 't Hooft-Polyakov magnetic monopole in $SU(2)$ Yang-Mills theory [2, 3]. The topological charges are associated with the homotopy groups $\pi_1(U(1))$ and $\pi_2(SU(2)/U(1))$, respectively. Domain walls also often appear in models with degenerate and discrete vacua which are characterized by the homotopy group $\pi_0(\mathcal{M}_{\text{vac}})$, where \mathcal{M}_{vac} is a vacuum manifold.

In addition to these elementary solitons, there are also composite solitons, which include two or more different kinds of elementary solitons. They are sometimes called D-brane solitons or field theoretical D-branes, because they share many properties with D-branes in superstring theories [4]. Among various configurations, in this paper we are especially interested in composite solitons, where vortex strings attach to domain walls. Such configurations are natural field theory counterparts to the D-branes on which fundamental strings end in superstring theory. These configurations have been studied for a long time. A simple field theoretical model possessing the composite soliton was provided in Ref. [5]. Numerical analysis based on the specific scalar field theory was performed in [6]. Existence of such configurations in $\mathcal{N} = 1$ supersymmetric (SUSY) QCD was found in [7], and inspired by this result, qualitative explanation of existence of a vortex-string ending on a domain wall was shown in [8, 9]. It was found that annihilation of domain wall and anti-domain wall produces stable solitons of lower dimensionality [10] in a modified model of $\mathcal{N} = 1$ SUSY QCD [7].

A remarkable progress was done in [11], in which an exact solution of a lump-string ending on a domain wall was found as a Bogomol'nyi-Prasad-Sommefield

(BPS) state preserving 1/4 SUSY in $\mathcal{N} = 2$ SUSY massive nonlinear sigma model on the cotangent bundle over the complex projective space, $T^*\mathbb{C}P^1$. It was also shown there that Dirac-Born-Infeld (DBI) action correctly describes the low energy effective dynamics on the domain wall's world-volume. The lump string ending on the domain wall can be seen as a Born-Infeld-on (BIon), a spiky soliton of DBI action, which provides a natural interpretation for the string end point as an electric charge on the domain wall. Furthermore, it was observed that the vortex-string pulls the domain wall, and consequently the domain wall is logarithmically bent, which is again intriguingly similar to the D-branes.

Perhaps one of the best playgrounds to study composite state of the vortex string and the domain wall are $\mathcal{N} = 2$ SUSY gauge theories. Indeed, the massive $T^*\mathbb{C}P^1$ model can be realized as a strong (infinite) gauge coupling limit of $\mathcal{N} = 2$ SQED with $N_F = 2$ hypermultiplets in the presence of the Fayet-Iliopoulos term. The manifold $T^*\mathbb{C}P^1$ appears as the Higgs branch of SQED. One advantage of SUSY gauge theory with finite gauge coupling constant is that the vortex strings are regular with a finite width of the order $\sim 1/(gv)$, where g is the gauge coupling constant and v is the vacuum expectation value (VEV) of the charged scalar fields. On the other hand, lump strings in the massive nonlinear sigma models are singular if put into the bulk without ending on any domain walls. When the lump string is attached to the domain wall, its transverse size falls off asymptotically as $\sim e^{-mL}$ with the distance from the domain wall L and with m being a massive parameter of dimension one [11]. Therefore, the lump string is asymptotically singular. A disadvantage of SUSY gauge theories is that analytic solutions of solitons are hard to obtain, whereas sigma models solitons are often found analytically. Due to this lack of analytical solutions, studies of composite solitons in the gauge theories seldom goes beyond their qualitative features.

Nevertheless, much progress has been done within SUSY gauge theories in the past decade. In $\mathcal{N} = 2$ SQED, seen as a low energy effective theory of $\mathcal{N} = 2$ SQCD with $SU(2)$ gauge group with $N_F = 2$ hypermultiplets, perturbed by a small mass term for the adjoint scalar field, the 1/4 BPS equations for the Abelian vortex strings ending on the domain walls were first derived in [12]. End points of the vortex strings on the domain wall were identified with electric particles in a low energy effective theory of the domain wall. Then the model was extended to $\mathcal{N} = 2$ $SU(2) \times U(1)$ SQCD with $N_F = 4$ hypermultiplets [13] and the 1/4 BPS equations including the non-Abelian vortex strings [14, 15] were found. A low energy effective theory on the composite domain walls was studied and it was found that the end points of the non-Abelian vortex strings play the role of a non-Abelian charge coupled with localized dual non-Abelian gauge fields at linear level of small fluctuations [13], see also related works [16, 17, 18, 19, 20].

Almost in the same period, the different kind of the 1/4 BPS composite configurations of the non-Abelian vortex and the magnetic monopoles were found in $\mathcal{N} = 2$

$U(N_C)$ SQCD with $N_F = N_C$ flavors [15, 21, 22, 23, 24], see also recent related works [25, 26, 27, 28, 29]. Afterwards, all these kinds of topological solitons, the vortex strings, domain walls and the magnetic monopoles were found to coexist as the 1/4 BPS composite states in $\mathcal{N} = 2$ $U(N_C)$ SQCD with $N_F \geq N_C$ flavors. The most generic 1/4 BPS equations for these were found in [30]. The BPS equations are a set of first order differential equations for the gauge fields A_μ^a , the adjoint scalar fields Σ^a ($a = 1, 2, \dots, N_C^2$), and $N_C \times N_F$ squark fields H and \hat{H} , which depends on three spacial coordinates x^k ($k = 1, 2, 3$). Since, except for several simplest configurations, the generic solutions have no spacial symmetries, it is quite hard to solve the BPS equations, even though they are first order differential equations. To make things worse, no analytic solutions to the 1/4 BPS equations have been found in the model with finite gauge coupling constants. In order to overcome these difficulties a powerful technique, so-called moduli matrix formalism, was invented for the 1/2 BPS domain walls [31, 32], 1/2 BPS vortex strings [33] and for the full 1/4 BPS equations [30]. It is so powerful that not only the dimension of the moduli space but also all the information on the moduli parameters for all topological sectors are easily exhausted. Notably, the moduli matrix formalism provides all exact solutions in the strong gauge coupling limit where the model reduces to the massive nonlinear sigma model whose target space is a cotangent bundle over Grassmannian manifold $Gr_{N_F, N_C} \simeq SU(N_F)/SU(N_C) \times SU(N_F - N_C) \times U(1)$ [30]. The case with $N_C = 1$ and $N_F = 2$ corresponds to the massive $T^*\mathbb{C}P^1$ nonlinear sigma model and the moduli matrix formalism correctly reproduces the results in Ref. [11] mentioned above. There is another advantage of the moduli matrix formalism, though less emphasized in the literature, that the complicated first order differential equations for $2N_C^2$ fields in the vector multiplet and $2N_C N_F$ fields in the hypermultiplet ($\hat{H} = 0$) are converted into $N_C(N_C + 1)/2$ second order equations, collectively called the master equation

$$\frac{1}{g^2} \partial_k (\Omega^{-1} \partial_k \Omega) = v^2 (\mathbf{1}_{N_C} - \Omega^{-1} \Omega_0), \quad (1.1)$$

for real positive $N_C \times N_C$ matrix field Ω [30], where g is the $U(N_C)$ gauge coupling constant, v^2 is the FI parameter and Ω_0 stands for a source term, which can be chosen quite freely up to certain rules [30]. Even in the case $N_F = N_C$, for which the moduli matrix formalism gives a minimal benefit, the degrees of freedom reduces by half. Details of the moduli matrix formalism are summarized in the review paper [34]. Also, there are good reviews covering many studies of the topological solitons in $\mathcal{N} = 2$ SQCD [35, 36, 37, 38].

While many properties are shared by BPS topological solitons in field theory and D-branes in string theory, there is a BPS object, which is inherently field theoretical and has no analog in string theory. It appears at a junction point where two different kind of topological solitons meet. Interestingly, it has a negative BPS mass and can be interpreted as a binding energy. The first example of this kind of object was

found as the domain wall junction [39, 40, 41, 42, 43, 44]. When a vortex string ends on a domain wall, a different type of BPS object with negative mass appears [30]. Like the domain wall junctions, it was shown that the negative BPS mass is nothing but the binding energy of the vortex string and the domain wall [45]. In particle physics context it is now called the boojum [45] because a similar configuration, coined Boojum¹ by Mermin, is known in the context of ³He superfluid [46, 47]. Recently, the boojums are getting more popular in various fields. For example, it has been studied in the 2 component Bose Einstein condensates [48, 49], and also in the dense QCD [50, 51]. The negative BPS binding energy was also found for intersections of vortex sheets in 5 dimensions [22, 52, 53]. Typically, these negative BPS masses appear in Abelian-Higgs model and these three different binding energies in different dimensions can be reasonably understood through a descent relations given by Kaluza-Klein dimensional reductions [54].

Our main aim in this paper is to study the 1/4 BPS boojums in details in $\mathcal{N} = 2$ SUSY QED with $N_F \geq 2$ flavors in the presence of the Fayet-Iliopoulos term. If one desires, one can think of this theory as a low energy effective theory of the mass perturbed $SU(2)$ SQCD as considered in [12]. As mentioned above, fundamental results such as the derivation of the BPS equations, the BPS masses and the structure of the moduli space were already done [30, 34], and the interaction rules of various solitons and some qualitative features were clarified [45]. However, we would like to point out that these understandings still remain at qualitative level. This is because neither analytic nor numerical solutions to the 1/4 BPS equations have been obtained. Although all exact solutions to the 1/4 BPS equations were obtained [30], it was done only in the strong gauge coupling limit where the BPS boojum masses becomes zero and the lump strings in the bulk are singular. In order to fill this hole, we will provide both numerical solutions for generic case and analytical solutions for particular cases with the gauge coupling constant kept finite. To this end, we are greatly helped by the moduli matrix formalism [30, 34], which reduces the complicated 1/4 BPS equations to a mere second order equation for a single real scalar field $u(x^k)$

$$\frac{1}{2g^2} \partial_k^2 u = v^2 (1 - \Omega_0 e^{-u}), \quad (k = 1, 2, 3), \quad (1.2)$$

which is the Abelian version of the master equation given in Eq. (1.1) with identification $\Omega = e^u$. In this paper, we will in particular explain how to solve this Abelian master equation.

At this point, it is worth mentioning that the two dimensional version of Eq. (1.2) is the well-known Taubes equation for the BPS vortices in the Abelian-Higgs theory [55]. Unfortunately, no analytic solutions are known for the Taubes equation in \mathbb{R}^2 . This is in contrast to the familiar BPS Yang-Mills instantons, for which the

¹The word “boojum” originates from Lewis Carroll’s poem *Hunting of the Snark*.

well-known Atiyah-Drinfeld-Hitchin-Manin construction is established [56]. However, Taubes equation on the hyperbolic plane \mathbb{H}^2 of curvature $-1/2$ is slightly modified from Eq. (1.2), such that the first term in the parentheses on the right hand side vanishes and the equation becomes integrable [57]. This is a consequence of the fact that these vortices are obtained as a dimensional reduction from $SO(3)$ -symmetric Yang-Mills instantons on \mathbb{R}^4 [57]. Recent progress for integrable vortex models are found in [58, 59, 60, 61, 62, 63, 64]. In short, no analytic solutions have been found for the Taubes equation in \mathbb{R}^2 , much less for the master equation (1.2) in \mathbb{R}^3 . Thus, it seems almost hopeless to find analytic solutions to the master equations (1.2). Surprisingly, we will provide some exact solutions in both \mathbb{R}^2 and \mathbb{R}^3 .

In contrast to simplicity of the master equation (1.2), physics behind it is very rich. We will encounter various interesting phenomena during the process of solving numerically/analytically the master equation (1.2). A technical but important result of this paper is finding a *global* approximation to solutions of the master equation (1.2), which supports almost all other results in this paper. In general, solving the Cauchy boundary problem in \mathbb{R}^3 for configuration of identical topological solitons, such as parallel domain walls or parallel vortex strings, is not difficult because finding appropriate boundary conditions offers no complications. Even when two identical topological solitons coexist with a finite slanting angle, say domain wall junctions, one may not encounter any difficulties in specifying boundary conditions because the solitons extend linearly to boundary. However, when two or more topological solitons of different kind coexist, giving an appropriate boundary condition is not always straightforward task. A prototype example is a vortex string attached to a domain wall from one side. The vortex string has codimension two while the domain wall has codimension one. As was mentioned above, the domain wall is pulled and it logarithmically bends toward spacial infinity along the string axis. Thus, in order to solve the Cauchy boundary problem for this kind of configuration, we have to have asymptotic solution for bent domain wall. We will provide a simple but very generic method to construct globally correct approximate solutions from the solutions of constituent isolated solitons. The global approximation offers us quite good approximate solutions which are valid for not only spacial infinity but also almost all regions except vicinity of the junction points. What we need is only flat domain wall solution and straight vortex strings solutions. We will use global approximations not only for determining the boundary condition of the master equation (1.2) but also for a suitable initial function consistent with the boundary condition to solve Eq. (1.2) by the gradient flow (imaginary time relaxation) method. The closer initial function is to the true solution, the faster the gradient flow converges. Therefore, the global approximate solution is useful for numerical works. Whatever the solutions for the constituent solitons are, numerical or analytical, our method works very efficiently. Namely, with the global approximations we can solve the Cauchy problem for any kind of configuration in the theory with arbitrary coupling constants.

As a direct consequence of solving the BPS equations for the finite gauge coupling, we will reveal shape of the boojums, see Fig. 4. So far, only schematic picture such as a simple hemisphere for the boojum have been given in the literature. We will also show how the shape of the boojums is modified when the coupling constants of the model are changed. It is also interesting to observe how they deform when multiple boojums coalesce. Do they behave similarly to the BPS magnetic monopoles, that it that two separate balls collide and form a donut [65]? Our numerical computations show that the boojums behave very differently from the monopoles, see Figs. 24, 25 and 31.

Furthermore, the global approximation developed in this paper would settle down a problem raised in [66]: Based on approximate solutions it was pointed out that there is an ambiguity in the definition of the Boojum mass, which stems from the ambiguity of definition of the geometric parameters such as domain wall area and vortex string length caused by logarithmic bending of the domain wall. As mentioned above, the boojum mass was originally computed in [45] and it was shown that it is negative half mass of 't Hooft-Polyakov monopole without any ambiguity. To reach this value, they simplified their calculation by taking a mean value for the scalar field in the vector multiplet at a cross section of logarithmically bend domain wall [45]. Although the result – the negative half of 't Hooft-Polyakov monopole – seems to be plausible, the validity for taking the average is not very clear because the cross section is exponentially large far away from the junction point. We will recalculate the boojum mass using the global approximation and confirm that the calculation in [45] is correct without any ambiguity. In [66], they also considered the case of two vortex-strings attached from the both sides of the domain wall, ending at different points (see Fig. 26). According to [66], this setting raises another problem about localization of the binding energy. Two possibilities are considered: One is that the binding energy locates around the junction points only and the other is that the binding energy is also localized half way between the strings endings. Our numerical computation confirms the former scenario, as is clearly visible in Fig. 21.

With the solutions at hand, we can clearly observe the magnetic fields expanding in the domain walls which are injected through the vortex strings. The figures drawn from the solutions, see Fig. 18 as a typical example, naturally invite an identification of the end points of the vortex strings with point-like sources in the domain wall. We would like to emphasize that this identification works quite well before integrating over the normal direction to the domain walls. Often, the end points are interpreted as *electric* point charges in low energy effective theory in $2 + 1$ dimensional world volume of the domain walls [11, 12, 13]. On the contrary, we will identify the end points with *magnetic* point-like sources from the $3 + 1$ dimensional view point by taking the thickness of the domain walls into account. We will show that the two dimensional distribution of the magnetic flux inside the domain wall can be correctly reproduced by gradient of a scalar function, which we will call the *magnetic* scalar

potential. Interestingly, the magnetic scalar potential corresponds to “height” of the domain wall. Namely, we will prove that the shape of the domain wall determines the magnetic force inside the domain walls. Further insights along this direction will be brought by the global approximate solutions. We will show that the domain wall’s position can be approximately – but precisely enough – identified with the solution $u(x^1, x^2)$ to the Taubes equation, Eq. (1.2) with $k = 1, 2$, up to a constant.

Thanks to the usefulness of the global approximations, we can now engineer any kind of configurations, no matter how complicated they are. As an interesting example, we will obtain numerical solution to a configuration of periodically aligned vortex strings attached to the domain wall. The shape of the domain wall exhibits a linear rather than logarithmic structure. This is expected once we identify the end points to the point-like charges. Suppose that infinite number of point charges are placed periodically on a line. The flux lines from those charges asymptotically become parallel, therefore the scalar potential too becomes linear sufficiently far away. In the setup, as mentioned above, the point charges are magnetic charges and the magnetic scalar potential corresponds to the domain wall’s position/shape. Then we will consider the configuration, where periodically aligned vortex strings end on the domain wall from one side and another infinite series of the vortex strings end on the opposite side. As can be easily imagined, such configuration resembles *magnetic* capacitor. We compute the magnetic capacitance per unit length and energy stored there. When we separate the two parallel lines of end points far away, flat but slant domain wall remains in between with non-zero magnetic flux inside. This is similar to a D-brane with magnetic flux. Putting additional vortex string ending on the tilt domain wall, the magnetic flux spreading inside the domain wall shows again one dimensional structure, which is almost the same as an electric charge placed in an electric capacitor. Similar configuration was already obtained in the strong gauge coupling limit [30] and our solution is for the finite gauge coupling case. This offers a field theoretical D-brane resembling the fundamental string ending on the D-brane with magnetic flux [67, 68].

We also study a dyonic extension of the 1/4 BPS solutions. Although the BPS equations were derived in [54, 69], no solutions have been obtained in the literature, except for the strong gauge coupling limit [11]. We will first study the 1/2 BPS dyonic domain walls which are finite gauge coupling version of the Q-kinks [70, 71]. We will find that positive and negative electric charges are induced on the skin of the domain wall. As a consequence, the dyonic domain wall in the weak gauge coupling region is an *electric* capacitor. Then, we will numerically solve the master equation for the dyonic 1/4 BPS configuration again with an aid of the global approximate solutions. When a vortex string attaches to the dyonic domain wall, both the magnetic and electric fluxes coexist inside the domain wall. We will show that almost everywhere except for the vicinity of the junction point, the electric flux \vec{E} and the magnetic flux \vec{B} are perpendicular. \vec{E} and \vec{B} becomes parallel around the junctions points, and,

indeed, we can show the boojum charge is proportional to $\vec{E} \cdot \vec{B}$, which is CP-violating interaction.

As a novel solution, which has not been studied previously, we find a semi-local boojum which appears at the end point of the semi-local vortex string [72] on the domain wall in the model with multiple flavors $N_F \geq 3$ with partially degenerate masses for the hypermultiplets. It has an additional zero mode related to size of the string diameter. We find that the semi-local boojum change its size unison with the size of the attached semi-local vortex string.

We have another progress. We have stressed that no analytic solutions have been found for the master equation (1.2) so far. Situation is the same even for much simpler case of the Taubes equation, Eq. (1.2) in \mathbb{R}^2 , for the local vortices. Thus, one might think that there is no hope to find analytic solutions to the master equations (1.2) either in \mathbb{R}^2 or \mathbb{R}^3 . Contrary to expectations, we will obtain several analytic exact solutions to the Taubes equation for specific semi-local vortices in \mathbb{R}^2 . Furthermore, combining this with the known exact solutions to the master equation in \mathbb{R}^1 for the domain walls [73] in a similar way with which we made the global approximate solution, we will, surprisingly, succeed in constructing analytic solutions to the master equation (1.2) in \mathbb{R}^3 . In connection with these results, we will also develop accurate approximation to the individual vortex string and domain wall solutions, which are useful to quickly obtain the global approximation for the 1/4 BPS solutions.

Finally, we will study the 1/4 BPS configuration from the view point of the low energy effective action, the Nambu-Goto action and the DBI action, for the domain wall. This kind of study was already performed for example, in [11, 12, 13, 16]. In these previous works, as the low energy effective action, the DBI action (or its linearization) which is obtained by dualizing the internal moduli of the domain wall to the Abelian gauge field was studied. In our paper, we study both the Nambu-Goto action and the DBI action. We first investigate the domain wall and its Q-extension (dyonic extension) in the Nambu-Goto action and find that the energy of those configuration coincides with one in the field theoretical model. Secondly, we study the case that a point source of zero size deforms the domain wall to a spike configuration in the Nambu-Goto action. This is precisely counter part of the Q-lump string ending on the domain wall in the strong gauge coupling limit in the original field theory. After that we study the relation between the Nambu-Goto action and the DBI action. We briefly explain how the Nambu-Goto action is dualized to the DBI action. By using the relations so obtained, we also transform the energy and the BPS equation for the dyonic extension of the spike configuration in terms of the DBI language. We show that the results are the same one as in [11]. By using the DBI action, we also study a point-like source with a finite size which should be a counterpart of the semi-local boojum. We find the semi-local BIon which, contrary to local BIon, has the tip of its spike smoothed out with the same order as the size

of the source.

This paper is organized as follows. In Section 2, we review our model, which is $\mathcal{N} = 2$ supersymmetric $U(1)$ gauge theory in $(3 + 1)$ -dimensions coupled to N_F hypermultiplets. We derive the BPS equations for the boojum configuration, preserving $1/4$ supersymmetry and shows that they reduce to one differential equation (1.2). In Section 3, we deal with the axially symmetric configuration, namely one vortex string ending on the domain wall. We show all the basic properties of the boojum there. Then, we demonstrate more complicated solutions, where multiple vortex strings end on the domain walls in Section 4. Section 5 is devoted to study periodically aligned vortex strings. We investigate the magnetic capacitor there. In Section 6, we study the dyonic extension of the $1/4$ BPS states. We find that the domain wall plays a role of an electric capacitor and show several numerical solutions. We develop a useful and accurate approximation for the ANO vortex and the domain walls in Section 7. We give several exact solutions to the $1/2$ and $1/4$ BPS equations in Section 8. Section 9 is devoted to analysis from the perspective of Nambu-Goto action together with analysis in terms of the DBI action. A brief discussion of the future work is given in Section 10.

2. The Model

2.1 Abelian vortex-wall system

Let us consider $\mathcal{N} = 2$ supersymmetric $U(1)$ gauge theory in $(3+1)$ -dimensions with $2N_F$ complex scalar fields in the charged hypermultiplets. We assemble them into a row vector $H \equiv (H^1, H^2, \dots, H^{N_F})$ and $\hat{H}^\dagger \equiv (\hat{H}^{1*}, \hat{H}^{2*}, \dots, \hat{H}^{N_F*})$. The vector multiplet include the photon A_μ and a real scalar field σ . The bosonic Lagrangian is given as

$$\mathcal{L} = -\frac{1}{4g^2}(F_{\mu\nu})^2 + \frac{1}{2g^2}(\partial_\mu\sigma)^2 + |D_\mu H|^2 + |D_\mu \hat{H}^\dagger|^2 - V, \quad (2.1)$$

$$V = \frac{g^2}{2}(v^2 - HH^\dagger + \hat{H}^\dagger \hat{H})^2 + \frac{g^2}{2} |H \hat{H}|^2 + |\sigma H - HM|^2 + |\sigma \hat{H}^\dagger - \hat{H}^\dagger M|^2, \quad (2.2)$$

where g is a gauge coupling constant, M is a real diagonal matrix

$$M = \text{diag}(m_1, \dots, m_{N_F}), \quad (2.3)$$

and v is the Fayet-Illiopoulos D-term. Without loss of generality we can take M to be traceless, namely $\sum_{A=1}^{N_F} m_A = 0$,² and align the masses as $m_A > m_{A+1}$. Since \tilde{H} will play no role, we will set $\tilde{H} = 0$ in the rest of this paper. Throughout this paper,

²Any overall factor $M = m\mathbf{1}_{N_F} + \dots$ can be absorbed into σ by shifting $\sigma \rightarrow \sigma - m$

we use the conventions:

$$\eta_{\mu\nu} = \text{diag}(+, -, -, -), \quad (2.4)$$

$$F_{\mu\nu} = \partial_\mu A_\nu - \partial_\nu A_\mu, \quad (2.5)$$

$$D_\mu H = \partial_\mu H + iA_\mu H. \quad (2.6)$$

The quartic coupling in the potential term is written by the gauge coupling constant g while in general it is not necessary to choose it like this. Such a non-generic value of the coupling constant allows us to embed this model into a supersymmetric model with eight supercharges by adding appropriate bosonic and fermionic fields. Such a choice of coupling constants make possible reduce the full equations of motion

$$\frac{1}{g^2} \partial_\mu F^{\mu\nu} + i(HD^\nu H^\dagger - D^\nu H H^\dagger) = 0, \quad (2.7)$$

$$\frac{1}{g^2} \partial_\mu \partial^\mu \sigma + H(H^\dagger \sigma - M H^\dagger) + (H \sigma - H M) H^\dagger = 0, \quad (2.8)$$

$$D_\mu D^\mu H = g^2(v^2 - |H|^2)H - \sigma(\sigma H - H M) + (\sigma H - H M)M. \quad (2.9)$$

into BPS equations, which are first order differential equations. Solutions to the BPS equations are called BPS solitons. These field configurations possess many special properties, such as saturating the energy bound in a given topological sector and preserving a fraction of supercharges in the supersymmetric theory. These facts simplify construction and discussion of topological solutions significantly. Of course, one can consider more general values of coupling constants without qualitatively changing the results. We will focus on the BPS solutions because generic case would involve much complicated analysis for solving the full equations of motion.

In the absence of the mass matrix M , the Lagrangian (2.1) is invariant under $SU(N_F)$ flavour transformation of Higgs fields $H \rightarrow HU$, $U \in SU(N_F)$. The non-degenerate masses in M explicitly break this down to $U(1)^{N_F-1}$, which we from now on assume to be the case unless stated otherwise.

There are N_F discrete vacua with representative field values

$$H_{\langle A \rangle} = (0, \dots, \underbrace{v}_{A\text{-th}}, \dots, 0), \quad \sigma_{\langle k \rangle} = m_A, \quad (A = 1, \dots, N_F). \quad (2.10)$$

We can act on each of these configurations by N_F global $U(1)$ transformations, which make each vacuum topologically a circle. Thus, the space of all vacuum configurations – the manifold \mathcal{V} – is isomorphic to N_F -torus $\mathcal{V} \sim S^1 \times S^1 \times \dots \times S^1$. A direct consequence of this fact is that the model (2.1) has a rich spectrum of topological excitations [21, 30, 45].

Non-trivial homotopy groups $\pi_0(\mathcal{V}) = \mathbb{Z}_{N_F}$ and $\pi_1(\mathcal{V}) = \mathbb{Z} \times \mathbb{Z} \times \dots \times \mathbb{Z}$ give rise to a large variety of domain walls and vortex strings. These solitons are 1/2 BPS solitons, as they preserve half of the supercharges if the model is extended to have

supersymmetry. In addition, there are also lots of composite solitons, where vortex strings attach to the domain walls. These configurations preserve 1/4 of supercharges and hence are known as 1/4 BPS solitons, which we are interested in.

2.2 1/4 BPS state

Let us now construct the 1/4 BPS solitons. We will arrange vortex strings to be parallel to the x^3 axis and the domain walls to be perpendicular to the x^3 axis. We let $A_0 = 0$ and consider static configurations, so that the Higgs field H , the scalar σ and the gauge field $A_k (k = 1, 2, 3)$ are independent on x^0 . The Bogomol'nyi bound is then obtained as³

$$\begin{aligned} \mathcal{E} = & \frac{1}{2g^2} \left\{ (\xi F_{12} - \eta \partial_3 \sigma - g^2 (HH^\dagger - v^2))^2 + (\xi F_{23} - \eta \partial_1 \sigma)^2 + (\xi F_{31} - \eta \partial_2 \sigma)^2 \right\} \\ & + |(D_1 + i\xi D_2)H|^2 + |D_3 H + \eta(\sigma H - HM)|^2 \\ & + \eta v^2 \partial_3 \sigma - \xi v^2 F_{12} + \frac{\xi \eta}{g^2} \epsilon_{klm} \partial_k (\sigma F_{lm}) + \partial_k j_k, \end{aligned} \quad (2.11)$$

where ϵ_{klm} is a totally antisymmetric symbol in three dimensions ($\epsilon_{123} = 1$) and j_k are non-topological currents defined by

$$j_a = \frac{\xi^i}{2} \epsilon_{ab} (H D_b H^\dagger - D_b H H^\dagger), \quad (a = 1, 2) \quad (2.12)$$

$$j_3 = -\eta(\sigma H - HM)H^\dagger. \quad (2.13)$$

The energy density (2.11) saturates the so-called Bogomol'nyi bound

$$\mathcal{E} \geq \mathcal{T}_W + \mathcal{T}_S + \mathcal{T}_B + \partial_k j_k, \quad (2.14)$$

with

$$\mathcal{T}_W = \eta v^2 \partial_3 \sigma, \quad \mathcal{T}_S = -\xi v^2 F_{12}, \quad \mathcal{T}_B = \frac{\eta \xi}{g^2} \epsilon_{klm} \partial_k (F_{lm} \sigma), \quad (2.15)$$

if the following 1/4 BPS equations

$$D_3 H + \eta(\sigma H - HM) = 0, \quad (2.16)$$

$$(D_1 + i\xi D_2)H = 0, \quad (2.17)$$

$$\eta \partial_1 \sigma = \xi F_{23}, \quad \eta \partial_2 \sigma = \xi F_{31}, \quad (2.18)$$

$$\xi F_{12} - \eta \partial_3 \sigma + g^2 (v^2 - |H|^2) = 0. \quad (2.19)$$

³The following useful identity holds:

$$D_a H (D_a H)^\dagger = (D_1 + i\xi D_2)H ((D_1 + i\xi D_2)H)^\dagger + \partial_a j_a - \xi F_{12} H H^\dagger.$$

are satisfied. It is easy to verify that these equations are compatible with the equations of motion (2.7)-(2.9) for all values of parameters $\eta^2 = \xi^2 = 1$, where $\xi = (-1)1$ labels (anti-)vortices and $\eta = (-1)1$ denotes (anti-)walls.

\mathcal{T}_W and \mathcal{T}_S , the domain wall and the vortex string energy density respectively, are positive definite. \mathcal{T}_B is the so-called *boojum* energy density, which is interpreted as binding energy of vortex string attached to the domain wall, since it is negative irrespective the signs of η and ξ [45, 66]. The total energy of 1/4 BPS soliton is obtained upon the space integration and it consists of three parts⁴

$$E_{1/4} = T_W A + T_S L + T_B, \quad (2.20)$$

where we have denoted sum of tensions of the domain walls $T_W = \int dx^3 \mathcal{T}_W$, and that of the vortex strings $T_S = \int dx^1 dx^2 \mathcal{T}_S$, respectively. $A = \int dx^1 dx^2$ and $L = \int dx^3$ stand for the domain wall's area and length of the vortex string. Only masses of the boojums $T_B = \int d^3x \mathcal{T}_B$ are finite. Let $t_W(A, A+1)$ be the tension of elementary domain wall interpolating the vacua $\langle A \rangle$ and $\langle A+1 \rangle$ [30]

$$t_W(A, A+1) = v^2 |m_{A+1} - m_A|. \quad (2.21)$$

Summing up all the elementary domain walls and vortex strings, we have

$$T_W = \sum t_W = v^2 |\Delta m|, \quad T_S = 2\pi v^2 |k|, \quad (2.22)$$

where we have denoted $\Delta m = [\sigma]_{x^3=-\infty}^{x^3=+\infty}$ and $k \in \mathbb{Z}$ stands for the number of vortex strings. T_B has been also calculated in [30, 45, 66]. But, there is a discussion about determining the mass of a single boojum which appears as a junction of the semi-infinite string ending on a logarithmically bent domain wall. In what follows, we will confirm without doubt that the boojum mass even for bent domain walls is given by the following formula [45]

$$T_B = \sum -\frac{2\pi}{g^2} |m_{A+1} - m_A|, \quad (2.23)$$

where the sum is taken for all the junctions of domain walls and vortex strings in the solution under consideration.

2.3 The moduli matrix formalism

With the use of the moduli matrix approach [31, 30, 34] the set of the equations (2.16)–(2.19) amounts to solving one equation called the master equation. It is easy to see that the following ansatz solves (2.16)–(2.18)

$$H = v e^{-\frac{v}{2}} H_0(z) e^{\eta M x^3}, \quad A_1 + i\xi A_2 = -i\partial_{\bar{z}} u, \quad \eta\sigma + iA_3 = \frac{1}{2}\partial_3 u, \quad (2.24)$$

⁴The total energy of any 1/4 BPS configuration is, of course, infinite, thus the equality has meaning only after employing some regularization procedure.

where $H_0(z)$ is the so-called the moduli matrix which is holomorphic in a complex coordinate $z \equiv x^1 + i\xi x^2$. Our notation is $\partial_{\bar{z}} = (\partial_1 + i\xi\partial_2)/2$. By using the $U(1)$ gauge transformation, we fix $u = u(z, \bar{z}, x^3)$ to be real. Then we have $A_3 = 0$. The last equation (2.19) turns into the master equation

$$\frac{1}{2g^2v^2}\partial_k^2 u = 1 - \Omega_0 e^{-u}, \quad \Omega_0 = H_0(z)e^{2\eta Mx^3}H_0^\dagger(\bar{z}). \quad (2.25)$$

Now, all fields can be expressed in terms of u as follows

$$\sigma = \frac{\eta}{2}\partial_3 u, \quad F_{12} = -2\xi\partial_z\partial_{\bar{z}}u, \quad F_{23} = \frac{\xi}{2}\partial_3\partial_1 u, \quad F_{31} = \frac{\xi}{2}\partial_2\partial_3 u. \quad (2.26)$$

The energy densities are also written as

$$\mathcal{T}_W = \frac{v^2}{2}\partial_3^2 u, \quad (2.27)$$

$$\mathcal{T}_S = 2v^2\partial_z\partial_{\bar{z}}u = \frac{v^2}{2}(\partial_1^2 + \partial_2^2)u, \quad (2.28)$$

$$\mathcal{T}_B = \frac{1}{2g^2}\{(\partial_1\partial_3 u)^2 + (\partial_2\partial_3 u)^2 - (\partial_1^2 + \partial_2^2)u\partial_3^2 u\}. \quad (2.29)$$

The non-topological current j_k given in Eqs. (2.12) and (2.13) can be rewritten in the following expression by using the BPS equations

$$j_k = \frac{1}{2}\partial_k(HH^\dagger). \quad (2.30)$$

Thus, we also have

$$\mathcal{T}_4 = \partial_k j_k = \frac{1}{2}\partial^2(HH^\dagger) = -\frac{1}{4g^2}\partial^2\partial^2 u, \quad (2.31)$$

with $\partial^2 \equiv \partial_k^2$. Collecting all pieces, the total energy density is given by

$$\mathcal{E} = \frac{v^2}{2}\partial_k^2 u + \frac{1}{2g^2}\{(\partial_1\partial_3 u)^2 + (\partial_2\partial_3 u)^2 - (\partial_1^2 + \partial_2^2)u\partial_3^2 u\} - \frac{1}{4g^2}(\partial_k^2)^2 u. \quad (2.32)$$

Thus, the scalar function u determines everything.

The moduli matrix formalism is an easy tool for describing the 1/4 BPS solitons. Indeed, one can construct any kind of configurations by preparing appropriately the moduli matrix $H_0(z) = (h_1(z), h_2(z), \dots, h_{N_F}(z))$. As a simple example, let us consider the case that only h_1 and h_2 are non-zero. The vacuum $\langle i \rangle$ is given by $h_j = \delta_{ij}$ ($j = 1, 2$). If they are both non zero constants, the corresponding configuration has the domain wall separating $\langle 1 \rangle$ and $\langle 2 \rangle$ vacua. Since we assume $m_A > m_{A+1}$, the vacuum $\langle 1 \rangle$ appears on the left hand side of the domain wall while the vacuum $\langle 2 \rangle$ on the right hand side. When one wants to put N_1 vortex strings in the vacua $\langle 1 \rangle$, one only needs to prepare $h_1 = P_1(z)$ where $P_1(z)$ stands

for a polynomial with degree N_1 . This can be straightforwardly extended for generic $H_0(z)$.

Hence, the moduli matrix formalism allows us to handle the complicated 1/4 BPS solitons. One can even deal with the solutions belonging to different topological sectors simultaneously. It is nice that all information about the moduli parameters are included in H_0 . For these reasons, the moduli matrix formalism has been frequently used in the literature since its inception. Nevertheless, a finishing touch has been omitted in the sense that no analytic or numerical solutions have been constructed for the master equation (2.25) except for the strong gauge coupling limit $g^2 \rightarrow \infty$ [31] as was mentioned in the Introduction. In the literature, only schematic pictures in the weak/strong gauge coupling region has been given []. This lack of solutions also caused some confusion about the definition of the boojum [66], which we will mention later.

3. Axially symmetric solutions

In this section we explain how we numerically solve the master equation (2.25). Throughout this section, we will concentrate on $N_F = 2$ case but everything addressed here can be straightforwardly extended to generic case. For ease of notation, we will use the following dimensionless coordinates and mass

$$\tilde{x}^k = \sqrt{2}gvx^k, \quad \tilde{M} = \frac{1}{\sqrt{2}gv}M = \text{diag} \left(\frac{\tilde{m}}{2}, -\frac{\tilde{m}}{2} \right). \quad (3.1)$$

The dimensionless fields are similarly defined by

$$\tilde{H} = \frac{H}{v} = e^{-\frac{u}{2}} H_0 e^{\eta \tilde{M} \tilde{x}^3}, \quad \tilde{\sigma} = \frac{\sigma}{\sqrt{2}gv} = \frac{\eta}{2} \tilde{\partial}_3 u. \quad (3.2)$$

We will also use the dimensionless magnetic fields

$$\tilde{F}_{12} = \frac{1}{g^2v^2} F_{12} = -\xi \left(\tilde{\partial}_\rho^2 + \frac{1}{\tilde{\rho}} \tilde{\partial}_\rho \right) u, \quad (3.3)$$

$$\tilde{F}_{23} = \frac{1}{g^2v^2} F_{23} = \xi \tilde{\partial}_3 \tilde{\partial}_\rho u \cos \theta, \quad (3.4)$$

$$\tilde{F}_{31} = \frac{1}{g^2v^2} F_{31} = \xi \tilde{\partial}_3 \tilde{\partial}_\rho u \sin \theta. \quad (3.5)$$

Then, the dimensionless energy density $\tilde{\mathcal{E}}$ is defined by

$$\mathcal{E} = g^2v^4 \tilde{\mathcal{E}} = \tilde{\mathcal{T}}_W + \tilde{\mathcal{T}}_S + \tilde{\mathcal{T}}_B + \tilde{\mathcal{T}}_4, \quad (3.6)$$

where

$$\tilde{\mathcal{T}}_W = 2\eta\tilde{\partial}_3\tilde{\sigma} = \tilde{\partial}_3^2 u, \quad (3.7)$$

$$\tilde{\mathcal{T}}_S = -\xi\tilde{F}_{12} = \left(\tilde{\partial}_\rho^2 + \frac{1}{\tilde{\rho}}\tilde{\partial}_\rho\right)u, \quad (3.8)$$

$$\tilde{\mathcal{T}}_B = 2\eta\xi\tilde{\partial}_i\left(\epsilon_{ijk}\tilde{\sigma}\tilde{F}_{jk}\right) = 2\left[\left(\tilde{\partial}_\rho\tilde{\partial}_3u\right)^2 - \left(\tilde{\partial}_\rho^2 + \frac{1}{\tilde{\rho}}\tilde{\partial}_\rho\right)u\tilde{\partial}_3^2u\right], \quad (3.9)$$

$$\tilde{\mathcal{T}}_4 = -\left(\tilde{\partial}_\rho^2 + \frac{1}{\tilde{\rho}}\tilde{\partial}_\rho + \tilde{\partial}_3^2\right)^2 u. \quad (3.10)$$

The relations to the original values are given as

$$T_W = \int dx^3 \mathcal{T}_W = \frac{gv^3}{\sqrt{2}} \int d\tilde{x}^3 \tilde{\mathcal{T}}_W = \frac{gv^3}{\sqrt{2}} \tilde{T}_W \quad (3.11)$$

$$T_S = \int d^2x \mathcal{T}_S = \frac{v^2}{2} \int d^2\tilde{x} \tilde{\mathcal{T}}_S = \frac{v^2}{2} \tilde{T}_S, \quad (3.12)$$

$$T_B = \int d^3x \mathcal{T}_B = \frac{v}{2\sqrt{2}g} \int d^3\tilde{x} \tilde{\mathcal{T}}_B = \frac{v}{2\sqrt{2}g} \tilde{T}_B. \quad (3.13)$$

In what follows, we will not distinguish x^k and \tilde{x}^k , unless stated otherwise. An exception is the mass: we will use the notation \tilde{m} in order not to forget that we are using the dimensionless variables. Then the master equation (2.25) is expressed as

$$\partial_k^2 u - 1 + \Omega_0 e^{-u} = 0, \quad \Omega_0 = H_0^\dagger e^{2\eta\tilde{M}x^3} H_0^\dagger. \quad (3.14)$$

If the moduli matrix is constant, we have flat domain walls and the function $u = u_W(x^3)$ depend only on x^3 coordinate. The reduced master equation reads

$$\partial_3^2 u_W - 1 + \Omega_0 e^{-u_W} = 0. \quad (3.15)$$

Similarly, when the moduli matrix has only one non-zero component, say $H_0 = (P_n(z), 0, \dots, 0)$, the configuration has n vortex strings in the vacuum $\langle 1 \rangle$. One can eliminate the x^3 dependence by defining

$$u(x^k) = u_S(x^1, x^2) + \eta\tilde{m}x^3. \quad (3.16)$$

Then the master equation reduces to

$$(\partial_1^2 + \partial_2^2)u_S - 1 + |P_n|^2 e^{-u_S} = 0. \quad (3.17)$$

3.1 Gradient flow

Now we are ready to solve the master equation Eq. (3.14) numerically. But, instead of solving it directly, we will solve the so-called gradient flow equation

$$\partial_k^2 U - 1 + \Omega_0 e^{-U} = \partial_t U, \quad (3.18)$$

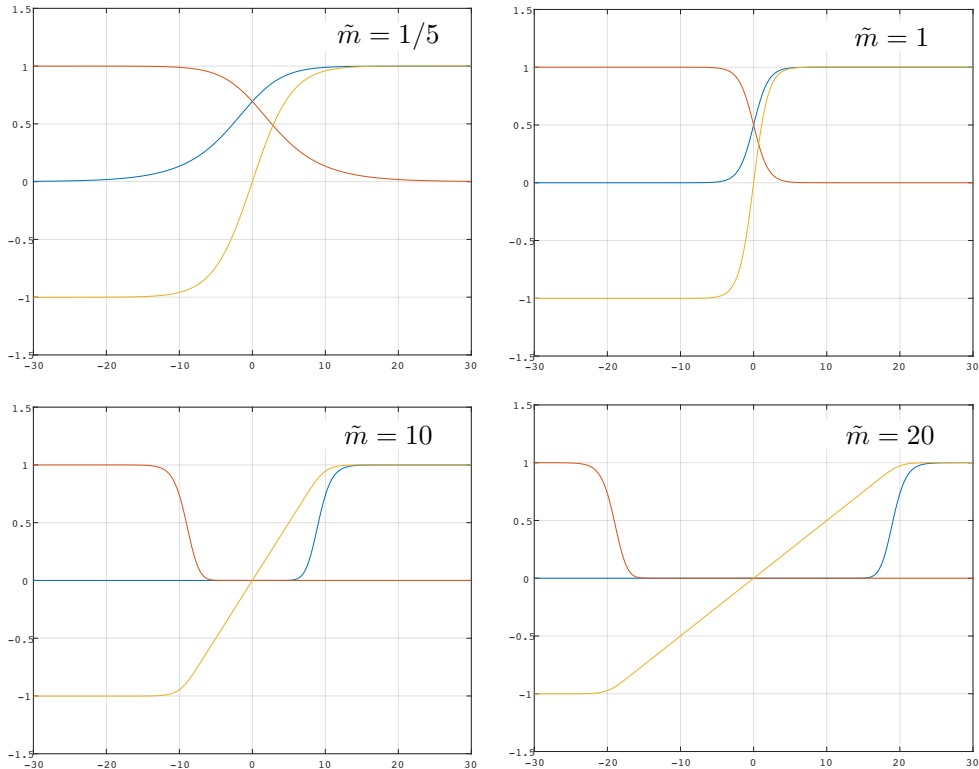


Figure 1: The numerical solutions of the domain wall in $N_F = 2$ case with $\tilde{M} = (\tilde{m}/2, -\tilde{m}/2)$ where \tilde{m} is taken to be $1/5$ (strong coupling), 1 , and $10, 20$ (weak coupling), respectively. The horizontal axis is in dimensionless coordinate $\tilde{x}^3 = gv x^3$. The blue and red lines are \tilde{H}_1 and \tilde{H}_2 . The yellow line is $2\tilde{\sigma}/\tilde{m}$.

for $U = U(x^k, t)$, using appropriate initial configuration $U(x^k, 0)$ and boundary conditions. Normally, $U(x^i, t)$ rapidly converges to a static function. When $\partial_t U(x^k, t)$ becomes negligibly small at a sufficiently large t , we regard $U(x^k, t)$ as a solution $u(x^k)$ of the original master equation,

$$u(x^k) = \lim_{t \rightarrow \infty} U(x^k, t). \quad (3.19)$$

Final state obtained in this way depends on the initial configuration and the boundary conditions. Thus, the necessary step to successfully solve Eq. (3.18) is to provide an initial configuration compatible with the boundary conditions.

3.1.1 Domain wall solutions

Solving the gradient flow equation is not difficult especially for a single type of solitons like the flat domain walls or the straight vortex strings. For the domain walls perpendicular to the x^3 axis, the master equation reduces to Eq. (3.15). The

solution $u_W(x^3)$ can be obtained by solving the corresponding gradient flow equation for $U = U_W(x^3, t)$

$$\partial_3^2 U_W - 1 + \Omega_0(x^3)e^{-U_W} = \partial_t U_W. \quad (3.20)$$

A convenient choice of the initial configuration and the boundary conditions at $x^3 = \pm L_3$ ($L_3 \gg \tilde{m}$) is

$$U_W(x^3, 0) = \log \Omega_0(x^3), \quad U_W(\pm L_3, t) = \log \Omega_0(\pm L_3). \quad (3.21)$$

The true solution can be obtained as the asymptotic function $u_W(x^3) = \lim_{t \rightarrow \infty} U_W(x^3, t)$ which satisfies

$$u_W(x^3) \rightarrow \begin{cases} \tilde{m}x^3 & \text{for } x^3 \gg \tilde{m}, \\ -\tilde{m}x^3 & \text{for } x^3 \rightarrow -\tilde{m}. \end{cases} \quad (3.22)$$

Several numerical solutions are shown in Fig. 1. There are two qualitatively different domain walls according to \tilde{m} [12]. In the strong gauge coupling limit, $\tilde{m} \ll 1$, the domain wall has a simple structure as shown in the left panel of Fig. 1. The traverse size of the domain wall is $\tilde{d}_W = 2/\tilde{m}$. On the other hand, in the weak coupling region, $\tilde{m} \gg 1$, the domain walls consists of two layers [12]: the fundamental Higgs field decays in the outer thin layer whose transverse size is of order 1 (in the dimensionless unit), whereas the singlet scalar field $\tilde{\sigma}$ interpolates $\tilde{m}/2$ and $-\tilde{m}/2$ through the inner fat layer whose transverse size is about $\tilde{d}_W = 2\tilde{m}$. In the latter case, the inside of the domain wall remains almost the Coulomb phase since the charged fundamental fields are exponentially small there.

3.1.2 Vortex string solutions

The vortex strings can be obtained similarly. As an example, let us consider n vortex strings in the $\langle 1 \rangle$ vacuum. It is given by the moduli matrix $H_0 = (P_n(z), 0)$ with $P_n(z)$ being the n -th order polynomial. This yields $\Omega_0 = |P_n|^2 e^{\eta \tilde{m} x^3}$. Then we define

$$U(x^k, t) = U_S(x^1, x^2) + \eta \tilde{m} x^3. \quad (3.23)$$

This yields $\tilde{\sigma} = \eta \tilde{m}$. The master equation to U_S for the vortex strings reduces to

$$(\partial_1^2 + \partial_2^2)U_S - 1 + |P_n|^2 e^{-U_S} = \partial_t U_S. \quad (3.24)$$

Note that \tilde{m} disappears due to the shift given in Eq. (3.23). There are no dimensionful parameters in this equation, so that everything is of order one. A convenient choice for the initial and boundary conditions is

$$U_S(x^1, x^2, 0) = \log \left(|P_n|^2 + e^{-\rho^2} \right), \quad (3.25)$$

$$U_S(\pm L_1, \pm L_2, t) = \log \left(|P_n|^2 \Big|_{x^1=\pm L_1, x^2=\pm L_2} \right), \quad (3.26)$$

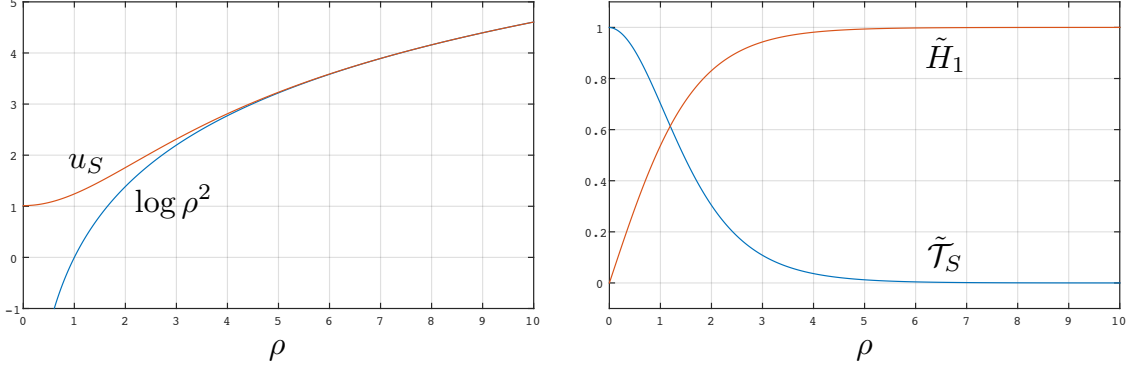


Figure 2: Profiles of the vortex string solutions. The red and blue curves correspond to u_S and $\log \rho^2$ in the left panel. In the right panel, the red line stands for \tilde{H}_1 and the blue line shows the magnetic flux density \tilde{T}_S .

where, of course, we assume $|L_{1,2}| \gg 1$ so that $e^{-\rho^2}$ can be neglected. The exponential term appearing in Eq. (3.25) is there in order to avoid singular behavior at the center of the vortex strings in the initial configuration. It is exponentially small at the boundary $x^1 = \pm L_1$ and $x^2 = \pm L_2$, so that the initial configuration does not contradict to the boundary conditions. As before, the true vortex solution u_S for Eq. (3.17) can be obtained as the asymptotic function $u_S(x^1, x^2) = \lim_{t \rightarrow \infty} U_S(x^1, x^2, t)$.

The single vortex string ($P_1 = z$) leads to an axially symmetric configuration $U_S(\rho, t)$ satisfying the master equation

$$\left(\partial_\rho^2 + \frac{1}{\rho} \partial_\rho \right) U_S - 1 + \rho^2 e^{-U_S} = \partial_t U_S. \quad (3.27)$$

This should be solved with the boundary conditions

$$\partial_\rho U_S(0, t) = 0, \quad U_S(L_\rho, t) = \log L_\rho^2. \quad (3.28)$$

The asymptotic behavior of $u_S(\rho) = \lim_{t \rightarrow \infty} U_S(\rho, t)$ is

$$u_S \rightarrow \log \rho^2 \quad (\rho \gg 1). \quad (3.29)$$

The numerical solution for a single vortex string is given in Fig. 2.

3.2 1/4 BPS solutions

Let us now address how to get the 1/4 BPS solutions by again taking the simplest configuration with the moduli matrix $H_0 = (z, 1)$. The corresponding gradient flow equation is given by

$$\left(\partial_3^2 + \partial_\rho^2 + \frac{1}{\rho} \partial_\rho \right) U - 1 + \left(\rho^2 e^{\tilde{m}x^3} + e^{-\tilde{m}x^3} \right) e^{-U} = \partial_t U. \quad (3.30)$$

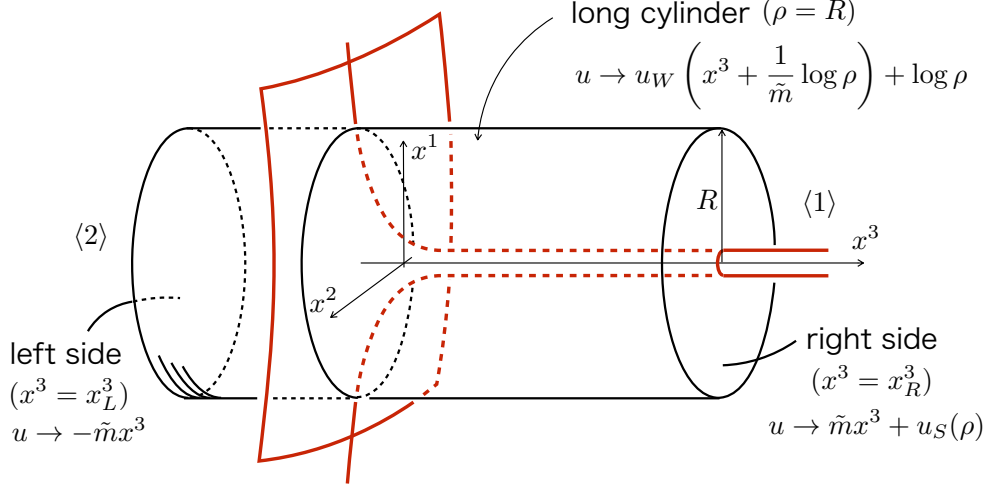


Figure 3: The vortex trumpet: vortex string ending on a logarithmically curved domain wall. The asymptotic behavior of the function $u(\rho, x^3)$ is shown on each part of the boundary (the ‘long cylinder’).

A significant difference from the homogeneous solitons is that the boundaries of the 3D box parallel to the vortex string intersect with the curved domain wall and one of the boundary parallel to the domain wall intersects with the vortex string, see Fig. 3. Thus, we have to figure out an appropriate boundary condition consistent with the curved domain wall.

Let us first look at the region far from the vortex string axis, namely $\rho \gg 1$. Since u depends on x^1 and x^2 only through $\log \rho$, we can drop $\partial_\rho^2 + (1/\rho)\partial_\rho$ term from the master equation

$$\partial_3^2 u - 1 + \left(\rho^2 e^{\tilde{m}x^3} + e^{-\tilde{m}x^3} \right) e^{-u} = 0. \quad (3.31)$$

This can be rewritten as

$$\partial_3^2 (u - \log \rho) - 1 + \left(e^{\tilde{m}(x^3 + \frac{1}{\tilde{m}} \log \rho)} + e^{-\tilde{m}(x^3 + \frac{1}{\tilde{m}} \log \rho)} \right) e^{-u + \log \rho} = 0. \quad (3.32)$$

This is nothing but the master equation for the domain wall if we regard $u - \log \rho$ as $u_W(x^3) = \lim_{t \rightarrow \infty} U_W(x^3, t)$, so we find

$$u \rightarrow u_W \left(x^3 + \frac{1}{\tilde{m}} \log \rho \right) + \log \rho, \quad (\rho \rightarrow \infty). \quad (3.33)$$

The shift $(\log \rho)/\tilde{m}$ in the argument of u_W reflects the fact that the domain wall asymptotically bends as

$$x^3 \simeq -\frac{1}{\tilde{m}} \log \rho. \quad (3.34)$$

Next, going far from the domain wall, u approaches to the vortex string $u \rightarrow \tilde{m}x^3 + u_S$ for $x^3 \gg 0$ while becomes close to the vacuum $u \rightarrow -\tilde{m}x^3$ for $x^3 \ll 0$.

$$u(\rho, x^3) \rightarrow \begin{cases} \tilde{m}x^3 + u_S(\rho) & \text{for } x^3 \rightarrow \infty, \\ -\tilde{m}x^3 & \text{for } x^3 \rightarrow -\infty, \end{cases} \quad (3.35)$$

with $u_S(\rho) = \lim_{t \rightarrow \infty} U_S(\rho, t)$.

A suitable function possessing these asymptotic behaviors can be obtained by replacing ρ by $e^{u_S/2}$ in the asymptotic function u given in Eq. (3.33). This is our choice for the initial configuration to solve the gradient flow

$$U(\rho, x^3, t=0) = u_W \left(x^3 + \frac{1}{2\tilde{m}} u_S(\rho) \right) + \frac{1}{2} u_S(\rho) \equiv \mathcal{U}(\rho, x^3). \quad (3.36)$$

Since $u_S(\rho) \rightarrow \log \rho^2$ as $\rho \rightarrow \infty$, this function is consistent with Eq. (3.33). Furthermore, since $u_W(x^3) \rightarrow \pm \tilde{m}x^3$ for $x^3 \rightarrow \pm \infty$ we have $\mathcal{U} \rightarrow \pm \tilde{m} \left(x^3 + \frac{1}{2\tilde{m}} u_S(\rho) \right) + \frac{1}{2} u_S(\rho)$, which is desired asymptotic behavior of Eq. (3.35). The boundary conditions consistent with the initial configuration are

$$\partial_\rho U(0, x^3, t) = 0, \quad U(L_\rho, x^3, t) = \mathcal{U}(L_\rho, x^3), \quad U(\rho, \pm L_3, t) = \mathcal{U}(\rho, \pm L_3). \quad (3.37)$$

Note that the first condition is ensured by $\partial_\rho u_S(\rho=0) = 0$. The initial configuration (3.36) gives us an important information about the domain wall's position for whole ρ as

$$x^3(\rho) = -\frac{1}{2\tilde{m}} u_S(\rho), \quad (3.38)$$

which is consistent with the asymptotic behavior given in Eq. (3.34). In the strong gauge coupling limit, we have the exact solution $u_S = \log \rho^2$, so the asymptotic relation (3.34) becomes exact for whole ρ . As shown in the left panel of Fig. 2, the domain wall is smooth everywhere in the finite gauge coupling, but it gets logarithmically sharp at the origin in the strong gauge coupling limit.

Having the appropriate initial configuration \mathcal{U} , we now solve the gradient flow equation (3.30). We solve it by using a standard finite difference method with the Crank-Nicolson scheme. A typical solution with $\tilde{m} = 1$ is shown in Fig. 4. One can clearly see that the straight vortex string with a *finite* diameter ends on the logarithmically curved domain wall. This is obvious contrast to previously obtained solutions with singular vortex strings [11, 30]. Furthermore, most importantly, our solution has the boojum which contributes to the total energy (the boojum disappears in the strong coupling limit since the boojum charge is proportional to $1/g^2$). With our numerical solution at hand, we figure out correct shape of the boojum as shown in Fig. 4. So far, the shape of boojum have been only schematically realized. For example, in Ref. [45], the boojum was expressed as just a hemisphere which is little

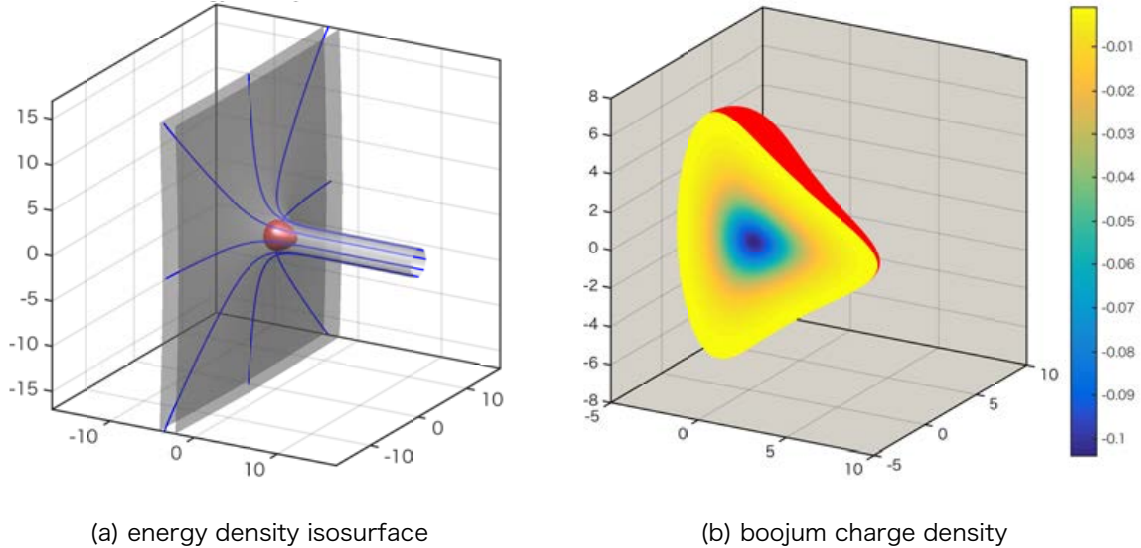


Figure 4: (a) The dimensionless energy density isosurface and (b) the dimensionless boojum charge density for the finite vortex string ending on the bent domain wall for $\tilde{m} = 1$. In the panel (a), the gray surface corresponds to the dimensionless energy isosurface, the red one to the dimensionless boojum charge isosurface, and the blue lines show the flows of the magnetic fields.

too simple compared to our numerical solution. The third advantage to have the numerical solution for a finite gauge coupling is that we can clearly see distribution of the magnetic flux which enters from the vortex string into the domain wall. In Fig. 4 we show several lines of the magnetic field (blue solid curves). They form a flux tube inside the vortex string and radially spread out once they enter the domain wall. This picture can correctly be obtained only for the finite gauge coupling since electromagnetic interaction disappears in the strong coupling limit.

The numerical solutions also shed light on both qualitative and quantitative difference between the 1/4 BPS configurations in the strong ($\tilde{m} \gg 1$) and the weak ($\tilde{m} \ll 1$) gauge coupling regions. Especially, the vicinity of a junction point of the domain wall and vortex string is hard to correctly understand without numerical methods. We show the several solutions in details; the profiles of the fields, the topological charge densities, and the energy densities are displayed in Fig. 5 ($\tilde{m} = 1/5$), Fig. 6 ($\tilde{m} = 1$) and Fig. 7 ($\tilde{m} = 10$).

Since we have rescaled out gv dependence, the asymptotic vortex string configuration is common for all the cases. This can be seen in regions near the top-left edges of the middle panels of Figs. 5 – 7 in which the topological charge densities of the vortex string $\tilde{\mathcal{T}}_S$ are shown. The bottom-middle panels show the magnitude of the magnetic fields which are slightly different from the string topological charge density $\tilde{\mathcal{T}}_S$.

The three panels in the first row of Figs. 5-7 show \tilde{H}_1 , \tilde{H}_2 and $\tilde{\sigma}$. The field \tilde{H}_1 develops the non-zero VEV in the upper region ($x^3 \gg 0$). Namely, the light yellow regions of the top-left panels correspond to the vacuum $\langle 1 \rangle$. Similarly, the yellow parts of the top-middle panels show region of the vacuum $\langle 2 \rangle$. Since the phase of \tilde{H}_1 has the winding number 1 for the vortex string, \tilde{H}_1 vanishes at the core of the vortex string (on the top-left edge ($\rho = 0, x^3 \gg 0$)). Since neither \tilde{H}_1 nor \tilde{H}_2 develops non-zero VEV there, the $U(1)$ gauge symmetry is recovered.

Shape of the bent domain wall can be seen in the middle-left panels where the topological charge density $\tilde{\mathcal{T}}_W$ is plotted. The yellow-line region of $\tilde{\mathcal{T}}_W$ is consistent with the yellow-blue transit region of $\tilde{\sigma}$ in the top-right panels. The domain wall strongly bends for the strong coupling ($\tilde{m} \ll 1$) while it seems to be almost flat for the weak coupling ($\tilde{m} \gg 1$). This difference comes from the wall to string tension ratio, which can be found by comparing the scales of the color bars of the middle-left and middle-middle panels.

The domain wall tends to strongly bent when the tension of the vortex string is larger than that of the domain wall. This can be also understood from Eq. (3.34), which tells that the asymptotic wall curve is $x^3 \simeq -\log \rho^{1/\tilde{m}}$. For example, $x^3(\rho = 10) = -\log 10$ for the case of $\tilde{m} = 1$. To get the same amount of bending in the case of $\tilde{m} = 10$, one needs to go to $\rho = 10^{10}$! This is the reason why the domain wall seems almost flat for $\tilde{m} = 10$ in the middle-left panel of Fig. 7. It is also seen that the domain wall at $\rho = 0$ is not singular for any \tilde{m} . In contrast to the inside of the vortex string, there are no topological reasons for the domain wall core to be in the unbroken phase. Indeed, both \tilde{H}_1 and \tilde{H}_2 are non-zero inside the domain wall with $\tilde{m} = 1/5$ and 1. This is consistent with the single domain wall solutions given in Fig. 1. Only when the gauge coupling is very weak ($\tilde{m} \gg 1$), the domain wall core develops the fat inner layer of the unbroken phase. While the diameter of the vortex string is fixed to be of order one, width of the domain wall varies as \tilde{m} is changed, see Fig. 1. The domain wall is sharpest when $\tilde{m} \simeq 1$, while it becomes much fatter than the vortex string for both weak and strong gauge coupling limits, see the bottom-left panels showing the full energy density including the surface term.

Our prime interest is to understand the junction point of the domain wall and the vortex string. Especially in the weak coupling limit, since the cores of the vortex string and domain wall are in the unbroken phase. The top-left and top-middle panels of Fig. 7 clearly show that the two unbroken regions are just smoothly connected. We are also interested in the boojum, the binding energy appearing at the junction point. The middle-right panels exhibit variety of the shape of boojum depending on \tilde{m} . It is basically a smoothed cone which becomes thinner for $\tilde{m} \ll 1$ and fatter for $\tilde{m} \gg 1$.

Finally, in the bottom-right panels we plot the mass square of the gauge field

defined by

$$m_v^2 \equiv \left| \tilde{H}_1 \right|^2 + \left| \tilde{H}_2 \right|^2. \quad (3.39)$$

The gauge symmetry is recovered in the deep-blue region, while is strongly broken in the light-yellow region. In addition, we also plot flow of the magnetic field (magnetic force lines). In general, the flow tend to be concentrated into the region where the gauge symmetry is unbroken or weakly broken. In the case of the strong gauge coupling ($\tilde{m} = 1/5$ given in Fig. 5), the incoming magnetic force lines through the vortex string are forced to bend when they encounter the domain wall. They scatter and then spread out along the domain wall because the breaking of the gauge symmetry is milder inside the domain wall. However, the lines running near the core of the vortex string are pushed out of the domain wall. This happens because the energy cost to bend the lines all the way into the core of domain wall is larger than that to have mildly bending lines going through the bulk. In contrast, in the intermediate case with $\tilde{m} = 1$ given in Fig. 6, the magnetic force lines go along the domain wall. This is because the mass of the gauge field inside the domain wall is sufficiently small, so that the magnetic force lines bend and tend to go inside the domain wall. The weak coupling case with $\tilde{m} = 10$ shown in Fig. 7 has totally different structure. Inside the fat domain wall is the unbroken phase. The incoming magnetic force lines spread out *linearly* in the domain wall until they encounter the other side of the domain wall beyond which is the broken phase.

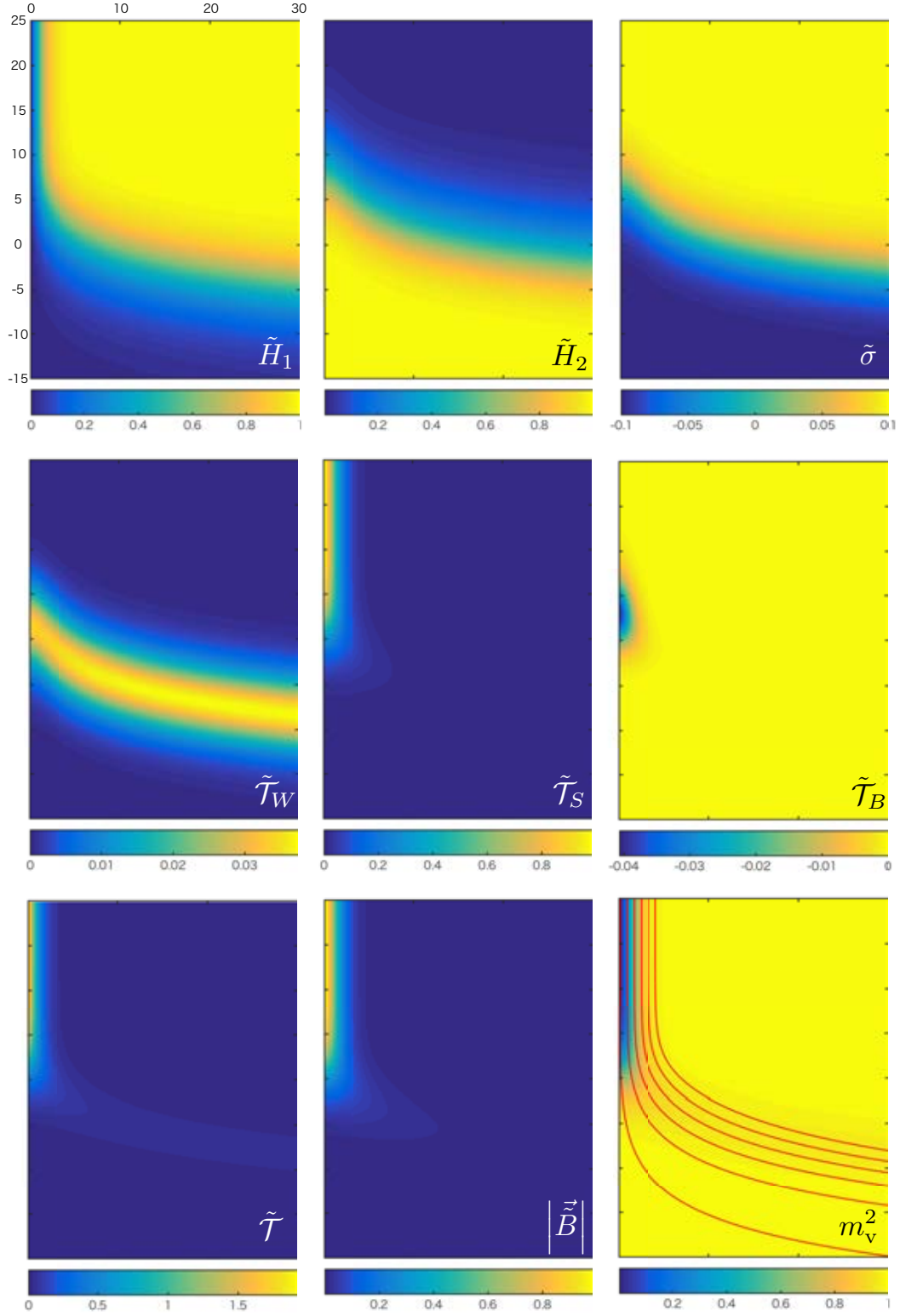


Figure 5: The numerical solution for $\tilde{m} = 1/5$, the strong gauge coupling region where the domain wall strongly bends. The 1st row shows the scalar fields, and the 2nd row shows the constituent topological charge densities. The right-bottom panel shows the effective photon mass m_v^2 and the red lines are magnetic force lines.

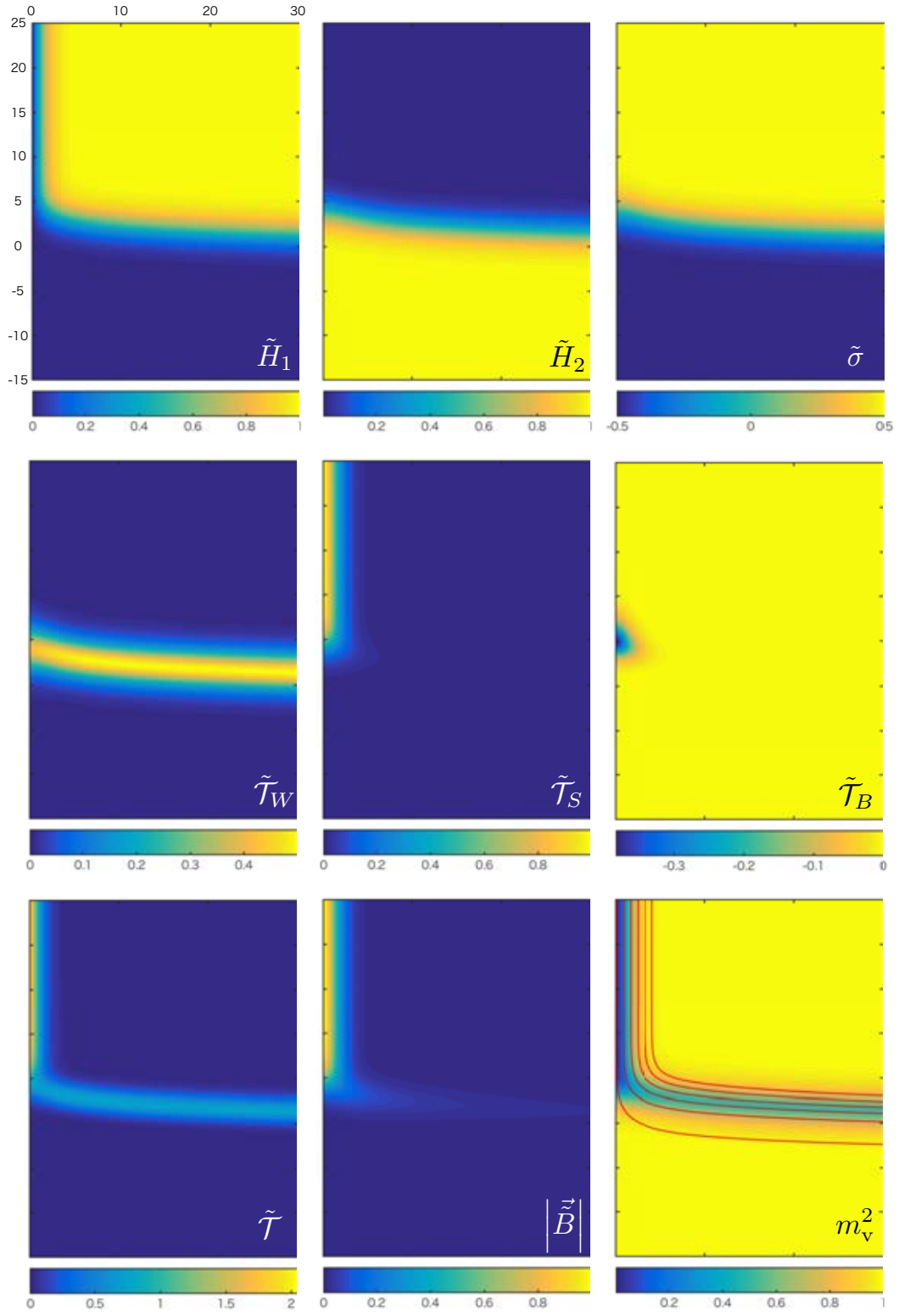


Figure 6: The numerical solution for $\tilde{m} = 1$, an intermediate gauge coupling constant. See also the caption of Fig. 5.

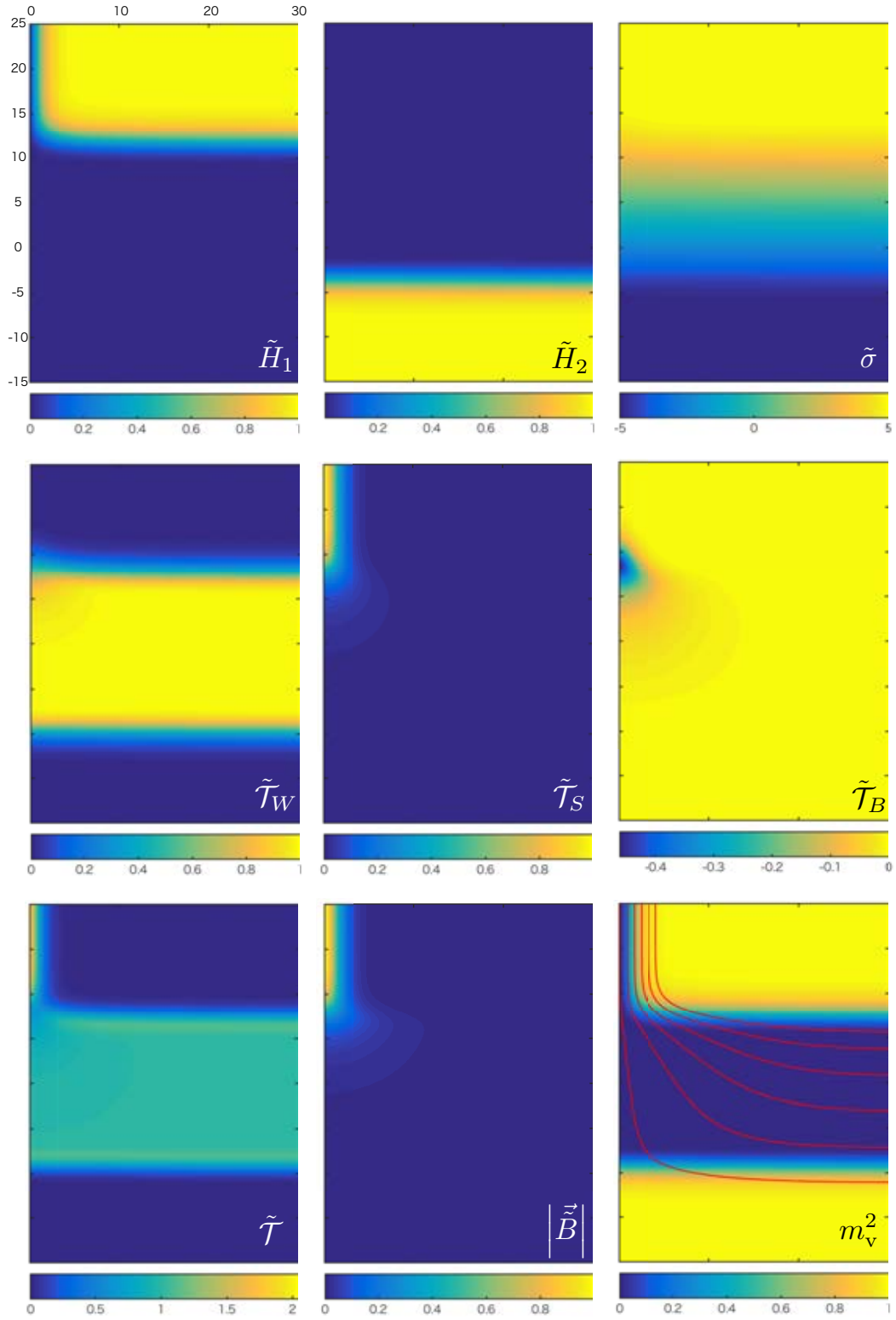


Figure 7: The numerical solution for $\tilde{m} = 10$, the weak gauge coupling region where the domain wall slowly bends. See also the caption of Fig. 5.

Finally, let us compute the tensions of the topological objects: The domain wall tension is everywhere constant in the x^1 - x^2 plane and it is given as

$$\begin{aligned}
\tilde{T}_W(\rho) &= \int_{-\infty}^{\infty} dx^3 \tilde{\mathcal{T}}_W(\rho, x^3) \\
&= \partial_3 u(x^3 \rightarrow \infty) - \partial_3 u(x^3 \rightarrow -\infty) \\
&= 2\tilde{m}.
\end{aligned} \tag{3.40}$$

The string tension is a constant along the x^3 direction

$$\begin{aligned}
\tilde{T}_S(x^3) &= \int dx^1 dx^2 \tilde{\mathcal{T}}_S(\rho, x^3) \\
&= 2\pi \int_0^{\infty} d\rho \partial_\rho (\rho \partial_\rho u) \\
&= 2\pi \left[\frac{1}{\tilde{m}} u'_W \left(x^3 + \frac{1}{\tilde{m}} \log \rho \right) \Big|_{\rho \rightarrow \infty} + 1 \right] \\
&= 4\pi,
\end{aligned} \tag{3.41}$$

where we used the asymptotic behavior given in Eq. (3.33) and $u_W(x^3) \rightarrow \tilde{m}x^3$ for $x^3 \gg 0$. In terms of the original variables, these are rewritten as

$$T_W = \frac{gv^3}{\sqrt{2}} \times 2\tilde{m} = \sqrt{2} gv^3 \frac{m}{\sqrt{2} gv} = mv^2 \tag{3.42}$$

$$T_S = \frac{v^2}{2} \times 4\pi = 2\pi v^2. \tag{3.43}$$

One should be careful that the (dimensionless) string tension is always 4π even in the vacuum $\langle 2 \rangle$ side of the domain wall ($x^3 \ll 0$) where we do not put the vortex string. This is simply a consequence of the flux conservation. The magnetic flux cannot invade the vacuum $\langle 2 \rangle$, so that it flows along the surface of the domain wall which logarithmically bends. Therefore, regardless of x^3 , we always have total flux of 4π . In other words, the vortex string *is not* chopped by the domain wall but exponentially inflates. This observation can also be justified by seeing the profile of the scalar field H_1 . The amplitude of the scalar field whose phase has the winding number must necessarily vanish somewhere by a topological reason. Therefore, we can think of the deep-blue region in the top-left panels of Figs. 5 – 7 as the *inside* the vortex trumpet.

The total magnetic flux outgoing through a sufficiently long cylinder (the right side is at $x_R^3 \gg \tilde{m}$ and the left side is at $x_L^3 \ll -\tilde{m}$) of sufficiently large radius R

($\gg 1$) surrounding the vortex trumpet, see Fig. 3, can be calculated as follows

$$\begin{aligned}
\tilde{\Phi}_C &= \int_{\text{cylinder}} dS_i \frac{1}{2} \epsilon_{ijk} \tilde{F}_{jk} \\
&= 2\pi R \int_{x_L^3}^{x_R^3} dx^3 \tilde{F}_{23} \Big|_{\rho=R, \theta=0} \\
&= 2\pi R \int_{x_L^3}^{x_R^3} dx^3 \partial_3 \partial_\rho u \Big|_{\rho=R} \\
&= 2\pi R \int_{x_L^3}^{x_R^3} dx^3 \partial_3 \partial_\rho u_W \left(x^3 + \frac{1}{\tilde{m}} \log \rho \right) \Big|_{\rho=R} \\
&= \frac{2\pi}{\tilde{m}} \int_{x_L^3}^{x_R^3} dx^3 \partial_3^2 u_W \left(x^3 + \frac{1}{\tilde{m}} \log R \right) \\
&= \frac{2\pi}{\tilde{m}} \left[\partial_3 u_W \left(x^3 + \frac{1}{\tilde{m}} \log R \right) \right]_{x^3=x_L^3}^{x^3=x_R^3} \\
&= 4\pi,
\end{aligned} \tag{3.44}$$

where we used Eqs. (3.22) and (3.33). The incoming magnetic flux passing the right side of the cylinder can be similarly obtained as

$$\begin{aligned}
\tilde{\Phi}_R &= \int dx^1 dx^2 \tilde{F}_{12} \Big|_{x^3=x_R^3} \\
&= \int dx^1 dx^2 - \left(\partial_\rho^2 + \frac{1}{\rho} \partial_\rho \right) u \Big|_{x^3=x_R^3} \\
&= -2\pi \int d\rho \rho \left(\partial_\rho^2 + \frac{1}{\rho} \partial_\rho \right) (\tilde{m} x^3 + u_S(\rho)) \\
&= -2\pi \int d\rho \partial_\rho (\rho \partial_\rho u_S) \\
&= -4\pi,
\end{aligned} \tag{3.45}$$

where we have used the boundary conditions, $\partial_\rho u_S \rightarrow 0$ for $\rho \rightarrow 0$ and $u_S \rightarrow \log \rho^2$ for $\rho \rightarrow \infty$. As expected, we have $\tilde{\Phi}_C + \tilde{\Phi}_R = 0$ and $\tilde{T}_S = -\tilde{\Phi}_R$ due to the flux conservation. This conservation implies there is no magnetic flux passing the left side of the cylinder, namely $\tilde{\Phi}_L = 0$. In order to express this in a conventional way, we need to use the original variables and rescale $A_\mu \rightarrow g A_\mu$. Then we have

$$\Phi_C = \frac{1}{2g} \tilde{\Phi}_C = \frac{2\pi}{g}, \quad \Phi_R = \frac{1}{2g} \tilde{\Phi}_R = -\frac{2\pi}{g}. \tag{3.46}$$

Similarly, the boojum mass is calculated as follows.

$$\begin{aligned}
\tilde{T}_B &= 2 \int d^3x \epsilon_{ijk} \partial_i \left(\tilde{\sigma} \tilde{F}_{jk} \right) \\
&= 2 \int_{\text{cylinder}} dS_i \epsilon_{ijk} \left(\tilde{\sigma} \tilde{F}_{jk} \right) + 4 \int dx^1 dx^2 \tilde{\sigma} \tilde{F}_{12} \Big|_{x^3=x_R^3} \\
&= 2\tilde{m} \tilde{\Phi}_R \\
&= -8\pi \tilde{m},
\end{aligned} \tag{3.47}$$

where we used $\tilde{\sigma} \rightarrow \tilde{m}/2$ for $x^3 = x_R^3 \gg \tilde{m}$ and the following identity

$$\begin{aligned}
\int_{\text{cylinder}} dS_i \epsilon_{ijk} \left(\tilde{\sigma} \tilde{F}_{jk} \right) &= 4\pi R \int_{x_L^3}^{x_R^3} dx^3 \tilde{\sigma} \tilde{F}_{23} \Big|_{\rho=R, \theta=0} \\
&= 2\pi R \int_{x_L^3}^{x_R^3} dx^3 \partial_3 u \partial_3 \partial_\rho u \Big|_{\rho=R} \\
&= 2\pi R \int_{x_L^3}^{x_R^3} dx^3 \partial_3 u_W \left(x^3 + \frac{1}{\tilde{m}} \log \rho \right) \partial_3 \partial_\rho u_W \left(x^3 + \frac{1}{\tilde{m}} \log \rho \right) \Big|_{\rho=R} \\
&= \frac{2\pi}{\tilde{m}} \int_{x_L^3}^{x_R^3} dx^3 \partial_3 u_W \partial_3^2 u_W \\
&= \frac{\pi}{\tilde{m}} \left[(\partial_3 u_W)^2 \right]_{x_L^3}^{x_R^3} \\
&= 0.
\end{aligned} \tag{3.48}$$

Note that the above result reflects an accidental Z_2 symmetry for our specific choice of the mass matrix $\tilde{M} = \text{diag}(\tilde{m}/2, -\tilde{m}/2)$. For generic case with $\tilde{M} = \text{diag}(\tilde{m}_1, \tilde{m}_2)$ ($\tilde{m}_1 > \tilde{m}_2$), the asymptotic behavior of u at a larger ρ becomes $u \rightarrow u_W (x^3 + \frac{1}{\tilde{m}_1 - \tilde{m}_2} \log \rho) + \log \rho + (\tilde{m}_1 + \tilde{m}_2)x^3$ with $u_W \rightarrow (\tilde{m}_1 - \tilde{m}_2)x^3$ for $x^3 \gg \tilde{m}_1 - \tilde{m}_2$ while $u_W \rightarrow -(\tilde{m}_1 - \tilde{m}_2)x^3$ for $x^3 \ll -(\tilde{m}_1 - \tilde{m}_2)$. It is straightforward to verify the following identity

$$\int_{\text{cylinder}} dS_i \epsilon_{ijk} \left(\tilde{\sigma} \tilde{F}_{jk} \right) = 4\pi (\tilde{m}_1 + \tilde{m}_2). \tag{3.49}$$

Thus, we find the generic form

$$\tilde{T}_B = 8\pi(\tilde{m}_1 + \tilde{m}_2) - 16\pi\tilde{m}_1 = -8\pi(\tilde{m}_1 - \tilde{m}_2). \tag{3.50}$$

In terms of the original variables, this can be expressed as

$$T_B = \frac{v}{2\sqrt{2g}} \tilde{T}_B = \frac{-4\pi v}{\sqrt{2g}} (\tilde{m}_1 - \tilde{m}_2) = -\frac{2\pi}{g^2} (m_1 - m_2). \tag{3.51}$$

This is consistent with the previously obtained value in Ref. [45].

As a closing comment for this subsection, we would like to emphasize that we were able to rigorously calculate the charges thanks to the asymptotic behavior given in Eq. (3.33). In particular, we calculated the charges by surrounding them with the *finite* size cylinder as shown in Fig. 3. Since we have not touched the spacial infinity, the above computations do not suffer from any complications coming from logarithmic bending at all. In the literature, several attempts to avoid this problem have been done. In Ref. [30], the mass of two coaxial boojums was calculated for the flat domain wall on which one coaxial vortex string ends on from both sides and found $2T_B = -4\pi(m_1 - m_2)/g^2$. Since the domain wall is flat in this case, there are no anxieties. Then, in the proceeding work [66], it was proposed that the mass of the single boojum can be obtained by just dividing the mass of the two coaxial boojums by 2. In the same paper [66], they also discussed that there is an uncertainty for determining the mass of the single boojum in the case of logarithmically bent domain wall due to a geometrical ambiguity. Ref. [45] is the first work which showed $T_B = -2\pi(m_1 - m_2)/g^2$ for the isolated single boojum in the logarithmically curved domain wall. They reached this value by integrating the mass density \mathcal{T}_B at $x^3 = \pm\infty$ as $T_B = \int dx^1 dx^2 \mathcal{T}_B|_{x^3=\infty} - \int dx^1 dx^2 \mathcal{T}_B|_{x^3=-\infty}$ under the assumption that no flux goes through the boundary transverse to the vortex string axis. The first term unambiguously equals to $-2\pi m_1/g^2$. The second term is somewhat tricky since one needs to consider intersection of the logarithmically bent domain wall with the boundary at $x^3 = -\infty$. In Ref. [45], σ was simply replaced by a mean value $(m_1 + m_2)/2$ and made use of the flux conservation, then the second term was found to be $-\pi(m_1 + m_2)/g^2$. Summing up the two contribution gives us $T_B = -2\pi(m_1 - m_2)/g^2$. This way of computing the boojum mass is plausible, but it might be better to confirm it by a more rigorous way. We believe that our calculations above contribute to this point. For further confirmation, we perform the integrations numerically and find $-\tilde{T}_B/8\pi\tilde{m} = 0.976, 0.996, 1.010, 0.997$ for $\tilde{m} = 1, 10, 20, 30$, respectively. In conclusion, we agree with [45] that the boojum mass can be cleanly separated from the semi-infinite vortex string and the logarithmically bent domain wall.

3.3 Weak coupling regime

3.3.1 Boojum as a fractional magnetic monopole and monostick

There are no magnetic sources, namely no magnetic monopoles, in our $U(1)$ gauge theory. Indeed, Bianchi identity $\epsilon_{ijk}\partial_i F_{jk} = 0$ always holds. The non-zero boojum charge T_B seems to yield non-zero magnetic charge, but it is not true. The boojum has $\epsilon_{ijk}\partial_i \hat{F}_{jk} \neq 0$ with $\hat{F}_{ij} = \sigma F_{ij}$ while it has $\epsilon_{ijk}\partial_i F_{jk} = 0$. Of course, $\hat{F}_{ij} = \sigma F_{ij}$ is not a genuine magnetic field. Nevertheless, there is a case that the boojum can be naturally identified as a magnetic source in the weak gauge coupling region $\tilde{m} \gg 1$. In this region, the domain wall has a fat inner layer of the width $\sim \tilde{m}$, where the $U(1)$ gauge symmetry is almost recovered. When the magnetic flux is injected into

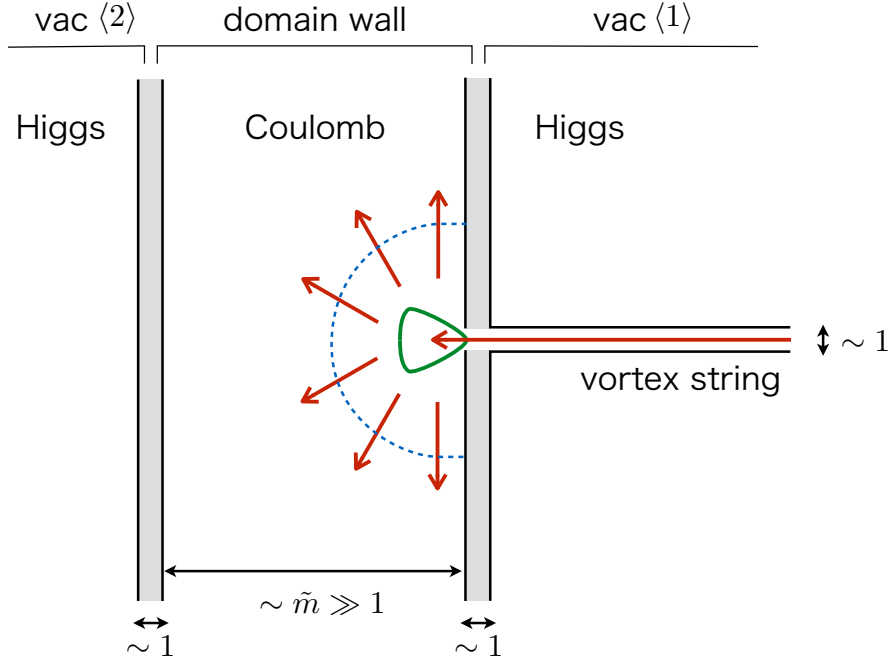


Figure 8: A sketch of a boojum inside the domain wall in the weak coupling region. The boojum is naturally identified with the magnetic source with a fractional magnetic charge $(2\pi/g)$ which sticks to the inner boundary of the domain wall.

the domain wall through the vortex string, the magnetic flux almost freely spreads out inside the domain wall, see Fig. 8. Therefore, for one living inside the domain wall, who is blind to outside world, the boojum is really magnetic source. It is a point-like source, so one may call it the magnetic monopole. The difference from the ordinary magnetic monopole, be it Dirac or 't Hooft-Polyakov monopole, is that the boojum sticks to the boundary of the semi-compact world, where he lives.

Note that, here, we are trying to identify the boojum as the magnetic monopole in the semi-compact space $d = 2+1$ where 2 corresponds to the 2 dimensional infinite plane and 1 to the finite segment of width $\sim \tilde{m}$. This is different from the well-known arguments that the end point of the vortex string can be identified with an *electric* charge in the $1+2$ dimensional (1 is time and 2 space) effective theory of the domain wall. To this end, one needs to integrate out the normal direction to the domain wall (x^3) and then to dualize the S^1 internal moduli parameter to the dual $U(1)$ gauge field in $1+2$ dimensional spacetime *à la* Polyakov. Here, we do not do this and instead are dealing with the original $U(1)$ gauge field.

In Fig. 7, we have already seen that the magnetic flux inside the fat domain wall ($\tilde{m} = 10$) linearly spreads for a while until it encounters the boundary. Characteristic length of this linear spreading is proportional to the width of the inner layer. For this, we show three extremely wide domain walls in Fig. 9.

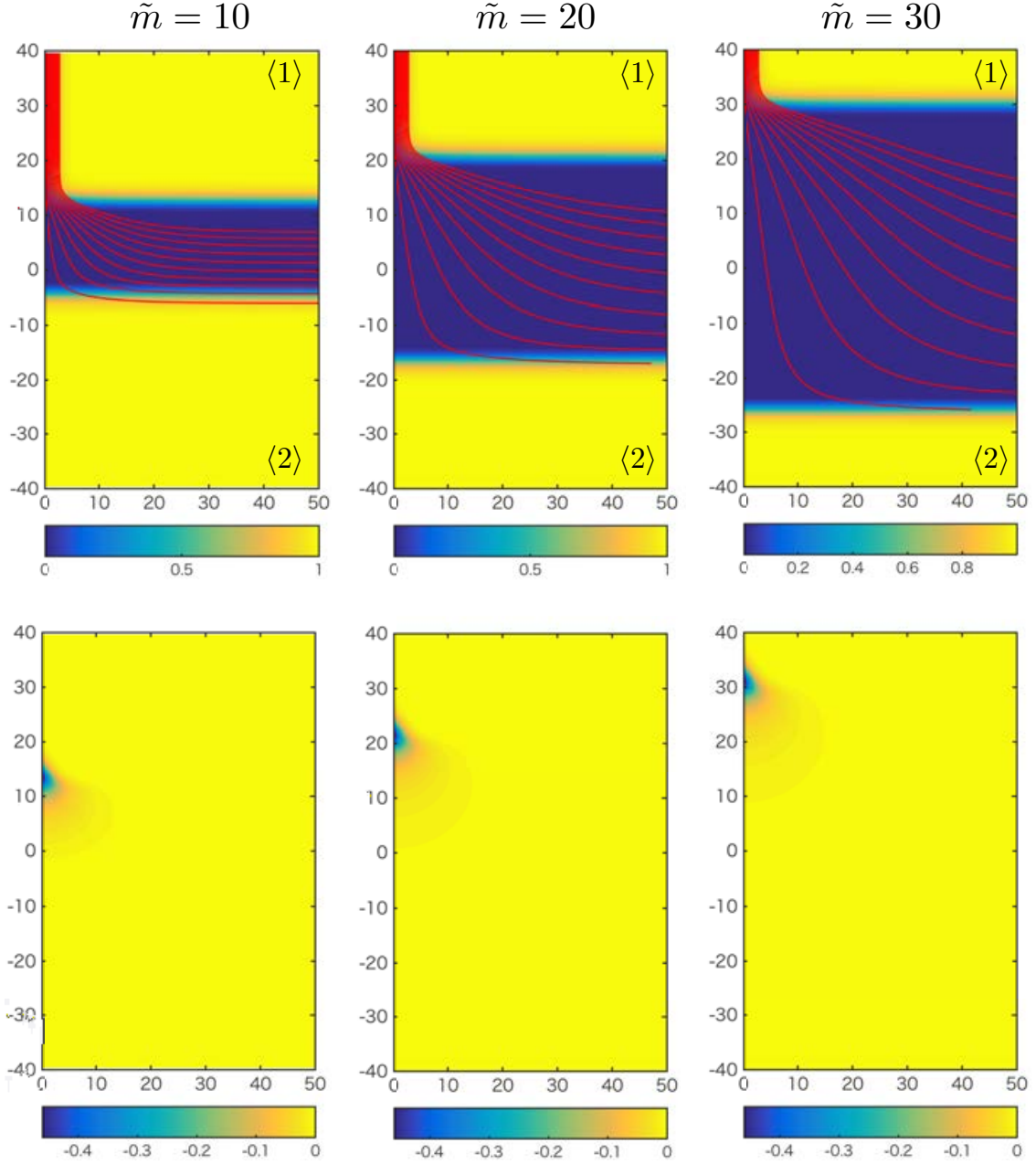


Figure 9: Fat domain walls with $\tilde{m} = 10, 20, 30$. The 1st row shows the effective photon mass m_v^2 and the magnetic force lines. The 2nd row shows the boojum charge density.

An observer inside the domain wall can measure the magnetic charge of the boojum by counting the magnetic flux flowing through a hemisphere enclosing the boojum (blue dotted line in Fig. 8) as

$$\tilde{\Phi}_{\text{boojum}} = \int_{\text{hemisphere}} dS_i \frac{1}{2} \epsilon_{ijk} \tilde{F}_{jk} = 4\pi. \quad (3.52)$$

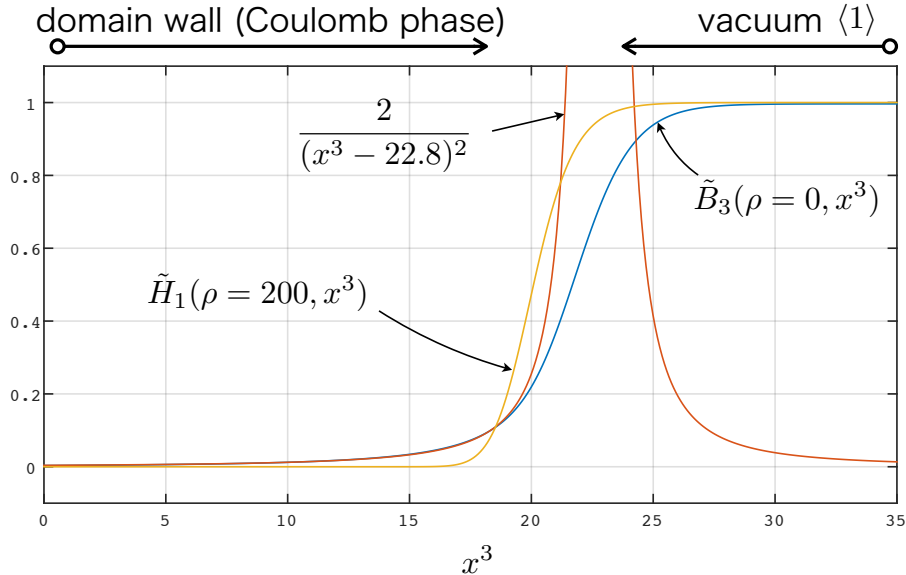


Figure 10: The magnitude of magnetic field \tilde{B}_3 on the string axis (the x^3 axis) for $\tilde{m} = 20$ is shown in the blue curve. The red curve shows the Coulomb force with an appropriate shift $x^3 \rightarrow x^3 - 22.8$. The yellow curve corresponds to \tilde{H}_1 on the x^3 axis. The region $\tilde{H}_1 = 0$ is in the Coulomb phase. $\tilde{B}_3 \rightarrow 1$ at the vacuum $\langle 1 \rangle$ corresponds to the magnitude of the magnetic field at the center of the vortex string.

Here we integrated only on the hemisphere with excluding the boundary of the wall from the surface integral. We have 4π simply due to the flux conservation, $\tilde{\Phi}_{\text{boojum}} = -\tilde{\Phi}_{\text{in}}$. From the Gauss's law (the integration is taken only on the hemisphere) we conclude that the magnetic charge of the boojum is

$$\tilde{\mathcal{M}}_B = 4\pi. \quad (3.53)$$

Note that this is calculated with the dimensionless variables. In terms of the original variables and with respect to the usual notation $A_\mu \rightarrow gA_\mu$, the magnetic charge of the boojum in a conventional notation is given by

$$\mathcal{M}_B = \frac{2\pi}{g}. \quad (3.54)$$

This is a half of the magnetic charge $\mathcal{M}_{\text{TP}} = 4\pi/g$ of 't Hooft-Polyakov type magnetic monopole. Thus, the boojum can be identified with a fractional magnetic monopole from the point of view of wall-bound observers.

Since we have solved the equation of motion for the finite gauge coupling constant, we can check this statement numerically. In the Coulomb phase, the magnetic field of the magnetic charge $\tilde{\mathcal{M}}$ stuck on a wall at $x^3 = X$ should obey the normal 1 + 3 dimensional Coulomb's law

$$\tilde{B}_i \equiv \frac{1}{2}\epsilon_{ijk}\tilde{F}_{jk} = \frac{\tilde{\mathcal{M}}}{2\pi r^2} \frac{x^i - \delta^{i3}X}{r}, \quad x^3 < X, \quad (3.55)$$

with $r = \sqrt{(x^1)^2 + (x^2)^2 + (x^3 - X)^2}$. Note that not $4\pi r^2$ but $2\pi r^2$ (the area of hemisphere surrounding the boojum) appears in the denominator reflecting the fact that the magnetic flux spread for one side ($x^3 < X$) of the right boundary of the domain wall at $x^3 = X$. Thus magnitude of the magnetic field from the boojum with $\tilde{\mathcal{M}}_B = 4\pi$ is given by

$$|\vec{\tilde{B}}| = \frac{2}{(x^1)^2 + (x^2)^2 + (x^3 - X)^2}. \quad (3.56)$$

We show the magnetic flux $\tilde{B}_3(\rho = 0, x^3)$ on the x^3 axis for $\tilde{m} = 20$ in Fig. 10 and find that it asymptotically approaches to the Coulomb law as

$$\tilde{B}_3(\rho = 0, x^3) \simeq \frac{-2}{(x^3 - 22.8)^2}, \quad (x^3 \lesssim 20). \quad (3.57)$$

Thus, the boojum is identical to the magnetic point particle put on $X = 22.8$ with the magnetic charge $\tilde{\mathcal{M}}_B = 4\pi$, if it is observed sufficiently far away. Since the boundary of the inner layer at the vortex string side is about $x^3 \sim 22$, it is quite natural that the above approximation works well.

Let us now leave the boojum and travel inside the domain wall along $x^1 - x^2$ plane. When we reach the distance much farther than the domain wall width $\sim 2\tilde{m}$, the magnetic flux expands as if in 2-dimensional plane. Therefore, the magnetic field should behave as $|\tilde{B}| \propto 1/\rho$. Thus, one may expect for $\rho \gg 2\tilde{m}$

$$\tilde{B}_a = \frac{\tilde{\mathcal{M}}_B x^a}{2\pi\rho}, \quad (a = 1, 2), \quad (3.58)$$

where $2\pi\rho$ in the denominator is the circumference of an circle surrounding the boojum. However, this is too naive. We should not forget that the inner layer is not a 2 dimensional plane, but it has the thickness $\tilde{d}_W = 2\tilde{m}$. Therefore, the magnetic field lines are parallelly distributed along the x^3 direction and, effectively, the magnetic charge is weakened by $1/2\tilde{m}$. Thus, the correct asymptotic behavior of the magnetic field for $\rho \gg 2\tilde{m}$ should be

$$\tilde{B}_a = \frac{\tilde{\mathcal{M}}_B x^a}{2\pi\tilde{d}_W\rho}, \quad B_a = \frac{2\pi g^2 v^2 x^a}{m 2\pi\rho^2}. \quad (3.59)$$

In order to verify this, we plot $\tilde{B}_1(x^1, 0, x^3 = X_0)$, where $x^3 = X_0$ is the center of the domain wall for $\tilde{m} = 10, 20, 30$ in Fig. 11. We read $x^3 = X_0$ at which σ becomes zero, and find $X_0 = 2.07, 2.26, 2.36$ for $\tilde{m} = 10, 20, 30$, respectively. As seen from Fig. 11, the numerical solution perfectly supports the formula Eq. (3.59). Thus, when seen at a distance, the boojum is suitable to be called *magnetic monostick* of height $2\tilde{m}$.

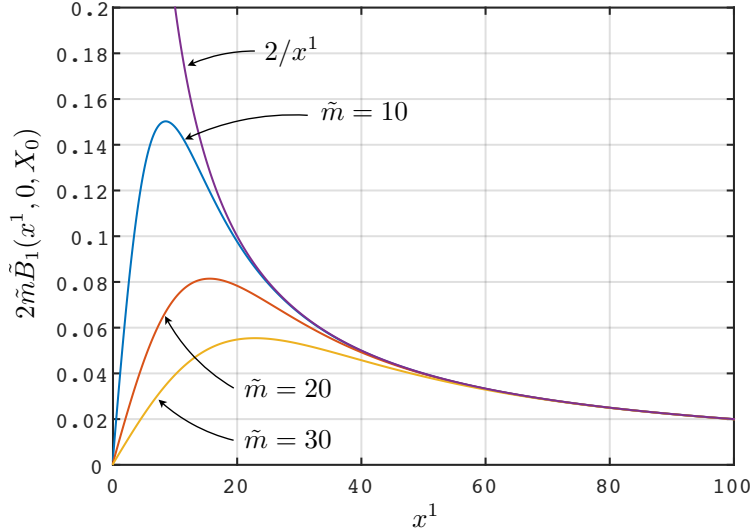


Figure 11: A numerical verification for the formula (3.59). We plot $2\tilde{m}\tilde{B}_1(x^1, 0, X_0)$ for $\tilde{m} = 10, 20, 30$ which is numerically obtained. All functions approach to $\tilde{\mathcal{M}}_B/(2\pi x^1) = 2/x^1$ for $x^1 > 2\tilde{m}$.

3.3.2 Colinear Vortex strings from both sides

Let us next consider collinear vortex strings ending on the domain wall from both sides. Since the tensions of the vortex strings are the same, the domain wall remains flat. For $N_F = 2$ case with $M = (\tilde{m}/2, -\tilde{m}/2)$, such configuration is given by the moduli matrix $H_0 = (z, z)$. The collinear vortex strings sit on the x^3 axis and the flat domain wall is at $x^3 = 0$. The corresponding master equation is

$$\left(\partial_3^2 + \partial_\rho^2 + \frac{1}{\rho}\partial_\rho\right)u - 1 + \rho^2 \left(e^{\tilde{m}x^3} + e^{-\tilde{m}x^3}\right)e^{-u} = 0. \quad (3.60)$$

Since $\partial_\rho^2 + (1/\rho)\partial_\rho \rightarrow 0$ for a large ρ , the scalar function asymptotically obeys

$$\partial_3^2(u - 2\log\rho) - 1 + \left(e^{\tilde{m}x^3} + e^{-\tilde{m}x^3}\right)e^{-u+2\log\rho} = 0, \quad (\rho \gg 1). \quad (3.61)$$

Then we have

$$u(\rho, x^3) \rightarrow u_W(x^3) + 2\log\rho, \quad (\rho \gg 1), \quad (3.62)$$

where $u_W(x^3)$ is the domain wall solution to $\partial_3^2 u_W - 1 + \left(e^{\tilde{m}x^3} + e^{-\tilde{m}x^3}\right)e^{-u_W} = 0$ with $u_W \rightarrow \pm\tilde{m}x^3$ for $x^3 \rightarrow \pm\infty$. For a large x^3 ($\gg \tilde{m}$), $\partial_3^2 u \rightarrow 0$ and the master equation reduces to

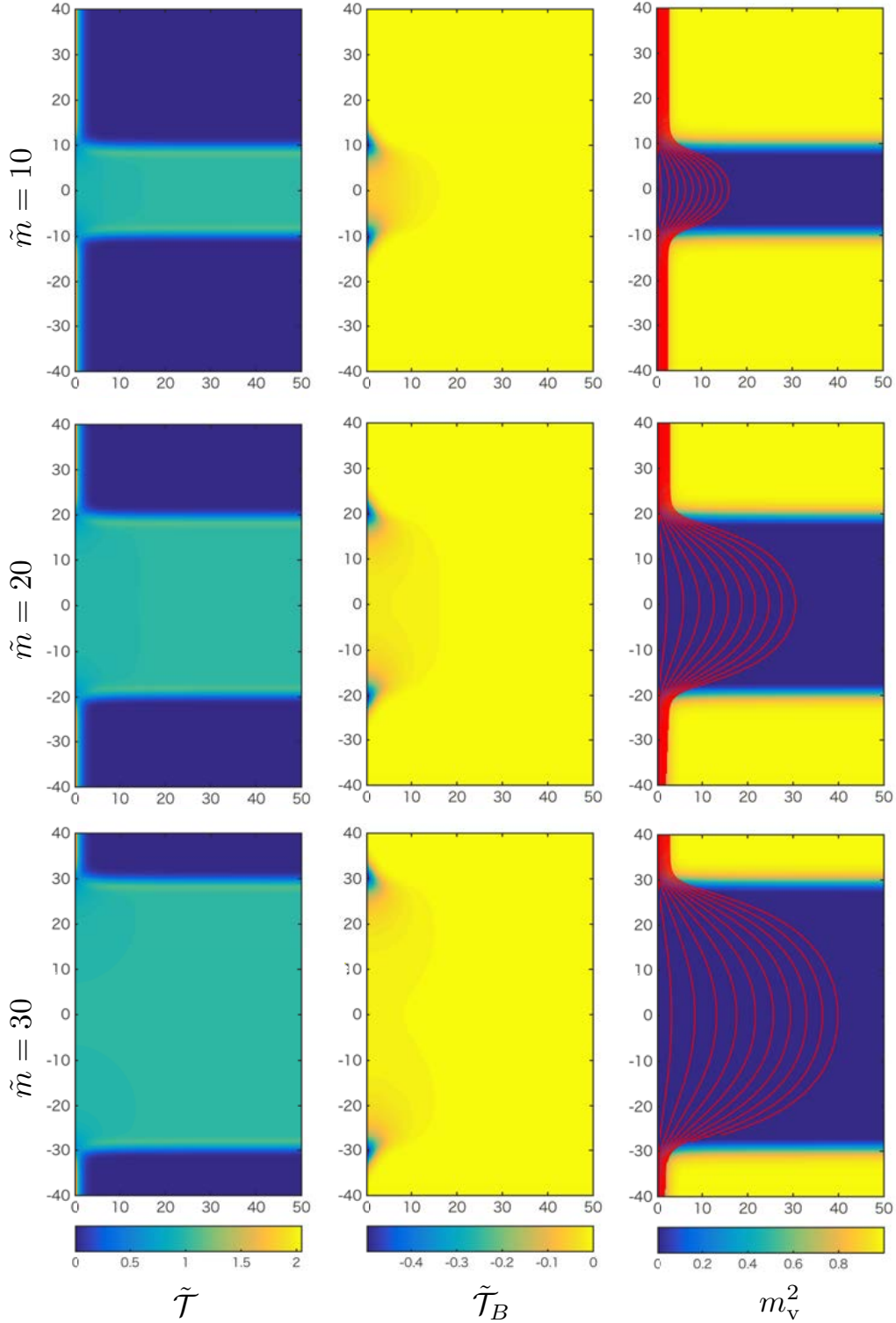


Figure 12: Collinear vortex strings ending of the thick flat domain wall for the weak coupling region ($\tilde{m} = 10, 20, 30$). The panels in left, middle, and right columns show density plots of the total energy density $\tilde{\mathcal{T}}$, the boojum charge density $\tilde{\mathcal{T}}_B$, and the the photon mass square m_V^2 , respectively. The red lines in the right column stand for the magnetic force lines incoming from the upper vortex string and outgoing to the lower one. The horizontal axis is ρ and the vertical one is x^3 .

$$\left(\partial_\rho^2 + \frac{1}{\rho}\partial_\rho\right)(u - \tilde{m}x^3) - 1 + \rho^2 e^{-u+\tilde{m}x^3} = 0. \quad (3.63)$$

Thus we find

$$u(\rho, x^3) \rightarrow u_S(\rho) + \tilde{m}x^3, \quad (x^3 \gg \tilde{m}), \quad (3.64)$$

where $u_S(\rho)$ is the vortex string solution to $(\partial_\rho^2 + (1/\rho)\partial_\rho)u_S - 1 + \rho^2 e^{-u_S} = 0$ with $u_S(\rho) \rightarrow 2 \log \rho$ for $\rho \gg 1$. Similarly, we have

$$u(\rho, x^3) \rightarrow u_S(\rho) - \tilde{m}x^3, \quad (x^3 \ll -\tilde{m}). \quad (3.65)$$

With these asymptotic behaviors taken into account, we now solve the gradient flow equation

$$\left(\partial_3^2 + \partial_\rho^2 + \frac{1}{\rho}\partial_\rho\right)U - 1 + \rho^2 \left(e^{\tilde{m}x^3} + e^{-\tilde{m}x^3}\right)e^{-U} = \partial_t U. \quad (3.66)$$

A natural choice for an initial configuration which is consistent with the above asymptotic behaviors is just superposition of u_W and u_S

$$U(\rho, x^3, t=0) = u_W(x^3) + u_S(\rho). \quad (3.67)$$

We show three typical configurations at weak gauge coupling with $\tilde{m} = 10, 20, 30$ in Fig. 12. The solution is symmetric under the reflection through the x^1 - x^2 plane. Since the domain walls have quite wide inner layers of the Coulomb phase, the upper and lower boojums are well isolated, see the panels in the middle column of Fig. 12. Incoming magnetic fluxes from the upper vortex string freely spread inside the domain walls, and then they are swallowed by the lower vortex string. There are no magnetic force lines going to infinity along the domain walls ($\rho = \infty$) due to the flux conservation. The expanse of the magnetic flux inside the domain wall is of the same order as the width of the domain wall, as expected in Ref. [45]. We numerically integrate the boojum charge density and get $-\tilde{T}_B/8\pi\tilde{m} = 1.95, 1.97, 1.98$ for $\tilde{m} = 10, 20, 30$, respectively. These numbers are in good agreement with the analytical result $-\tilde{T}_B/8\pi\tilde{m} = 2$.

For those who are sitting near the origin, the upper boojum is the fractional magnetic monopole with the magnetic charge $\tilde{\mathcal{M}}_B = 4\pi$ whereas the lower boojum is the fractional anti-magnetic monopole with $\tilde{\mathcal{M}}_{\bar{B}} = -4\pi$. The magnetic field observed by them should be a simple superposition

$$\tilde{B}_i = \frac{\tilde{\mathcal{M}}_B}{2\pi r_+^2} \frac{x^i - \delta^{i3}X}{r_+} + \frac{\tilde{\mathcal{M}}_{\bar{B}}}{2\pi r_-^2} \frac{x^i + \delta^{i3}X}{r_-}, \quad (3.68)$$

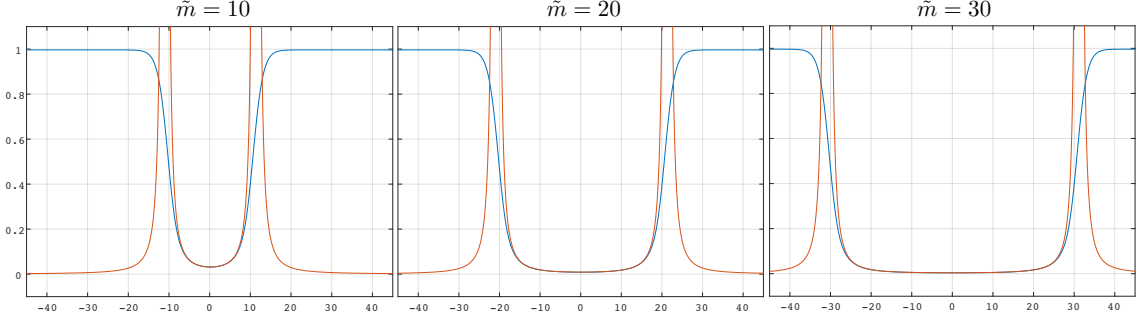


Figure 13: The blue lines show the magnitude of \tilde{B}_3 on the string axis ($\rho = 0$), which are numerically obtained. The red lines correspond to the magnetic fields from the point-like monopole approximations given in Eq. (3.69) with $X = 11.2, 21.1, 31.0$ for $\tilde{m} = 10, 20, 30$. The horizontal axis is x^3 .

with $r_{\pm} = \sqrt{(x^1)^2 + (x^2)^2 + (x^3 \mp X)^2}$ and $X \geq 0$. Especially, the third element on the x^3 axis for $|x^3| \ll X$ is

$$\begin{aligned} \tilde{B}_3(\rho = 0, x^3) &= \frac{\tilde{\mathcal{M}}_B}{2\pi(x^3 - X)^2} \frac{x^3 - X}{|x^3 - X|} + \frac{\tilde{\mathcal{M}}_B}{2\pi(x^3 + X)^2} \frac{x^3 + X}{|x^3 + X|} \\ &= -\frac{2}{(x^3 - X)^2} - \frac{2}{(x^3 + X)^2}. \end{aligned} \quad (3.69)$$

The parameter X should be tuned to fit the numerically obtained solutions for each \tilde{m} . For example, we find $X = 11.2, 21.1, 31.0$ for $\tilde{m} = 10, 20, 30$ respectively, see Fig. 13. The right and left boundary of the inner layer are at $x^3 = \pm\tilde{m}$. So the boojums, fractional magnetic monopoles, are really stuck on the boundaries.

3.3.3 Semi-local Boojums, semi-local magnetic monostick

So far, we have mostly considered $N_F = 2$ model which has three kind of topological objects, the domain wall, the vortex string and the boojum. In the models with higher number of flavors $N_F > 2$, other kinds of topological object enters the game. Namely, the semi-local vortex strings [72] and the semi-local boojums. They appear when some of the masses are degenerate. The minimal model is $N_F = 3$ with $\tilde{M} = \text{diag}(\tilde{m}/2, \tilde{m}/2, -\tilde{m}/2)$. The model has a non-Abelian flavor symmetry $SU(2) \times U(1)$, and two isolated vacua: the first vacuum $\langle 1 \rangle$ is determined by $|\tilde{H}_1|^2 + |\tilde{H}_2|^2 = 1$, $\tilde{H}_3 = 0$ and $\tilde{\sigma} = \tilde{m}/2$, while the second vacuum $\langle 2 \rangle$ is determined by $\tilde{H}_1 = \tilde{H}_2 = 0$, $\tilde{H}_3 = 1$ and $\tilde{\sigma} = -\tilde{m}/2$. Thus, the vacuum manifold for $\langle 1 \rangle$ is $\mathbb{C}P^1$, while that for $\langle 2 \rangle$ is a point. The vortex string put in the degenerate vacuum $\langle 1 \rangle$ is the so-called semi-local vortex string [72]. The semi-local vortex string can change its transverse size with its tension preserved. Namely, it has a size moduli. To prevent confusion, vortex string in the non-degenerate vacuum $\langle 2 \rangle$ is sometimes called the local vortex

string. Size zero limit of the semi-local vortex string corresponds to the local vortex string.

Here we consider 1/4 BPS configuration of the semi-local vortex string ending on the domain wall. Naturally, the boojum at the junction point changes its size with the semi-local string, therefore we may call it *semi-local Boojum*. The simplest configuration is generated by the moduli matrix

$$H_0 = (z, a, 1), \quad (3.70)$$

where a is a complex constant. We can assume that a is a positive real number without loss of generality. This yields an axially symmetric configuration with the master equation

$$\left(\partial_3^2 + \partial_\rho^2 + \frac{1}{\rho} \partial_\rho \right) u - 1 + \left[(\rho^2 + a^2) e^{\tilde{m}x^3} + e^{-\tilde{m}x^3} \right] e^{-u} = 0. \quad (3.71)$$

Let $u_{SLS}(\rho)$ be a solution to the master equation for the purely semi-local vortex string

$$\left(\partial_\rho^2 + \frac{1}{\rho} \partial_\rho \right) u_{SLS} - 1 + (\rho^2 + a^2) e^{-u_{SLS}} = 0. \quad (3.72)$$

The asymptotic behavior of u_{SLS} is

$$u_{SLS} \rightarrow \log(\rho^2 + a^2), \quad (\rho \gg a). \quad (3.73)$$

Repeating the similar analysis done in Sec. 3.2, we find the following function as a suitable initial function to the gradient flow equation for Eq. (3.71)

$$U(x^3, \rho, t = 0) = u_W \left(x^3 + \frac{1}{2\tilde{m}} u_{SLS} \right) + \frac{1}{2} u_{SLS}, \quad (3.74)$$

which is just a replacement $u_S \rightarrow u_{SLS}$ in Eq. (3.36).

We show the numerical solutions with $\tilde{m} = 10$ (in the weak coupling region) and $a = 5, 10, 20$ in Fig. 14. This should be compared with the panels in the left column of Fig. 9, which shows $\tilde{m} = 10$ with $a = 0$ (the local vortex string and local boojum). Increasing the size of the parameter a , the cross-section of the semi-local vortex string grows linearly. At the same time, the semi-local boojum is inflated. Fig. 14 clearly shows that the transverse size in the x^1 - x^2 plane follows the semi-local vortex string but the vertical size along the x^3 axis is limited by the domain wall size.

There is an advantage for making use of the moduli matrix formalism. As listed at the beginning of Sec. 3, all the physical quantities are expressed by the single scalar function u . Thanks to this, we can immediately conclude that the mass of the semi-local boojum is the same as that of the local boojum, namely

$$\tilde{T}_{SLB} = -8\pi\tilde{m}, \quad T_{SLB} = -\frac{2\pi m}{g^2}. \quad (3.75)$$

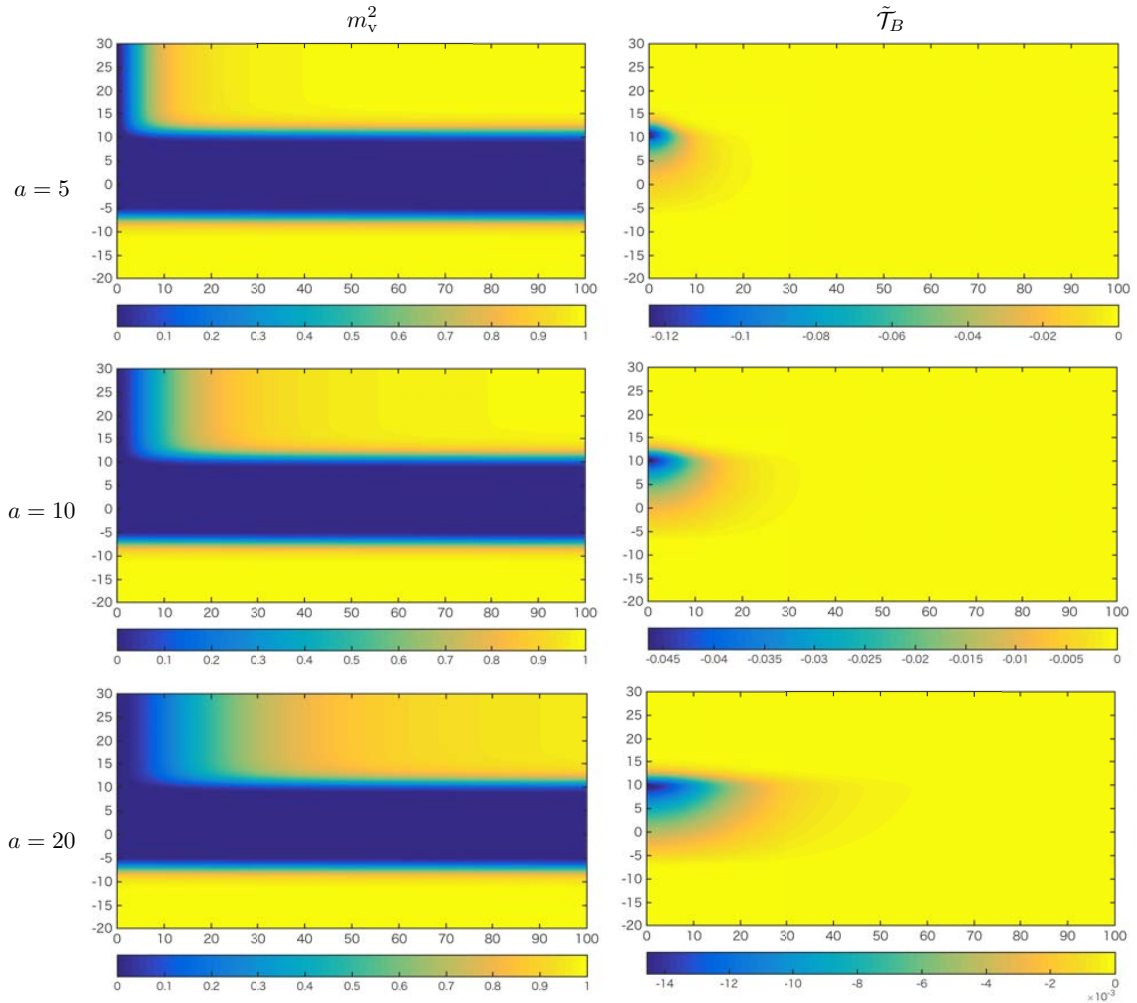


Figure 14: Semi-local vortex string and semi-local boojum for $\tilde{m} = 10$ and $a = 5, 10, 20$ (top, middle, bottom). The left panels show $m_v^2 = |\tilde{H}_1|^2 + |\tilde{H}_3|^2$ and the boojum charge density is plotted in the right panels.

This is because the change in the calculations in Eqs. (3.47) and (3.48) is that ρ is replaced by $\sqrt{\rho^2 + a^2}$, which does not affect the result. Similarly, due to the flux conservation, the magnetic charge of the semi-local boojum is

$$\tilde{\mathcal{M}}_{\text{SLB}} = 4\pi, \quad \mathcal{M}_{\text{SLB}} = \frac{2\pi}{g}. \quad (3.76)$$

Thus, the quantum numbers of the semi-local boojum are the same as those for the local boojum. Where can we find the effect of the size moduli? It appears in the Coulomb's law. When the boojum is seen far from the string axis, the magnetic field should spread according to the 1 + 2 dimensional Coulomb's law as in Eq. (3.59) for the local boojum. In the semi-local case, we find the following modified Coulomb's

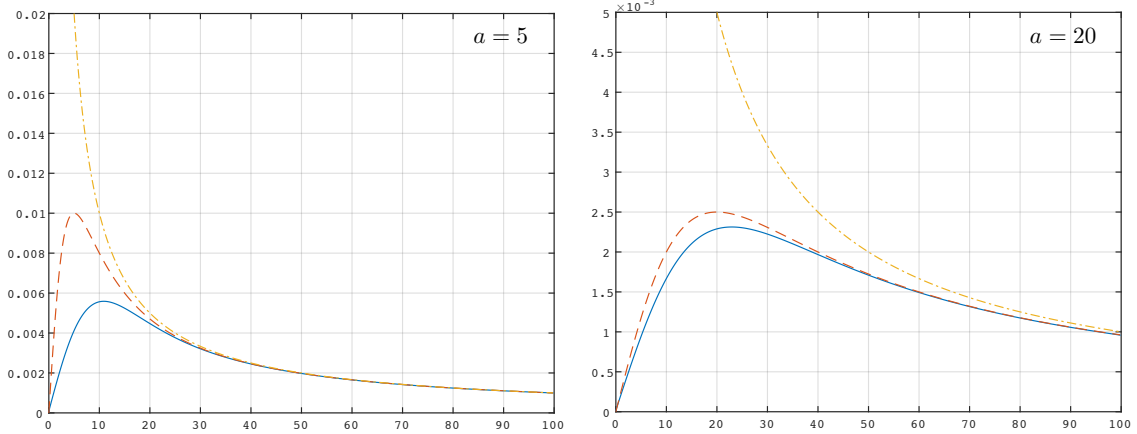


Figure 15: The modified Coulomb's law $\tilde{B}_1(x^1, 0, x^3 = 2.07)$ for $\tilde{m} = 10$ given in Eq. (3.73) is plotted (red dashed line). The blue solid line shows the numerical result and the yellow dot-dashed line is the normal Coulomb's law. The left (right) panel corresponds to the case with $a = 5$ ($a = 20$). The horizontal axis is x^1 .

law

$$\tilde{B}_b = \frac{\tilde{\mathcal{M}}_{\text{SLB}}}{2\pi\tilde{d}_W} \frac{x^b}{\rho^2 + a^2}, \quad B_b = \frac{2\pi g^2 v^2}{m} \frac{x^b}{2\pi(\rho^2 + a^2)}, \quad \text{for } \rho \gg a, \quad (3.77)$$

with $b = 1, 2$ and $\tilde{d}_W = 2\tilde{m}$. We compare it to the numerically obtained magnetic field for $\tilde{m} = 10$ and $a = 5, 20$ in Fig. 15 by plotting $\tilde{B}_1(x^1, 0, x^3 = X_0)$ with $X_0 = 2.07$ ($\tilde{\sigma}(x^3 = X_0) = 0$ as before). We also show the magnetic field with $a = 0$ (the ordinary Coulomb's law). As clearly seen in Fig. 15, the modified Coulomb's law reproduces the numerical result much better than the normal Coulomb's law.

If we extrapolate the magnetic field in Eq. (3.77) to $\rho = 0$, it implies the following 1 + 2 dimensional Gauss's law for the magnetic field

$$\partial_a \tilde{B}_a = \tilde{f}, \quad \tilde{f} \simeq \frac{\tilde{\mathcal{M}}_{\text{SLB}}}{4\pi\tilde{m}} \frac{2a^2}{(\rho^2 + a^2)^2}. \quad (3.78)$$

Therefore, the semi-local boojum is not point-like. Roughly speaking, the magnetic charge is distributed into a cylinder of the height $2\tilde{m}$ and the radius $\rho = a$. Thus, it is suitable to call the semi-local boojum as *semi-local magnetic monostick*.

Finally, we show collinear semi-local vortex strings with different sizes ending on the domain wall. A minimal model for this is $N_F = 4$ with $\tilde{M} = \text{diag}(\frac{\tilde{m}}{2}, \frac{\tilde{m}}{2}, -\frac{\tilde{m}}{2}, -\frac{\tilde{m}}{2})$. The moduli matrix is $H_0 = (z, a_1, z, a_2)$. A suitable initial function for the gradient flow equation in this case is

$$U(\rho, x^3, t = 0) = u_W \left(x^3 + \frac{u_{\text{SLS}}(a_1) - u_{\text{SLS}}(a_2)}{2\tilde{m}} \right) + \frac{u_{\text{SLS}}(a_1) + u_{\text{SLS}}(a_2)}{2}. \quad (3.79)$$

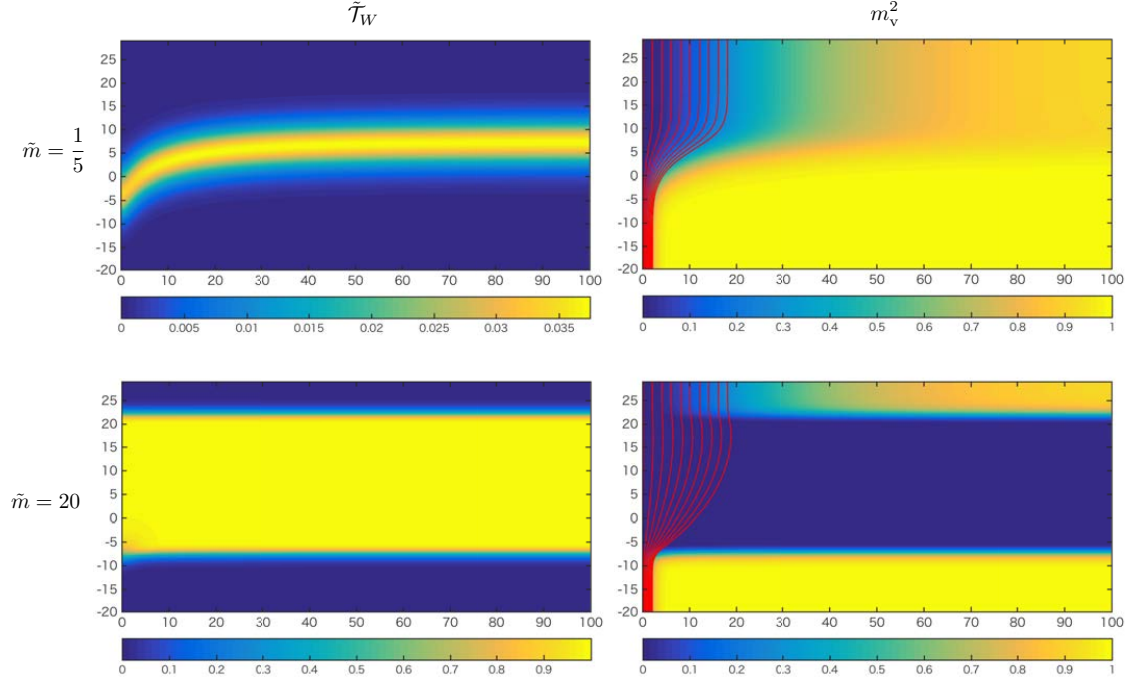


Figure 16: The collinear semi-local vortex strings with $a_2 = 0$ from blow and $a_1 = 30$ from top end on the asymptotically flat domain wall. The domain wall energy density $\tilde{\mathcal{T}}_W$ and $m_v^2 = |\tilde{H}_1|^2 + |\tilde{H}_3|^2$ are shown in the left and right panels, respectively. The horizontal axis is ρ and the vertical axis is x^3 .

The domain wall is asymptotically flat, but it can be logarithmically bent around the junction point, when the sizes of two strings are very different. Such local bending is visible in the strong gauge coupling limit $\tilde{m} \ll 1$. In Fig. 16, we show two typical configurations that have two collinear strings, the single local vortex string ($a_2 = 0$) from $x^3 < 0$ side and the single very fat semilocal vortex string with $a_1 = 30$ from $x^3 > 0$ side, ending of the domain wall for $\tilde{m} = 1/5$ (strong gauge coupling) and $\tilde{m} = 20$ (weak gauge coupling). The domain wall steeply bends near the collinear string axis for $\tilde{m} = 1/5$, but it asymptotically becomes flat at large ρ due to the balance of the tensions of two vortex strings. On the other hand, the domain wall tension becomes sufficiently large for $\tilde{m} = 20$, so that the local curving structure near the string axis is almost invisible. The well-squeezed magnetic flux tube from the local vortex string is magnified, when it goes into the semi-local vortex string as is shown in the right panels of Fig. 16. This is a lens effect for the magnetic force lines.

3.4 Strong coupling regime

Let us next consider the strong gauge coupling limit⁵ where the kinetic term of the gauge field disappears in the Lagrangian (2.1), and the Higgs fields are restricted to satisfy $HH^\dagger = v^2$. Because of this, the domain wall has no internal structure, namely both inside and outside the domain wall are in the Higgs phase. The gauge fields are infinitely heavy and no longer dynamical. Indeed, their equations of motion give

$$A_\mu = \frac{-i}{2v^2} (H\partial_\mu H^\dagger - \partial_\mu HH^\dagger). \quad (3.80)$$

As a result, the Abelian-Higgs model with N_F flavor reduces to the massive $\mathbb{C}P^{N_F-1}$ nonlinear sigma model. One can introduce fictitious electromagnetic fields by $F_{\mu\nu} = \partial_\mu A_\nu - \partial_\nu A_\mu$ from the gauge fields given above as

$$F_{\mu\nu} = \frac{-i}{v^2} (\partial_\mu H\partial_\nu H^\dagger - \partial_\nu H\partial_\mu H^\dagger). \quad (3.81)$$

The BPS equations and the energy formulae obtained in Sec. 2.2 remain unchanged except for dropping the terms proportional to $1/g^2$. Furthermore, the moduli matrix formalism explained in Sec. 2.3 still works without any changes. One advantage is that the master equation is exactly solvable

$$u_{g \rightarrow \infty} = \log \Omega_0 = \log H_0 e^{2\eta M x^3} H_0^\dagger. \quad (3.82)$$

In the following we will set $\eta = \xi = +1$. Let us take the simplest example of a singular lump string (singular at a spacial infinity) ending on the domain wall, which is generated by the moduli matrix $H_0 = (z, 1)$ in $N_F = 2$ model with $M = (m/2, -m/2)$. The exact solution is given by

$$u_{g \rightarrow \infty} = \log \left(\rho^2 e^{mx^3} + e^{-mx^3} \right). \quad (3.83)$$

The domain wall's position can be read from the condition $\rho^2 e^{mx^3} = e^{-mx^3}$, namely, it is given by

$$x^3 = -\frac{1}{m} \log \rho. \quad (3.84)$$

The fictitious magnetic flux given in Eq. (3.81) can be easily calculated by making use of the formulae (2.26) as

$$B_a = \frac{2mx^a}{(\rho^2 e^{mx^3} + e^{-mx^3})^2}, \quad B_3 = -\frac{2}{(\rho^2 e^{mx^3} + e^{-mx^3})^2}. \quad (3.85)$$

At the domain wall, the $a = 1, 2$ components becomes

$$B_a \Big|_{x^3 = -\frac{1}{m} \log \rho} = \frac{m x^a}{2 \rho^2}. \quad (3.86)$$

⁵In this subsection, we will use the original variables x^μ , m and so on.

Similarly, the configuration with one regular lump string of the size a ending on the domain wall given by $H_0 = (z, a, 1)$ in $N_F = 3$ model with $M = (m/2, m/2, -m/2)$ can be obtained by just replacing $\rho \rightarrow \sqrt{\rho^2 + a^2}$ in the above results. Therefore, the $a = 1, 2$ components of the magnetic flux at the domain wall is given by

$$B_a \Big|_{x^3 = -\frac{1}{m} \log \sqrt{\rho^2 + a^2}} = \frac{m}{2} \frac{x^a}{\rho^2 + a^2}. \quad (3.87)$$

3.5 The magnetic scalar potential

As observed in the previous subsections, the boojum, precisely speaking the ending point of the vortex string on the domain wall, can be regarded as the magnetic source inside the domain wall. In order to pursue the identification, let us introduce the *magnetic* scalar potential, whose gradient gives the $a = 1, 2$ component of the magnetic fields:

$$B_a = -\partial_a \varphi(x^b), \quad (a = 1, 2). \quad (3.88)$$

In this subsection⁶ and we will concentrate on $B_{a=1,2}$ only, while ignoring the third component B_3 .

3.5.1 Strong coupling limit

Let us first consider the strong gauge coupling limit where the magnetic fields are given as in Eq. (3.86). The magnetic scalar potential for this is given by

$$\varphi = -\frac{q_B}{2\pi} \log \rho, \quad q_B = m\pi. \quad (3.89)$$

Because of $\partial_a^2(\log \rho)/2\pi = \delta^{(2)}(x^a)$, we see that the singular lump string can be thought of as a point magnetic source with the charge q_B :

$$\partial_a B_a = -\partial_a^2 \varphi = q_B \delta^{(2)}(x^a). \quad (3.90)$$

This identification of the lump string to the point magnetic source is consistent with the fact that the lump string is asymptotically singular far away from the domain wall.

The magnetic charge $q_B = m\pi$ can be understood as follows. The total magnetic flux coming from the lump string is 2π . Furthermore, as explained in Sec. 3.1.1, the width of domain wall in the strong gauge coupling is given by $d_W = 2/m$. Thus, the mean value of the total magnetic flux going through center of the domain wall corresponds to the magnetic charge

$$\frac{2\pi}{d_W} = m\pi = q_B. \quad (3.91)$$

⁶In this subsection, we will use the original variables x^μ , m and so on.

Now we come across an interesting coincidence: the domain wall curve given in Eq. (3.84) and the magnetic scalar potential introduced in Eq. (3.89) are related as

$$\varphi = \frac{m^2}{2}x^3 = \frac{mx^3}{d_W}. \quad (3.92)$$

Multiplication of m^2 is needed for consistency of the mass dimension. If we integrate all the magnetic flux going through the domain wall, we have the total magnetic scalar potential

$$\Phi = d_W\varphi = mx^3. \quad (3.93)$$

This coincidence tells us that the wall curve function $x^3(\rho)$ gives the magnetic scalar potential.

This is quite similar to another identification of an end point of the singular lump string on the domain wall in the massive $\mathbb{C}P^1$ nonlinear sigma model to an *electric* point source of a *dual* electromagnetic field on the $2+1$ dimensional domain wall world volume theory [11], as will be studied in Sec. 9. In this section, however, we do not take the dual viewpoint and we deal with the magnetic field of the original $U(1)$ gauge field.

The end point of the finite size lump string on the domain wall can be similarly regarded as a magnetic source, but as a source with finite size magnetic density. The magnetic scalar potential leading to Eq. (3.87) is given by

$$\varphi = -\frac{q_B}{4\pi} \log(\rho^2 + a^2), \quad (3.94)$$

As in the case of the singular lump string, the same relation (3.92) between the magnetic scalar potential and the wall curve function holds.

3.5.2 Weak coupling regime

Let us next consider the finite gauge coupling limit in which the vortex string has the finite size of order $1/gv$. The boojum also has finite size, so that it should be identified with a magnetic source with finite size distribution in $2+1$ dimensions. In the finite gauge coupling, the domain wall's position is given by Eq. (3.38). In terms of the original variables, it is rewritten as

$$x^3(\rho) = -\frac{1}{2m}u_S(\rho). \quad (3.95)$$

Now we identify this wall curve function with the magnetic scalar potential by Eq. (3.92). Before doing this, let us remember that the width of the domain wall in the weak gauge coupling region is $d_W = m/g^2v^2$. Thus the magnetic scalar potential in the weak gauge coupling region is given by

$$\varphi = \frac{mx^3}{d_W} = -\frac{g^2v^2}{2m}u_S. \quad (3.96)$$

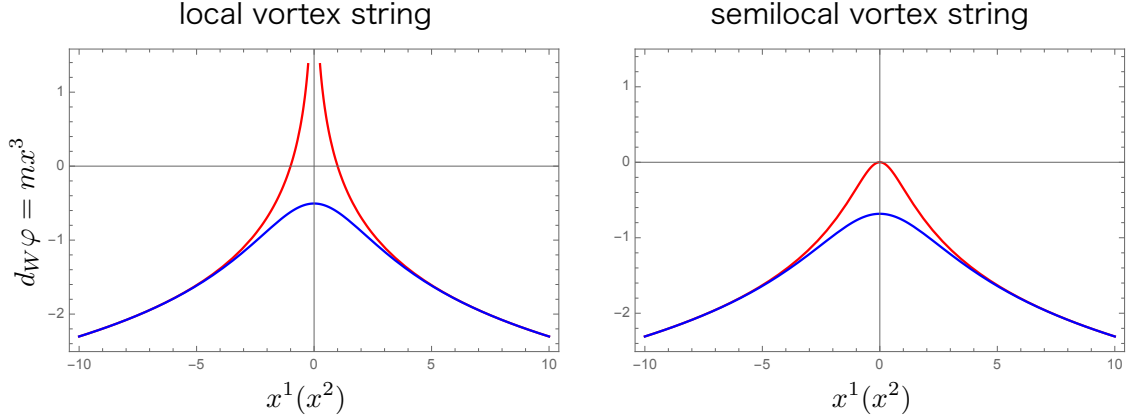


Figure 17: The magnetic scalar potentials corresponding to the local vortex string (singular lump string) in the left panel and the semi-local vortex string (regular lump string) with the size moduli $a = 1$ in the right panel for the strong gauge coupling limit (red) and the finite gauge coupling (blue). The horizontal axes is in the unit of $1/\sqrt{2}gv$.

Since u_S is asymptotically $\log \rho^2$, we read the magnetic charge as

$$q_B = \frac{2\pi g^2 v^2}{m} = \frac{2\pi}{d_W}. \quad (3.97)$$

This is consistent with the observation in the strong gauge coupling limit given in Eq. (3.91).

Let us verify if the magnetic scalar potential correctly reproduces the numerical results explained in Sec. 3.3.1. The corresponding magnetic field obtained from the magnetic scalar potential (3.96) is

$$B_a = \frac{q_B}{4\pi} \partial_a u_S. \quad (3.98)$$

This asymptotically behaves as $\rho \rightarrow \infty$

$$B_a \rightarrow \frac{q_B}{4\pi} \partial_a \log \rho^2 = \frac{2\pi g^2 v^2}{m} \frac{x^a}{2\pi \rho^2}, \quad (3.99)$$

which perfectly agrees with the previous result given in Eq. (3.59).

Distribution of the magnetic charge density can be found as

$$-\partial_a^2 \varphi = \frac{q_B}{4\pi} \partial_a^2 u_S = -q_B \frac{F_{12}}{2\pi}. \quad (3.100)$$

Thus, we are lead to a quite reasonable magnetic density $F_{12}/2\pi$, which corresponds to the magnetic field made by the vortex string.

The similar can be said for the semi-local boojum studied in Sec. 3.3.3. The domain wall's position can be read from Eq. (3.74), which leads to the magnetic scalar potential

$$\varphi = -\frac{q_{SLB}}{4\pi}u_{SLS} \rightarrow -\frac{q_{SLB}}{4\pi}\log(\rho^2 + a^2), \quad (\rho \rightarrow \infty), \quad (3.101)$$

with $q_{SLB} = 2\pi g^2 v^2/m$. From this, one can compute the asymptotic magnetic field as

$$B_b = -\partial_b\varphi \rightarrow \frac{q_{SLB}}{4\pi} \frac{2x^b}{\rho^2 + a^2} = \frac{2\pi g^2 v^2}{m} \frac{x^b}{2\pi(\rho^2 + a^2)}. \quad (3.102)$$

Again, this perfectly agrees with the previous result given in Eq. (3.77).

We plot the magnetic scalar potentials in Fig. 17 for the strong gauge coupling limit and the finite gauge coupling case. In the left panel, the red curve shows that the potential made by the point magnetic source at the origin which corresponds to the end point of the singular lump string in the strong gauge coupling limit. When the gauge coupling is finite, the string size becomes finite of order $1/gv$, and the charge distribution get fat with the same size. Then the magnetic potential written in the blue curve in the left panel becomes regular at the origin. In the right panel, we show the similar potentials for the semi-local configurations with the moduli matrix $H_0 = (z, a, 1)$ with the mass matrix $M = (m/2, m/2, -m/2)$. We set $a = 1$ so that the semi-local strings are non singular even in the strong gauge coupling limit.

The magnetic scalar potential can be explained in different way at more technical level as follows. As are given in Eq. (2.26), the BPS equations and the moduli matrix formalism give us

$$B_a = \partial_a \left(\frac{1}{2} \partial_3 u \right), \quad (3.103)$$

where u is a solution to the master equation for the full 1/4 BPS equations. Therefore, we should extract the magnetic scalar potential φ from $\partial_3 u/2$. How can we do it? A hint is in the approximate solution

$$\mathcal{U}(x^k) = u_W \left(x^3 + \frac{1}{2m} u_S(x^a) \right) + u_S(x^a). \quad (3.104)$$

Let us evaluate $\partial_a \partial_3 \mathcal{U}$ on the domain wall's position $x^3 = -u_S/2m$. We find

$$\begin{aligned} \partial_3 \partial_a \mathcal{U} \Big|_{x^3 = -\frac{u_S}{2m}} &= \partial_3 \left[\left(\frac{\partial_a u_S}{2m} \right) u'_W \left(x^3 + \frac{1}{2m} u_S \right) \right]_{x^3 = -\frac{u_S}{2m}} \\ &= \partial_a \left(\frac{u''_W(0)}{2m} u_S \right), \end{aligned} \quad (3.105)$$

where the prime stands for a x^3 derivative. From Eq. (2.26), we have $\sigma = \partial_3 u_W/2$, so that $u''_W(0)/2$ corresponds to $\sigma'(0)$, namely the derivative of σ at the center of the

domain wall. As is shown in Fig. 1, σ transits from $-m/2$ to $m/2$ inside the domain wall of the thickness d_W . Thus, we have $u_W''(0)/2 = \sigma'(0) = m/d_W$. Combining all the pieces, we reach the desired result

$$B_a \Big|_{x^3 = -\frac{u_S}{2m}} = -\partial_a \varphi, \quad \varphi = -\frac{u_S}{2d_W} = \frac{mx^3}{d_W}. \quad (3.106)$$

In summary, we found that the solution u_S to the master equation for the vortex string gives the magnetic scalar potential for $B_{a=1,2}$.

4. Non-axially symmetric solutions

In the previous section we have concentrated on studying the 1/4 BPS states which are all axially symmetric about the vortex-string axis. This symmetry reduces the problem from being three-dimensional to two-dimensional. Contrary to this, in this section we will show many numerical solutions, which require full three-dimensional treatment. We can again use the moduli matrix formalism introduced in Sec. (2.3) to reduce the 1/4 BPS equations (2.16)–(2.19) to the master equation (2.25) for a single scalar function $u(x^k)$.

4.1 $N_F = 2$

Let us first look at the 1/4 BPS solutions in $N_F = 2$ case with $\tilde{M} = (\tilde{m}/2, -\tilde{m}/2)$, which has two distinct vacua $\langle 1 \rangle$ and $\langle 2 \rangle$, and one domain wall separating those vacua. The moduli matrix for n_1 (n_2) vortex strings in the vacuum $\langle 1 \rangle$ ($\langle 2 \rangle$) is given by

$$H_0 = (P_{n_1}(z), P_{n_2}(z)), \quad (4.1)$$

where $P_n(z)$ stands for an arbitrary polynomial of n -th power in z . For this moduli matrix, we solve the master equation (3.14) written in terms of the dimensionless parameters (3.1). As before, we upgrade the master equation to the gradient flow (3.18) for the real scalar function $U(x^k, t)$,

$$\partial_k^2 U - 1 + \left(|P_{n_1}|^2 e^{\tilde{m}x^3} + |P_{n_2}|^2 e^{-\tilde{m}x^3} \right) e^{-U} = \partial_t U. \quad (4.2)$$

We need an appropriate initial function for solving this. It is given by

$$\mathcal{U}(x^k) = u_W \left(x^3 + \frac{u_S^{(n_1)} - u_S^{(n_2)}}{2\tilde{m}} \right) + \frac{u_S^{(n_1)} + u_S^{(n_2)}}{2}, \quad (4.3)$$

where $u_W(x^3)$ is the domain wall solution to the master equation (3.15) and $u_S^{(n)}(x^1, x^2)$ is the n vortex string solution to the master equation (3.17). One can easily check that this correctly reproduces the initial functions given in Sec. 3 for $n_{1,2} = 0$ or 1.

Two vortex strings in the first vacuum $\langle 1 \rangle$ ending on the domain wall can be generated by

$$P_{n_1=2}(z) = (z - L)(z + L), \quad P_{n_2=0}(z) = 1. \quad (4.4)$$

The vortex strings are asymptotically parallel and located at $z = \pm L$. In Fig. 18 we show a numerical solution with $L = 6$ for $\tilde{m} = 1$. The gray surfaces in the panels (a1) and (a2) on Fig. 18 are the energy density isosurfaces on which $\tilde{\mathcal{T}}_W + \tilde{\mathcal{T}}_S + \tilde{\mathcal{T}}_B$ takes one half of its maximum.

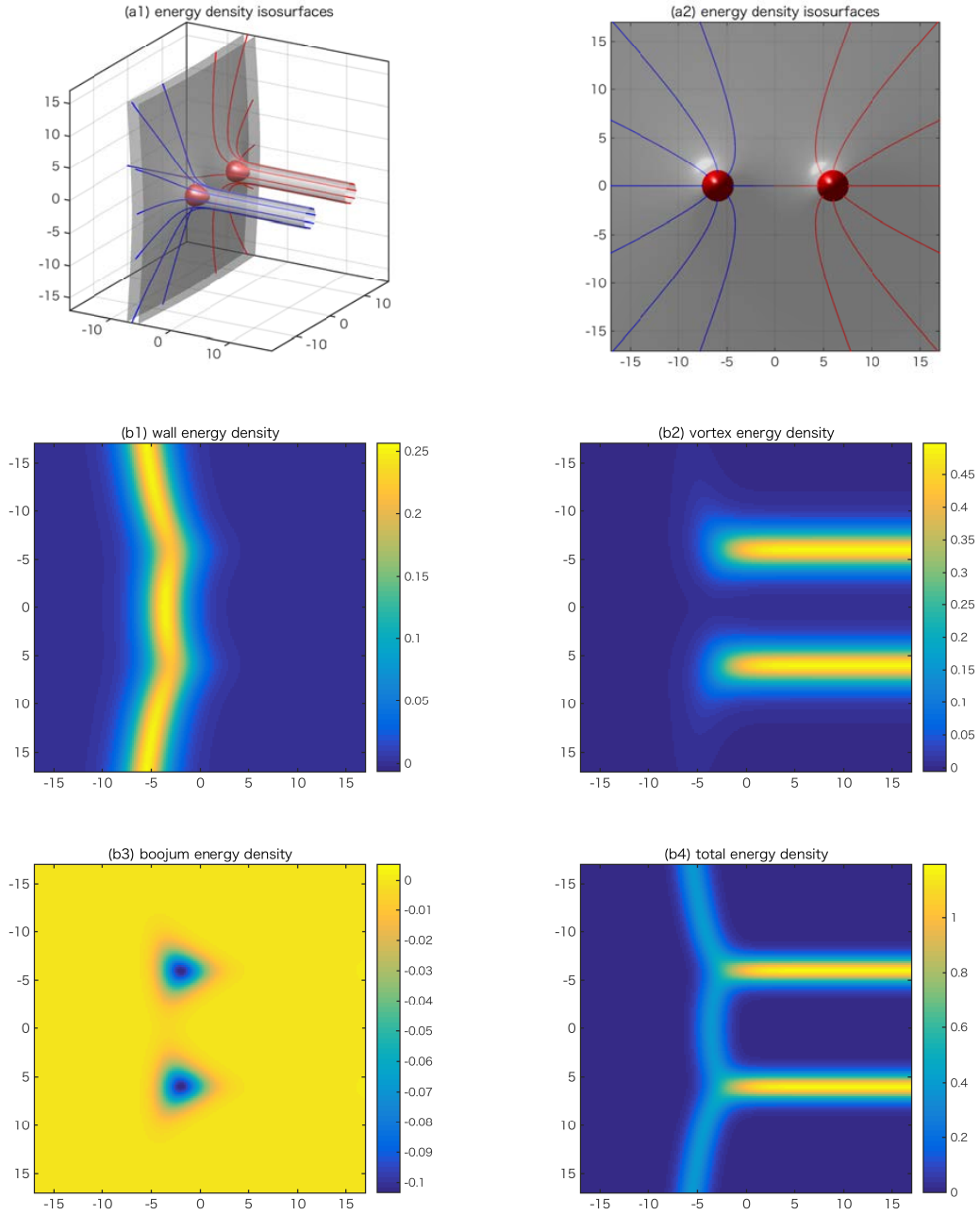


Figure 18: The plots show the energy density isosurfaces of two vortices ending on one wall (a1, a2), where the blue and the red curves show magnetic flux, the wall energy density (b1), the vortex energy density (b2), the boojum energy density (b3) and the total energy density (b4) with the distance between two vortices $L = 6$. The mass is set to be $\tilde{m} = 1$.

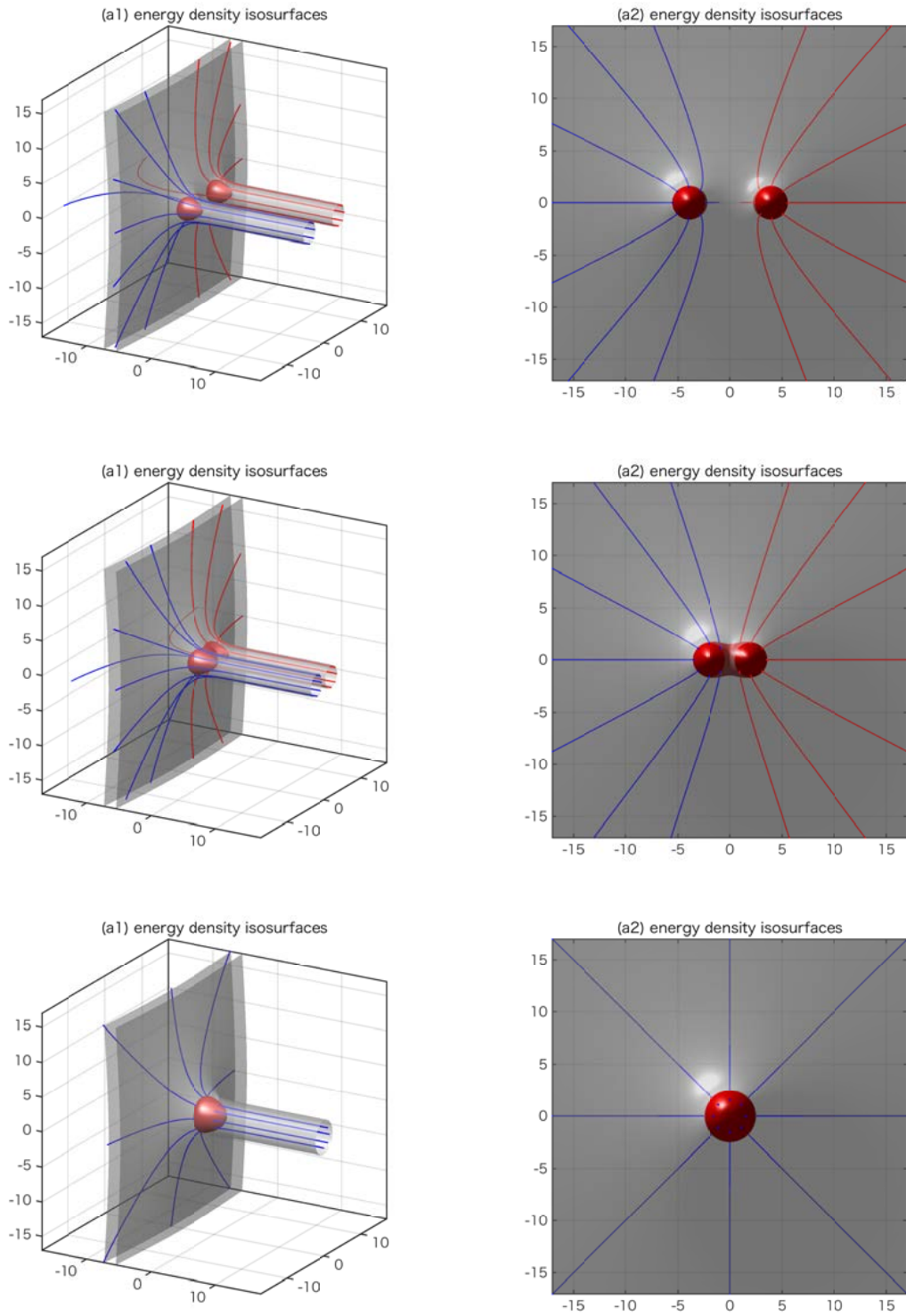


Figure 19: The plots show the energy density isosurfaces of two vortices ending on one wall. The distance between two vortices are taken to be $L = 4, 2, 0$ from top to bottom.

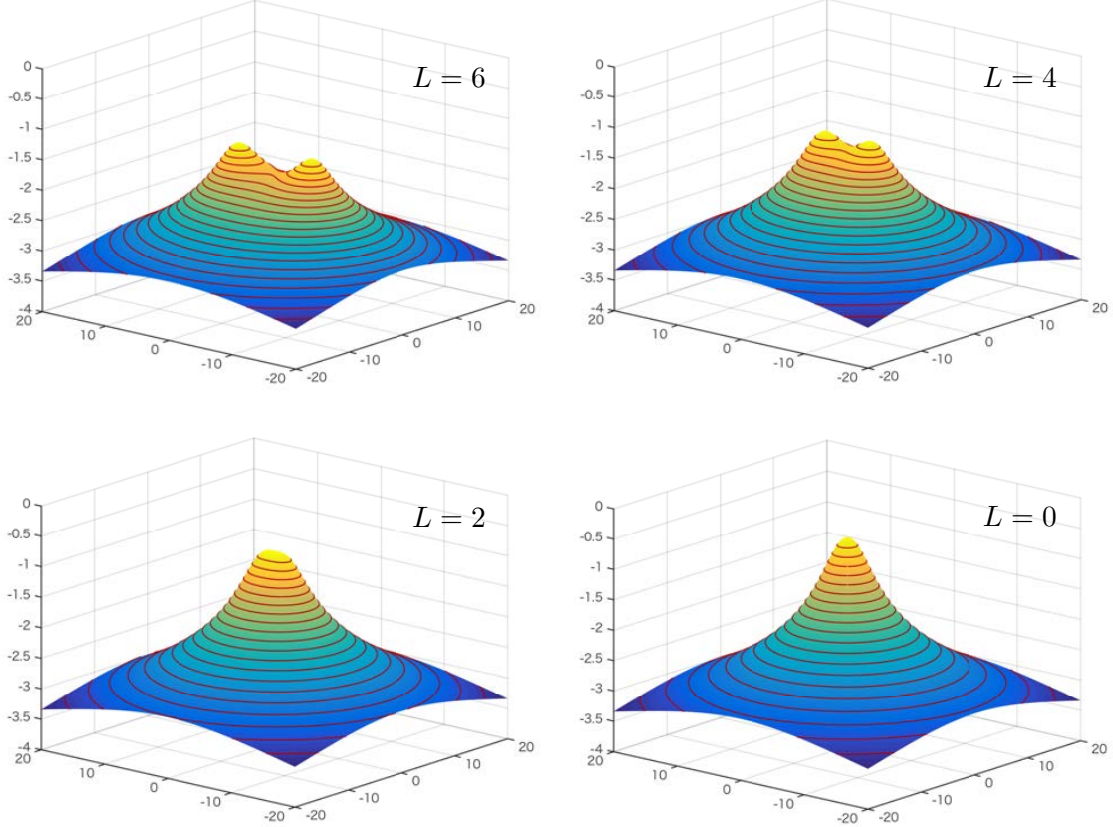


Figure 20: The 2 + 1 dimensional magnetic scalar potentials $\tilde{\varphi}$ for two vortex strings ending on the domain wall in $N_F = 2$ model with $\tilde{m} = 1$. The separation of two strings are $L = 6, 4, 2, 0$. The horizontal axes are x^1 and x^2 .

The red lumps in the panels (a1) and (a2) of Fig. 18 show the boojum density isosurface on which $\tilde{\mathcal{T}}_B$ takes one half of its minimum (a negative value), and the red and blue curves correspond to the magnetic force lines going through the vortex strings. In the panels (b1), (b2), and (b3) we show the topological charge densities $\tilde{\mathcal{T}}_W$, $\tilde{\mathcal{T}}_S$, and $\tilde{\mathcal{T}}_B$ on the cross section which passes the centers of vortex strings, respectively. The panel (b4) of Fig. 18 depicts the total energy density $\tilde{\mathcal{T}}$ including the surface terms on the same cross section.

One can easily change the distance of two vortex strings by varying L in Eq. (4.4). The numerical solutions for $L = 4, 2, 0$ are shown in Fig. 19. It is clearly seen that the two individual boojums coalesce into one large boojum as the distance between two vortex strings becomes small.

Looking at the magnetic force lines injecting inside the domain wall via the vortex strings shown in the panels (a1) of Figs. 18 and 19, the red and blue lines repel on the domain wall. This is quite similar to expansion of the magnetic force lines from two point-like magnetic sources in 2 + 1 dimensions. As is seen for the

single magnetic source in Sec. 3.5, we indeed regard them as the 2 + 1 dimensional magnetic sources and the corresponding magnetic scalar potential is given by the domain wall curve function. It can be read from Eq. (4.3) as

$$\tilde{\varphi} = \frac{\tilde{m}x^3}{\tilde{d}_W} = -\frac{u_S^{(n_1=2)} - u_S^{(n_2=0)}}{2\tilde{d}_W} = -\frac{u_S^{(n_1=2)}}{4}, \quad (4.5)$$

with $\tilde{d}_W \simeq 2$ for $\tilde{m} = 1$. We show the numerical plots for the magnetic scalar potentials in Fig. 20. They are asymptotically close to the log function $\tilde{\varphi} \rightarrow -(\log \rho^4)/4$ for large ρ . Note that the solution $u_S^{(n_1=2)}$ is well approximated by a superposition of $u_S^{(n_1=1)}$ when the separation L is sufficiently large:

$$u_S^{(n_1=2)}|_{P_{n_1}=(z-L)(z+L)} \simeq u_S^{(n_1=1)}|_{P_{n_1}=z-L} + u_S^{(n_1=1)}|_{P_{n_1}=z+L}, \quad (4.6)$$

with $u_S^{(n_1=1)}$ shown in Fig. 2. When L is comparable to the size of the vortex string, the superposition is no longer good approximation and we should solve the master equation directly as the numerical solutions shown in Fig. 20.

Let us next consider the asymptotically flat domain wall on which a vortex strings end from both sides. The moduli matrix is

$$P_{n_1=1}(z) = z - L, \quad P_{n_2=1}(z) = z + L. \quad (4.7)$$

The parameters $z = \pm L$ correspond to positions of the string end points. We show a typical solution with $L = 6$ for $\tilde{m} = 1$ case in Fig. 21. The six panels in Fig. 21 show the same quantities plotted in the panels in Fig. 18. The magnetic force lines incoming from the vortex string on the positive x^3 side go into the other vortex string on the negative x^3 side. Seen from the x^3 axis, the distribution of the magnetic force lines is like a magnetic dipole, see the panel (a2) of Fig. 21. This is remarkable contrast to the two vortex strings ending on the domain wall from one side. The former can be thought of as the dipole with opposite magnetic charges and the latter is as the dipole with the same magnetic charges. As we reduce the separation L of the two strings, the region in which the magnetic flux expands gets smaller, see Fig. 22 where we plot the numerical solutions for $L = 4, 2, 0$. Note that when $L = 0$ the two vortex strings become collinear and the magnetic charges in the 2 + 1 dimensional sense exactly cancel. Even in the limit $L \rightarrow 0$, the boojums do not disappear because the domain wall has the finite width and the boojums are separate in x^3 direction.

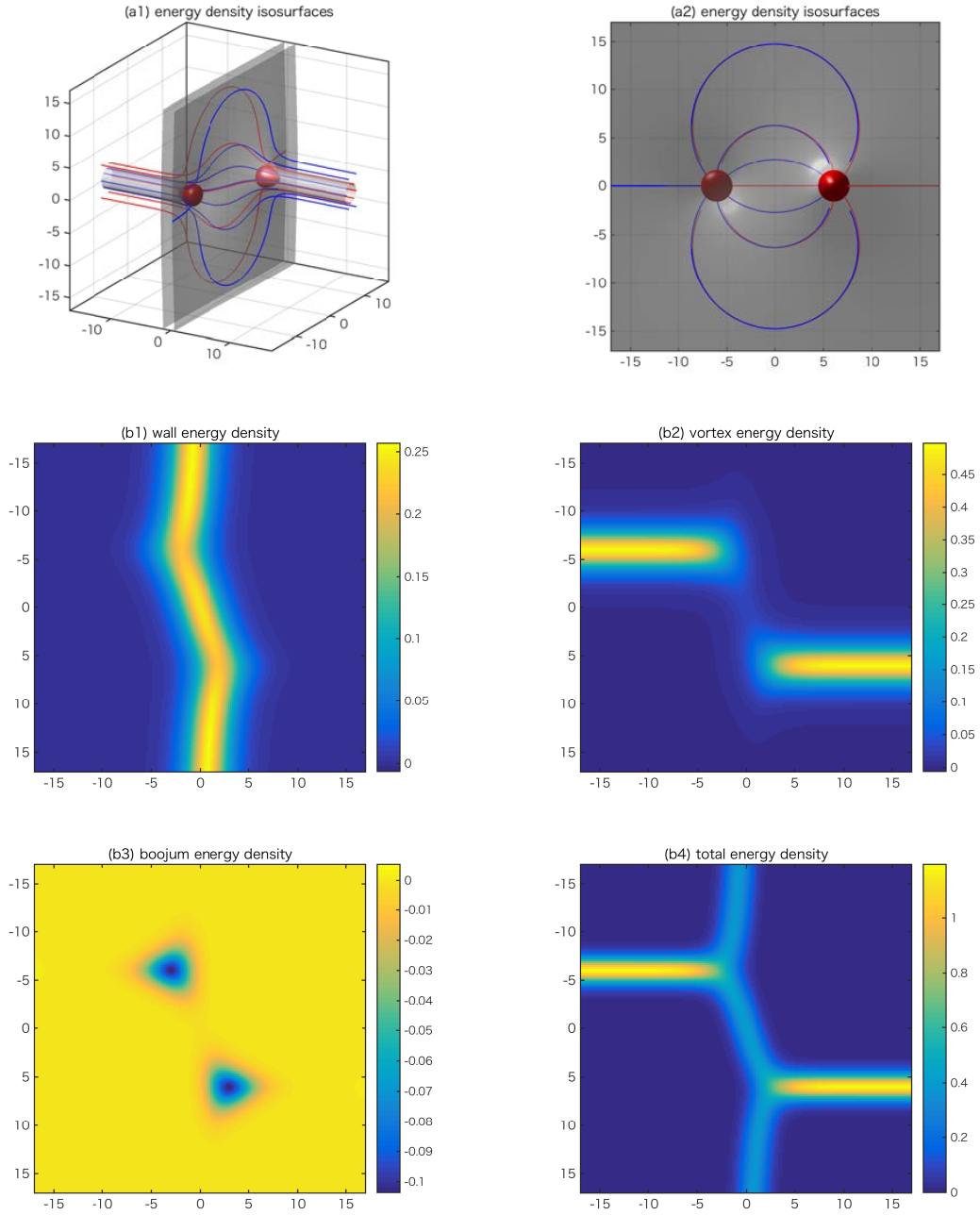


Figure 21: The plots show the energy density isosurfaces of two vortices ending on one wall from two sides (a1, a2), where the blue and the red curves show magnetic fluxes, the wall energy density (b1), the vortex energy density (b2), the boojum energy density (b3) and the total energy density (b4) with the distance between two vortices $L = 6$.

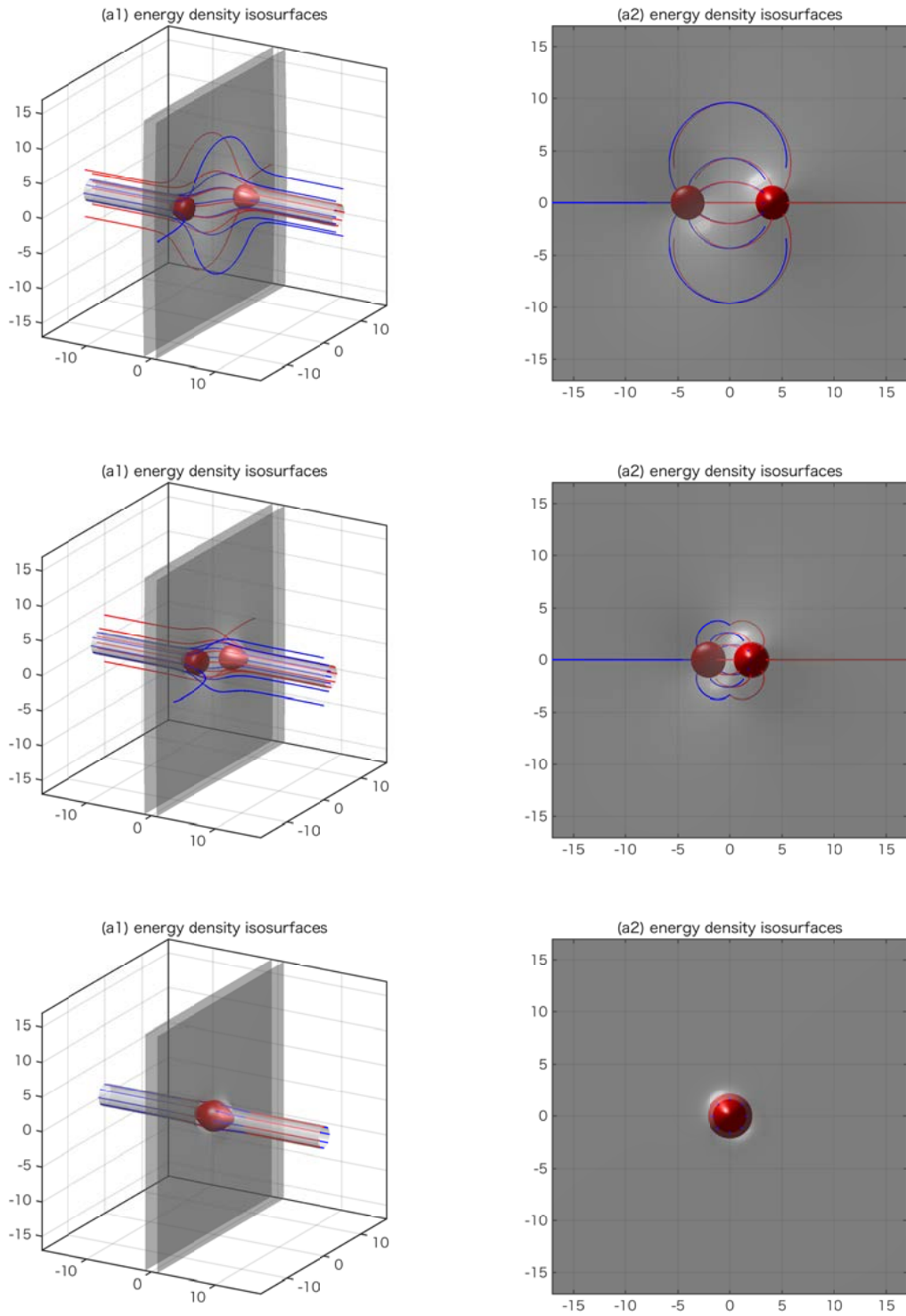


Figure 22: The plots show the energy density isosurfaces of two vortices ending on one wall from two sides. The distance between two vortices are taken to be $L = 4, 2, 0$ from top to bottom.

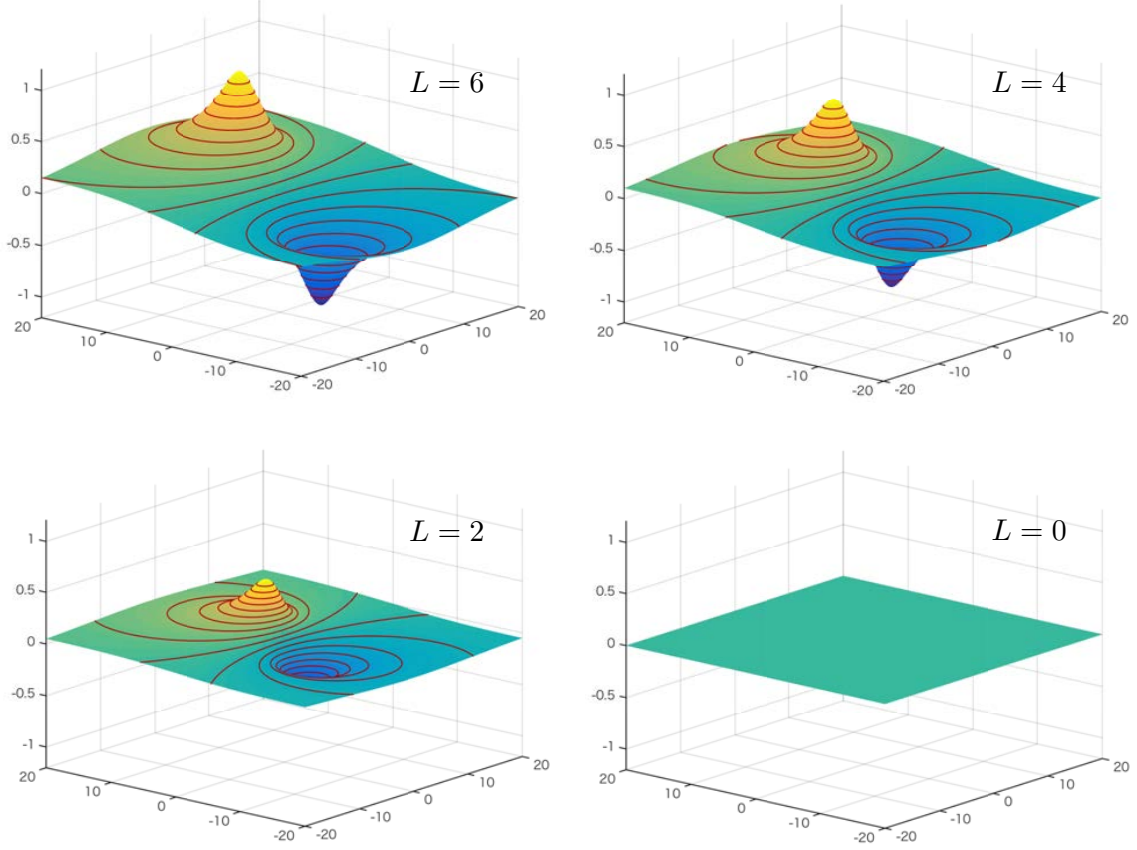


Figure 23: The 2 + 1 dimensional magnetic scalar potentials $\tilde{\varphi}$ for vortex strings ending on the domain wall from both sides in $N_F = 2$ model with $\tilde{m} = 1$. The separation of two strings are $L = 6, 4, 2, 0$. The horizontal axes are x^1 and x^2 .

Now we expect that the end point of the vortex string on the positive (negative) x^3 side should be identified with the positive (negative) point-like magnetic source. The corresponding magnetic scalar potential is again given by the domain wall curve function, which we read from Eq. (4.3) as

$$\tilde{\varphi} = -\frac{u_S^{(n_1=1)}}{2\tilde{d}_W} + \frac{u_S^{(n_2=1)}}{2\tilde{d}_W}, \quad (4.8)$$

where $u_S^{(n_1)}$ is the solution for the vortex string at $z = L$ and $u_S^{(n_2)}$ is for the vortex string at $z = -L$, while $\tilde{d}_W = 2$ for $\tilde{m} = 1$ as before. This is just a superposition of the potentials of the positive and negative sources. Unlike the case of two charges of the same kind, the potential is given by the superposition irrespective the value of L .

Let us make a comment on the shapes of the boojums. When they are well separated, shape of the individual boojum is approximately the same as that drawn in the right panel of Fig. 4. When the vortex strings are closer to each other than

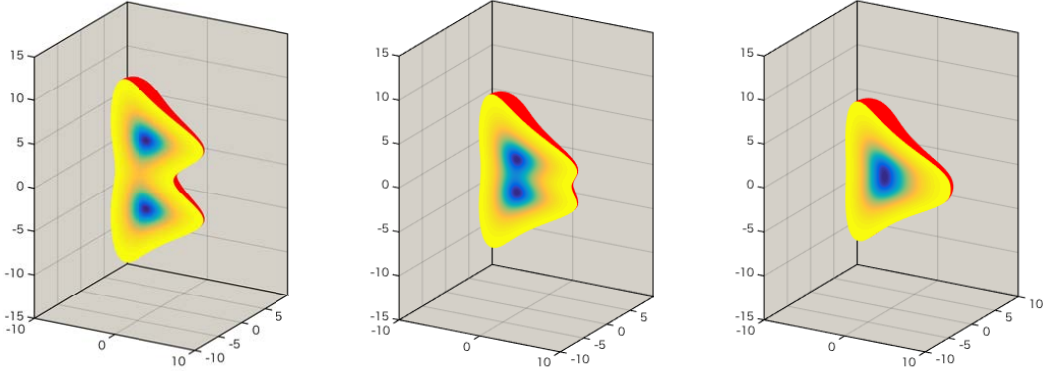


Figure 24: The plots of the boojum energy density for the case that two vortices ending on one wall. The distances of two vortices are $L = 4, 2, 0$ from left to right.

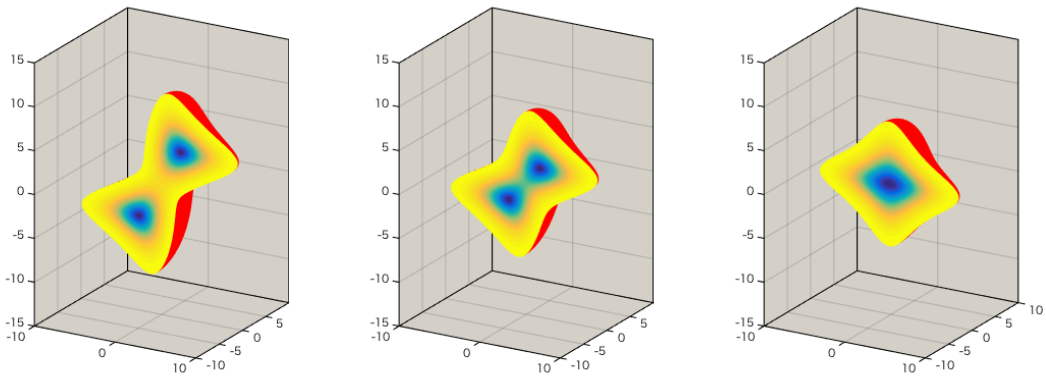


Figure 25: The plots of the boojum energy density for the case that two vortices ending on one wall from two sides. The distance of two vortices are $L = 4, 2, 0$ from left to right.

the vortex string size, the boojums merge. One may recall that rich 3D structure appears when several BPS 't Hooft-Polyakov monopoles in $SU(2)$ gauge theory get close. For the boojums in the Abelian-Higgs theory, such drastic change in the shape is not observed, see Figs. 24 and 25.

Our last comment here is about the question of definition of the binding energy raised in [66]. Consider two vortex-strings attached to the domain wall from both sides, see Fig. 26. Two vortex-strings are separated by the distance d . For this configuration the authors of Ref. [66] argued that there are two possibilities where the binding energy is located. First possibility is that the binding energy only localizes around the junction points. Second one is that it localizes not only around the junction points but also near the origin (dotted-circled domain in the right figure in Fig. 26). Our numerical solutions, for example Fig. 21, strongly supports that the former is true.

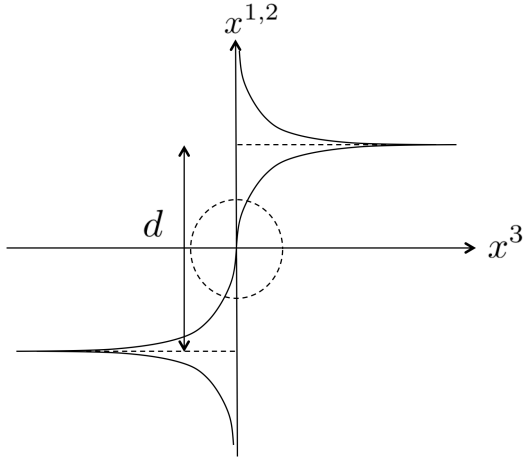


Figure 26: Schematic picture of the configuration of two vortices attached to the wall from both sides.

4.2 $N_F \geq 3$

4.2.1 Non-degenerate masses

Next we will explain how to obtain the 1/4 BPS configurations with two domain walls separating three different vacua $\langle A \rangle$ ($A = 1, 2, 3$) in which n_A vortex strings exist. The minimal model is $N_F = 3$ with non-degenerate mass matrix $\tilde{M} = (\tilde{m}_1/2, (\tilde{m}_2 - \tilde{m}_1)/2, -\tilde{m}_2/2)$. The tension of the domain wall interpolating $\langle 1 \rangle$ and $\langle 2 \rangle$ is $v^2(2\tilde{m}_1 - \tilde{m}_2)/2$ and that of the domain wall interpolating $\langle 2 \rangle$ and $\langle 3 \rangle$ is $v^2(2\tilde{m}_2 - \tilde{m}_1)/2$. For simplicity, we will focus on the case $\tilde{m}_1 = \tilde{m}_2 = \tilde{m}$, namely that the two domain walls have the same tension.

First of all, let us consider the configuration with no vortex strings. The moduli matrix is characterized by only one real parameter δ as

$$H_0 = (1, \delta, 1). \quad (4.9)$$

When $\delta \gg 1$ the physical meaning of this parameter is related to the separation of walls, since the position of the walls can be estimated as

$$x^3 = \pm \frac{1}{\tilde{m}} \log \delta^2. \quad (4.10)$$

Thus the separation R is

$$R = \frac{2}{\tilde{m}} \log \delta^2, \quad (4.11)$$

see Fig. 27. When δ is close to or smaller than 1, two domain walls coalesce and $2(\log \delta^2)/\tilde{m}$ can no longer be understood as the distance. When $\delta \rightarrow -\infty$, the

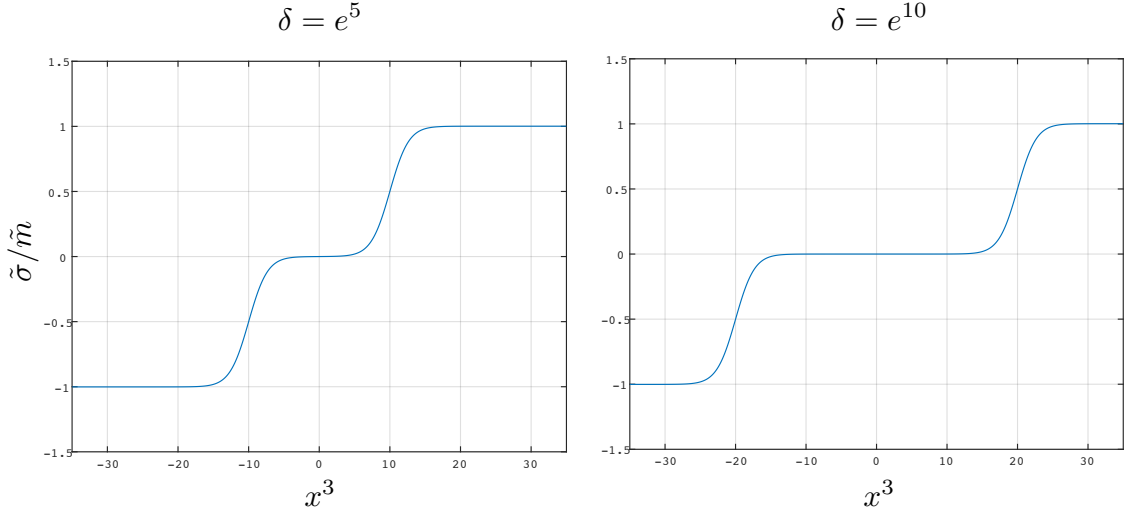


Figure 27: $\tilde{\sigma}$ for two separated domain walls for $\tilde{m}_1 = \tilde{m}_2 = \tilde{m} = 1$ in $N_F = 3$ case. The left panel is for $\delta = e^5$ ($R = 20$) and the right panel is for $\delta = e^{10}$ ($R = 40$).

two walls collapse into one heavier domain wall. The solution is parametrized as $u = u_W(x^3; \delta)$ which satisfies the following reduced master equation

$$\partial_3^2 u_W(x^3; \delta) - 1 + \left(e^{\tilde{m}x^3} + \delta^2 + e^{-\tilde{m}x^3} \right) e^{-u_W(x^3; \delta)} = 0. \quad (4.12)$$

Next, we put n_A vortex strings in the $\langle A \rangle$ vacuum. The moduli matrix for this is given by

$$H_0 = (P_{n_1}(z), \delta P_{n_2}(z), P_{n_3}(z)), \quad (4.13)$$

where $P_{n_A}(z)$ stands for a monomial of n_A -th degree. The corresponding gradient flow equation is

$$\partial_k^2 U - 1 + \left(|P_{n_1}|^2 e^{\tilde{m}x^3} + \delta^2 |P_{n_2}|^2 + |P_{n_3}|^2 e^{-\tilde{m}x^3} \right) e^{-U} = \partial_t U. \quad (4.14)$$

One can rewrite this as

$$\partial_k^2 U - 1 + \left(e^{\tilde{m}x^3 + \log \left| \frac{P_{n_1}}{P_{n_3}} \right|} + \frac{\delta^2 |P_{n_2}|^2}{|P_{n_1} P_{n_3}|} + e^{-\tilde{m}x^3 - \log \left| \frac{P_{n_1}}{P_{n_3}} \right|} \right) e^{-U + \log |P_{n_1} P_{n_3}|} = \partial_t U. \quad (4.15)$$

Comparing this with Eq. (4.12), one finds a suitable initial configuration for solving the 3 dimensional master equation

$$\mathcal{U}(x^k) = u_W \left(x^3 + \frac{u_S^{(n_1)} - u_S^{(n_3)}}{2\tilde{m}}; \delta \frac{|P_{n_2}|}{\sqrt{|P_{n_1} P_{n_3}|}} \right) + \frac{u_S^{(n_1)} + u_S^{(n_3)}}{2}. \quad (4.16)$$

Validity of this initial configuration is ensured by the asymptotic behavior $u_S^{(n)} \rightarrow \log |P_n|^2$ for $\rho \gg 1$. The positions of the two domain walls are estimated as

$$x^3|_{\langle 1 \rangle \leftrightarrow \langle 2 \rangle} = \frac{1}{\tilde{m}} \left(\log \delta^2 + u_S^{(n_2)} - u_S^{(n_1)} \right), \quad (4.17)$$

$$x^3|_{\langle 2 \rangle \leftrightarrow \langle 3 \rangle} = -\frac{1}{\tilde{m}} \left(\log \delta^2 + u_S^{(n_2)} - u_S^{(n_3)} \right). \quad (4.18)$$

Then the separation of the two domain walls is

$$\begin{aligned} R &= \frac{2}{\tilde{m}} \left(\log \delta^2 + u_S^{(n_2)} - \frac{u_S^{(n_1)} + u_S^{(n_3)}}{2} \right), \quad (4.19) \\ &\simeq \frac{2}{\tilde{m}} \log \delta^2 \frac{|P_{n_2}|^2}{|P_{n_1} P_{n_3}|}, \\ &\rightarrow \frac{2}{\tilde{m}} \log \delta^2 \rho^{2n_2 - n_1 - n_3} \quad (\rho \rightarrow \infty). \end{aligned}$$

The domain walls are asymptotically parallel when $2n_2 = n_1 + n_3$ and are asymptotically flat only when $n_1 = n_2 = n_3$.

In Fig. 28, we show the numerical solution for $n_1 = n_3 = 0$ and $n_2 = 1$ with $\delta = e^5$ for the model with $\tilde{m} = 2$. Namely, we put a single vortex string in the middle vacuum $\langle 2 \rangle$. Reasons for taking $\tilde{m} = 2$ here is, first, that the mass of each domain wall is $\tilde{m}/2 = 1$, and, second, that we have the exact solution u_W to the domain wall master equation in this case [73]. Having the exact solution benefits our numerical works. We will mention more about this in Sec. 7. The panel (b2) of Fig. 28 clearly shows that the vortex string of the finite length $\ell = \frac{2}{\tilde{m}} \log \delta^2 \simeq 10$ exists in the middle vacuum. The string length ℓ is the same as the domain wall distance with no vortex strings. The magnetic fluxes expressed by the blue curve in the panels (a1) and (a2) in the domain wall at the negative side of x^3 are squeezed and run through the vortex string, and then expand inside the domain wall at the positive side of x^3 . The end points of the vortex strings on the domain walls are accompanied with the boojums as shown in the panel (b3).

As δ gets small, the domain walls get close. At the same time, the distance between the boojums becomes smaller and the vortex string gets shorter. We show the solutions for $\delta = e^{4,2,0}$ in Fig. 29. When the domain walls start to merge it is difficult to find a clear boundary between them. In this situation it is difficult to speak about the length of the string. However, the diameter of the string becomes very wide, while the magnitude of the magnetic flux weakens, see Fig. 30 for $\delta = e^{-2}$. The panels (b2) and (b3) in Fig. 30 show the vortex and boojum charges and we see that the vortex is indeed sandwiched by the domain walls. Ultimately, at $\delta = 0$, the middle vacuum completely disappears, so that the vortex vanishes as well. Fig. 31 shows change of the shape of two boojums living in the different domain walls. As the domain walls close on each other, the boojums merge into a flat disk.

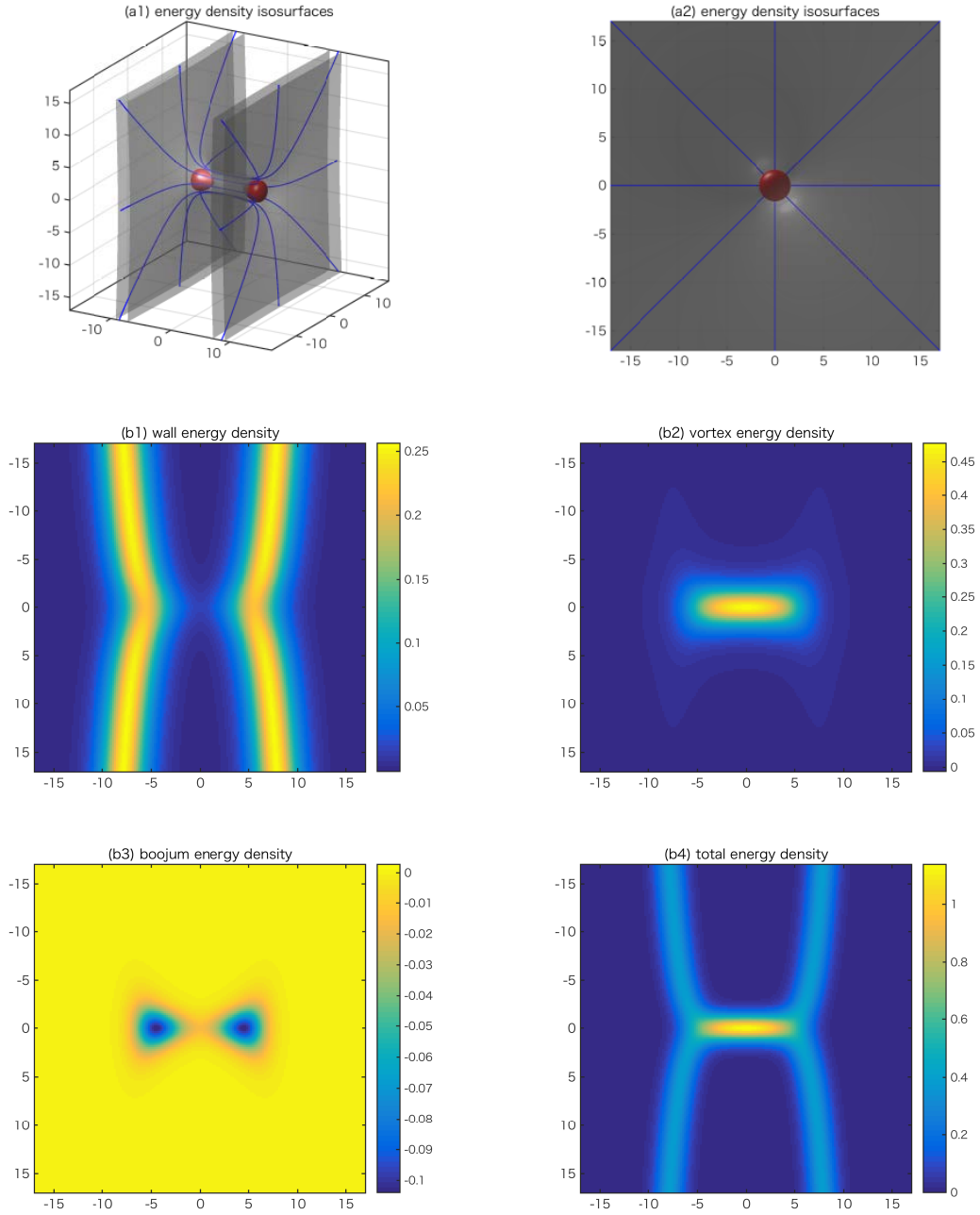


Figure 28: The plots show the energy density isosurfaces of one vortex stretching between two walls (a1, a2), where the blue and the red curves show magnetic fluxes, the wall energy density (b1), the vortex energy density (b2), the boojum energy density (b3) and the total energy density (b4) with the half distance between two vortices $R = 5$.

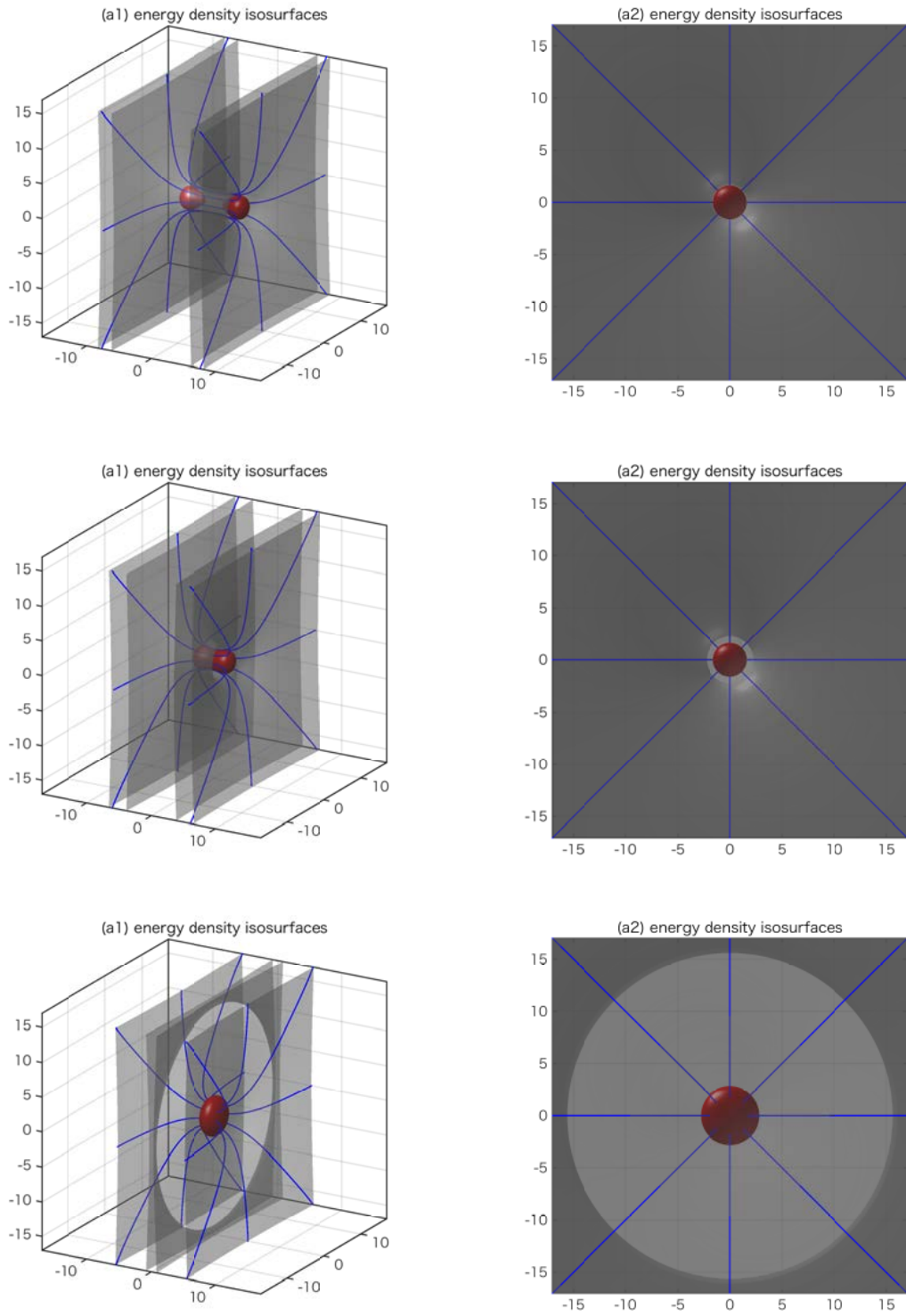


Figure 29: The plots show the energy density isosurfaces of one vortex ending on two walls. The half distance between two vortices are taken to be $R = 4, 2, 0$ from top to bottom.

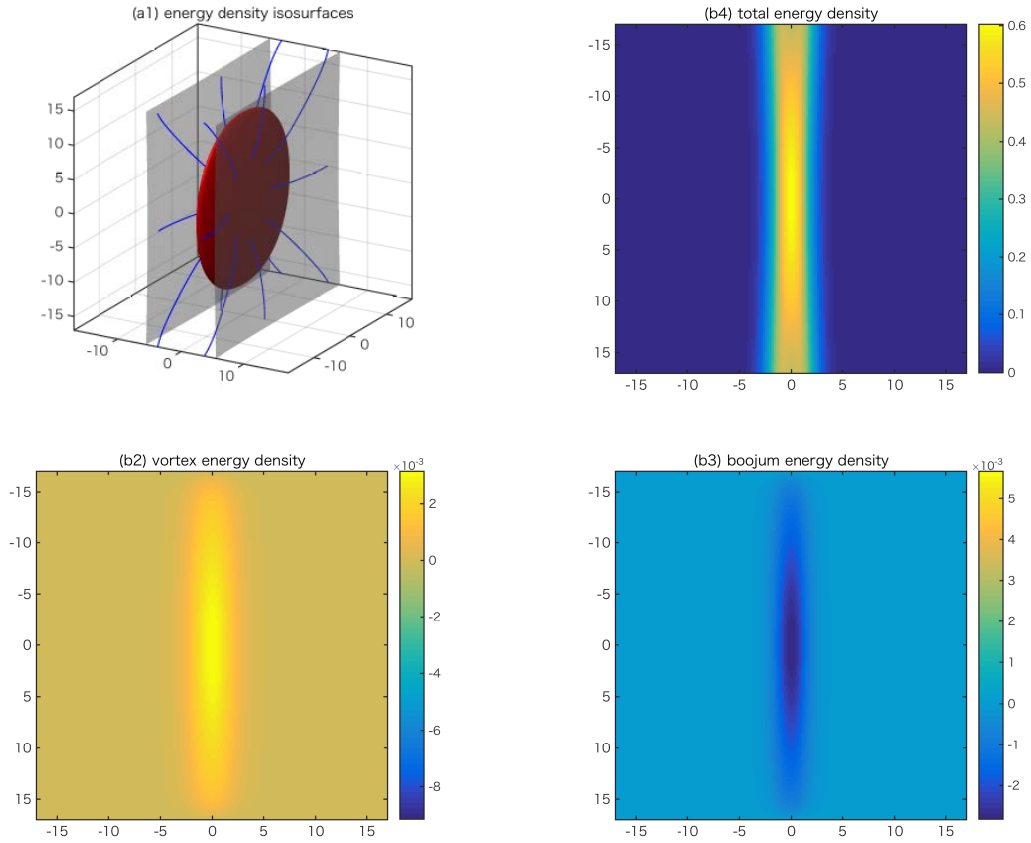


Figure 30: The plots show the energy density isosurfaces of two vortices ending on one wall from two sides (a1), where the blue and the red curves show magnetic fluxes, the vortex energy density (b2), the boojum energy density (b3) and the total energy density (b4) with $\delta = e^{-2}$.

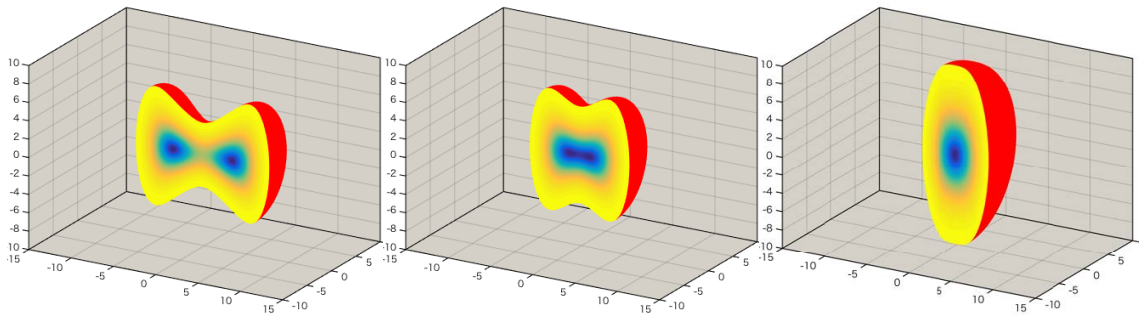


Figure 31: The plots of the boojum energy density for the case that two vortices ending on one wall from one side (top), two vortices ending on one wall from two sides (middle) and one vortex ending on two walls (bottom). The half distance of two boojums are $R = 4, 2, 0$ from left to right.

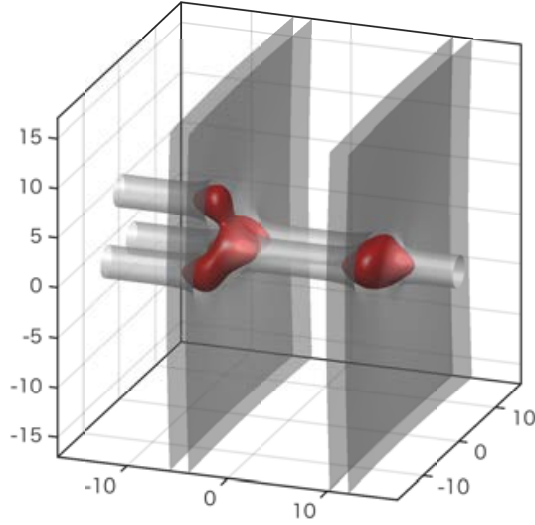


Figure 32: The two logarithmically bent but parallel domain walls in $N_F = 3$ model. The number of the vortices are 3, 2 and 1 in the vacua $\langle 1 \rangle$, $\langle 2 \rangle$ and $\langle 3 \rangle$, respectively.

Observing the expansion of the magnetic flux in the two domain walls shown in Figs. 28 and 29, it is natural to regard the vortex string as a magnetic source as before. Clearly, the vortex string should be regarded as a positive magnetic source for one of the domain wall (on the x^3 positive side) and as a negative magnetic source for the other (on the x^3 negative side). The corresponding magnetic scalar potentials for 2 + 1 dimensional worlds inside the domain walls are given by x^3 positions of the domain walls. From Eqs. (4.17) and (4.18), we have

$$\tilde{\varphi}|_{\langle 1 \rangle \leftrightarrow \langle 2 \rangle} = \frac{\tilde{m}/2}{\tilde{d}_W} x^3|_{\langle 1 \rangle \leftrightarrow \langle 2 \rangle} = \frac{1}{2\tilde{d}_W} \left(\log \delta^2 - u_S^{(n_1=1)} \right), \quad (4.20)$$

$$\tilde{\varphi}|_{\langle 2 \rangle \leftrightarrow \langle 3 \rangle} = \frac{\tilde{m}/2}{\tilde{d}_W} x^3|_{\langle 2 \rangle \leftrightarrow \langle 3 \rangle} = -\frac{1}{2\tilde{d}_W} \left(\log \delta^2 - u_S^{(n_3=1)} \right). \quad (4.21)$$

Here we have put $\tilde{m}/2$ instead of \tilde{m} on the numerators of the middle equations, since the mass difference of the first (second) and second (third) flavor is $\tilde{m}/2$. Correspondingly, the domain wall thickness is given by $\tilde{d}_W \simeq 2(\tilde{m}/2) = 2$ for $\tilde{m} = 2$. Except for the unphysical constant parts, these two potentials are equal but have different signs. This is consistent with our interpretation of the vortex string as the magnetic sources to the domain walls. The magnetic potential is shown in the left panel of Fig. 17.

As an example for more complicated configuration, in Fig. 32, we show the solution which have single, double and triple vortex strings in the vacuum $\langle 1 \rangle$, $\langle 2 \rangle$

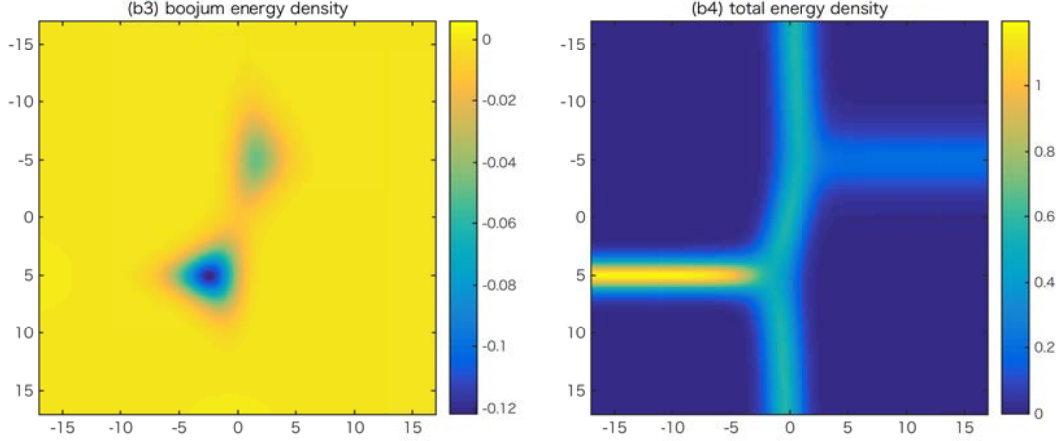


Figure 33: The semi-local vortex string with $a = 3$ at $z = -5$ ending of the domain wall from the x^3 positive side and the local vortex string at $z = 5$ ending on the domain wall from the x^3 negative side. The panel (b3) shows the boojum charge density and (b4) shows the total energy density on the $x^2 = 0$ plane.

and $\langle 3 \rangle$, respectively. The number of vortex strings satisfy the relation $2n_2 = n_1 + n_3$, so that the domain walls are logarithmically bending but are asymptotically parallel.

4.2.2 Partially degenerate masses

When some masses are partially degenerate, the corresponding vacua are degenerate. Then the vortex strings there become the semi-local vortex strings, as seen in Sec. 3.3.3. As before, we consider the minimal model $N_F = 3$ with $\tilde{M} = \text{diag}(\tilde{m}/2, \tilde{m}/2, -\tilde{m}/2)$. The relevant moduli matrix is given by

$$H_0 = (P_{n_1}(z), Q_{n_1-1}(z), P_{n_2}(z)), \quad (4.22)$$

where $P_n(z)$ is a monomial of power n and $Q_n(z)$ stands for a polynomial of power n . The n_1 semi-local vortex strings in the degenerate vacuum $\langle 1 \rangle$ are determined by P_{n_1} and Q_{n_1-1} , while the n_2 local vortex strings in the vacuum $\langle 2 \rangle$ are determined by P_{n_2} .

The gradient flow equation to be solved is

$$\partial_k^2 U - 1 + \left((|P_{n_1}|^2 + |Q_{n_1-1}|^2)e^{\tilde{m}x^3} + |P_{n_2}|^2 e^{-\tilde{m}x^3} \right) e^{-U} = \partial_t U. \quad (4.23)$$

This is identical to Eq. (4.2) if we replace $|P_{n_1}|^2 \rightarrow |P_{n_1}|^2 + |Q_{n_1-1}|^2$. Thus, a suitable initial configuration is given by

$$\mathcal{U}(x^k) = u_W \left(x^3 + \frac{u_{SLS}^{(n_1)} - u_S^{(n_2)}}{2\tilde{m}} \right) + \frac{u_{SLS}^{(n_1)} + u_S^{(n_2)}}{2}, \quad (4.24)$$

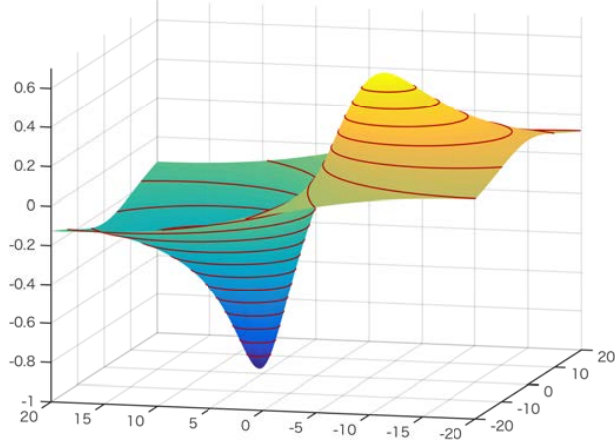


Figure 34: The magnetic scalar potential for the semi-local vortex string (the positive magnetic charge with the size parameter $a = 3$) at $z = -5$ and the local vortex string (the negative magnetic charge) at $z = 5$.

where $u_{SLS}^{(n_1)}$ stands for a solution to the master equation for the semi-local vortex string

$$\partial_a^2 u_{SLS} - 1 + (|P_{n_1}|^2 + |Q_{n_1-1}|^2)e^{-u_{SLS}} = 0. \quad (4.25)$$

In Fig. 33, we show a solution for a generic choice

$$P_{n_1=1} = z + L, \quad Q_{n_1-1=0} = a, \quad P_{n_2=1} = z - L, \quad (4.26)$$

with $a = 3$ and $L = 5$.

The magnetic scalar potential for this model is given by

$$\tilde{\varphi} = \frac{\tilde{m}x^3}{\tilde{d}_W} = -\frac{u_{SLS}^{(n_1)} - u_S^{(n_2)}}{2\tilde{d}_W}. \quad (4.27)$$

We show $\tilde{\varphi}$ for the choice in Eq. (4.26) with $a = 3$ and $L = 5$ in Fig. 34. The positive part corresponding the end point of the semi-local vortex string is lower and broader compared with the negative part for the end point of the local vortex string.

For closing this section, we show several funny solutions in order to demonstrate that we can have any kind of numerical configurations, see Fig. 35.

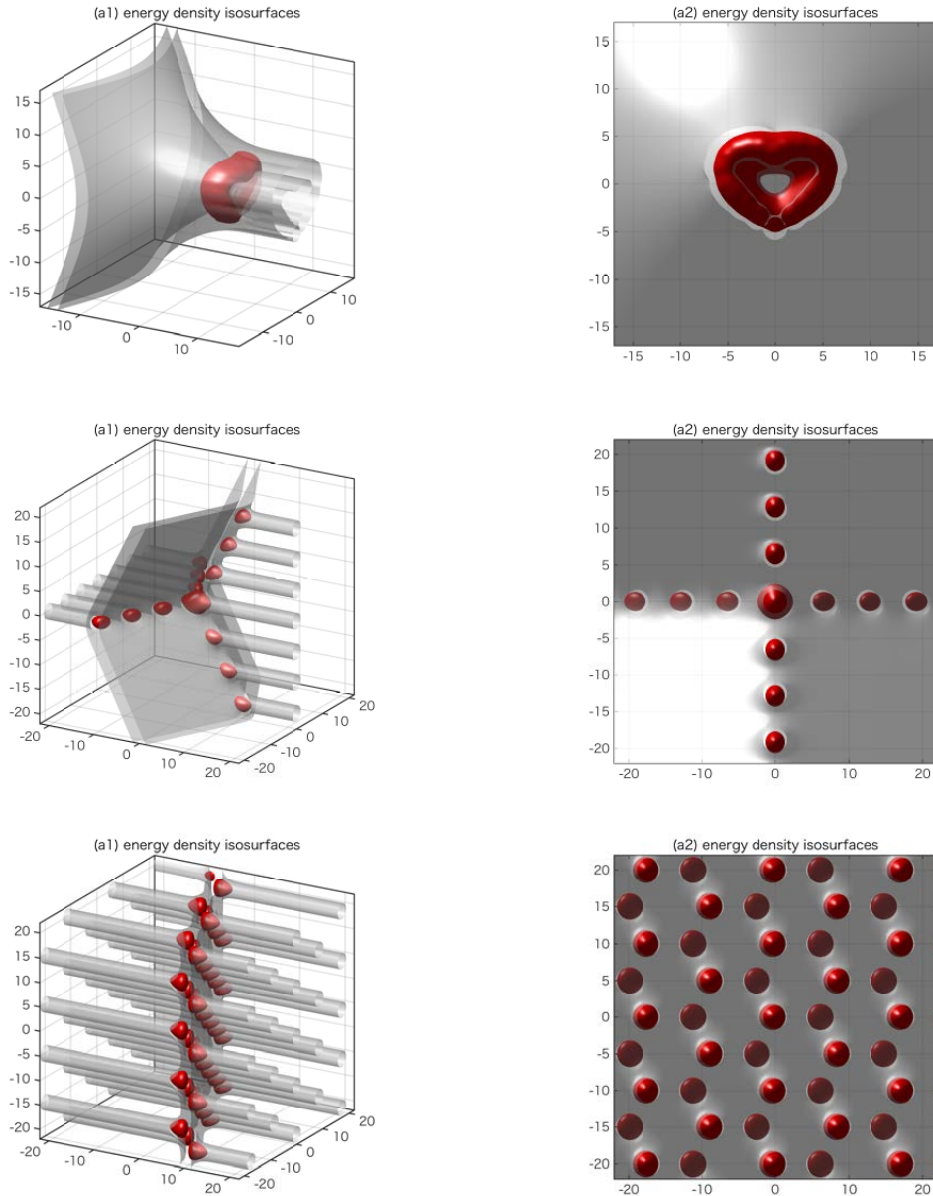


Figure 35: The plots show the energy density isosurfaces of various configurations of vortices-wall-boojum system. The top plots show that the energy density isosurface of the boojum is a heart mark shape. The middle plots show that the energy density isosurface of periodic vortices on cross lines ending on one wall from two sides. The bottom plots show that the energy density isosurface of the so-called Abrikosov lattices ending on one wall from two sides.

5. A magnetic capacitor

In this section we will study the $1/4$ BPS solutions which have a lot of vortex strings aligned in a line on one end of the domain wall in the model with $N_F = 2$ and $M = (\tilde{m}/2, -\tilde{m}/2)$. The details for solving the master equation have been already explained in Sec. 4.1. The moduli matrix which we will consider in this section is given in Eq. (4.1).

5.1 Linearly aligned vortex strings ending on a domain wall from one side

First, we align n_1 vortex strings in the vacuum $\langle 1 \rangle$ on a line, while we set no vortex strings in the opposite vacuum $\langle 2 \rangle$. We will consider the following moduli matrix given in Eq. (4.1) with

$$P_{n_1}(z) = e^{-\tilde{m}X/2} \prod_{k=-(n_1-1)/2}^{(n_1-1)/2} (z - Lk), \quad P_{n_2=0}(z) = e^{\tilde{m}X/2}, \quad (5.1)$$

with L and X begin real constants. For this moduli matrix, the n_1 string axes in the vacuum $\langle 1 \rangle$ are alined on the x^1 axis with the separation L . The other real parameter X is introduced to shift the configuration along the x^3 direction.

In Fig. 36, we show two examples for $n_1 = 7$ and $n_1 = 15$. We set $X = 20$ for $n_1 = 7$ and $X = 40$ for $n_1 = 15$, and $L = 3$ for both solutions. Since the vortex strings are degenerate if they are seen very far from the junction points, the asymptotic bending of the domain wall is logarithmic $\sim \log \rho^{2n_1}$. However, the structure near the junction points is not logarithmic. The panels (b1) of Fig. 36 show the domain wall energy density on the cross-section at $x^1 = 0$. Increasing the number of aligned vortex strings, the domain wall at the vicinity of junction points becomes locally flat. Area of the flat region increases if we put more and more vortex strings on the line.

Emergence of the flat part can be understood as follows. As before, the domain wall's position can be read from the master equation as

$$x^3(x^1, x^2) = -\frac{1}{2\tilde{m}} u_S^{(n_1)}(x^1, x^2) + X, \quad (5.2)$$

where $u_S^{(n_1)}$ is a solution of the vortex master equation

$$\partial_a^2 u_S^{(n_1)} - 1 + \prod_k |z - kL|^2 e^{-u_S^{(n_1)}} = 0. \quad (5.3)$$

If the separation L is sufficiently larger than 1, the solution $u_S^{(n_1)}$ to the vortex master equation can be well approximated by a simple superposition of $u_S^{(1)}$ as

$$u_S^{(n_1)}(x^1, x^2) \simeq \hat{u}_S^{(n_1)}(x^1, x^2) \equiv \sum_k u_S^{(1);k}(x^1, x^2), \quad (L \gg 1), \quad (5.4)$$

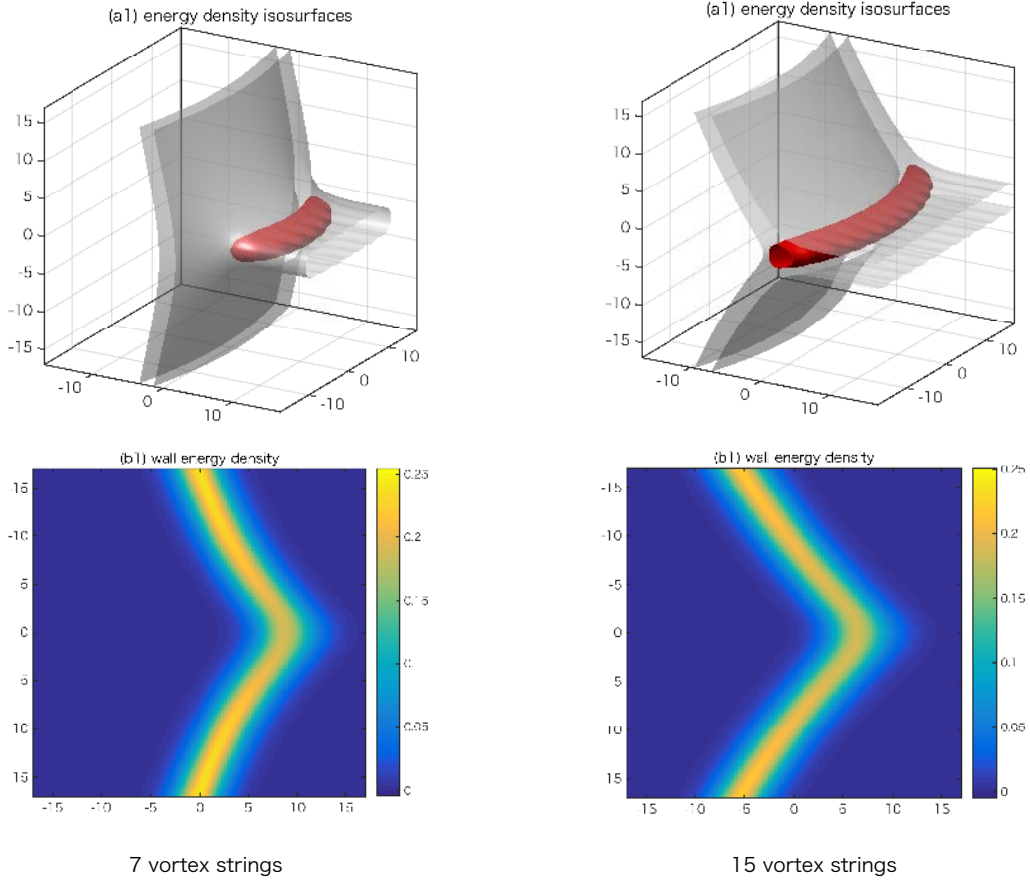


Figure 36: The $n_1 = 7$ (left) and $n_1 = 15$ (right) vortex strings ending on the domain wall from one side. The separation of neighbouring strings is $L = 3$. The gray surfaces in the panels (a1) are energy density isosurfaces and the red ones correspond to a boojum charge density isosurfaces. The panels (b1) show the domain wall energy density on the cross-section at $x^2 = 0$.

where $u_S^{(1);k}(x^1, x^2)$ is the single vortex string at $z = kL$, namely solution to the master equation

$$\partial_a^2 u_S^{(1);k} - 1 + |z - kL|^2 e^{-u_S^{(1);k}} = 0. \quad (5.5)$$

In the region around $z = kL$, we have $u_S^{(1);k'} \simeq \log |z - k'L|^2$ for $k' \neq k$. Therefore, the approximate solution there becomes

$$\hat{u}_S^{(n_1)}(x^1, x^2) = u_S^{(1);k} + \sum_{k'(\neq k)} \log |z - k'L|^2, \quad (|z - kL| \ll 1). \quad (5.6)$$

Plugging this into Eq. (5.3), one can confirm that the approximation works well.

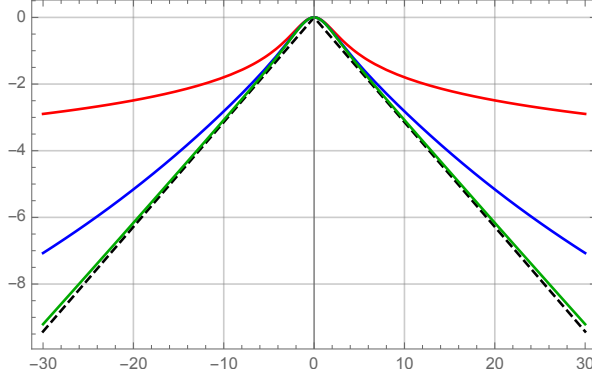


Figure 37: The approximate solution $-\frac{1}{2} \left(\hat{u}_S^{(n_1)}(x^1 = 0, x^2) - \hat{u}_S^{(n_1)}(0, 0) \right)$ is shown for $n_1 = 1$ (red), $n_1 = 7$ (blue), and $n_1 = 101$ (green). The black dashed line is $-\frac{\pi}{L}|x^2|$. L is set to be 10.

Thus, the domain wall's position in the $x^1 = 0$ plane is approximated by

$$\begin{aligned} x^3(0, x^2) &\simeq -\frac{1}{2\tilde{m}} \sum_k \hat{u}_S^{(1);k}(0, x^2) + X, \\ &\sim -\frac{1}{2\tilde{m}} \sum_k \log((x^2)^2 + k^2 L^2) + X. \end{aligned} \quad (5.7)$$

We choose $X = (\sum_k \log kL)/\tilde{m}$, so that the junction point at $z \simeq 0$ is independent of k . In Fig. 37 we show $x^3(0, x^2)$ for $n_1 = 1, 7, 101$ for $L = 10$ and $\tilde{m} = 1$. The domain wall becomes linear as n_1 is increased, and it gets close to the linear function at $n_1 \rightarrow \infty$ limit

$$\begin{aligned} \lim_{n_1 \rightarrow \infty} \tilde{m} x^3(0, x^2) &= -\frac{1}{2} \sum_{k=-\infty}^{\infty} \log((x^2)^2 + k^2 L^2) + \sum_{k=1}^{\infty} \log(kL) \\ &= -\log|x^2| - \sum_{k=1}^{\infty} \log\left(1 + \frac{(x^2)^2}{k^2 L^2}\right) \\ &= -\log|x^2| - \log \frac{\sinh \frac{\pi|x^2|}{L}}{\frac{\pi|x^2|}{L}} \\ &= -\log \sinh \frac{\pi|x^2|}{L} - \log \frac{L}{2\pi} \\ &\rightarrow -\frac{\pi}{L}|x^2| - \log \frac{L}{2\pi}, \quad (\pi|x^2| \gg L), \end{aligned} \quad (5.8)$$

where we have used the relation $\prod_{k=1}^{\infty} \left(1 + \frac{\alpha^2}{k^2}\right) = \frac{\sinh \pi\alpha}{\pi\alpha}$.

There is nice physical observation which explains the appearance of the factor π/L in the asymptotic angle of the flat domain wall. From the view point of the

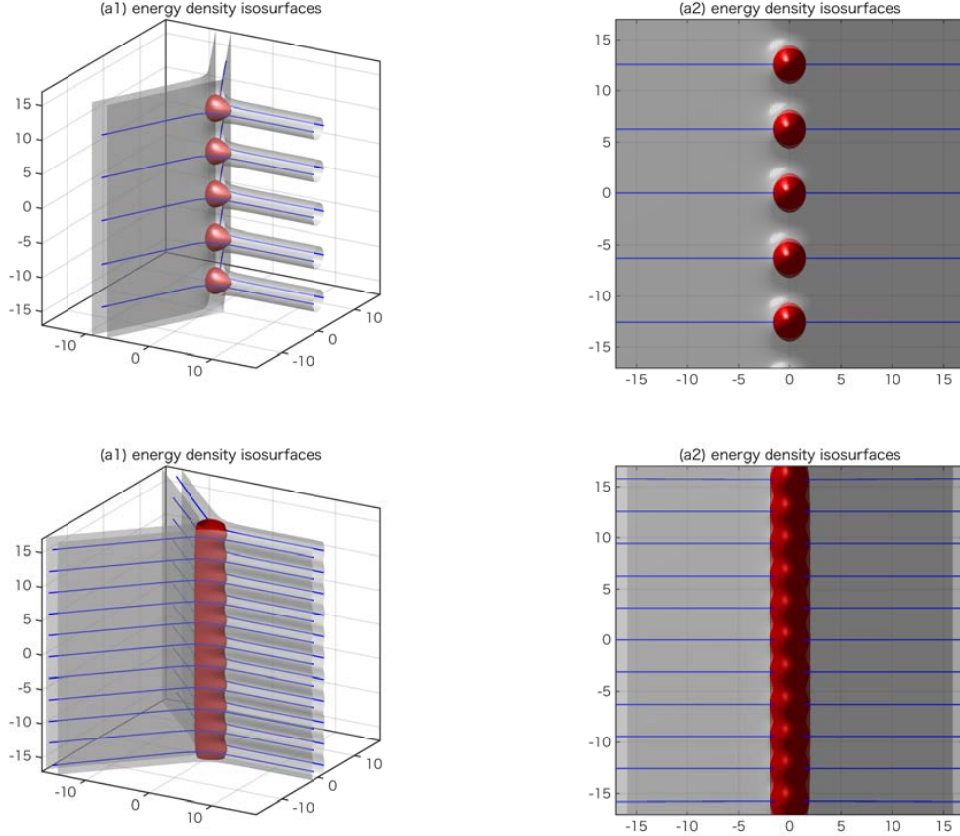


Figure 38: Periodically aligned vortex strings with period 2π (upper panels) and π (lower panels) are shown. The gray surfaces show the energy density isosurfaces, the red surfaces show the boojum density isosurfaces and the blue lines show several magnetic force lines.

domain wall the end points of vortex strings are interpreted as the magnetic sources in $2 + 1$ dimensional sense. Consider the magnetic scalar potential defined by

$$\tilde{\varphi}(x^1, x^2) = \frac{\tilde{m}}{\tilde{d}_W} x^3(x^1, x^2) = \frac{-1}{2\tilde{d}_W} u_S^{(n_1)}(x^1, x^2). \quad (5.9)$$

Suppose that we have the infinite point-like magnetic sources on a line, say the x^1 axis, with the period L . Due to the symmetry of this source arrangement, the magnetic force lines far from the x^1 axis become parallel to the x^2 axis. There is one magnetic source of the magnetic charge $\tilde{q}_B = 2\pi/\tilde{d}_W$ (see the discussions in in Sec. 3.5) at every finite segment $x^1 \in [x_0, x_0 + L]$ for an arbitrary x_0 . Therefore, seen far from the sources, the magnetic charge density is \tilde{q}_B/L . The magnetic force lines from these source equally expand both to $x^2 > 0$ and $x^2 < 0$ regions. Thus, we should have

$$\tilde{\varphi} \simeq -\frac{\tilde{q}_B}{2L} |x^2| = -\frac{\pi}{\tilde{d}_W L} |x^2|. \quad (5.10)$$

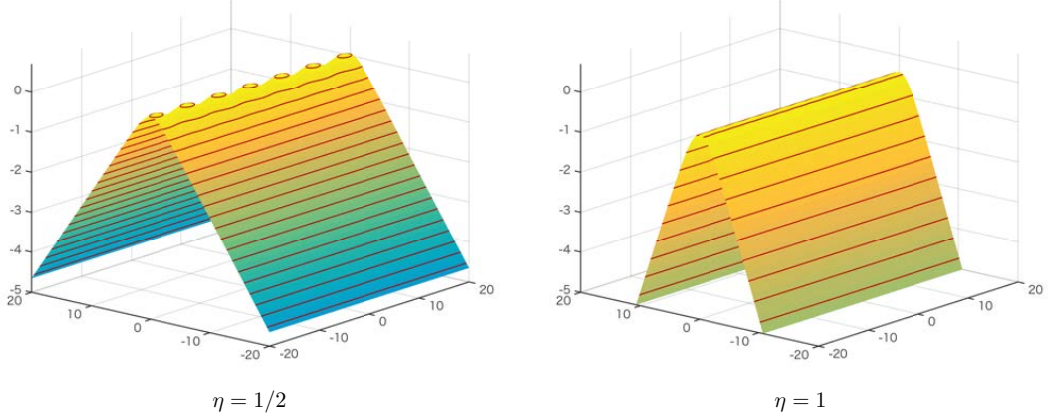


Figure 39: The magnetic scalar potentials for the periodically aligned vortex strings with periods 2π ($\eta = 1/2$) and π ($\eta = 1$).

Combining this with Eq. (5.9), we correctly find the asymptotic behavior given in Eq. (5.8).

In order to get vortex strings periodically aligned on a line, it is better to use holomorphic trigonometric functions rather than polynomial functions [52]. For example, we choose the following moduli matrix

$$H_0 = (\sin i\eta z, 1). \quad (5.11)$$

The positions of the vortex strings correspond to the zeros of the first elements, namely $z = (\pi i/\eta)n$ ($n \in \mathbb{Z}$). An advantage of using the trigonometric function is that one does not need to shift the domain wall's position by adjusting the X parameter for the polynomial case in Eq. (5.1). In Fig. 38, we show two examples with sparsely aligned ($\eta = 1/2$: the period is 2π) and densely aligned ($\eta = 1$: the period π) vortex strings ending on the domain wall from one side. Since the moduli matrix includes the infinite number of vortex strings, the domain wall becomes asymptotically exactly flat with the slanting angle η . Namely, the domain wall's position is estimated by $e^{-2\tilde{m}x^3} \simeq |\sin i\eta z|^2$,

$$\begin{aligned} x^3 &= -\frac{1}{2\tilde{m}} \log (\cosh^2 \eta x^1 \sin^2 \eta x^2 + \sinh^2 \eta x^1 \cos^2 \eta x^2) \\ &\rightarrow -\frac{\eta}{\tilde{m}} |x^1| + \frac{1}{\tilde{m}} \log 2, \quad (|x^1| \rightarrow \infty). \end{aligned} \quad (5.12)$$

The magnetic scalar potentials $\tilde{\varphi} = -u_S/2\tilde{d}_W$ for $\eta = 1/2, 1$ are shown in Fig. 39 for $\tilde{m} = 1$ ($\tilde{d}_W = 2$). As expected, it is clear that the potentials are asymptotically exactly linear in $|x^1|$, reflecting the asymptotic flatness of domain wall.

5.2 Linearly aligned vortex strings ending on a domain wall from two sides

Let us next consider configurations with periodically aligned infinite vortex strings ending on the domain wall from both sides. The corresponding moduli matrix is given by

$$H_0 = (\sin i\eta_1(z - Z_1), \sin i\eta_2(z - Z_2)), \quad (5.13)$$

with $Z_{1,2}$ being complex constants. We set $\eta_1 = \eta_2 = \eta$ to be real constants, so that the vortex strings are aligned on the lines $x^1 = \text{Re}(Z_{1,2})$ parallel to the x^2 axis with period π/η . We show two examples of this kind in Figs. 40 and 41 with $\tilde{m} = 1$. In the former figure, we take $Z_1 = -Z_2 = 10, 5, 0$ with $\eta = 1/2$ (the period is 2π). In the latter figure, we shift the vortex strings at the negative x^3 side by $\delta x^2 = \pi$. Namely, we take $Z_1 = -Z_2 + i\pi = 10, 5, 0$. Far from the vortex strings the domain wall is flat and perpendicular to the $x^1 - x^2$ plane. On the other hand, between the vortex strings the domain wall is flat but slanted as $x^3 \simeq 2\eta x^1$, which is twice steeper than for the domain wall with the vortex strings just on the one side, see Eq. (5.12). This is, of course, because we have two lines of vortex strings. The shape of the domain wall is determined by superposition, as was discussed in Eq. (4.8). For example, the domain wall's position can be estimated for real positive $Z > 0$ as follows,

$$\tilde{m}x^3 \simeq -\eta|x_1 - Z| + \eta|x_1 + Z| = \begin{cases} 2\eta Z & 2Z < x^1 \\ 2\eta x^1 & \text{for } -2Z < x^1 < 2Z \\ -2\eta Z & x^1 < -2Z \end{cases}. \quad (5.14)$$

Comparing Figs. 40 and 41 we can see that the shift $\delta x^2 = \pi$ in Fig. 41 did not affect the resulting configuration very much. Only the local structure around the end points received small deformation but the asymptotic structure is not changed. The formula (5.14) also remains correct.

Let us interpret the above 1/4 BPS configurations from the view point of 2 + 1 dimensions. The corresponding magnetic scalar potential is given as follows

$$\begin{aligned} \tilde{\varphi} &= -\frac{1}{2\tilde{d}_W} u_S|_{+Z} + \frac{1}{2\tilde{d}_W} u_S|_{-Z} \\ &= \frac{\tilde{m}}{\tilde{d}_W} \left(x^3|_{+Z} + x^3|_{-Z} \right) \\ &\simeq \frac{\eta}{\tilde{d}_W} (-|x_1 - Z| + |x_1 + Z|). \end{aligned} \quad (5.15)$$

We plot the magnetic scalar potential $\tilde{\varphi}$ in Fig. 42 which reproduces the correct structure of the kinky domain wall.

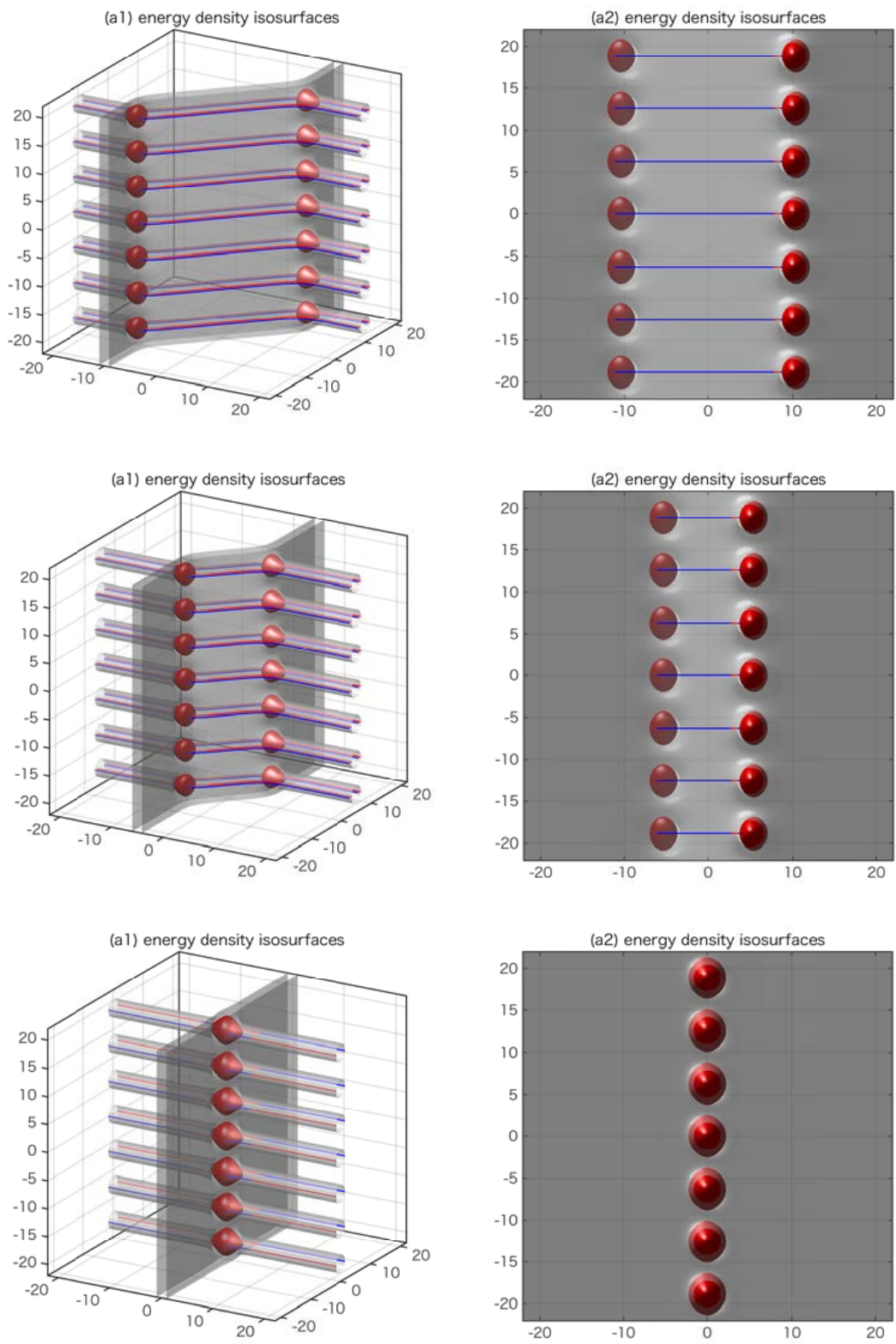


Figure 40: The plots of the energy density isosurfaces of periodic vortices ending on 1 wall from two sides. The distances between vortices are $Z = 10$ (top), $Z = 5$ (middle), and $Z = 0$ (bottom).

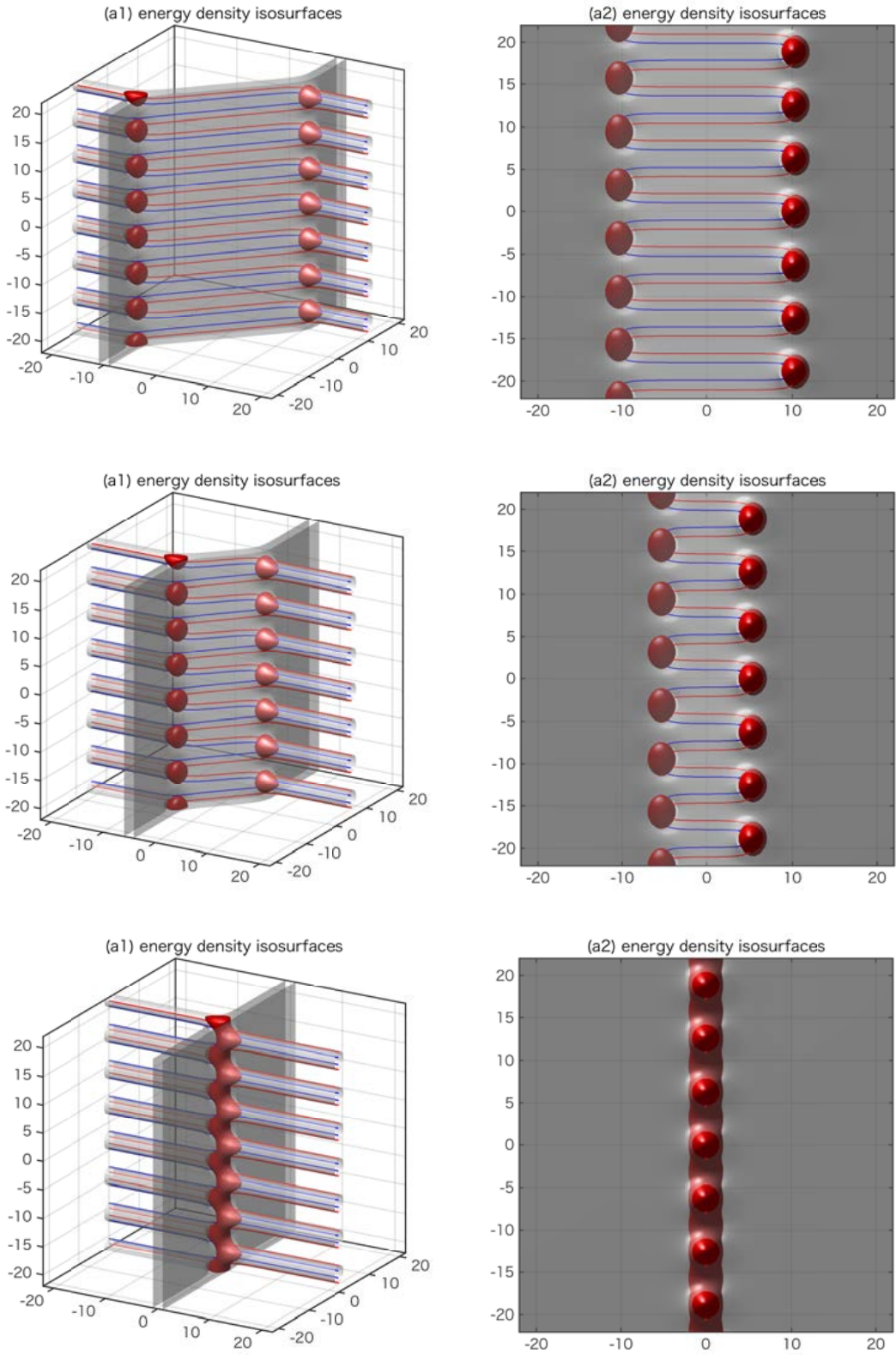


Figure 41: The plots of the energy density isosurfaces of periodic vortices aligned alternately ending on 1 wall from two sides. The distances between vortices are $Z = 10$ (top), $Z = 5$ (middle), and $Z = 0$ (bottom).

The last expression in Eq. (5.15) is reminiscent of the electric scalar potential for an electric capacitor. Hence, we may call the configuration with the magnetic scalar potential given in Eq. (5.15) a *magnetic capacitor* in $2 + 1$ dimensions. Let us define a density of magnetic capacitance \tilde{c}_M by

$$\tilde{c}_M \delta \tilde{V}_B = \frac{\tilde{Q}_B}{\pi/\eta}, \quad (5.16)$$

where $\delta \tilde{V}_B = \tilde{d}_W \tilde{\varphi}|_{x^2=Z} - \tilde{d}_W \tilde{\varphi}|_{x^2=-Z}$ stands for the difference of the magnetic potential and $\tilde{Q}_B = \tilde{q}_B \tilde{d}_W$ is the magnetic charge per unit length. We have $\delta \tilde{\varphi} = 4\eta Z/\tilde{d}_W$ and $\tilde{q}_B = 2\pi/\tilde{d}_W$, thus we conclude that the domain wall has the magnetic capacitance

$$\tilde{c}_M = \frac{1}{2Z}. \quad (5.17)$$

As an ordinary electric capacitance of a flat capacitor, the capacitance is inversely proportional to the distance of the charges.

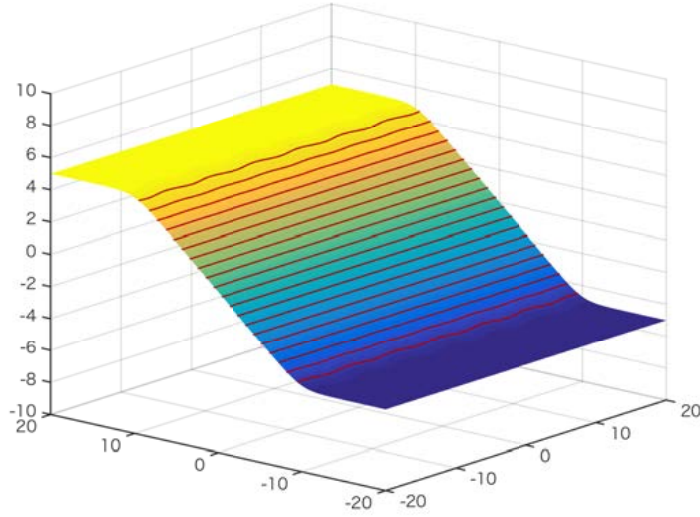


Figure 42: The magnetic scalar potential (5.15) for the moduli matrix given in Eq. (5.13) with $Z = Z_1 = -Z_2 = 10$, $\eta = 1/2$ and $\tilde{m} = 1$.

The energy stored in the magnetic capacitor is given by

$$\delta \tilde{\mathcal{E}}_M = \frac{1}{2} \tilde{c}_M \delta \tilde{V}_M^2 = 4\eta^2 Z. \quad (5.18)$$

This can be accounted by the following geometric consideration about the domain wall and the vortex strings. Suppose the domain wall did not bend by the vortex strings. Then the energy for the part between two linearly aligned vortex strings, namely $x^1 \in [-Z, Z]$ are proportional to the distance $2Z$ as is depicted in the left

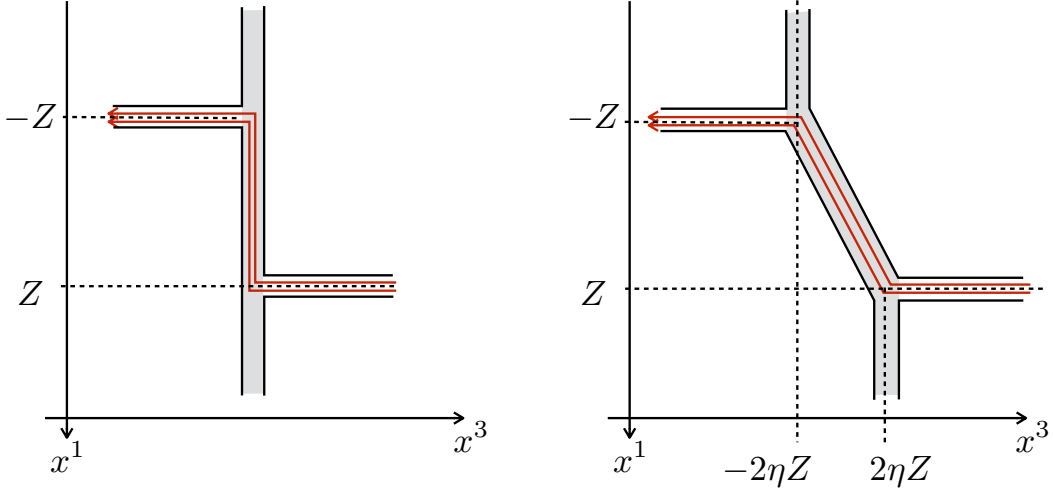


Figure 43: Schematic picture for the ideal (real) domain wall (gray region) with periodically aligned vortex strings from both sides is shown in the left (right) panel. Red lines stand for the incoming and outgoing magnetic fluxes from the vortex strings.

panel of Fig. 43. In reality, of course, the domain wall linearly bends as is shown in the right panel of Fig. 43. The bent domain wall is longer than flat one by

$$\delta\tilde{L} = 2Z\sqrt{1+4\eta^2} - 2Z \simeq 4\eta^2 Z, \quad (5.19)$$

for $\eta \ll 1$. This coincides with the energy stored in the magnetic capacitor given in Eq. (5.18).

5.3 Vortex strings ending on a slanting domain wall

Next, we consider the following moduli matrix which is slightly different from the one given in Eq. (5.13)

$$\begin{aligned} H_0 &= \left(\frac{e^{-\eta(z-Z)} - e^{\eta(z-Z)-2\xi}}{2i}, \frac{e^{-\eta(z+Z)-2\xi} - e^{\eta(z+Z)}}{2i} \right) \\ &= e^{-\xi} \left(\sin i\eta \left(z - Z - \frac{\xi}{\eta} \right), \sin i\eta \left(z + Z + \frac{\xi}{\eta} \right) \right). \end{aligned} \quad (5.20)$$

As is discussed in the previous subsection, this moduli matrix generates the configuration with the linearly aligned vortex strings at $z = i\frac{\pi}{\eta}n \pm \left(Z + \frac{\xi}{\eta} \right)$ with $n \in \mathbb{Z}$. Now, we send all the vortex strings to the spatial infinity by taking the limit $\xi \rightarrow \infty$. We are left with

$$H_0 = \left(\frac{e^{-\eta(z-Z)}}{2i}, \frac{-e^{\eta(z+Z)}}{2i} \right) \simeq (1, -e^{2\eta z}), \quad (5.21)$$

where we used the so-called V -transformation that transforms the moduli matrix as $H_0 \rightarrow V(z)H_0$ and $u \rightarrow 2\log V(z)$ with arbitrary invertible holomorphic function

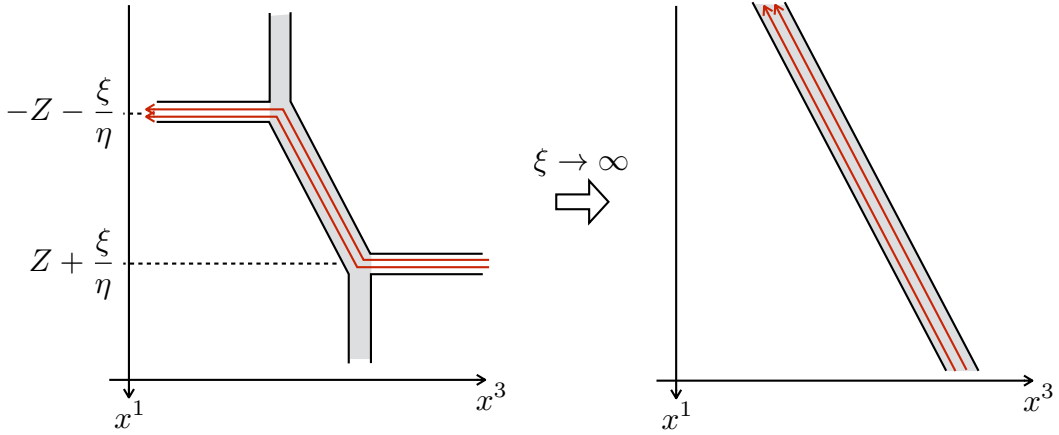


Figure 44: The slant domain wall as a limit of sending the vortex strings toward the spacial infinities.

$V(z)$ [31, 30, 34]. The V -transformation does not change any physics. Since we just shifted the vortex strings to the spacial infinities, the domain wall shape is given by the Eq. (5.14) with replacement Z by $Z + \xi/\eta$. Especially, the domain wall between the lines of the vortex strings keeps being slant with the same angle, see Fig. 44. This holds even in the limit $\xi \rightarrow \infty$. Furthermore, we know the existence of the vortex strings behind the spacial boundaries $x^1 = \pm\infty$, which provides a background magnetic fluxes $4\pi/(\pi/\eta) = 2\eta$ per unit length. In short, the flat domain wall slants when a background magnetic field is turned on [30]. The 1/4 BPS master equation for the moduli matrix (5.21) is given by

$$\partial_k^2 u - 1 + \left(e^{\tilde{m}x^3} + e^{4\eta x^1} e^{-\tilde{m}x^3} \right) e^{-u} = 0. \quad (5.22)$$

This can be rewritten as

$$\partial_k^2 u - 1 + \left(e^{\tilde{m}x^3 - 2\eta x^1} + e^{-\tilde{m}x^3 + 2\eta x^1} \right) e^{-u + 2\eta x^1} = 0. \quad (5.23)$$

Introducing the new coordinate by

$$\begin{pmatrix} y_3 \\ y_1 \end{pmatrix} = \begin{pmatrix} \cos \alpha & -\sin \alpha \\ \sin \alpha & \cos \alpha \end{pmatrix} \begin{pmatrix} x_3 \\ x_1 \end{pmatrix}, \quad \tan \alpha = \frac{2\eta}{\tilde{m}}, \quad (5.24)$$

and define a function by

$$\hat{u} = u - 2\eta x^1, \quad (5.25)$$

we find that \hat{u} is the solution to

$$\left(\frac{\partial^2}{\partial y_3^2} + \frac{\partial^2}{\partial y_2^2} \right) \hat{u} - 1 + \left(e^{\hat{m}y^3} + e^{-\hat{m}y^3} \right) e^{-\hat{u}} = 0, \quad (5.26)$$

where we defined $\hat{m} \equiv \sqrt{\tilde{m}^2 + 4\eta^2}$. Clearly, \hat{u} does not depend on y^1 , so that we identify that \hat{u} is identical to the domain wall solution written in the rotated coordinate y^3 with the mass parameter \hat{m} . In the original coordinates, the solution is given by

$$u(x^k) = u_W(x^3 - x^1 \tan \alpha) + 2\eta x^1. \quad (5.27)$$

The position of domain wall is determined by the condition $x^3 \cos \alpha - x^1 \sin \alpha = 0$, namely it is

$$x^3 = (\tan \alpha)x^1 = \frac{2\eta}{\tilde{m}}x^1. \quad (5.28)$$

This is consistent with the previous result given in Eq. (5.14).

Next, we put a single vortex string in the first vacuum $\langle 1 \rangle$. The corresponding moduli matrix is given by

$$H_0 = (z, -e^{2\eta z}). \quad (5.29)$$

The master equation for this can be expressed as follows

$$\partial_k^2 u - 1 + \left(e^{\tilde{m}x^3 - 2\eta x^1 + \log |z|} + e^{-\tilde{m}x^3 + 2\eta x^1 - \log |z|} \right) e^{-u + 2\eta x^1 + \log |z|} = 0. \quad (5.30)$$

An appropriate initial configuration for the gradient flow equation to this is

$$\mathcal{U}(x^k) = u_W \left(x^3 - \frac{2\eta}{\tilde{m}}x^1 + \frac{1}{2\tilde{m}}u_S(x^a) \right) + 2\eta x^1 + \frac{u_S(x^a)}{2}. \quad (5.31)$$

We show a numerical solution for $\tilde{m} = 1$ and $\eta = 1/4$ in Fig. 45 which clearly demonstrates the vortex string parallel to the x^3 axis ends on the slanting and logarithmically bending domain wall. The junction point is accompanied with the boojum which is also sheared as shown in the panel (b3) of Fig. 45. Interestingly, the magnetic force lines supplied by the vortex string do not spread out in the domain wall but flow toward a direction as forming a stringy flux in $2 + 1$ dimensions, see the panel (a1) and (a2) in Fig. 45. This squeezing of the magnetic flux inside the domain wall occurs because the magnetic force lines from the vortex string repel with those of the background magnetic flux on the slanting domain wall.

This magnetic scalar potential can be read from Eq. (5.31) as

$$\tilde{\varphi} = -\frac{1}{2\tilde{d}_W}u_S + \frac{2\eta}{\tilde{d}_W}x^1 \quad (5.32)$$

and again correctly capture these features. The first term corresponds to the potential generated by the end point of the vortex string and the second one expresses the potential for the background magnetic field. We plot stream lines of the magnetic fields $\tilde{B}_a = -\partial_a \tilde{\varphi}$ for $\eta = 0, 1/10, 1/4$ in Fig. 46 where we compare two cases: the

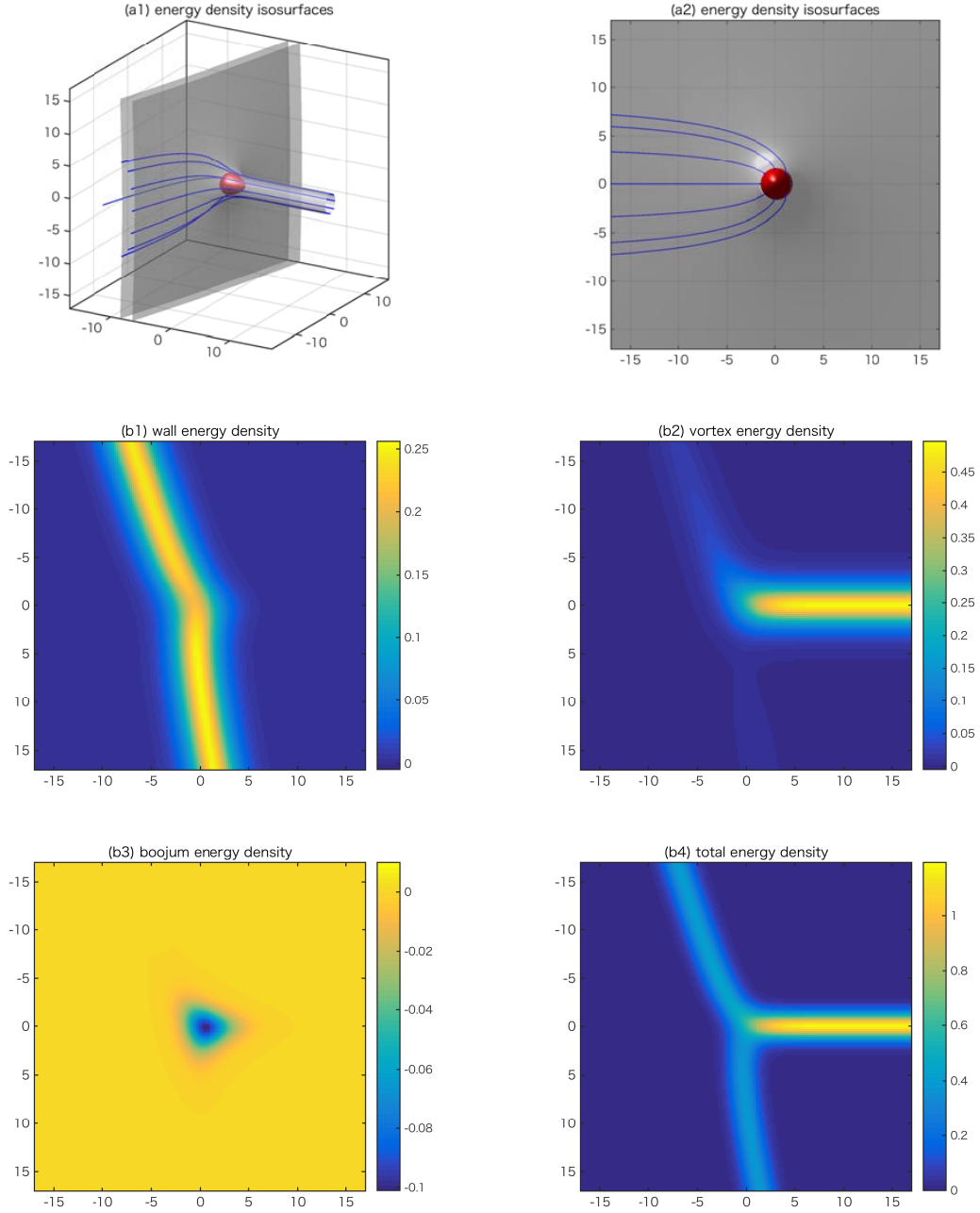


Figure 45: The plots show the energy density isosurfaces of one vortex ending on one slant wall (a1, a2), where the blue and the red curves show magnetic fluxes, the wall energy density (b1), the vortex energy density (b2), the boojum energy density (b3) and the total energy density (b4).

strong gauge coupling limit with $u_s = \log \rho^2$ (the first row) and the finite gauge coupling case (the second row). The flux lines emitted from the positive magnetic source are absorbed into the negative magnetic charges aligned periodically at $x^1 \rightarrow -\infty$,

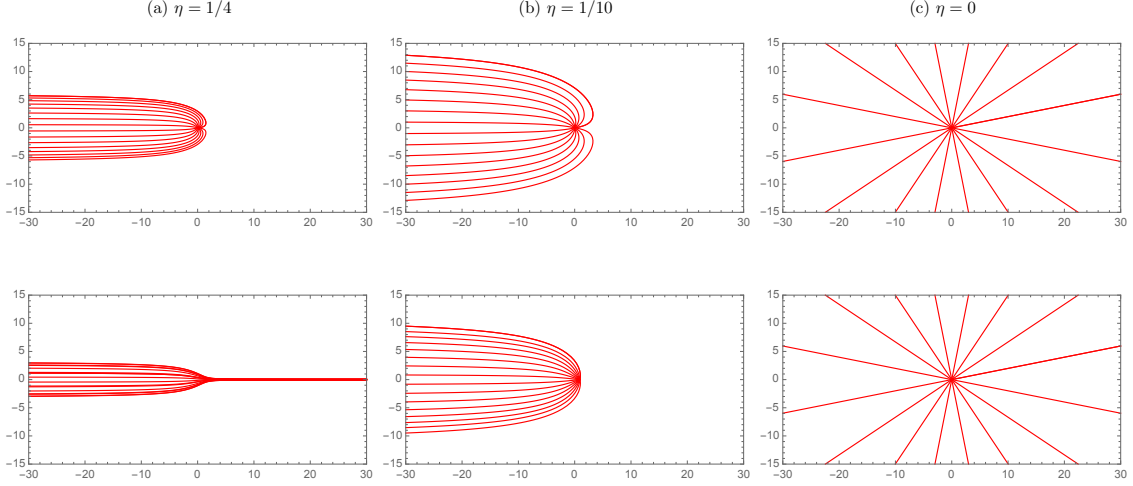


Figure 46: The stream lines of the magnetic field $\tilde{B}_a = -\partial_a \tilde{\varphi}$. We plot the lines which pass the points on the unit circle surrounding the origin. The figures in the first row are for the point charge with $u_S = \log \rho^2$. The figures in the second row are for the finite size source with u_S for the finite gauge coupling.

so that they are squeezed. This situation is quite similar to the squeezing of the magnetic fluxes by the Higgs mechanism but it is not the case because no further symmetries are broken in the domain wall.

Finally, we put another vortex string from the other side of the domain wall. The moduli matrix is

$$H_0 = ((z - Z)e^{\eta z}, -(z + Z)e^{-\eta z}). \quad (5.33)$$

The vortex string on the positive (negative) x^3 side is at $z = Z$ ($z = -Z$), and the domain wall is asymptotically flat but slanting as

$$x^3 = -\frac{1}{2\tilde{m}}u_S|_{z=+Z} + \frac{1}{2\tilde{m}}u_S|_{z=-Z} + \frac{2\eta}{\tilde{m}}x^1 \rightarrow \frac{2\eta}{\tilde{m}}x^1, \quad (\rho \rightarrow \infty). \quad (5.34)$$

We show several numerical solutions in Figs. 47 and 48 for $\tilde{m} = 1$ and $\eta = 1/4$. We set $Z = 6$ in Fig. 47 and $Z = 4, 2, 0$ in Fig. 48. The configurations are similar to those given in Figs. 21 and 22 which show the solutions of the flat and non-slanting domain wall with vortex strings from both sides. A remarkable difference between non-slant and slant configurations can be found in distribution of the magnetic force lines inside the domain wall. The flux lines are quite similar to those around an ordinary magnetic dipole in the non-slanting domain wall, see Fig. 22. On the other hand, they are squeezed in the slanting domain wall, so if we arrange the vortex strings in such a way that the line segment connecting two end points is exactly parallel to the steepest direction of the slanting domain wall (the injecting vortex

string is on the upper side and the ejecting one is on the lower side), the flux lines are as if confined, see Fig. 48.

Now we can naturally generalize the configuration to have any slanting angle and any number of vortex strings from both sides. The magnetic scalar potential is the most useful tool to describe it by

$$\tilde{d}_W \tilde{\varphi} = - \sum_{k_1=1}^{n_1} \frac{1}{2} u_S|_{z=Z_{k_1}} + \sum_{k_2=1}^{n_2} \frac{1}{2} u_S|_{z=Z_{k_2}} + \tilde{B}_a^{(\text{bg})} x^a, \quad (5.35)$$

where $u_S|_{z=Z_k}$ stands for the solution of vortex string at $z = Z_k$, and $\tilde{B}_a^{(\text{bg})}$ is the background magnetic field.

The magnetic flux lines for $(n_1, n_2) = (1, 1)$ are shown in Fig. 49. We put the vortex string at $Z_{n_1=1} = -Z_{n_2=1} = 20e^{i\theta}$ with $\theta = 0, \frac{\pi}{4}, \frac{\pi}{2}, \frac{3\pi}{4}, \pi$ for $\tilde{B}_a^{(\text{bg})} = 2\eta\delta_{1a}$ with $\eta = \frac{1}{15}$ and $\tilde{m} = 1$ ($\tilde{d}_W = 2$). As shown in (a1) of Fig. 49, the magnetic sources are confined only when $\theta = 0$, where the magnetic flux lines from the positive source go into the negative magnetic source. When we rotate the sources, a part of flux lines run toward the boundaries, see (a2) – (a5) of Fig. 49. When we turn off the background magnetic field, we have the magnetic dipole regardless of the rotating angle as (b) of Fig. 49.

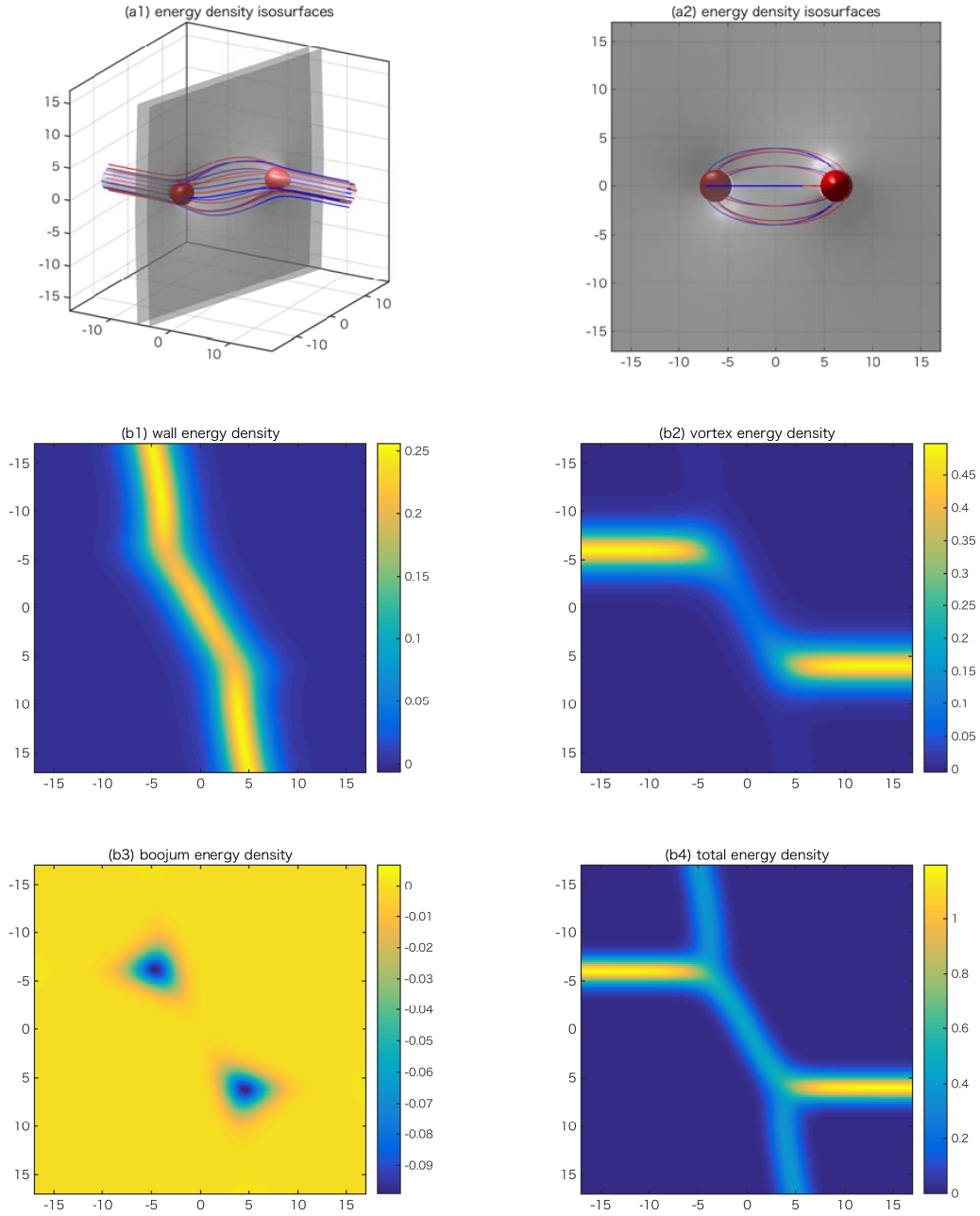


Figure 47: The plots show the energy density isosurface of two vortices ending on one slant wall (a1, a2), where the blue and the red curves show magnetic fluxes, the wall energy density (b1), the vortex energy density (b2), the boojum energy density (b3) and the total energy density (b4). The distance of two vortices is taken to be $Z = 6$.

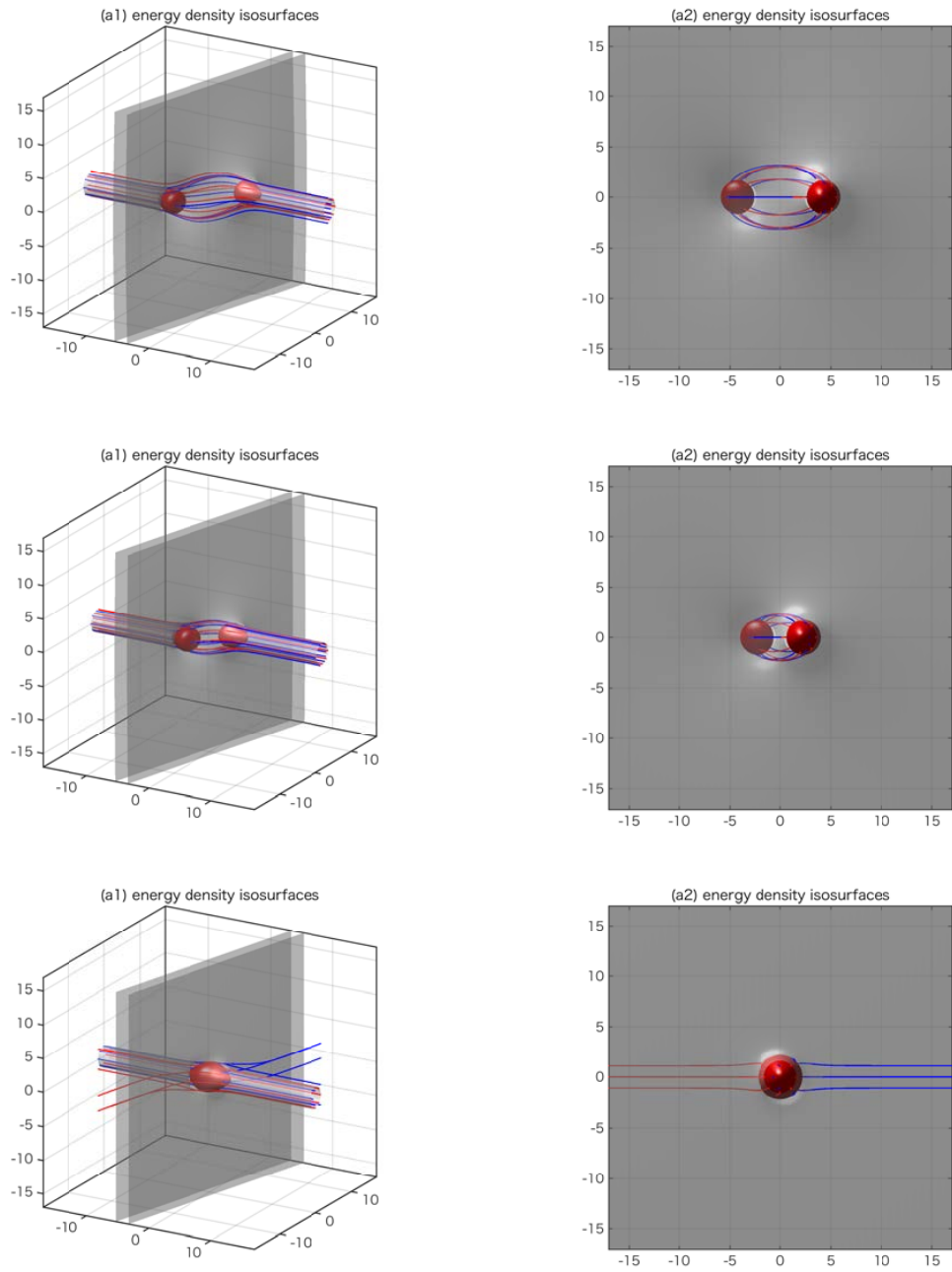


Figure 48: The plots show the energy density isosurfaces of two vortices ending on one slant wall from two sides. The distance between two vortices are taken to be $Z = 4, 2, 0$ from top to bottom.

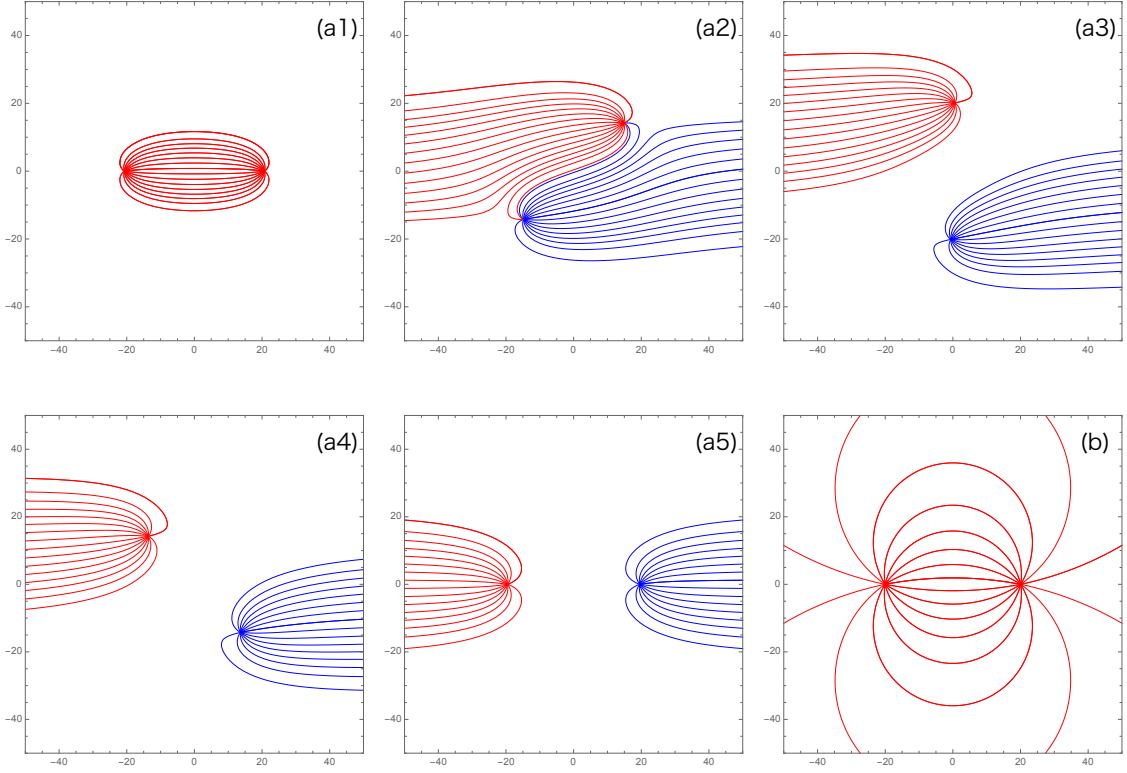


Figure 49: The stream lines of the magnetic field $\tilde{B}_a = -\partial_a \tilde{\varphi}$. The red lines are fluxes from the positive charge and the blue ones are those going into the negative charge. The panels (a1) – (a5) are with the background magnetic field while the panel (b) is without it.

6. Dyonic extension

6.1 Basic formulae

In this section we will study a dyonic extension of the purely magnetic 1/4 BPS equations (2.16)–(2.19) [69, 74]. A perfect square of the energy density including time dependence is given by

$$\begin{aligned}
\mathcal{E} = & \frac{1}{2g^2} \left\{ (\xi F_{12} - \eta \cos \alpha \partial_3 \sigma - g^2 (HH^\dagger - v^2))^2 + (F_{0k} - \sin \alpha \partial_k \sigma)^2 + (\partial_0 \sigma)^2 \right. \\
& + (\xi F_{23} - \eta \cos \alpha \partial_1 \sigma)^2 + (\xi F_{31} - \eta \cos \alpha \partial_2 \sigma)^2 \left. \right\} \\
& + |(D_1 + i\xi D_2)H|^2 + |D_0 H + i \sin \alpha (\sigma H - HM)|^2 \\
& + |D_3 H + \eta \cos \alpha (\sigma H - HM)|^2 \\
& + v^2 \eta \cos \alpha \partial_3 \sigma - \xi v^2 F_{12} + \xi \eta \cos \alpha \partial_i \left(\frac{\sigma}{g^2} \epsilon_{ijk} F_{jk} \right) \\
& + i \sin \alpha (HMD_0 H^\dagger - D_0 H M H^\dagger) \\
& + \partial_k j_k + \sin \alpha \partial_k \left(\frac{\sigma}{g^2} F_{0k} \right) \\
& - \sin \alpha \left\{ \frac{1}{g^2} \partial_k F_{0k} + i (HD_0 H^\dagger - D_0 H H^\dagger) \right\}, \tag{6.1}
\end{aligned}$$

where we restrict α to satisfy $\alpha \in (-\pi/2, \pi/2)$ because $\cos \alpha$ always appears accompanied with $\eta = \pm 1$. The non-topological currents $j_{a=1,2}$ are the same as in (2.12) while $j_{k=3}$ is given by

$$j_3 = -\eta \cos \alpha (\sigma H - HM) H^\dagger. \tag{6.2}$$

Vanishing of the squared terms leads to the dyonic extension to 1/4 BPS equations

$$D_0 H + i \sin \alpha (\sigma H - HM) = 0, \tag{6.3}$$

$$D_3 H + \eta \cos \alpha (\sigma H - HM) = 0, \tag{6.4}$$

$$(D_1 + i\xi D_2)H = 0, \tag{6.5}$$

$$\eta \cos \alpha \partial_1 \sigma = \xi F_{23}, \quad \eta \cos \alpha \partial_2 \sigma = \xi F_{31}, \tag{6.6}$$

$$\sin \alpha \partial_k \sigma = F_{0k}, \tag{6.7}$$

$$\xi F_{12} - \eta \cos \alpha \partial_3 \sigma - g^2 (|H|^2 - v^2) = 0, \tag{6.8}$$

$$\partial_0 \sigma = 0. \tag{6.9}$$

Also, one has to include the Gauss's law

$$\frac{1}{g^2} \partial_k F_{0k} + i (HD_0 H^\dagger - D_0 H H^\dagger) = 0, \tag{6.10}$$

which is obtained from (2.7). The parameters $\eta^2 = \xi^2 = 1$ labels (anti-)vortices $\xi = (-1)1$ and (anti-)walls $\eta = (-1)1$. In the strong gauge coupling limit, our Abelian-Higgs model reduces to the massive nonlinear sigma model whose target space is $\mathbb{C}P^{N_F-1}$, and the above dyonic extension reduces to the Q-kink lump configuration without the boojums, first studied in Ref. [11].

When the BPS equations (6.3)–(6.9) and the Gauss’s law are satisfied, the total energy density saturates the Bogomol’nyi bound

$$\mathcal{E} \geq (\mathcal{T}_W \cos \alpha + \mathcal{Q}_W \sin \alpha) + \mathcal{T}_S + (\mathcal{T}_B \cos \alpha + \mathcal{Q}_B \sin \alpha) + \partial_k j_k, \quad (6.11)$$

where $\mathcal{T}_{W,S,B}$ is defined in Eq. (2.15), and the Noether charge density and the electric Boojum charge density are defined by

$$\mathcal{Q}_W = i (HMD_0H^\dagger - D_0HMH^\dagger), \quad (6.12)$$

$$\mathcal{Q}_B = \partial_k \left(\frac{\sigma}{g^2} F_{0k} \right). \quad (6.13)$$

The set of the BPS equations (6.3)–(6.7) are solved via the moduli matrix formalism

$$H = ve^{-\frac{u}{2}} H_0(z) e^{M(x^3 \eta \cos \alpha + ix^0 \sin \alpha)}, \quad (6.14)$$

$$a_1 + i\xi a_2 = -i\partial_z u, \quad (6.15)$$

$$\sigma \eta \cos \alpha + ia_3 = \frac{1}{2} \partial_3 u, \quad (6.16)$$

$$\sigma \sin \alpha + a_0 = -\frac{i}{2} \partial_0 u. \quad (6.17)$$

We demand u to be real by fixing the gauge freedom. Thus, the equation (6.16) gives us

$$a_3 = 0, \quad \sigma = \frac{\eta}{2 \cos \alpha} \partial_3 u. \quad (6.18)$$

From Eq. (6.9) σ is independent of t . Then, Eq. (6.17) gives

$$a_0 = -\sigma \sin \alpha = -\frac{\eta}{2} \tan \alpha \partial_3 u. \quad (6.19)$$

Note that this also solves the Gauss’s law (6.10). Now, we can express the electric and magnetic field in terms of the single real function u as

$$E_k = \frac{\eta \tan \alpha}{2} \partial_k \partial_3 u, \quad (B_1, B_2, B_3) = \frac{\xi}{2} (\partial_3 \partial_1 u, \partial_2 \partial_3 u, -(\partial_1^2 + \partial_2^2)u). \quad (6.20)$$

Similarly, the topological charge densities are also expressed as

$$\mathcal{T}_W = \eta v^2 \partial_3 \sigma = \frac{v^2}{2 \cos \alpha} \partial_3^2 u, \quad (6.21)$$

$$\mathcal{T}_S = -\xi v^2 F_{12} = \frac{v^2}{2} (\partial_1^2 + \partial_2^2) u, \quad (6.22)$$

$$\begin{aligned} \mathcal{T}_B &= \frac{\eta \xi}{g^2} \epsilon_{klm} \partial_k (F_{lm} \sigma) \\ &= \frac{1}{2g^2 \cos \alpha} \{ (\partial_1 \partial_3 u)^2 + (\partial_2 \partial_3 u)^2 - (\partial_1^2 + \partial_2^2) u \partial_3^2 u \}. \end{aligned} \quad (6.23)$$

Finally, we are left with the equation (6.8) which turns into the master equation

$$\frac{1}{2g^2 v^2} \partial_k^2 u = 1 - \Omega_0 e^{-u}, \quad \Omega_0 = H_0 e^{2\eta \cos \alpha M x^3} H_0^\dagger. \quad (6.24)$$

Comparing this with the master equation (2.25) for the purely magnetic case, the only difference is the replacement M by $M \cos \alpha$.

The tension of the domain wall is the same as in the purely magnetic case

$$T_W = \int dx^3 \mathcal{T}_W = \eta v^2 [\sigma]_{x^3=-\infty}^{x^3=\infty} = v^2 \eta \Delta m = v^2 |\Delta m|. \quad (6.25)$$

The similar holds for the Noether charge. Combining Eqs. (6.3) and (6.4), we find

$$D_0 H = i \eta \tan \alpha D_3 H. \quad (6.26)$$

By using this, we have the following expression for \mathcal{Q}_W ,

$$\mathcal{Q}_W = \eta \tan \alpha \partial_3 (H M H^\dagger). \quad (6.27)$$

Thus, the Noether charge density upon the integration over x^3 gives a constant.

$$Q_W = \int dx^3 \mathcal{Q}_W = \eta \tan \alpha \left[H M H^\dagger \right]_{x^3=-\infty}^{x^3=\infty} = v^2 \Delta m \eta \tan \alpha. \quad (6.28)$$

Hence, the Noether charge per unit area is proportional to the domain wall tension

$$\frac{Q_W}{T_W} = \tan \alpha. \quad (6.29)$$

Therefore, the volume integral of \mathcal{Q}_W diverges as the domain wall mass which is proportional to $A = \int dx^1 dx^2$. Now, a part of the BPS mass can be calculated as

$$\int d^3 x (\mathcal{T}_W \cos \alpha + \mathcal{Q}_W \sin \alpha) = \frac{T_W}{\cos \alpha} A = \sqrt{T_W^2 + Q_W^2} A. \quad (6.30)$$

Contribution of the vortex string to the total mass is independent of $\cos \alpha$. Therefore, we have $T_S = 2\pi v^2 |k|$ where k stands for the vortex winding number, and then the mass of the vortex string is given by

$$\int d^3x \mathcal{T}_S = \int dx^3 T_S = 2\pi v^2 |k| L. \quad (6.31)$$

Let us next evaluate T_B , the boojum mass,

$$T_B = \frac{\eta \xi}{g^2} \int d^3x \partial_i (\sigma B_i). \quad (6.32)$$

This is easy to do for the case of flat domain walls since we have the same number k of straight vortex strings at both sides of the domain walls. The magnetic flux at $x^3 \rightarrow \pm\infty$ is given by $\int dx^1 dx^2 \xi B_i = -\delta_{i3} 2\pi |k|$. Therefore, we have

$$T_B = \frac{\eta}{g^2} \times (-2\pi |k|) \times [\sigma]_{x^3=-\infty}^{x^3=+\infty} = -\frac{2\pi}{g^2} |\Delta m| |k|. \quad (6.33)$$

This is independent of α as T_S . For configurations including bent domain walls, we should repeat the same computation as we have done in Sec. 3.2. But it is clear even for such cases that T_B is independent of α . Hence, the formula Eq. (6.33) is valid for any configurations. Contribution of the boojum to the total mass is then found as

$$\cos \alpha T_B = \frac{T_W}{\sqrt{T_W^2 + Q_W^2}} T_B. \quad (6.34)$$

Since T_B is negative definite, this makes the total mass larger. Next, we evaluate contribution from \mathcal{Q}_B given in Eq. (6.13). Using the BPS equations, it can be written as

$$\mathcal{Q}_B = \partial_k \left(\frac{\sigma}{g^2} F_{0k} \right) = \frac{\sin \alpha}{g^2} \partial_k (\sigma \partial_k \sigma) = \frac{\sin \alpha}{2g^2} \partial_k^2 \sigma^2. \quad (6.35)$$

Since the electric field is proportional to the derivative of σ , $E_k \propto \partial_k \sigma$, it is non-zero only inside the domain wall. Therefore, upon integration along x^3 , \mathcal{Q}_B vanishes. The contribution from the non-topological terms $\partial_k j_k$ also vanishes upon integration. Summing up all the contributions, we conclude that the mass of the dyonic 1/4 BPS configuration is given by

$$E_{1/4} = \sqrt{T_W^2 + Q_W^2} A + T_S L + \frac{T_W}{\sqrt{T_W^2 + Q_W^2}} T_B. \quad (6.36)$$

The electric charge density appearing in the Gauss' law (6.10) can be written as

$$\mathcal{Q}_E = i (D_0 H H^\dagger - H D_0 H^\dagger) = -\eta \tan \alpha \partial_3 (H H^\dagger). \quad (6.37)$$

This is very similar to \mathcal{Q}_W . Since we have $HH^\dagger = v^2$ at any vacua, $\int dx^3 \mathcal{Q}_E = 0$, so that net electric charge is zero. However, note that the electric charge density is non-zero everywhere.

As a final remark, the following relation

$$\begin{aligned}\vec{E} \cdot \vec{B} &= \frac{\eta\xi}{4} \tan \alpha \{ (\partial_1 \partial_3 u)^2 + (\partial_2 \partial_3 u)^2 - (\partial_1^2 + \partial_2^2) u \partial_3^2 u \} \\ &= \frac{g^2}{2} \xi \eta \sin \alpha \mathcal{T}_B,\end{aligned}\tag{6.38}$$

implies that E_k is perpendicular to B_k far from the boojums, while in their vicinity they are not.

6.2 The dyonic domain wall as an electric capacitor

The Q-extension of the domain wall was first found in nonlinear sigma models in Ref. [70, 71], and lots of works have followed them. The Q-extended domain walls in gauge theories are sometimes called the dyonic domain walls [69, 74, 35]. They are characterized by the topological and the Noether charges, so it is suitable to call them dyonic solitons. In the previous works [69, 74, 35], the dyonic domain wall was not a main focus. Some qualitative properties such as derivation of the BPS equations, topological charges, and the BPS mass formula have been given. To the best of our knowledge, very little has been done for solving the BPS equations, especially in the weak gauge coupling region. Furthermore, while the Noether charge, which gives a finite contribution to the BPS mass, has been studied very well, the electric and/or magnetic charge densities have not been discussed. Therefore, before studying the dyonic 1/4 BPS states, we stop for a while to clarify the dyonic domain wall in the weak gauge coupling region.

The master equation for the dyonic domain wall in the dimensionless coordinates (3.1) is given by

$$\partial_3^2 u - 1 + \Omega_0 e^{-u} = 0, \quad \Omega_0 = H_0^\dagger e^{2\eta \tilde{M} \cos \alpha x^3} H_0^\dagger.\tag{6.39}$$

This is formally the same equation as the master equation for the purely magnetic domain wall. If we write $\tilde{M} = \tilde{M}' / \cos \alpha$, the solutions $u(x^3)$ are identical to those which have already obtained in Sec. 3.1.1. In order to avoid inessential complications, we will consider $\eta = +1$ and $\tilde{M}' = \text{diag}(\tilde{m}'/2, -\tilde{m}'/2)$ with $\tilde{m}' > 0$ in what follows. Thus, we *reuse* the solutions given in Fig. 1 under the understanding that the yellow line corresponds to $2 \cos \alpha \tilde{\sigma} / \tilde{m}'$. On the other hand, the profile functions (the red and blue lines in Fig. 1) of $\tilde{H}_{1,2}$ are unchanged. The tension of the domain wall becomes

$$\tilde{T}_W = \frac{2\tilde{m}'}{\cos \alpha}, \quad \left(T_W = \frac{gv^3}{\sqrt{2}} \tilde{T}_W = \frac{m'v^2}{\cos \alpha} \right),\tag{6.40}$$

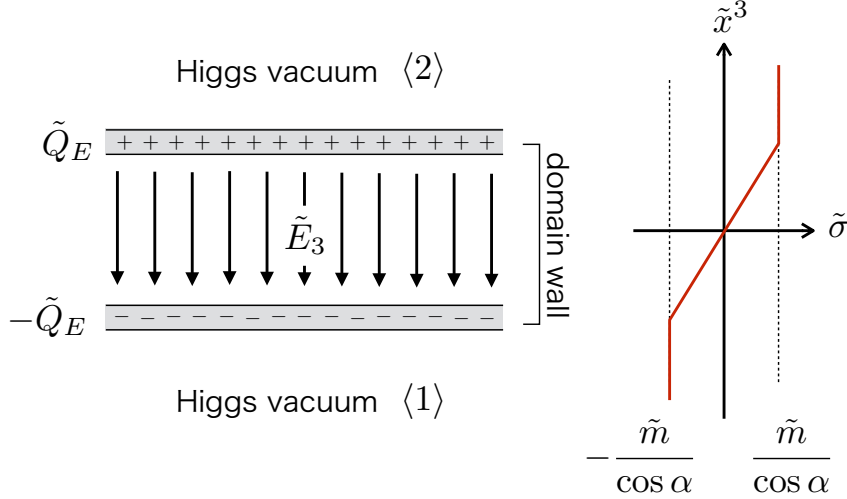


Figure 50: The dyonic domain wall as an electric capacitor.

because of $\tilde{m} = \tilde{m}'/\cos\alpha$.

Since $u = u(x^3)$ and from Eq. (6.20), no magnetic fields are involved. On the other hand, the third component of the electric field does appear

$$\tilde{E}_3 = 2 \tan\alpha \partial_3 \tilde{\sigma} = \tan\alpha \partial_3^2 u. \quad (6.41)$$

Remember, ∂_3 means the derivative in terms of \tilde{x}^3 and $\tilde{E}_k = E_k/g^2 v^2$. When $N_F = 2$, as can be seen from Fig. 1, $\tilde{\sigma}$ is constant outside the domain wall, so no electric fields exist there. On the other hand, a constant electric E_3 appears inside the domain wall, as $\tilde{\sigma}$ is linear in x^3 there. Since the width of the domain wall is $2\tilde{m}'$ and $\tilde{\sigma}$ changes from $-\tilde{m}'/2\cos\alpha$ to $\tilde{m}'/2\cos\alpha$, we have $\partial_3 \tilde{\sigma} \simeq 1/2\cos\alpha$. Therefore, the electric field inside the domain wall for the weak coupling is

$$\tilde{E}_k = \frac{\sin\alpha}{\cos^2\alpha} \delta_{k3}. \quad (6.42)$$

The induced electric charges which generate this electric fields can be found from Eq. (6.37). In terms of the dimensionless coordinates, the electric charge density is rewritten as follows

$$\tilde{Q}_E = \frac{\tilde{Q}_E}{\sqrt{2}g v^3} = -\tan\alpha \partial_3 (\tilde{H}\tilde{H}^\dagger) = -\tan\alpha \partial_3 m_v^2, \quad (6.43)$$

where $m_v^2 = \tilde{H}\tilde{H}^\dagger$ is 1 in the vacua, while $m_v^2 = 0$ inside the domain wall. Therefore, electric charges are induced on the outer layers, see Fig. 50: positive (negative) electric charges on the left outer skin and negative (positive) charges on the right outer skin for $\tan\alpha > 0$ ($\tan\alpha < 0$). Then the electric charge per unit area is given by

$$\tilde{Q}_E = \pm [\tilde{H}\tilde{H}^\dagger \tan\alpha]_{\text{outside}}^{\text{inside}} = \pm \tan\alpha. \quad (6.44)$$

Since the distance between two outer layers is $2\tilde{m}'$, the difference of electric potential is

$$\tilde{V} = 2\tilde{m}'\tilde{E}_3 = \frac{2\tilde{m}'}{\cos\alpha} \tan\alpha = \frac{2\tilde{m}'}{\cos\alpha} |\tilde{Q}_E|. \quad (6.45)$$

Hence, the electric capacitance per unit area is given by

$$\tilde{c} = \frac{\cos\alpha}{2\tilde{m}'} = \frac{1}{\tilde{T}_W}. \quad (6.46)$$

Note that the electric capacitance, in the usual sense, is infinity because the domain wall has infinite area. The energy stored in the capacitor is

$$\frac{1}{2}\tilde{c}\tilde{V}^2 = \frac{1}{2}\tilde{T}_W \tan^2\alpha, \quad (6.47)$$

which is the excess of the domain wall's tension for small α

$$\sqrt{\tilde{T}_W^2 + \tilde{Q}_W^2} - \tilde{T}_W \simeq \frac{1}{2}\frac{\tilde{Q}_W^2}{\tilde{T}_W} = \frac{1}{2}\tilde{T}_W\frac{\tilde{Q}_W^2}{\tilde{T}_W^2} = \frac{1}{2}\tilde{T}_W \tan^2\alpha. \quad (6.48)$$

Note that the dyonic domain wall behaves as the electric capacitor only in the weak gauge coupling region. This is because $HH^\dagger \simeq v^2$ holds everywhere in the strong gauge coupling region, so that no electric charge can be stored on the outer skins, see Eq. (6.43).

6.3 1/4 BPS dyonic configurations

Let us next consider the simplest 1/4 BPS dyonic solution $H_0 = (z, 1)$ in the $N_F = 2$ case. As mentioned below Eq. (6.24), the difference between the master equation for the purely magnetic and the dyonic cases amounts to the replacement of M by $M \cos\alpha$. Therefore, as in the case of dyonic domain walls, all the numerical solutions which we have obtained previously are still valid for the dyonic configurations. Indeed, the master equation (6.24) in terms of the dimensionless parameters given in Eq. (3.1) reduces to

$$\partial_\rho^2 u + \frac{1}{\rho}\partial_\rho u + \partial_3^2 u = 1 - (\rho^2 e^{\eta\tilde{m}'x^3} + e^{-\eta\tilde{m}'x^3})e^{-u}, \quad (6.49)$$

where we have written $\tilde{m} = \tilde{m}'/\cos\alpha$. Solutions to this equation can be obtained by solving the gradient flow equation (3.30) and identifying \tilde{m} with \tilde{m}' . Thus, we can recycle all the numerical solutions to (3.30).

The energy density consists of six parts; the domain wall \mathcal{T}_W , vortex string \mathcal{T}_S , boojum \mathcal{T}_B , $\mathcal{T}_4 = \partial_k j_k$, \mathcal{Q}_W and \mathcal{Q}_B . The first four contributions have no changes

from the purely magnetic case because of cancellation of $\cos \alpha$

$$\tilde{\mathcal{T}}_{W;\alpha} = \frac{1}{g^2 v^4} \mathcal{T}_W \cos \alpha = \partial_3^2 u, \quad (6.50)$$

$$\tilde{\mathcal{T}}_{S;\alpha} = \frac{1}{g^2 v^4} \mathcal{T}_S = (\partial_1^2 + \partial_2^2) u, \quad (6.51)$$

$$\tilde{\mathcal{T}}_{B;\alpha} = \frac{1}{g^2 v^4} \mathcal{T}_B \cos \alpha = 2 \{ (\partial_1 \partial_3 u)^2 + (\partial_2 \partial_3 u)^2 - (\partial_1^2 + \partial_2^2) u \partial_3^2 u \}, \quad (6.52)$$

$$\tilde{\mathcal{T}}_{4;\alpha} = \frac{1}{g^2 v^4} \mathcal{T}_4 = -\partial_k^2 \partial_k^2 u. \quad (6.53)$$

Another quantities depends on α as

$$\tilde{\mathcal{Q}}_{W;\alpha} = \frac{1}{g^2 v^4} \mathcal{Q}_W \sin \alpha = \eta \partial_3 \left(\tilde{H} \tilde{M}' \tilde{H}^\dagger \right) \tan^2 \alpha, \quad (6.54)$$

$$\tilde{\mathcal{Q}}_{B;\alpha} = \frac{1}{g^2 v^4} \mathcal{Q}_B \sin \alpha = \partial_k^2 [(\partial_3 u)^2] \tan^2 \alpha. \quad (6.55)$$

The electric and magnetic fields are given by

$$\tilde{E}_k = \frac{1}{g^2 v^2} E_k = \eta \tan \alpha \partial_k \partial_3 u, \quad (6.56)$$

$$(\tilde{B}_1, \tilde{B}_2, \tilde{B}_3) = \frac{1}{g^2 v^2} (B_1, B_2, B_3) = \xi (\partial_3 \partial_1 u, \partial_2 \partial_3 u, -(\partial_1^2 + \partial_2^2) u). \quad (6.57)$$

The electric charge density is

$$\tilde{\mathcal{Q}}_{E;\alpha} = \frac{\mathcal{Q}_E}{\sqrt{2} g v^3} = -\eta \tan \alpha \partial_3 \left(\tilde{H} \tilde{H}^\dagger \right). \quad (6.58)$$

Remember that the derivatives are with respect to the rescaled variables \tilde{x}^k .

In the following, we will set $\alpha = \pi/4$ and consider the masses $\tilde{m}' = 1/5, 1, 10$ ($\tilde{m} = \sqrt{2}/5, \sqrt{2}, 10\sqrt{2}$), as examples for the strong, intermediate and weak gauge couplings, respectively.

Let us first look at Fig. 51 in which the dyonic charge densities for $\tilde{m}' = 1/5$ are shown (the corresponding topological charge densities are shown in Fig. 5). The distributions are quite different from those in the weak coupling solution. The domain wall steeply bends. Since $HH^\dagger \simeq v^2$ holds everywhere for the strong gauge coupling, the induced electric charge is tiny ($\partial_3(HH^\dagger) \simeq 0$), so that it is no longer suitable to regard it as an electric capacitor, see the top-left panel of Fig. 51. Only the region near the junction point is evidently charged positively, whereas the electric charge densities become diluted far away from the junction point. The electric and magnetic force lines are shown in the top-right panel of Fig. 51. The region, having the boojum shown in the middle-right panel of Fig. 5, is where the electric and magnetic fields are not orthogonal.

Fig. 52 shows the electric charge densities for the intermediate mass $\tilde{m}' = 1$ (the corresponding topological charge densities are shown in Fig. 6). Since the curvature of the domain wall is now smaller, the separation between the positive and negative electric charges is visible. Mean distance is of the same order as the domain wall width $2\tilde{m}' = 2$. Unlike the strong coupling case, both the positive and negative electric charge densities are not localized near the junction point, but they extend along the domain wall. The positive charges are distributed across the whole domain wall, whereas the negative charges have no support around the junction point. Therefore, the electric force lines bends near the junction point and asymptotically becomes vertical far from the boojum (see the top-right panel of Fig. 52).

Finally, we show the dyonic solution for $\tilde{m}' = 10$ in Fig. 53. As expected, it is clearly similar to an electric capacitor with a large distance $2\tilde{m}' = 20$ between positive and negative charges. The electric force lines are vertical except for the region near the boojum. From Fig. 53 one clearly sees that the electric charge and Noether charge appear on the outer skins of the domain wall in the weak coupling region. The Noether charge densities on the two outer skins have the same sign, so that the total Noether charge does not vanish. The charge \tilde{Q}_B is negative on the outer skins but it is positive inside the domain wall, which is consistent with the fact that $\int_{-\infty}^{\infty} dx^3 \tilde{Q}_B = 0$.

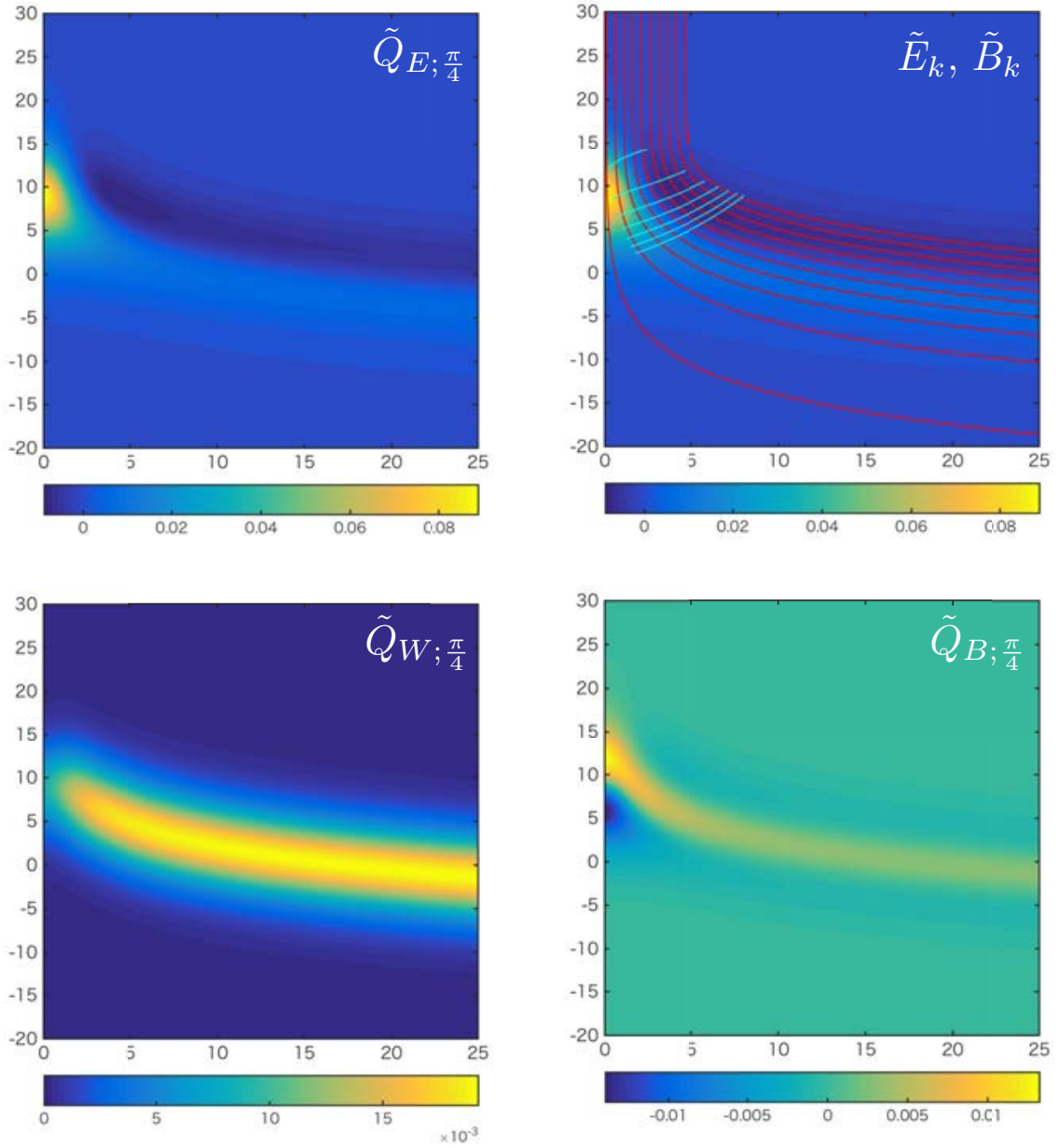


Figure 51: The dyonic charges $\tilde{Q}_{E,W,B;\alpha=\pi/4}$ are shown for $\tilde{m}' = 1/5$ (strong gauge coupling region). The topological charge densities are given in Fig. 5. The red curves show the magnetic force lines and the cyan ones correspond to the electric force lines.

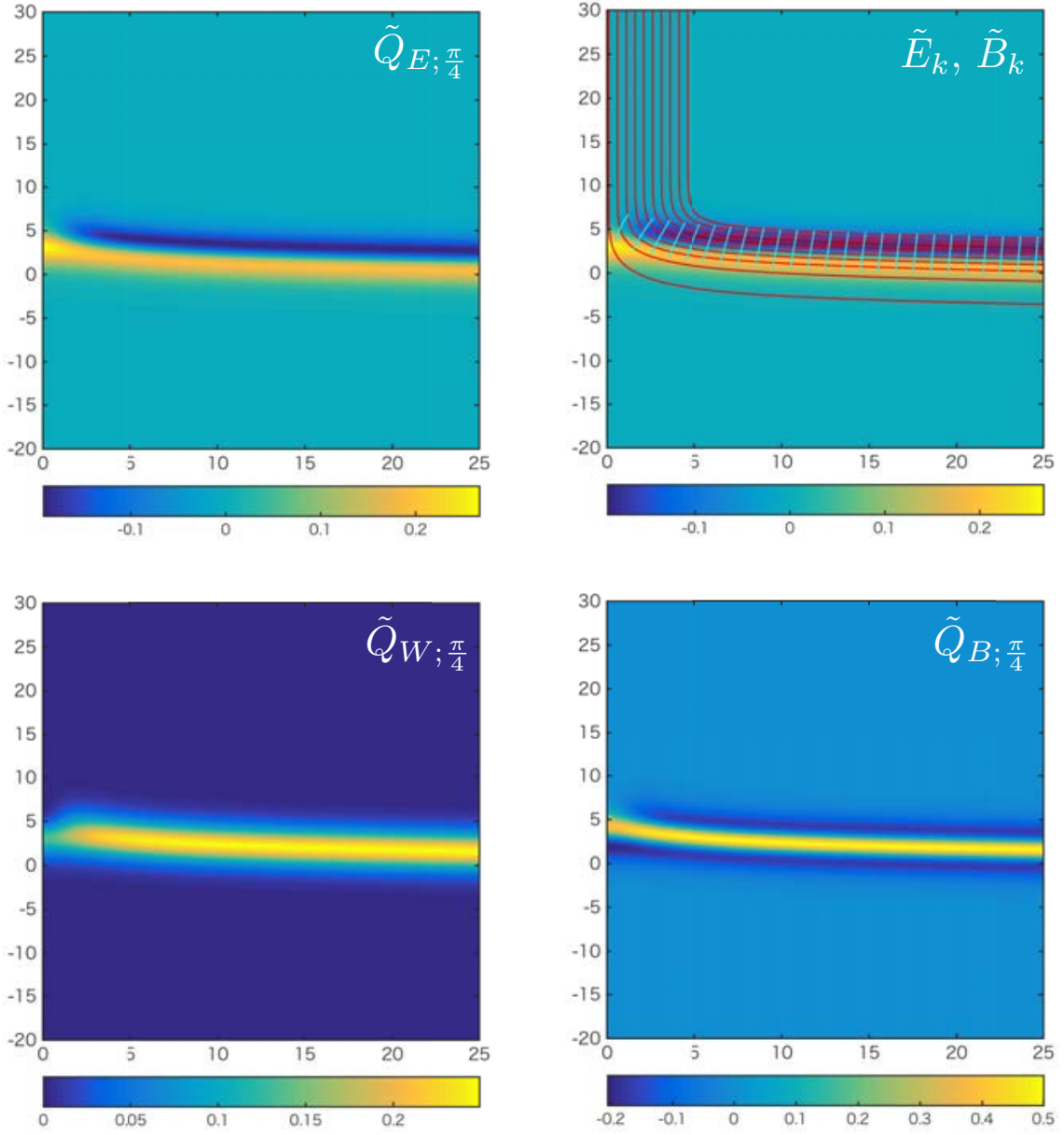


Figure 52: The dyonic charges $\tilde{Q}_{E,W,B;\alpha=\pi/4}$ are shown for $\tilde{m}' = 1$ (strong gauge coupling region). The topological charge densities are given in Fig. 6. The red curves show the magnetic force lines and the cyan ones correspond to the electric force lines.

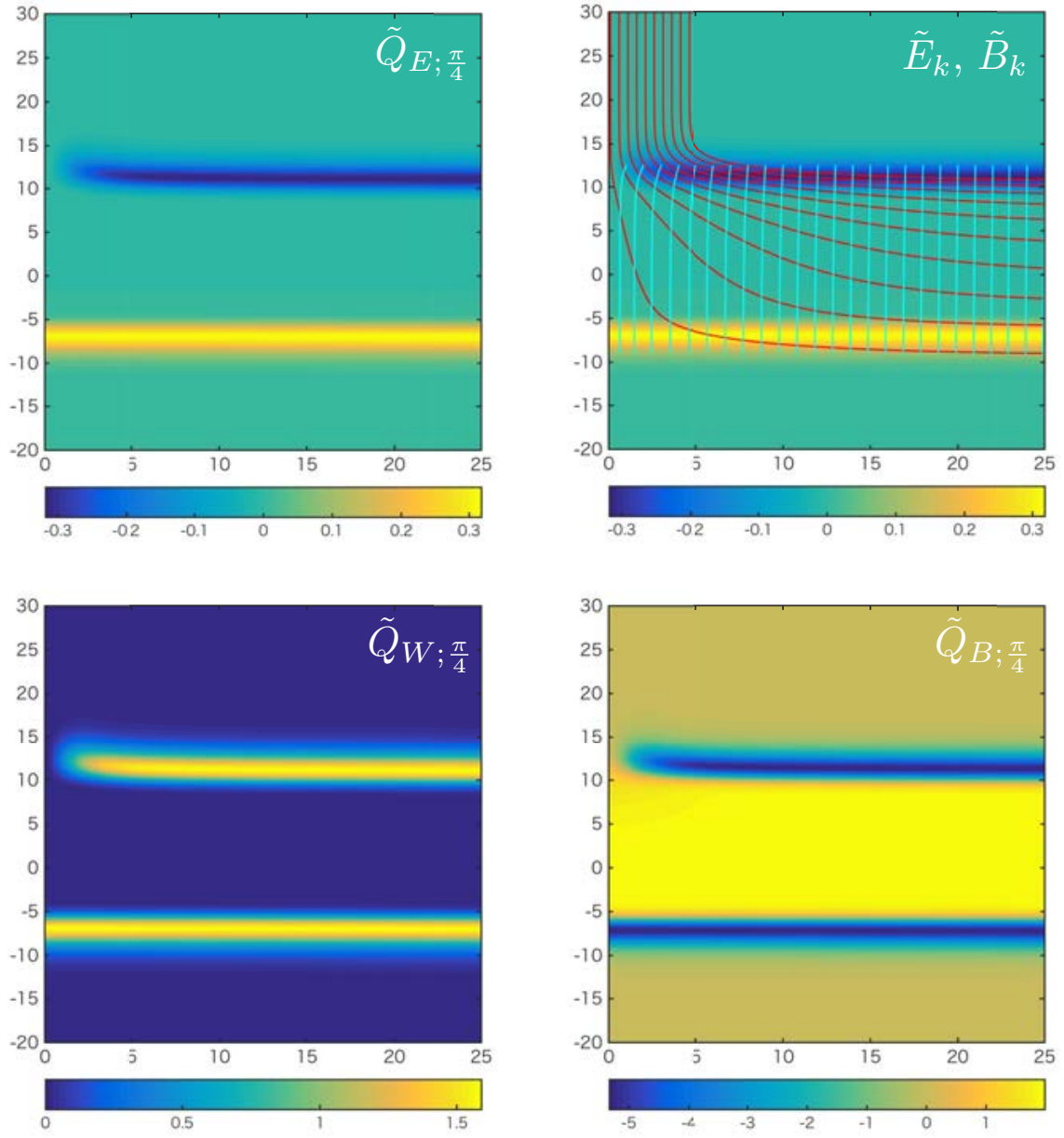


Figure 53: The dyonic charges $\tilde{Q}_{E,W,B;\alpha=\pi/4}$ are shown for $\tilde{m}' = 10$ (strong gauge coupling region). The topological charge densities are given in Fig. 7. The red curves show the magnetic force lines and the cyan ones correspond to the electric force lines.

7. Approximate solutions to Abelian master equations

In this paper we have analysed various 1/4 BPS configurations by numerically solving the corresponding master equations. However, in doing so, the need for asymptotically well-behaving initial configurations led us to the novel method, how to approximate composite solitons. Let us illustrate this method by recalling the simplest 1/4 BPS configuration, that is a vortex string attached to the domain wall, which we have studied in Sec. 3. In moduli matrix formalism, the corresponding master equation in dimensionless coordinates reads

$$\partial_3^2 u - 1 + \left(\rho^2 e^{\tilde{m}x^3} + e^{-\tilde{m}x^3} \right) e^{-u} = 0. \quad (7.1)$$

In Sec. 3 we argued that an approximate solution, which asymptotically approaches the true solution in all directions is

$$\mathcal{U} \equiv u_W \left(x^3 + \frac{1}{2\tilde{m}} u_S(\rho) \right) + \frac{1}{2} u_S(\rho), \quad (7.2)$$

where $u_W(x^3)$ is a solution to a domain wall ‘part’ and $u_S(\rho)$ a solution to the vortex string ‘part’ of the composite soliton. In other words, these functions are solutions to 1/2 BPS master equations

$$\partial_3^2 u_W = 1 - \left(e^{\tilde{m}x^3} + e^{-\tilde{m}x^3} \right) e^{-u_W}, \quad (7.3)$$

$$\partial_\rho^2 u_S + \frac{1}{\rho} \partial_\rho u_S = 1 - \rho^2 e^{-u_S}. \quad (7.4)$$

The function \mathcal{U} is designed to solve Eq. (7.1) in regions far away from vortex string, where $|\partial_\rho \mathcal{U}| \ll 1$. Indeed, using asymptotic behavior of the string solution $u_S(\rho) \sim \log \rho^2$ we can easily see that the function

$$u_W \left(x^3 + \log \rho / \tilde{m} \right) + \log \rho, \quad (7.5)$$

solves Eq. (7.1), if we neglect derivatives with respect to ρ . On the other hand, if we look at region dominated by the vortex string, that is $x^3 \gg 1$, we see from the asymptotic property of the domain wall part $u_W(x^3) \sim \tilde{m}x^3$ that the approximate solution takes the form

$$\mathcal{U} \sim u_S(\rho) + \tilde{m}x^3, \quad x^3 \gg 1. \quad (7.6)$$

This indeed solves Eq. (7.1), if we neglect the term $e^{-\tilde{m}x^3}$ on the right hand side. The only place where \mathcal{U} fails to solve the master equation is the junction point of the vortex string and the domain wall – the boojum. Thus, \mathcal{U} approximates the true solution *globally*, which is not the case for the commonly used infinite gauge coupling approximation $\mathcal{U}_\infty \equiv \log \left(\rho^2 e^{\tilde{m}x^3} + e^{-\tilde{m}x^3} \right)$. Indeed, if we evaluate the left hand side

of the master equation (7.1) along the domain wall's position $x^3 = -\log \rho/\tilde{m}$ we obtain

$$\partial_k^2 \mathcal{U}_\infty(\rho, x^3) \Big|_{x^3 = -\log \rho/\tilde{m}} = \tilde{m}^2 + \frac{1}{\rho^2}. \quad (7.7)$$

This shows that region of discrepancy between the true solution and \mathcal{U}_∞ is not bound to a finite region like in the case of \mathcal{U}_∞ .

Amongst other advantages, the approximation \mathcal{U} also enabled us in Sec. 3 to calculate all topological charges *exactly* and helped us to refine the arguments, which lead to the derivation of the general formula for the boojum charge in Eq. (3.51).

More importantly, the same strategy can be used to create approximations to virtually any 1/4 BPS configuration. Let us briefly summarize all composite solitons, which we have treated in this way.

A collinear vortex strings attached from both sides of the domain wall is approximated as:

$$\partial_k^2 u = 1 - \rho^2 \left(e^{\tilde{m}x^3} + e^{-\tilde{m}x^3} \right) e^{-u}, \quad (7.8)$$

$$\mathcal{U} = u_W(x^3) + u_S(\rho). \quad (7.9)$$

A semi-local vortex string of the size a attached to the wall is approximated as:

$$\partial_k^2 u = 1 - \left((\rho^2 + a^2) e^{\tilde{m}x^3} + e^{-\tilde{m}x^3} \right) e^{-u}, \quad (7.10)$$

$$\mathcal{U} = u_W \left(x^3 + \frac{1}{2\tilde{m}} u_{SLS}(a) \right) + \frac{u_{SLS}(a)}{2}, \quad (7.11)$$

where $u_{SLS}(a)$ is a solution to semi-local vortex master equation

$$\partial_\rho^2 u_{SLS} + \frac{1}{\rho} \partial_\rho u_{SLS} = 1 - (\rho^2 + a^2) e^{-u_{SLS}}. \quad (7.12)$$

Two semi-local vortex strings of sizes a_1 and a_2 attached from both sides can be approximated as

$$\partial_k^2 u = 1 - \left((\rho^2 + a_1^2) e^{\tilde{m}x^3} + (\rho^2 + a_2^2) e^{-\tilde{m}x^3} \right) e^{-u}, \quad (7.13)$$

$$\mathcal{U} = u_W \left(x^3 + \frac{u_{SLS}(a_1) - u_{SLS}(a_2)}{2\tilde{m}} \right) + \frac{u_{SLS}(a_1) + u_{SLS}(a_2)}{2}. \quad (7.14)$$

A general formula for approximate solution for arbitrary configuration of n_1 vortices attached from the right and n_2 vortices attached from the left is

$$\partial_k^2 u = 1 - \left(|P_{n_1}|^2 e^{\tilde{m}x^3} + |P_{n_2}|^2 e^{-\tilde{m}x^3} \right) e^{-u}, \quad (7.15)$$

$$\mathcal{U} = u_W \left(x^3 + \frac{u_S^{(n_1)} - u_S^{(n_2)}}{2\tilde{m}} \right) + \frac{u_S^{(n_1)} + u_S^{(n_2)}}{2}, \quad (7.16)$$

where the string solutions obey

$$\partial_\rho^2 u_S^{(n)} + \frac{1}{\rho} \partial_\rho u_S^{(n)} = 1 - |P_n|^2 e^{-u_S^{(n)}}. \quad (7.17)$$

Generalizing further to a configuration of two domain walls with n_1 vortex strings attached to the right wall, n_2 vortex strings in the middle and n_3 vortex strings attached to the left wall, we find the approximation in the form:

$$\partial_k^2 u = 1 - \left(|P_{n_1}|^2 e^{\tilde{m}x^3} + \delta^2 |P_{n_2}|^2 + |P_{n_3}|^2 e^{-\tilde{m}x^3} \right) e^{-u}, \quad (7.18)$$

$$u = u_W \left(x^3 + \frac{u_S^{(n_1)} - u_S^{(n_3)}}{2\tilde{m}}; \delta \frac{|P_{n_2}|}{\sqrt{|P_{n_1} P_{n_3}|}} \right) + \frac{u_S^{(n_1)} + u_S^{(n_3)}}{2}. \quad (7.19)$$

Here, we must supply double wall solution $u_W(x^3; \delta)$

$$\partial_3^2 u_W(x^3; \delta) = 1 - \left(e^{\tilde{m}x^3} + \delta^2 + e^{-\tilde{m}x^3} \right) e^{-u_W(x^3; \delta)}. \quad (7.20)$$

Arbitrary configuration of semi-local vortex strings attached from the right and arbitrary configuration of vortex strings attached from the left is given as

$$\partial_k^2 u = 1 - \left((|P_{n_1}|^2 + |Q_{n_1-1}|^2) e^{\tilde{m}x^3} + |P_{n_2}|^2 e^{-\tilde{m}x^3} \right) e^{-u}, \quad (7.21)$$

$$u = u_W \left(x^3 + \frac{u_{SLS}^{(n_1)} - u_S^{(n_2)}}{2\tilde{m}} \right) + \frac{u_{SLS}^{(n_1)} + u_S^{(n_2)}}{2}, \quad (7.22)$$

where

$$\partial_\rho^2 u_{SLS}^{(n)} + \frac{1}{\rho} \partial_\rho u_{SLS}^{(n)} = 1 - (|P_n|^2 + |Q_{n-1}|^2) e^{-u_{SLS}^{(n)}}. \quad (7.23)$$

And lastly, vortex string attached to a domain wall under the angle $\tan \alpha = 2\eta/\tilde{m}$ is approximated as

$$\partial_k^2 u = 1 - \left(e^{\tilde{m}x^3} + e^{4\eta x^1} e^{-\tilde{m}x^3} \right) e^{-u}, \quad (7.24)$$

$$u = u_W \left(x^3 - \frac{2\eta}{\tilde{m}} x^1 + \frac{1}{2\tilde{m}} u_S \right) + 2\eta x^1 + \frac{u_S}{2}. \quad (7.25)$$

This ends our recounting of approximate solutions given in previous sections. As we see, the general way how to construct approximations to composite solitons is to first solve the corresponding domain wall ‘part’ u_W by ignoring x^1 and x^2 derivatives and then replace these coordinates inside u_W by appropriate vortex string solutions.

The 1/2 BPS pieces entering our approximations are solutions to single domain wall $u_W(x^3)$, double domain wall $u_W(x^3; \delta)$, vortex strings $u_S^{(n)}$ and semi-local vortex strings $u_{SLS}^{(n)}$. These pieces can be supplied as numerical solutions of corresponding 1/2 BPS master equations, which are generally much easier to solve than the full three-dimensional 1/4 BPS master equations. A complementary way is to obtain

analytic approximations to 1/2 BPS solitons. This is the goal of this section. In the following subsections we will develop accurate analytic approximations to both vortex string and domain wall.

Especially accurate approximations can be found for vortex string master equation Eq. (7.4), since there is no intrinsic mass scale as in the case of domain wall master equation Eq. (7.3). This allows easy use of the so-called global Padé method, which we describe in the next subsection.

7.1 Approximations to ANO vortex

The master equation for single vortex string reads

$$\partial_\rho^2 u_S + \frac{1}{\rho} \partial_\rho u_S = 1 - \rho^2 e^{-u_S}. \quad (7.26)$$

No analytic solution of Eq. (7.26) is known. In order to construct global approximations, we take advantage of what we can learn about u_S locally. In particular, let us investigate behaviour of u_S close to $\rho = 0$ and for large $\rho \gg 1$. Expanding u_S in Taylor series around origin and matching coefficients on both sides of Eq. (7.26) we obtain

$$u_S(\rho) = u_0 + \frac{1}{4}\rho^2 - \frac{e^{-u_0}}{16}\rho^4 + \frac{e^{-u_0}}{144}\rho^6 + O(\rho^8), \quad (7.27)$$

where $u_0 \equiv u_S(0)$. Note that we have used the regularity condition $u'_S(0) = 0$. On the other hand, the asymptotic behaviour of u_S is

$$u_S(\rho) \sim 2 \log(\rho) + qK_0(\rho) \sim \log(\rho^2 + q\rho^{3/2}e^{-\rho}) \quad \text{as } \rho \rightarrow \infty. \quad (7.28)$$

Here, $K_0(\rho)$ is the modified Bessel function and $q > 0$ is some constant.

Both u_0 and q are locally undetermined; their values cannot be ascertained neither by Taylor series nor by asymptotic series. In other words, these numbers characterize global properties of u_S and as such, they are very hard to study analytically. Recently, a detailed study of Eq. (7.26) was published [75], where based on a perturbative expansion around small winding number, the numbers u_0 and q ($2D_1$ and $2C_1$ in their notation) were obtained with high precision, both analytically and numerically. In the following, we shall adopt the values $u_0 = 1.01072165$ and $q = 3.41572835$ (Eq. (2.66) in [75]) in all our approximations.

A (global) Padé approximant is a widely used tool to model a function based on its series expansion(s). The basic idea is to find a rational function which, when expanded, matches all series to given orders. Generally, such approximant tends to be very accurate even outside radii of convergence and for sufficiently nice functions (such as meromorphic functions) it remains close to the true solution everywhere.

Nevertheless, there is only so much a rational function can do. In particular, as we see from Eq. (7.28), the asymptotic formula for u_S contains log, exp and square root (suggesting essential singularity at infinity), neither of which can be

globally approximated by rational functions. Therefore, simple Padé approximants are insufficient in this case.

A way to overcome these difficulties, originally discussed in [76], is to put the Padé approximant directly into the asymptotic series, in such a way that singular terms are replaced by rational functions, which coefficients are fixed to match Taylor series at origin. In this way, the resulting function is guaranteed to behave in a desired way both at origin and at infinity.

Let us, therefore, propose the following ansatz:

$$u_{(p+3,p)} = \log\left(\rho^2 + e^{-\rho} \sqrt{\frac{P_{p+3}(\rho)}{Q_p(\rho)}}\right), \quad (7.29)$$

where $P_{p+3}(\rho)$ and $Q_p(\rho)$ are polynomials of order $p+3$ and p respectively. The coefficients are chosen such that they give correct large ρ behaviour

$$\frac{P_{p+3}(\rho)}{Q_p(\rho)} \xrightarrow{\rho \rightarrow \infty} q^2 \rho^3, \quad (7.30)$$

and the remaining ones are fixed to match the Taylor series (7.27) up to $O(\rho^{2p+3})$. After this procedure is done, it needs to be checked that both $P_{p+3}(\rho)$ and $Q_p(\rho)$ are strictly positive for $\rho \geq 0$, as we require that $u_{(p+3,p)}$ is regular on the positive semi-axis. It turns out that this is satisfied only up to $p=4$ and for higher p singularities appear.

We have found the following Padé approximants

$$P_3(\rho) = 7.54921285 + 15.0984\rho + 13.37786594\rho^2 + 11.66720016\rho^3, \quad (7.31)$$

$$P_4(\rho) = 7.54921285 + 17.82022676\rho + 18.82146806\rho^2 + 11.44776733\rho^3 + 4.20650447\rho^4, \quad (7.32)$$

$$P_5(\rho) = 7.54921285 + 14.95444855\rho + 13.29529829\rho^2 + 6.7801308\rho^3 + 2.05572318\rho^4 + 0.31742204\rho^5, \quad (7.33)$$

$$P_6(\rho) = 7.54921285 + 16.30163555\rho + 16.01574815\rho^2 + 9.27493053\rho^3 + 3.39472576\rho^4 + 0.76276929\rho^5 + 0.08549070\rho^6, \quad (7.34)$$

$$P_7(\rho) = 7.54921285 + 15.37863036\rho + 14.48581026\rho^2 + 8.23429824\rho^3 + 3.07646819\rho^4 + 0.76371628\rho^5 + 0.11835967\rho^6 + 0.00902282\rho^7, \quad (7.35)$$

and

$$Q_0(\rho) = 1, \quad (7.36)$$

$$Q_1(\rho) = 1 + 0.36054103\rho, \quad (7.37)$$

$$Q_2(\rho) = 1 - 0.01907181\rho + 0.02720636\rho^2, \quad (7.38)$$

$$Q_3(\rho) = 1 + 0.15938215\rho + 0.03066048\rho^2 + 0.00732744\rho^3, \quad (7.39)$$

$$Q_4(\rho) = 1 + 0.03711706\rho + 0.07252875\rho^2 + 0.00240865\rho^3 + 0.00077335\rho^4. \quad (7.40)$$

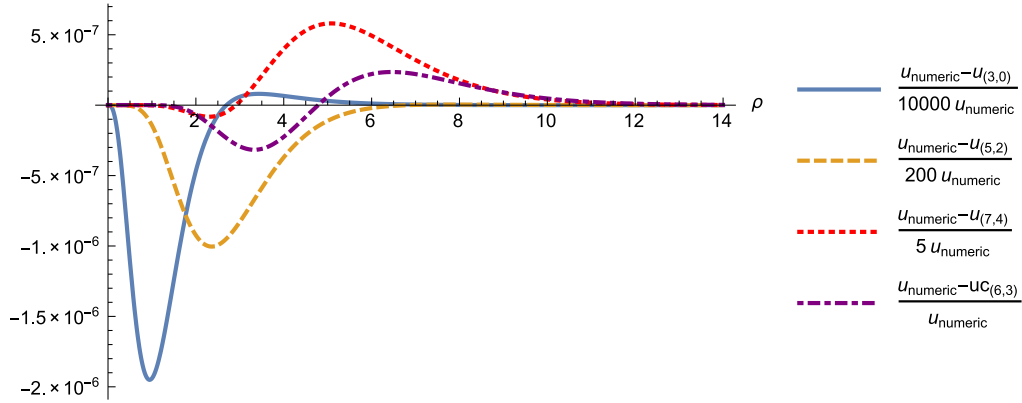


Figure 54: Relative difference between numerical and approximate solutions $u_{(3,0)}$ (blue solid line), $u_{(5,2)}$ (dashed yellow line), $u_{(7,4)}$ (red dotted line) and $u_{C(6,3)}$ (purple dash-dotted line). Notice that we had to scale down the first graph by a factor 10000, second graph by 200 and the third graph by 5 fit them comfortably into the picture.

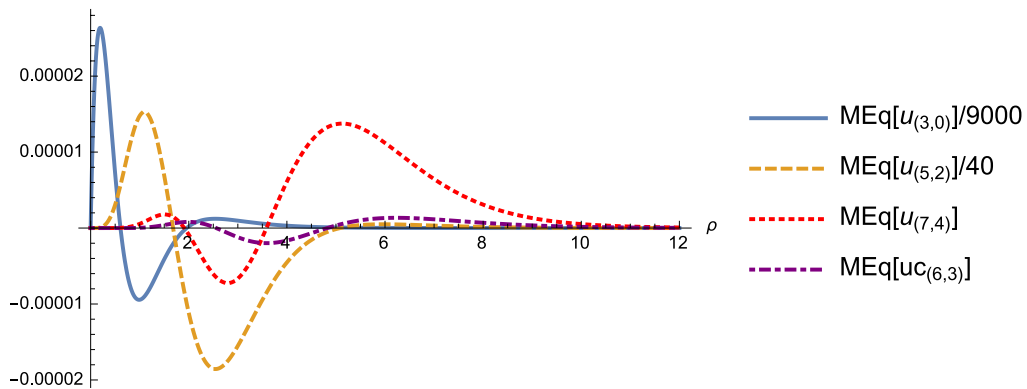


Figure 55: The master equation for approximate solutions $u_{(3,0)}$ (blue solid line), $u_{(5,2)}$ (dashed yellow line), $u_{(7,4)}$ (red dotted line) and $u_{C(6,3)}$ (purple dash-dotted line). Notice that we had to scale down first graph by a factor 9000 and the second graph by 20 to fit them comfortably into the picture.

Let us illustrate the accuracy of our approximations for $p = 0, 2, 4$. In Fig. 54 we show relative difference between $u_{(p+3,p)}$ and numerical solution and in Fig. 55 we show the master equation evaluated for each approximation. It demonstrates that $u_{(p+3,p)}$ is increasingly more accurate for larger p . As we already mentioned $u_{(8,5)}$ is not a regular function. This seems to persist even for higher values of p , indicating that capacity of this particular ansatz to approximate true solution has been exhausted.

Approximations $u_{(p+3,p)}$ have, however, one disadvantage, namely that they depend on odd powers of ρ . In contrast, series (7.27) contains only even powers. The coefficients must be therefore fine-tuned to eliminate all odd powers, especially the first power, since its presence cause a singularity in the master equation (7.26) at $\rho = 0$. Due to the finite precision of decimal representation of real numbers, this fine tuning is realised only imperfectly, which means that all odd powers, although strongly suppressed, are still present.

To overcome this technical issue we also considered the following ansatz

$$uc_{(p+3,p)} = \log\left(\rho^2 + \frac{1}{\cosh(\rho)} \sqrt[4]{\frac{P_{p+3}(\rho^2)}{Q_p(\rho^2)}}\right), \quad (7.41)$$

with the condition

$$\frac{P_{p+3}(\rho^2)}{Q_p(\rho^2)} \xrightarrow{\rho \rightarrow \infty} q^4 \frac{\rho^6}{16}. \quad (7.42)$$

The advantage is that $uc_{(p+3,p)}$ have only even powers of ρ in the expansion around origin. Curiously, only for $p = 0$ and $p = 3$ we get regular functions.

$$P_3(\rho^2) = 56.99061470 + 88.00348570\rho^2 + 49.40766370\rho^4 + 8.50772247\rho^6, \quad (7.43)$$

$$P_6(\rho^2) = 56.99061470 + 95.87543618\rho^2 + 61.81840575\rho^4 + 18.61295952\rho^6 \\ + 2.46701666\rho^8 + 0.09435195\rho^{10} + 2.59235211 \times 10^{-5}\rho^{12}, \quad (7.44)$$

$$Q_0(\rho^2) = 1, \quad (7.45)$$

$$Q_3(\rho^2) = 1 + 0.13812713\rho^2 + 0.00447569\rho^4 + 3.04705768 \times 10^{-6}\rho^6. \quad (7.46)$$

While $uc_{(3,0)}$ ranks somewhere between $u_{(3,0)}$ and $u_{(5,2)}$, as far as accuracy is concerned, $uc_{(6,3)}$ is roughly an order of magnitude better than $u_{(7,4)}$ and it is the best approximation to $u_s(\rho)$, which we have found.

7.2 Approximations to domain wall

In this subsection we shall for notational convenience relabel third coordinate as $y \equiv x^3$ and we also omit the \sim on the parameter $m \equiv \tilde{m}$, even though we are still using the dimensionless coordinates. The master equation for a single domain wall thus reads

$$\partial_y^2 u_W = 1 - \left(e^{my} + e^{-my}\right) e^{-u_W}. \quad (7.47)$$

For generic value of the parameter m , no analytic solution is known. However, for particular values of m , some exact solutions are available [73]. In our notation they are given as

$$u_1 = y + \log\left(1 + 2e^{-y} + e^{-2y}\right), \quad m = 1, \quad (7.48)$$

$$u_{3/2} = \frac{3}{2}y + \log\left(1 + 3e^{-y} + 3e^{-2y} + e^{-3y}\right), \quad m = \frac{3}{2}, \quad (7.49)$$

$$u_2 = 2y + \log\left(1 + 2\sqrt{6}e^{-y} + 8e^{-2y} + 2\sqrt{6}e^{-3y} + e^{-4y}\right), \quad m = 2. \quad (7.50)$$

In order to construct analytic approximations, let us see how the generic solution behaves for large positive values of y . The dominant term is clearly $u_W \sim my$. If we set $u_W \sim my + \delta u$ and neglect higher order terms (i.e. $e^{-2my}\delta u_W, (\delta u_W)^2$) we obtain the equation

$$\partial_y^2 \delta u_W = \delta u_W - e^{-2my}, \quad (7.51)$$

which gives $\delta u_W = c e^{-y} + \frac{1}{1-4m^2} e^{-2my}$, where c is an arbitrary constant (the second independent solution to homogenous equation e^y is discarded, since δu_W must be negligible compared with my for large values of y). This formula does not apply in the case $m = 1/2$, where instead we have $\delta u_W(m = 1/2) = c e^{-y} + \frac{1}{4} e^{-y}(1 + 2y)$. As this case is somewhat anomalous, we shall omit it and in the following we assume that $m > 1/2$.

Combining the δu_W correction with the dominant term into a single logarithm we obtain the asymptotic form

$$u_W \sim \log\left(e^{my} + c e^{(m-1)y} + \frac{1}{1-4m^2} e^{-my}\right), \quad y \gg 1. \quad (7.52)$$

At this point, we do not know the value of the constant c . However, for specific values of m , one can exploit reflection symmetry of the solution $u_W(-y) = u_W(y)$ to obtain a rather good estimate. In order to do that, let us look on additional sub-leading terms. Repeating the procedure outlined above, we obtain next order corrections combined into a single logarithm as:

$$u_W \sim \log\left(e^{my} + c e^{(m-1)y} + \frac{1}{1-4m^2} e^{-my} + \frac{c^2}{3} e^{(m-2)y} + \frac{c}{(1+m)(1-4m^2)} e^{-(m+1)y} - \frac{4m^2}{(1-4m^2)^2(1-16m^2)} e^{-3my}\right). \quad (7.53)$$

Notice that this asymptotic form contains (upon factoring out the dominant term e^{my}) either powers of e^{-2my} or powers of e^{-y} or their combinations. If we focus on half-integer values of m these factors can be the same, which we use to our advantage, since in that case we can force the reflection symmetry. Let us illustrate this on the case $m = 1$. We have

$$u_1 \sim \log\left(e^y + c + \frac{c^2 - 1}{3} e^{-y} - \frac{c}{6} e^{-2y} + \frac{4}{135} e^{-3y}\right). \quad (7.54)$$

The strategy of harvesting approximate solutions from the asymptotic forms, which we adopt from now on, is that we discard terms not compatible with the boundary condition $u \rightarrow -my$ as $y \rightarrow -\infty$. In the present case, the terms e^{-2y} and e^{-3y} would grow faster than e^{-y} as $y \rightarrow -\infty$, so we discard them. Doing so it only remains to ensure the reflection symmetry of u_1 , which fix the constant to be $c = 2$. Thus

$$u_1 \sim \log\left(e^y + 2 + e^{-y}\right). \quad (7.55)$$

Surprisingly, this approximation is in fact an exact solution (7.48)! It turns out that terms we have discarded are exactly cancelled by sub-leading terms.

The next case $m = 3/2$, including next-to-next leading order corrections to u , has the asymptotic form with incompatible terms already discarded given as

$$u_{3/2} \sim \log\left(e^{3y/2} + ce^{y/2} + \frac{c^2}{3}e^{-y/2} + \frac{c^3 - 3}{24}e^{-3y/2}\right). \quad (7.56)$$

We see that the choice $c = 3$ makes the above approximation an even function of y . Again $u_{3/2}$ with $c = 3$ is an exact solution (7.49). Repeating the same steps for $m = 2$, we obtain the form

$$u_2 \sim \log\left(e^{2y} + ce^y + \frac{c^2}{3} + \frac{c^3}{24}e^{-y} + \frac{c^4 - 36}{540}e^{-2y}\right) \quad (7.57)$$

and unique value of c , which ensures reflection symmetry, is now $c = 2\sqrt{6}$. Indeed, this choice of c makes u_2 an exact solution (7.50).

All three exact solutions u_1 , $u_{3/2}$ and u_2 were first reported in [73] and it seems that they are the only ones. Indeed, if we continue this procedure for $m = 5/2$ we obtain the asymptotic form

$$u_{5/2} \sim \log\left(e^{5y/2} + ce^{3y/2} + \frac{c^2}{3}e^{y/2} + \frac{c^3}{24}e^{-y/2} + \frac{c^4}{540}e^{-3y/2} + \frac{c^5 - 1080}{25920}e^{-5y/2}\right) \quad (7.58)$$

and upon inspection, we conclude there is no choice of the constant c , which would make the above approximation an even function of y .

At this point we adopt the attitude of ‘patching’ the asymptotic form in such a way, that it becomes symmetric under the reflection $y \rightarrow -y$. The condition for c is chosen in such a way that the patching affects only the inner-most terms. Thus, we choose $c^2/3 = c^3/24$, which yields $c = 8$. Then we fix the coefficients of $e^{-3y/2}$ and $e^{-5y/2}$ to match their reflected counterparts. In other words, we have

$$u_{5/2} \sim \log\left(e^{5y/2} + 8e^{3y/2} + \frac{64}{3}e^{y/2} + \frac{64}{3}e^{-y/2} + 8e^{-3y/2} + e^{-5y/2}\right), \quad (7.59)$$

which is however only approximative solution, but surprisingly accurate one, as can be seen on Fig. 56.

The process of creating approximations for higher half-integer masses can be now automated. Let us denote $m = p/2$. Based on the previous analysis let us adopt the ansatz:

$$u_{p/2} \sim \frac{p}{2}y + \log\left(1 + \frac{c}{c_1}e^{-y} + \dots + \frac{c^{p-1}}{c_{p-1}}e^{-(p-1)y} + e^{-py}\right), \quad (7.60)$$

where c and c_k , $k = 1, \dots, p-1$ are constants. The knowledge of exact solutions allow us to fix $c_1 = 1$, $c_2 = 3$ and $c_3 = 24$ (see Eq. (7.57)). The remaining coefficients c_k can be determined by requirement of reflection symmetry. In particular, we must demand

$$\frac{c^{p-1}}{c_{p-1}} = c, \quad \frac{c^{p-2}}{c_{p-2}} = \frac{c^2}{3}. \quad (7.61)$$

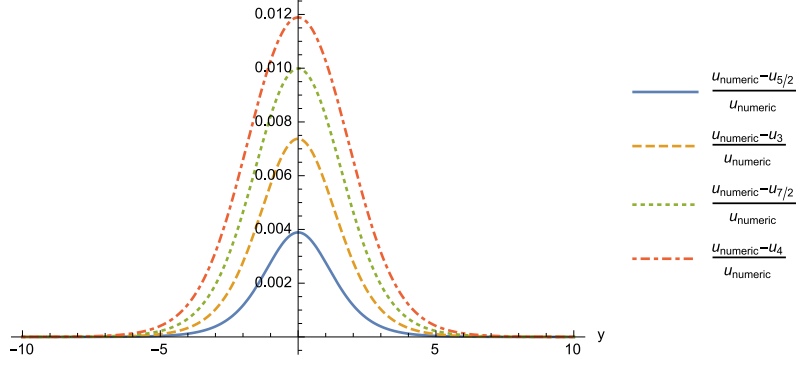


Figure 56: Relative errors between numerical and approximate solutions $u_{5/2}$, u_3 , $u_{7/2}$ and u_4 . The area below each curve is 0.013 ($p = 5$, solid blue), 0.023 ($p = 6$, dashed yellow), 0.042 ($p = 7$, dotted green) and 0.056 ($p = 8$, dot-dashed red).

These gives a recursion relation

$$c_{p-1} = \left(\frac{c_{p-2}}{3} \right)^{\frac{p-2}{p-4}}, \quad (p \geq 5) \quad (7.62)$$

with the solution

$$c_p = \left(\frac{8^{p-2}}{3^{p-4}} \right)^{\frac{p-1}{2}} \quad (p \geq 1), \quad (7.63)$$

$$c = \left(\frac{8^{p-2}}{3^{p-4}} \right)^{\frac{1}{2}} \quad (p \geq 2). \quad (7.64)$$

Remarkably, all additional symmetry conditions, such as $c^{p-k}/c_{p-k} = c^k/c_k$ for $k = 3, \dots, p-3$ are satisfied as well.

In summary, we have obtain the following family of approximate solutions

$$u_{p/2} = \frac{p}{2}y + \log \left(1 + \frac{9}{8} \sum_{k=1}^{p-1} \left(\frac{8}{3} \right)^{\frac{k(p-k)}{2}} e^{-ky} + e^{-py} \right), \quad (p \geq 3) \quad (7.65)$$

which are entirely determined by the reflection symmetry and few bits of "initial" data, namely the first three coefficients $c_1 = 1$, $c_2 = 3$ and $c_3 = 24$. Note that (7.65) does not include $m = 1$ ($p = 2$) case. It should be treated separately as in (7.55).

Given the spartan amount of information used in construction of these approximations, it is remarkable how accurate they are. We illustrate this fact on Fig. 56, where we compare $u_{p/2}$ to numerical solutions.

8. Exact solutions to 1/4 BPS solitons

In this paper we have so far relied on numerical methods to provide us with solutions to 1/2 and 1/4 BPS master equations (see Secs. 3-6). Although we have discussed

analytic approximations for 1/2 BPS solitons and a wide variety of 1/4 BPS solitons (see Sec. 7 for summary), these were primarily used as initial configurations for the numerical calculations. In this section we will complement both numerical and approximative analysis by discussing *exact* solutions of 1/4 BPS solitons, which we have found.

Any composite soliton, such as a vortex string attached to a domain wall, can be reduced to pure wall(s), or pure string(s) in some appropriate limit, i.e. either by shifting wall or string to infinity via the corresponding moduli parameter. Therefore, any exact 1/4 BPS solution potentially contains 1/2 BPS solutions as its limiting cases. Hence, before we can discuss exact composite soliton solutions we must first discuss exact domain wall and vortex string solutions.

In the following subsections we will present novel exact vortex string and exact domain wall solutions, out of which we construct new 1/4 BPS solutions. Throughout this section we use dimensionful coordinates.

8.1 $M = \text{diag}(m, 0, -m, -m)$

The master equation for the model with $N_F = 4$ and the mass matrix given as above reads in general

$$\frac{1}{2g^2v^2} \left(4\partial_z\partial_{\bar{z}}u + \partial_3^2u \right) = 1 - \left(e^{2mx^3} |h_1(z)|^2 + |h_2(z)|^2 + e^{-2mx^3} (|h_3(z)|^2 + |h_4(z)|^2) \right) e^{-u}, \quad (8.1)$$

where $H_0 = (h_1, h_2, h_3, h_4)$ are elements of the moduli matrix. The generic soliton configuration consists of a pair of domain walls, where the right wall has vortices attached from positive direction of x^3 axis (complex zeros of h_1), left wall has semi-local vortices attached from negative direction of x^3 axis (complex zeros of h_3 and/or h_4) and both walls have vortices stretched between them (complex zeros of h_2). The walls are bent if the net vorticity of incoming and outgoing vortex-strings is not equal. Asymptotically, the right wall has the profile $x^3 \approx \frac{1}{m} \log(|h_1|/|h_2|)$, while for the left wall it is $x^3 \approx -\frac{1}{2m} \log(|h_2|^2/(|h_3|^2 + |h_4|^2))$.

Let us first discuss an exact vortex string solution of this model. Since there are no known exact ANO vortices, based over non-degenerate vacua, we set $h_1 = h_2 = 0$ and look for exact solutions over the leftmost degenerate vacuum. Getting rid of the x^3 dependence by shifting $u \rightarrow u - 2mx^3$ in the master equation (8.1), we are left with the master equation for semi-local vortices:

$$\frac{2}{g^2v^2} \partial_z\partial_{\bar{z}}u = 1 - (|h_3(z)|^2 + |h_4(z)|^2) e^{-u}. \quad (8.2)$$

This equation has an exact solution, namely

$$u_{SLs}^{2F} = 2 \log \left(|z|^2 + \frac{4}{g^2v^2} \right), \quad (8.3)$$

for which $|h_3|^2 = \frac{8}{g^2 v^2} |z|^2$ and $|h_4|^2 = |z|^4$. Loosely, we could think about u_{SLS}^{2F} as a (non-linear) superposition of a local vortex and a semi-local vortex of the core size $\sqrt{8}/(gv)$. The vorticity of u_{SLS}^{2F} is indeed 2.

Now, let us consider domain wall solutions. We set $|h_1|^2 = 1$, $|h_2|^2 = e^{2R}$ and $|h_3|^2 = |h_4|^2 = 1$. The master equation (8.1) reduces to

$$\frac{1}{2g^2 v^2} \partial_3^2 u = 1 - \left(e^{2mx^3} + e^{2R} + e^{-2mx^3} \right) e^{-u}, \quad (8.4)$$

where the parameter $2R/m$ can be interpreted as the separation of walls for $R \gg m$. If R is close to or less than m , the domain walls cannot be distinguished from one another and they form a single (compressed) domain wall. In the limit $R \rightarrow -\infty$ the middle vacuum disappears completely and only a single elementary wall remains.

There are two exact solutions for this equation. The first one

$$u_{DW} = 2 \log \left(e^{mx^3} + \sqrt{e^{2R} - 6} + e^{-mx^3} \right), \quad \frac{m^2}{2g^2 v^2} = 1, \quad (8.5)$$

was originally reported in [73]. Notice that u_{DW} describes arbitrarily separated/compressed pair of walls (depending on the value of parameter R), but the ratio $m/(gv)$ is fixed. On the other hand, the second solution

$$u_{CW} = 2 \log \left(e^{mx^3} + e^{-mx^3} \right), \quad \frac{m^2}{2g^2 v^2} \leq \frac{1}{4}, \quad (8.6)$$

describes walls with separations up to $R = \frac{1}{2} \log \left(2 - \frac{4m^2}{g^2 v^2} \right) \leq \log \sqrt{2}$. In other words, walls in u_{CW} are always compressed, but unlike in the previous solution, ratio $m/(gv)$ can be varied up to the upper bound $1/\sqrt{2}$. Reaching this limit, we have $R \rightarrow -\infty$ and the solution u_{CW} reduces to an exact single wall solution, reported in [73], which we have denoted as u_1 in Sec. 7.

Now we have all the necessary pieces to discuss exact composite soliton solutions, which reads

$$u_{SW}^{4F} = 2 \log \left(e^{mx^3} + e^{-mx^3} \left(\frac{4}{g^2 v^2} + |z|^2 \right) \right), \quad \frac{m^2}{2g^2 v^2} = \frac{1}{8}, \quad (8.7)$$

with

$$|h_1|^2 = 1, \quad |h_2|^2 = |z|^2, \quad |h_3|^2 = \frac{8}{g^2 v^2} |z|^2, \quad |h_4|^2 = |z|^4. \quad (8.8)$$

The interpretation of this solution is most explicit if we rewrite it as

$$u_{SW}^{4F} = u_{CW} \left(x^3 - \frac{1}{4m} u_{SLS}^{2F} \right) + \frac{1}{2} u_{SLS}^{2F}. \quad (8.9)$$

Remarkably, this formulation is functionally identical to the analytic approximation (7.2) for a single vortex string attached to the domain wall (only this time, the string is attached from the left side).⁷

⁷The disparity of factors multiplying string solutions inside the wall solutions is due to the different choices of the mass matrix M for the approximate solution (7.2) and for the exact solution (8.7).

The bending of the compressed domain wall can be exactly obtained by equating both terms inside the logarithm in the solution (8.7), that is $x^3 = -\frac{2}{gv} \log(|z|^2 + \frac{4}{g^2v^2})$. Curiously, this bending is equivalent to the bending produced by a single semi-local vortex of the core size $\frac{4}{g^2v^2}$. However, by comparing the solution (8.7) with the Eq. (8.3) we recognize that the attached string is identical to u_{SLs}^{2F} . (The solutions become identical as $x^3 \rightarrow -\infty$.)

Thus, the solution u_{SW}^{4F} indeed describes a non-elementary wall u_{CW} with non-elementary string u_{SLs}^{2F} attached from the left. The same configuration with string attached from the right side can be achieved by reflection $x^3 \rightarrow -x^3$. Notice that position of the domain wall can be changed by shifting x^3 , while position of the string can be changed by shifting $z \rightarrow z - z_0$. We plot the total energy density and boojum charge density on Fig. 57.

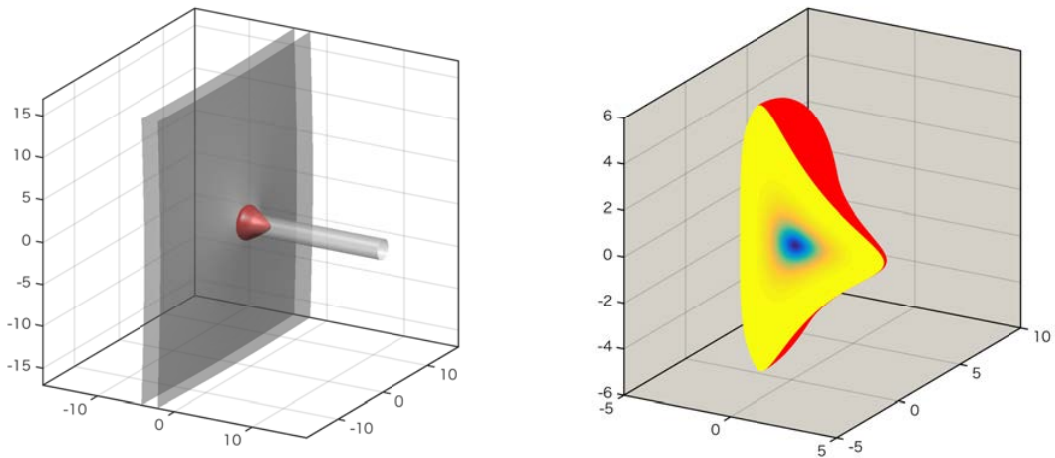


Figure 57: The energy density surface (left) and the boojum density (right) for u_{SW}^{4F} for $gv = 2$ and $m = -1$.

8.2 $M = \text{diag}(2m, m, 0, 0, -m, -2m)/2$

The master equation for the model with $N_F = 6$ case and with the mass matrix given as above reads in general

$$\frac{1}{2g^2v^2} \left(\partial_z \partial_{\bar{z}} u + \partial_3^2 u \right) = 1 - \left(e^{2mx^3} |h_1(z)|^2 + e^{mx^3} |h_2(z)|^2 + |h_3(z)|^2 + |h_4(z)|^2 + e^{-mx^3} |h_5(z)|^2 + e^{-2mx^3} |h_6(z)|^2 \right) e^{-u}, \quad (8.10)$$

where $H_0 = (h_1, h_2, h_3, h_4, h_5, h_6)$ are elements of the moduli matrix. The generic soliton configuration is composed of four domain walls. As in the previous example, the complex zeros of the moduli elements $h_i(z)$, $i = 1, \dots, 6$ determine number and positions of vortices, attached and stretched between successive walls (as well as their asymptotic profiles).

Since we have doubly degenerate vacuum between second and third wall, the exact vortex string solution of this model is again u_{SLS}^{2F} , as defined in Eq. (8.3). However, it is necessary to prove to introduce a more general solution of the semi-local vortex string based on $N_F = 3$ model, with the master equation

$$\frac{2}{g^2 v^2} \partial_z \partial_{\bar{z}} u = 1 - (|h_1|^2 + |h_2|^2 + |h_3|^2) e^{-u}. \quad (8.11)$$

That solution is

$$u_{SLS}^{3F}(s) = 2 \log(|z|^2 + s^2), \quad (8.12)$$

with

$$|h_1|^2 = |z|^4, \quad |h_2|^2 = 2s^2 |z|^2, \quad |h_3|^2 = s^2 \left(s^2 - \frac{4}{g^2 v^2} \right). \quad (8.13)$$

The solution u_{SLS}^{3F} is well-defined only if the core size s is sufficiently big, namely $s \geq \frac{2}{gv}$. Indeed, if $s = \frac{2}{gv}$ this solution reduces to the previous case $u_{SLS}^{3F}(\frac{2}{gv}) = u_{SLS}^{2F}$ and below this limit $|h_3|$ is imaginary. The interpretation of $u_{SLS}^{3F}(s)$ is best seen if we rewrite the master equation as

$$\frac{2}{g^2 v^2} \partial_z \partial_{\bar{z}} u = 1 - (|z|^2 + s^2 + \frac{2s}{gv}) (|z|^2 + s^2 - \frac{2s}{gv}) e^{-u}, \quad (8.14)$$

from which we see that u_{SLS}^{3F} describes a pair of coincident semi-local vortices with core sizes $s^2 \pm \frac{2s}{gv}$.

Let us now study the domain wall solution for the master equation (8.10), which is given as

$$u_{DCW}(x^3; R) = 2 \log \left(e^{mx^3} + e^R + e^{-mx^3} \right), \quad \frac{m^2}{2g^2 v^2} \leq \frac{1}{4}, \quad (8.15)$$

with

$$|h_1|^2 = |h_6|^2 = 1, \quad |h_2|^2 = |h_5|^2 = 2e^R \left(1 - \frac{m^2}{2g^2 v^2} \right), \quad (8.16)$$

$$|h_3|^2 + |h_4|^2 = e^{2R} + 2 - \frac{8m^2}{2g^2 v^2}. \quad (8.17)$$

Again, the parameter $2R/m$ can be interpreted as the separation of walls for $R \gg m$. However, we can rewrite u_{DCW} as

$$\begin{aligned} u_{DCW}(x^3; S) &= 2 \log \left(e^{m(x^3-S)/2} + e^{-m(x^3-S)/2} \right) \left(e^{m(x^3+S)/2} + e^{-m(x^3+S)/2} \right) \\ &= u_{CW}(x^3 - S; m/2) + u_{CW}(x^3 + S; m/2), \end{aligned} \quad (8.18)$$

where

$$e^R = 2 \cosh(mS). \quad (8.19)$$

In other words, the solution u_{DCW} describes a pair of compressed walls u_{CW} with separation $2S$.⁸

Now we have all the pieces to study an exact 1/4 BPS solution of Eq. (8.10). This solution is a combination of the wall solution u_{DCW} with the semi-local string solution u_{SLS}^{3F} stretched between its two domain walls:

$$u_{SW}^{6F} = 2 \log \left(e^{mx^3} + a + b|z|^2 + e^{-mx^3} \right), \quad \frac{1}{2} \leq \alpha^2 \leq 1, \quad (8.20)$$

with the moduli elements given as

$$|h_1|^2 = 1, \quad |h_2|^2 = 2b|z|^2(1 - \alpha^2), \quad |h_3|^2 = 2ab|z|^2 \quad (8.21)$$

$$|h_4|^2 = b^2|z|^4, \quad |h_5|^2 = 2b|z|^2(1 - \alpha^2), \quad |h_6|^2 = 1, \quad (8.22)$$

where we have denoted

$$\alpha^2 \equiv \frac{m^2}{2g^2v^2}, \quad a \equiv \sqrt{\frac{2 - 8\alpha^2}{1 - 2\alpha^2}}, \quad b \equiv \frac{g^2v^2}{2}(1 - \alpha^2)a. \quad (8.23)$$

The profile of the right compressed wall is asymptotically equal to $x^3 = \frac{1}{m} \log(a + b|z|^2)$, while that of the left wall is $x^3 = -\frac{1}{m} \log(a + b|z|^2)$. Therefore, the minimal separation between both composite walls is roughly $\frac{2}{m} \log a$. As in the previous case, we can rewrite this solution using its 1/2 BPS constituents:

$$u_{SW}^{6F} = u_{DCW}(x^3; u_{SLS}^{3F}(\frac{1}{gv} \sqrt{\frac{2}{1 - \alpha^2}}) + \frac{1}{2} \log \frac{ag^2v^2(1 - \alpha^2)}{2}). \quad (8.24)$$

This is functionally identical with the approximate solution for a similar configuration given in Eq. (7.18).

Notice that the ratio of mass and gauge coupling (parameter α) can only vary in a certain interval, outside of which the solution is not valid. The edges of the interval correspond to extreme cases. In the limit $\alpha^2 \rightarrow 1/2$ we see that $a, b \rightarrow \infty$, $a/b \rightarrow \frac{4}{g^2v^2}$ and the solution becomes $u_{SW}^{6F} \rightarrow u_{SLS}^{2F}$. In other words, this limit corresponds to infinite separation of walls. In the other extreme $\alpha^2 \rightarrow 1$ we have $a \rightarrow \sqrt{6}$, $b \rightarrow 0$ and $h_2, h_3, h_4, h_5 \rightarrow 0$ as a consequence. In other words, both domain walls are infinitely compressed and the vortex string disappears. This domain wall is an exact solution, which we denoted as u_2 is Sec. 7.

By shifting x^3 and z coordinates we can change the position of the configuration as a whole, but interestingly the separation between the walls is not a moduli of the solution, but rather it is controlled by parameters of the model. As we can see, as the walls are further apart the core size of the vortex string $\frac{1}{gv} \sqrt{\frac{2}{1 - \alpha^2}}$ shrinks

⁸Notice that the solution is defined for all values of R , but the parameter S is only defined for $R \geq \log 2$. If $R < \log 2$, it is possible to ascribe S a purely imaginary value $S = \frac{i}{m} \arccos(e^R/2)$, with which the solution (8.18) is still real. This confirms the intuition that the pair of wall merges at $R = \log 2$, where separation becomes zero $S = 0$.

ultimately to $\frac{2}{gv}$. But, when the wall approaches each other, the size of the semi-local string fattens and, ultimately, diverges. This is a direct confirmation of the numerical observation made in Sec. 4.

We plot the total energy density and boojum charge density on Fig. 58.

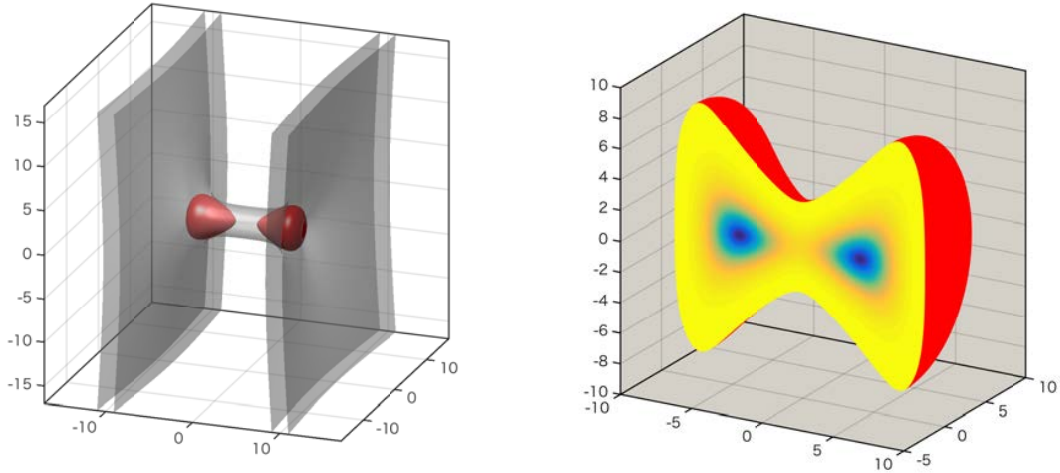


Figure 58: The energy density surface (left) and the boojum density (right) for u_{SW}^{6F} for $gv = 1$ and $m = 1.0001$.

8.3 Other exact solutions

The two exact 1/4 BPS solitons u_{SW}^{4F} and u_{SW}^{6F} are just illustrative examples of the rich hierarchy of exact solutions. We believe that there exists 1/4 BPS exact solutions in multi-flavour models. Our preliminary investigations show that many new configurations of domain walls and vortices can be constructed as a suitable combination of its 1/2 BPS constituents, in the same spirit as described in this section. The list is potentially infinite. To provide an exhaustive list of exact 1/4 BPS solution up to certain number of flavors seems to be important task, which however lies somewhat outside the scope of this paper. Therefore, we plan to address this issue fully in a separate work. For parallel domain walls, this was already achieved by one of us [Blaschke F., to appear].

All our exact solutions presented in this section shares the same trait: they are only a special configuration of solitons. The domain wall solution u_{CW} describes a pair of compressed elementary domain walls and both vortex string solutions $u_{SLS}^{2,3F}$ describes a pair of coincident semi-local vortices. In other words, some moduli are missing and we cannot provide exact results for generic configuration of solitons. Composite solitons u_{SW}^{4F} and u_{SW}^{6F} naturally inherit this trait.

As a closing comment of this section, the existence of exact solutions of Abelian master equations directly implies existence of exact solutions in non-Abelian case.

This can be seen from the fact, that non-Abelian analog of the master equation can be, for special $U(1)$ -factorizable solutions, decomposed into a set of independent Abelian master equations [32]. Thus, any exact solution in Abelian theory can be used to construct exact solutions in non-Abelian theories.

9. Low energy effective theory and Nambu-Goto/DBI action

In this section, we study 1/2 and 1/4 BPS configurations from the view point of the low energy effective actions, namely the Nambu-Goto (NG) action and the Dirac-Born-Infeld (DBI) action for the domain wall. As is well known, a low energy effective theory of a simple domain wall with translational zero modes is the NG action. The low energy effective action for the domain wall with not only the translational zero modes but also the internal moduli have been found to be the NG type [11, 77, 78] by regarding the internal space as extra dimensions. It is also known that the DBI action is dual to the NG action. In this section we show that the domain wall, the vortex string ending on the domain wall and their dyonic extension are reproduced in the NG action when the gauge coupling constant is taken to the infinity. In the strong gauge coupling limit, the vortex string asymptotically becomes the singular lump string attached to the domain wall. We call this configuration the spike domain wall. The dyonic extension of this configuration has been already studied in the massive nonlinear sigma model on $T^*\mathbb{C}P^1$, and it was shown that the configuration is realized as BIon in the DBI action [11]. We review the dyonic extension of the spike domain wall from the view point of the NG action. Finally we discuss whether the non-singular lump string with the size moduli, the semi-local boojums studied in subsection 3.3.3, can be realized in the DBI action.

9.1 Nambu-Goto action and Hamiltonian

We start with the NG action in $(2 + 1)$ -space-time dimensions [11]:

$$\mathcal{L}_{\text{NG}} = -\hat{T}_W \sqrt{\det(\eta_{\alpha\beta} - \partial_\alpha X \partial_\beta X - \partial_\alpha \phi \partial_\beta \phi)}, \quad \alpha, \beta = 0, 1, 2, \quad (9.1)$$

where X and ϕ are scalar fields, which will be identified with the position and the phase moduli of the domain wall solution and \hat{T}_W is the membrane tension. Here we have used the so-called physical gauge where the induced metric on the world-volume of the brane is flat (i.e. $\eta = \text{diag}(1, -1, -1)$). We can explicitly write this as

$$\mathcal{L}_{\text{NG}} = -\hat{T}_W \sqrt{D_{\text{NG}}}, \quad (9.2)$$

where

$$D_{\text{NG}} = 1 - (\partial_\alpha X \partial^\alpha X) - (\partial_\alpha \phi \partial^\alpha \phi) + (\partial_\alpha X \partial^\alpha X)(\partial_\beta \phi \partial^\beta \phi) - (\partial_\alpha X \partial^\alpha \phi)^2. \quad (9.3)$$

The canonical momenta for X and ϕ are given by

$$P_X = \frac{\partial \mathcal{L}}{\partial \dot{X}} = -\hat{T}_W D_{\text{NG}}^{-1/2} \left\{ \dot{X} - \dot{X}(\partial_\alpha \phi \partial^\alpha \phi) + \dot{\phi}(\partial_\alpha X \partial^\alpha \phi) \right\}, \quad (9.4)$$

$$P_\phi = \frac{\partial \mathcal{L}}{\partial \dot{\phi}} = \hat{T}_W D_{\text{NG}}^{-1/2} \left\{ \dot{\phi} - \dot{\phi}(\partial_\alpha X \partial^\alpha X) + \dot{X}(\partial_\alpha X \partial^\alpha \phi) \right\}, \quad (9.5)$$

so that the Hamiltonian is obtained as

$$\begin{aligned} \mathcal{H}_{\text{NG}} &= P_X \dot{X} + P_\phi \dot{\phi} - \mathcal{L}_{\text{NG}} \\ &= \hat{T}_W D_{\text{NG}}^{-1/2} \left\{ 1 + (\partial_i X)^2 + (\partial_i \phi)^2 + (\partial_i X)^2 (\partial_j \phi)^2 - (\partial_i X \partial_i \phi)^2 \right\}, \end{aligned} \quad (9.6)$$

where the index $i, j = 1, 2$ are summed over.

9.2 Domain wall, its dyonic extension and the NG action

Let us recall the domain wall solution discussed in section 2. The master equation for the flat domain wall is given in (2.25) when u is restricted to depend on x^3 coordinate only. In the strong gauge coupling limit, the master equation can be solved to give

$$u_{g \rightarrow \infty} = \log \Omega_0, \quad (9.7)$$

where Ω_0 is given in (2.25). For simplicity, let us consider $N_F = 2$ case. In this case, the moduli matrix $H_0(z)$ in (2.24) is just a constant. We choose

$$H_0(z) = \left(e^{-\frac{m}{2}(X+i\phi)}, e^{\frac{m}{2}(X+i\phi)} \right), \quad M = \text{diag}(m/2, -m/2). \quad (9.8)$$

with $\xi = \eta = 1$. Then (9.7) gives

$$u_{g \rightarrow \infty}(x^3) = \log(e^{m(x^3-X)} + e^{-m(x^3-X)}). \quad (9.9)$$

This shows that the constant parameter X corresponds to the position moduli. The other constant parameter ϕ is the internal moduli which is the Nambu-Goldstone mode associated with the spontaneously broken $U(1)_F$ symmetry. The energy of the domain wall is readily calculated by integrating (2.27) over all the space-directions

$$E_{\text{wall}} = \int d^3x \mathcal{T}_W = T_W A, \quad (9.10)$$

where $T_W = mv^2$ is the domain wall's tension and A is the area of the domain wall.

Now let us study the flat domain wall solution in the NG action. It is just given by considering constants for X and ϕ . The NG Hamiltonian (9.6) reduces to

$$\mathcal{H}_{\text{NG}} = \hat{T}_W. \quad (9.11)$$

The energy is obtained by integrating along the membrane directions:

$$E_{\text{NG}} = \int d^2x \mathcal{H}_{\text{NG}} = \hat{T}_W A. \quad (9.12)$$

The energy (9.10) and (9.12) completely coincide if the domain wall tension T_W is identified with the membrane tension \hat{T}_W . Therefore, as expected, the NG action with constant X and ϕ realizes the domain wall in the field theoretical model.

Next we consider the Q-extension (dyonic-extension) of domain wall. Let us first recall the field theory solution given in Eqs. (6.14) – (6.17). The dyonic extension of the master equation is given in (6.24). Substituting (9.8) with X and ϕ being constants into (6.24), we obtain the solution in the strong gauge coupling limit as

$$u_{g \rightarrow \infty}(x^3) = \log(e^{m \cos \alpha x^3 - mX} + e^{-m \cos \alpha x^3 + mX}). \quad (9.13)$$

The energy of the system is obtained from (6.30) with (6.21) and (6.27):

$$E_{\text{Q-wall}} = \int d^3x (\mathcal{T}_W \cos \alpha + \mathcal{Q}_W \sin \alpha) = \sqrt{T_W^2 + Q_W^2} A, \quad (9.14)$$

where we have used (6.29). The domain wall tension T_W and the Noether charge Q_W are calculated by (6.25) and (6.28): $T_W = mv^2$ and $Q_W = mv^2 \tan \alpha$.

Let us consider the corresponding configuration in the NG action. We take time-dependent phase

$$X = \text{const.}, \quad \phi = \frac{\omega}{\hat{m}} t, \quad (9.15)$$

where ω is a constant angular velocity and we have introduced a constant parameter \hat{m} of mass dimension one in order to make ϕ have mass dimension -1 . In this case, the energy is obtained as

$$E_{\text{NG}} = \frac{\hat{T}_W}{\sqrt{1 - (\omega/\hat{m})^2}} A. \quad (9.16)$$

The conserved momentum P_ϕ for this solution is given by

$$P_\phi = \hat{T}_W \frac{\omega/\hat{m}}{\sqrt{1 - (\omega/\hat{m})^2}}. \quad (9.17)$$

Then the energy can be written as

$$E_{\text{NG}} = \sqrt{\hat{T}_W^2 + P_\phi^2} A, \quad (9.18)$$

We identify $T_W = \hat{T}_W$ as before. Furthermore, we should identify $\omega/\hat{m} = \sin \alpha$ from Eq. (6.14), which tells us that the Q-charge (6.29) in the field theory is understood as

$$P_\phi = \hat{T}_W \tan \alpha = Q_W. \quad (9.19)$$

Thus, Eq. (9.18) coincides with (9.14). We conclude that the configuration (9.15) in the NG action realizes the Q-extension of the domain wall in the field theory.

9.3 Dyonic extension of spike domain wall and NG action

In this subsection, we study the 1/4 BPS dyonic extension of the spike domain wall that the lump vortex attaches on the domain wall. The master equation for this configuration is given in (6.24) where u depends on all the space coordinates. Considering $N_F = 2$ case, the moduli matrix and the mass matrix are given by

$$H_0(z) = (z, 1), \quad M = \text{diag}(m/2, -m/2). \quad (9.20)$$

In the strong gauge coupling limit the master equation (6.24) is solved as

$$u_{g \rightarrow \infty}(z, \bar{z}, x^3) = \log(\rho^2 e^{m \cos \alpha x^3} + e^{-m \cos \alpha x^3}), \quad (9.21)$$

where $|z|^2 = \rho^2$. The total energy of the configuration is

$$E_{1/4} = \int d^3x (\mathcal{T}_W \cos \alpha + \mathcal{Q}_W \sin \alpha + \mathcal{T}_S + \mathcal{T}_B), \quad (9.22)$$

where \mathcal{T}_S and \mathcal{T}_B are defined in (6.22) and (6.23), respectively. Taking into account the fact that in the strong gauge coupling limit (6.23) is vanishing, the energy is given as

$$E_{1/4} = \sqrt{T_W^2 + Q_W^2} A + T_S L. \quad (9.23)$$

Here we have used (6.29) and T_S is the string tension given in (6.31), $T_S = 2\pi v^2 |k|$ where k is the vortex winding number and L is length of the vortex string.

We consider the corresponding configuration in the NG action. We take the following configuration:

$$X \rightarrow X(x^1, x^2), \quad \phi \rightarrow \frac{\omega}{\hat{m}} t + \phi(x^1, x^2). \quad (9.24)$$

To simplify notation, let us introduce

$$a_i \equiv \partial_i X, \quad b_i \equiv \partial_i \phi. \quad (9.25)$$

Then the Hamiltonian (9.6) is expressed as

$$\mathcal{H}_{\text{NG}} = \hat{T}_W \frac{1 + a_i^2 + b_i^2 + (\epsilon_{ij} a_i b_j)^2}{\sqrt{1 + a_i^2 + b_i^2 + (\epsilon_{ij} a_i b_j)^2 - (\omega/\hat{m})^2 (1 + a_i^2)}}, \quad (9.26)$$

where $\epsilon_{12} = 1$ and we have used $a_i^2 b_j^2 - (a_i b_j)^2 = (\epsilon_{ij} a_i b_j)^2$. Let us further rewrite this in terms of $\tilde{b}_i \equiv b_i / \sqrt{1 - (\omega/\hat{m})^2}$,

$$\mathcal{H}_{\text{NG}} = \frac{\hat{T}_W}{\sqrt{1 - (\omega/\hat{m})^2}} \left(\mathcal{H}^{1/2} - \frac{(\omega/\hat{m})^2 (\tilde{b}_i^2 + (\epsilon_{ij} a_i \tilde{b}_j)^2)}{\mathcal{H}^{1/2}} \right), \quad (9.27)$$

where

$$\mathcal{H} = 1 + (a_i)^2 + (\tilde{b}_i)^2 + (\epsilon_{ij}a_i\tilde{b}_j)^2. \quad (9.28)$$

Now we are ready to minimize the Hamiltonian \mathcal{H}_{NG} . To this end, we first minimize \mathcal{H} as

$$\mathcal{H} = (a_i \pm \epsilon_{ij}\tilde{b}_j)^2 + (1 \mp \epsilon_{ij}a_i\tilde{b}_j)^2 \geq (1 \mp \epsilon_{ij}a_i\tilde{b}_j)^2. \quad (9.29)$$

The last inequality is saturated when the equation

$$a_i \pm \epsilon_{ij}\tilde{b}_j = 0 \quad (9.30)$$

is satisfied. The key observation is that when the equation (9.30) holds the first term in (9.27) is minimized while the second term is maximized. Indeed, the numerator in the second term is maximized because $(\epsilon_{ij}a_i\tilde{b}_j)^2$ becomes maximum when a_i is orthogonal to b_i , and at the same time the denominator is minimized. Taking account of the minus sign in front of the second term of Eq. (9.27), it is found that the Hamiltonian is minimized when the BPS equation (9.30) is satisfied. The BPS energy in terms of the original variable X is given by

$$\mathcal{H}_{\text{NG}} = \hat{T}_W \left\{ \frac{1}{\sqrt{1 - (\omega/\hat{m})^2}} + \sqrt{1 - (\omega/\hat{m})^2} (\partial_i X)^2 \right\}. \quad (9.31)$$

We now consider that a point particle corresponding to the end point of the lump string is placed on the membrane. Comparing Eqs. (9.8) and (9.20), one is naturally lead to the following identification

$$\phi = \pm \frac{1}{\hat{m}} \arctan \frac{x^2}{x^1}. \quad (9.32)$$

Again, we have introduced a certain parameter \hat{m} of mass dimension one. Combining (9.30) with (9.32) gives

$$X(\rho) = -\frac{1}{\sqrt{\hat{m}^2 - \omega^2}} \log \rho, \quad (9.33)$$

where $\rho = \sqrt{(x^1)^2 + (x^2)^2}$. With the solution (9.33), the Hamiltonian (9.31) turns out to be

$$\mathcal{H}_{\text{NG}} = \frac{\hat{T}_W}{\sqrt{1 - (\omega/\hat{m})^2}} \left(1 + \frac{1}{\hat{m}^2 \rho^2} \right). \quad (9.34)$$

The energy is

$$E_{\text{NG}} = \int d^2x \mathcal{H}_{\text{NG}} = \frac{\hat{T}_W}{\sqrt{1 - (\omega/\hat{m})^2}} A + \frac{2\pi\hat{T}_W}{\hat{m}\sqrt{\hat{m}^2 - \omega^2}} (\log R - \log \delta), \quad (9.35)$$

where we have introduced the ultraviolet cutoff $\rho = \delta$ and the infrared cutoff $\rho = R$. With the use of (9.19) and (9.33), the energy is rewritten as

$$E_{\text{NG}} = \sqrt{\hat{T}_W^2 + P_\phi^2} A + \frac{2\pi\hat{T}_W}{\hat{m}} \hat{L}, \quad (9.36)$$

where $\hat{L} \equiv X(\delta) - X(R)$. Identifying $T_W = \hat{T}_W$ and $m = \hat{m}$, it is found that $2\pi\hat{T}_W/\hat{m}$ ($T_W = mv^2$) coincides with the string tension $T_S = 2\pi v^2$ in the field theory. Respecting \hat{L} with the length of the vortex string, the energy (9.36) coincides with (9.23) in the field theoretical model.

9.4 Relation between solutions of NG action and DBI action

In this subsection, we show that the dyonic extension of the spike domain wall (9.20) in the field theory is also realized in the DBI action [11]. Rather than minimizing the Hamiltonian of the DBI action we derive the BPS equations in the DBI action by transforming Eq. (9.30).

First we derive (2 + 1)-dimensional DBI action from the NG action (9.1) by dualization

$$\mathcal{L}_{\text{DBI}} = \mathcal{L}_{\text{NG}} + \frac{\kappa}{2} \hat{T}_W \varepsilon_{\alpha\beta\gamma} \hat{F}^{\alpha\beta} \partial^\gamma \phi, \quad (9.37)$$

where the last term is called the BF term consisting of $\hat{F}_{\alpha\beta} = \partial_\alpha \hat{A}_\beta - \partial_\beta \hat{A}_\alpha$ being an abelian field strength and κ an arbitrary constant of mass dimension -2 . Notice that the term we added is a total divergence and it therefore has no effect on dynamics. Let us eliminate ϕ by using its equation of motion. Variation of the above Lagrangian with respect to $\partial_\alpha \phi$ leads to the condition

$$\kappa \hat{F}_\alpha^* = \frac{-1}{\sqrt{D_{\text{NG}}}} \left[\{1 - (\partial_\beta X \partial^\beta X)\} \partial_\alpha \phi + (\partial_\beta X \partial^\beta \phi) \partial_\alpha X \right], \quad (9.38)$$

where $\hat{F}_\alpha^* = \frac{1}{2} \varepsilon_{\alpha\beta\gamma} \hat{F}^{\beta\gamma}$ ($\epsilon_{123} = 1$). Contracting the above with $\partial^\alpha \phi$ we obtain

$$\kappa (\hat{F}_\alpha^* \partial^\alpha \phi) = \sqrt{D_{\text{NG}}} - \frac{1 - (\partial_\alpha X \partial^\alpha X)}{\sqrt{D_{\text{NG}}}}. \quad (9.39)$$

Substituting this into (9.37), we have

$$\mathcal{L}_{\text{DBI}} = -\hat{T}_W \frac{1 - (\partial_\alpha X \partial^\alpha X)}{\sqrt{D_{\text{NG}}}}. \quad (9.40)$$

In order to eliminate ϕ in D_{NG} , we consider contractions of (9.38) with $\partial^\alpha X$ and $\hat{F}^{*\alpha}$ as

$$\kappa (\hat{F}_\alpha^* \partial^\alpha \phi) = \frac{-1}{\sqrt{D_{\text{NG}}}} (\partial_\alpha \phi \partial^\alpha X), \quad (9.41)$$

$$\begin{aligned} \kappa (\partial_\alpha \phi \partial^\alpha \phi) (1 - (\partial_\beta X \partial^\beta X))^2 \\ = \frac{-1}{\sqrt{D_{\text{NG}}}} \left\{ (1 - (\partial_\alpha X \partial^\alpha X)) (\partial_\beta \phi \hat{F}^{\beta*}) + (\partial_\alpha X \partial^\alpha \phi) (\partial_\beta X \hat{F}^{\beta*}) \right\}. \end{aligned} \quad (9.42)$$

Eqs. (9.39)–(9.42) can be combined together to solve for D_{NG} :

$$D_{\text{NG}} = \frac{(1 - (\partial_\alpha X \partial^\alpha X))^2}{1 - (\partial_\beta X \partial^\beta X) + \kappa^2(\hat{F}_\beta^* \hat{F}^{\beta*}) - \kappa^2(\partial_\beta X \hat{F}^{\beta*})^2}. \quad (9.43)$$

With this expression at hand we use Eq. (9.39) to obtain the DBI action

$$\begin{aligned} \mathcal{L}_{\text{DBI}} &= -\hat{T}_W \sqrt{1 - (\partial_\alpha X \partial^\alpha X) + \kappa^2(\hat{F}_\alpha^* \hat{F}^{\alpha*}) - \kappa^2(\partial_\alpha X \hat{F}^{\alpha*})^2} \\ &= -\hat{T}_W \sqrt{\det(\eta_{\alpha\beta} - \partial_\alpha X \partial_\beta X + \kappa \hat{F}_{\alpha\beta})}, \end{aligned} \quad (9.44)$$

where the validity of the last equality can be checked by direct evaluation of the determinant.

Next we derive the Hamiltonian. In the following we set $\dot{X} = 0$ since we are not interested in the configuration where X depends on time. First we shall write the Lagrangian (9.44) in terms of the electric and magnetic fields defined by $\hat{F}_{0i} = \hat{E}_i$ ($i = 1, 2$) and $\hat{F}_{12} = \hat{B}$:

$$\mathcal{L}_{\text{DBI}} = -\hat{T}_W \sqrt{D_{\text{DBI}}}, \quad (9.45)$$

where

$$D_{\text{DBI}} = 1 + (\partial_i X)^2 - \kappa^2 \hat{E}_i^2 + \kappa^2 \hat{B}^2 - \kappa^2 \left(\epsilon_{ij} \hat{E}_i \partial_j X \right)^2. \quad (9.46)$$

Here the index i, j are summed over. In the following we rescale

$$\kappa \hat{E}_i \rightarrow \hat{E}_i, \quad \kappa \hat{B}_i \rightarrow \hat{B}_i. \quad (9.47)$$

A canonical momentum is obtained by differentiating (9.45) with respect to \hat{E}_i :

$$\Pi_i = \frac{\partial \mathcal{L}_{\text{DBI}}}{\partial \hat{E}_i} = -\hat{T}_W D_{\text{DBI}}^{-1/2} (\hat{E}_i - \epsilon_{ij} \partial_j X), \quad (9.48)$$

where

$$A = \epsilon_{ij} \partial_i X \hat{E}_j. \quad (9.49)$$

The Hamiltonian of the DBI action is then obtained as

$$\begin{aligned} \mathcal{H}_{\text{DBI}} &= \Pi_i \hat{E}_i - \mathcal{L}_{\text{DBI}} \\ &= \hat{T}_W D_{\text{DBI}}^{-1/2} (1 + (\partial_i X)^2 + \hat{B}^2). \end{aligned} \quad (9.50)$$

Remaining task for derivation of the Hamiltonian is to write D_{DBI} in terms of X, Π_i and \hat{B} . To this end, we calculate Π_i^2 and $\epsilon_{ij} \partial_i X \Pi_j$:

$$\Pi_i^2 = \hat{T}_W^2 D_{\text{DBI}}^{-1} \left\{ \hat{E}_i^2 + A^2 + (1 + (\partial_i X)^2) A^2 \right\}, \quad (9.51)$$

$$\epsilon_{ij} \partial_i X \Pi_j = \hat{T}_W D_{\text{DBI}}^{-1/2} (1 + (\partial_i X)^2) A. \quad (9.52)$$

From (9.52) we have

$$A = \frac{D_{\text{DBI}}^{1/2}}{\hat{T}_W(1 + (\partial_i X)^2)} (\epsilon_{kl} \partial_k \Pi_l). \quad (9.53)$$

From (9.46) we find

$$\hat{E}_i^2 + A^2 = 1 + (\partial_i X)^2 + \hat{B}^2 - D_{\text{DBI}}. \quad (9.54)$$

Substituting (9.53) and (9.54) into (9.51), we reach the following equation:

$$\Pi_i^2 = \hat{T}_W^2 D_{\text{DBI}}^{-1} \left\{ 1 + (\partial_i X)^2 + \hat{B}^2 - D_{\text{DBI}} + \frac{D_{\text{DBI}} (\epsilon_{ij} \partial_i X \Pi_j)^2}{1 + (\partial_k X)^2} \right\}. \quad (9.55)$$

Solving this equation with respect to D_{DBI} , we have

$$D_{\text{DBI}} = \frac{\hat{T}_W^2 (1 + (\partial_i X)^2 + \hat{B}^2) (1 + (\partial_i X)^2)}{\hat{T}_W^2 (1 + (\partial_i X)^2) + \Pi_i^2 + (\partial_i X \Pi_i)^2}. \quad (9.56)$$

We substitute (9.56) into the Hamiltonian (9.50) and obtain the final expression for the Hamiltonian

$$\mathcal{H}_{\text{DBI}} = \sqrt{\frac{\left\{ \hat{T}_W^2 (1 + (\partial_i X)^2) + \Pi_i^2 + (\partial_i X \Pi_i)^2 \right\} \left\{ 1 + (\partial_j X)^2 + \hat{B}^2 \right\}}{1 + (\partial_k X)^2}}. \quad (9.57)$$

Note that this is different from the DBI Hamiltonian obtained in Ref. [11].

Let us next rewrite the BPS equation (9.30) in terms of the DBI variables. To this end, we first show how \hat{B} and \hat{E}_i are written in terms of the fields X and ϕ in the NG action. For $X \rightarrow X(x^1, x^2)$ and $\phi \rightarrow (\omega/\hat{m})t + \phi(x^1, x^2)$ as is given in (9.24), from (9.38) we have

$$\hat{B} = -\frac{(\omega/\hat{m})}{\sqrt{D_{\text{NG}}}} (1 + (\partial_i X)^2), \quad (9.58)$$

$$\hat{E}_i = \frac{1}{\sqrt{D_{\text{NG}}}} \left\{ (1 + (\partial_k X)^2) \epsilon_{ij} \partial_j \phi - (\partial_k X \partial_k \phi) (\epsilon_{ij} \partial_j X) \right\}, \quad (9.59)$$

from which we find

$$\hat{B}^2 = \frac{(\omega/\hat{m})^2}{D_{\text{NG}}} (1 + (\partial_i X)^2)^2, \quad (9.60)$$

$$\hat{E}_i^2 = \frac{1}{D_{\text{NG}}} \left\{ (1 + (\partial_i X)^2)^2 (\partial_j \phi)^2 - (\partial_i X \partial_i \phi)^2 (\partial_j X)^2 - 2(\partial_i X \partial_i \phi)^2 \right\}. \quad (9.61)$$

Combining (9.49) with (9.61) we obtain

$$A^2 = (\partial_i X)^2 \hat{E}_j^2 - (\partial_i X \hat{E}_i)^2 = \frac{(\partial_i X \partial_i \phi)^2}{D_{\text{NG}}}. \quad (9.62)$$

Substituting (9.60)–(9.62) into D_{DBI} given in (9.46), it can be shown that

$$D_{\text{DBI}} = \frac{(1 + (\partial_i X)^2)^2}{D_{\text{NG}}}. \quad (9.63)$$

Now we are ready to rewrite the BPS equation (9.30) in terms of the DBI language. From (9.30) we have

$$\partial_i \phi \partial_i X = 0, \quad (9.64)$$

and

$$\begin{aligned} D_{\text{NG}} &= (1 + (\partial_i X)^2) (1 - (\omega/\hat{m})^2 + (\partial_j \phi)^2) \\ &= (1 - (\omega/\hat{m})^2) (1 + (\partial_i X)^2)^2. \end{aligned} \quad (9.65)$$

Substituting this into (9.63), we have

$$D_{\text{DBI}} = \frac{1}{1 - (\omega/\hat{m})^2}. \quad (9.66)$$

Furthermore, (9.59) gives us the relation

$$\hat{E}_i = \sqrt{D_{\text{DBI}}} \epsilon_{ij} \partial_j \phi. \quad (9.67)$$

Since $A = 0$, (9.48) is simplified as

$$\Pi_i = \hat{T}_W \frac{\hat{E}_i}{\sqrt{D_{\text{DBI}}}}. \quad (9.68)$$

Combining (9.67) and (9.68), tell us that

$$\epsilon_{ij} \partial_j \phi = \hat{T}_W^{-1} \Pi_i. \quad (9.69)$$

Substituting (9.30) into (9.58), we find

$$\hat{B} = -\frac{\omega}{\hat{m}} \sqrt{\frac{1 + (\partial_i X)^2}{1 - \omega^2 + (\partial_i \phi)^2}} = -\frac{\omega}{\sqrt{\hat{m}^2 - \omega^2}}. \quad (9.70)$$

Using (9.69) and (9.70), the BPS equation (9.30) in the NG action is rewritten as

$$\partial_i X = \pm \sqrt{1 + \hat{B}^2} \hat{T}_W^{-1} \Pi_i. \quad (9.71)$$

This is the BPS equation for the dyonic extension of the spike domain wall in terms of the DBI variables. Note that we eventually arrive at the same BPS equation given in [11], although our Hamiltonian (9.57) is different from one in [11].

In order to check that this equation leads to the desired result, we substitute (9.71) into the Hamiltonian (9.57). It yields

$$\mathcal{H}_{\text{DBI}} = \hat{T}_W \sqrt{1 + \hat{B}^2} \left(1 + \hat{T}_W^{-1} \Pi_i^2 \right). \quad (9.72)$$

We shall consider the following configuration:

$$\Pi_i = \frac{\hat{T}_W x_i}{\hat{m} \rho^2}. \quad (9.73)$$

This configuration represents that the unit electric charge is placed on the membrane. This fact is understood from the relation (9.68), which gives

$$\hat{E}_i = \hat{T}_W^{-1} \Pi_i = \frac{1}{\hat{m}} \frac{x_i}{\rho^2}. \quad (9.74)$$

Thus, the factor $1/\hat{m}$ is interpreted as an electric charge. A solution of the BPS equation (9.71) which is called the BIon is in this case

$$X = -\frac{1}{\hat{m}} \sqrt{1 + \hat{B}^2} \log \rho. \quad (9.75)$$

Substituting (9.73) into (9.72) and integrating over the membrane directions, we find the energy of the configuration as

$$E_{\text{DBI}} = \hat{T}_W \sqrt{1 + \hat{B}^2} A + \frac{2\pi \hat{T}_W}{\hat{m}} \sqrt{1 + \hat{B}^2} (\log R - \log \delta), \quad (9.76)$$

where we have introduced the infrared and ultraviolet cutoff $\rho = R$ and $\rho = \delta$, respectively. The energy is rewritten as

$$E_{\text{DBI}} = \hat{T}_W \sqrt{1 + \hat{B}^2} A + \frac{2\pi \hat{T}_W}{\hat{m}} \hat{L}, \quad (9.77)$$

where $\hat{L} = X(\delta) - X(R)$. Taking (9.70) with the choice $\omega/\hat{m} = \sin \alpha$, $\hat{T}_W = T_W$, and $\hat{m} = m$ into account, it is found that this expression is the same with (9.36) obtained in the NG action. Therefore it is concluded that the BPS equation (9.71) in the DBI action reproduces the dyonic extension of the spike domain wall (9.20) in the field theory.

Before closing this subsection, let us make a comment on the relation between the magnetic scalar potential φ introduced by (3.88) in Sec. 3.5 and X given in (9.75). φ is the scalar potential for the magnetic field $B_i(x^1, x^2)$ in the original gauge theory. We have found the relation $\varphi = m x^3(x^1, x^2)/d_W$ and $x^3(x^1, x^2) = -u_S(x^1, x^2)/2m$. In the strong gauge coupling limit, we have $u_S = \log \rho^2$, so that $x^3(x^1, x^2) = -(\log \rho)/m$, which precisely coincides with (9.75) in the case of $\hat{B} = 0$. On the other hand, from (9.74) and (9.75), X is the scalar potential for the dual electric field $\hat{E}_i(x^1, x^2)$. Thus, the magnetic field B_i in the original gauge theory and the dual electric field \hat{E}_i in the effective theory are generated by the same static potential.

9.5 The semi-local BIon: Round spike configuration and DBI action

In this subsection, we discuss the semi-local BIon – the round spike domain wall configuration, where the spike’s tip is smoothed out by introducing a lump size moduli. This configuration should be a DBI counterpart to the semi-local boojum which we studied for the finite gauge coupling in subsection 3.3.3. Our purpose in this subsection is to investigate whether the semi-local boojum in the strong gauge coupling limit in the field theory is realized in the DBI action.

As the simplest example of the semi-local vortex, let us consider $N_F = 3$ case with vanishing Q-charge. The moduli matrix of the configuration is

$$H_0(z) = (z, a, 1), \quad M = \text{diag}(m/2, m/2, -m/2). \quad (9.78)$$

where $a \in \mathbb{R}$ is a size moduli. Supposing that the u depends on all the space-directions, the master equation (2.25) is solved as

$$u_{g \rightarrow \infty} = \log \left\{ (\rho^2 + a^2)e^{mx^3} + e^{-mx^3} \right\}. \quad (9.79)$$

The domain wall position is read off from the condition $(\rho^2 + a^2)e^{mx^3} = e^{-mx^3}$, which gives

$$x^3(\rho) = -\frac{1}{2m} \log(\rho^2 + a^2). \quad (9.80)$$

In the strong gauge coupling limit, since the boojum energy density (2.29) is vanishing, the total energy (2.20) is just a sum of the domain wall tension and the vortex string tension:

$$E_{1/4} = \int d^3x (\mathcal{T}_W + \mathcal{T}_S), \quad (9.81)$$

where \mathcal{T}_W and \mathcal{T}_S are given in (2.27) and (2.28). We perform the integral along only x^3 -direction:

$$E_{1/4} = T_W A + \int d^2x \mathcal{E}_S(x^1, x^2), \quad (9.82)$$

where \mathcal{E}_S is given by

$$\mathcal{E}_S(x_1, x_2) = \frac{v^2}{m} \left[\frac{\rho^2}{(\rho^2 + a^2)^2} + \frac{a^2}{(\rho^2 + a^2)^2} \log \left\{ 1 + (\rho^2 + a^2)e^{2m\Lambda} \right\} \right]. \quad (9.83)$$

Here we have introduced the infrared cutoff $x_3 = \Lambda$. In the following, we focus on the contribution of the energy from the vortex string in (9.83). We separate it into two parts as

$$E_S = \int d^2x \mathcal{E}_S(x_1, x_2) = E_{S1} + E_{S2}, \quad (9.84)$$

where

$$E_{S1} = \frac{v^2}{m} \int d^2x \frac{\rho^2}{(\rho^2 + a^2)^2}, \quad (9.85)$$

$$E_{S2} = \frac{v^2}{m} \int d^2x \frac{a^2}{(\rho^2 + a^2)^2} \log \{1 + (\rho^2 + a^2)e^{2m\Lambda}\}. \quad (9.86)$$

Integration over ρ from a UV cutoff $\rho = \delta$ ($\delta \ll a$) to an IR cutoff $\rho = R$ ($R \gg a$), see Fig. 59, we find

$$E_{S1} = \frac{\pi v^2}{m} \left\{ \log(R^2 + a^2) - \left(\frac{a^2}{\delta^2 + a^2} + \log(\delta^2 + a^2) \right) \right\}, \quad (9.87)$$

$$E_{S2} \simeq \frac{\pi v^2 a^2}{m} \left\{ \frac{1 + \log(\delta^2 + a^2)}{\delta^2 + a^2} - 2m\Lambda \left(\frac{1}{R^2 + a^2} - \frac{1}{\delta^2 + a^2} \right) \right\}, \quad (9.88)$$

where we have assumed that the cutoff Λ is sufficiently large and that the second term in the logarithm in (9.86) is dominant. Taking account of (9.80) and assuming $a > \delta$, (9.87) and (9.88) are rewritten as

$$E_{S1} \simeq -2\pi v^2 \left(x^3(R) - x^3(\delta) + \frac{1}{2m} \right) + \mathcal{O} \left(\frac{\delta^2}{a^2} \right), \quad (9.89)$$

$$E_{S2} \simeq -2\pi v^2 (x^3(\delta) - \Lambda) + \mathcal{O} \left(\frac{\delta^2}{a^2} \right). \quad (9.90)$$

These results tell us that E_{S1} is the vortex string energy between $x^3(R)$ and $x^3(\delta)$ while E_{S2} is one between $x^3(\delta)$ and Λ . We show each contribution schematically in Fig. 59. As can be seen from Fig. 59, E_{S2} corresponds to the energy contributed by the lump string which is perpendicular to the domain wall. On the other hand, E_{S1} is contribution from a part of lump string ($\rho > a$) whose angle from the x^1 - x^2 plane is in the range of $[0, \pi/2)$. Thus, we expect that only E_{S1} is reproduced within the DBI theory.

For $a > 1$ the curve (9.80) does not cross the ρ axis (the upper panel in Fig. 59). As a is decreased, the curve crosses the ρ axis and $x^3(\delta)$ goes to right along x^3 axis and the contribution of E_{S1} is dominant (the lower panel in Fig. 59) in E_S . As a is decreased further, the expressions (9.89) and (9.90) are no longer valid. In such case, it is convenient to go back to the original expression (9.87) and (9.88). There we can safely take a to be zero and find that E_{S2} is vanishing while E_{S1} becomes

$$E_{S1} = \frac{2\pi v^2}{m} (\log R - \log \delta). \quad (9.91)$$

Using (9.80) with $a = 0$, this expression is rewritten as

$$E_{S1} = T_S L, \quad (9.92)$$

where $L = x^3(\delta) - x^3(R)$ is the string length. Therefore, E_{S1} at $a = 0$ is nothing but the lump string energy of zero size. Note that the lump string with $a = 0$ becomes singular at $x^3 \rightarrow \infty$. Thus, $a = 0$ lump string attached to the domain wall is regular except for $\rho = 0$, namely the angle to the x^1 - x^2 plane is always in the range of $[0, \pi/2)$ except for the junction point. Therefore, the lump string of zero size E_{S1} should be reproduced in the DBI theory for the whole region on the domain wall except for $\rho = 0$.

Now let us consider the corresponding configuration in the DBI action. The Hamiltonian and the BPS equation in the DBI action are (9.72) and (9.71) with $\hat{B} = 0$:

$$\mathcal{H}_{\text{DBI}} = \hat{T}_W \left(1 + \hat{T}_W^{-1} \Pi_i^2 \right), \quad (9.93)$$

$$\partial_i X = \pm \hat{T}_W^{-1} \Pi_i. \quad (9.94)$$

The energy of the configuration is

$$E_{\text{DBI}} = \hat{T}_W A + \hat{T}_W^{-1} \int d^2x \Pi_i^2. \quad (9.95)$$

We expect that the second term of (9.95) coincides with E_{S1} given in (9.87). In order to check this under the identification $T_W = \hat{T}_W$, the following relation should hold:

$$\frac{v^2}{m} \frac{\rho^2}{(\rho^2 + a^2)^2} = \hat{T}_W^{-1} \Pi_i^2 \quad (\hat{T}_W = mv^2). \quad (9.96)$$

This is solved by

$$\hat{T}_W^{-1} \Pi_i = \frac{1}{m} \frac{x_i}{\rho^2 + a^2}. \quad (9.97)$$

Combining this with (9.94), we find

$$X = -\frac{1}{2m} \log(\rho^2 + a^2). \quad (9.98)$$

This is precisely equal to (9.80)! Thus, we find the semi-local BIon that is the desired counterpart of the semi-local boojum in the original gauge theory. Note that E_{S1} in (9.89) with $\delta = 0$ does not depend on a , since we can absorb it into the IR cutoff by taking $R = (1 + \tilde{R})a$, where $\tilde{R} > 0$ is a new cutoff. In this sense, we can interpret a as a moduli parameter of the semi-local BIon.

While E_{S1} is correctly reproduced in the DBI action, E_{S2} is missing. As explained above, E_{S2} corresponds to a part of the lump string perpendicular to the domain wall. To reproduce this correctly, we should take additional zero modes into account. So far, we have considered only the zero modes localized on the domain wall. However, there are non-normalizable zero modes in the bulk because a part of flavor symmetry

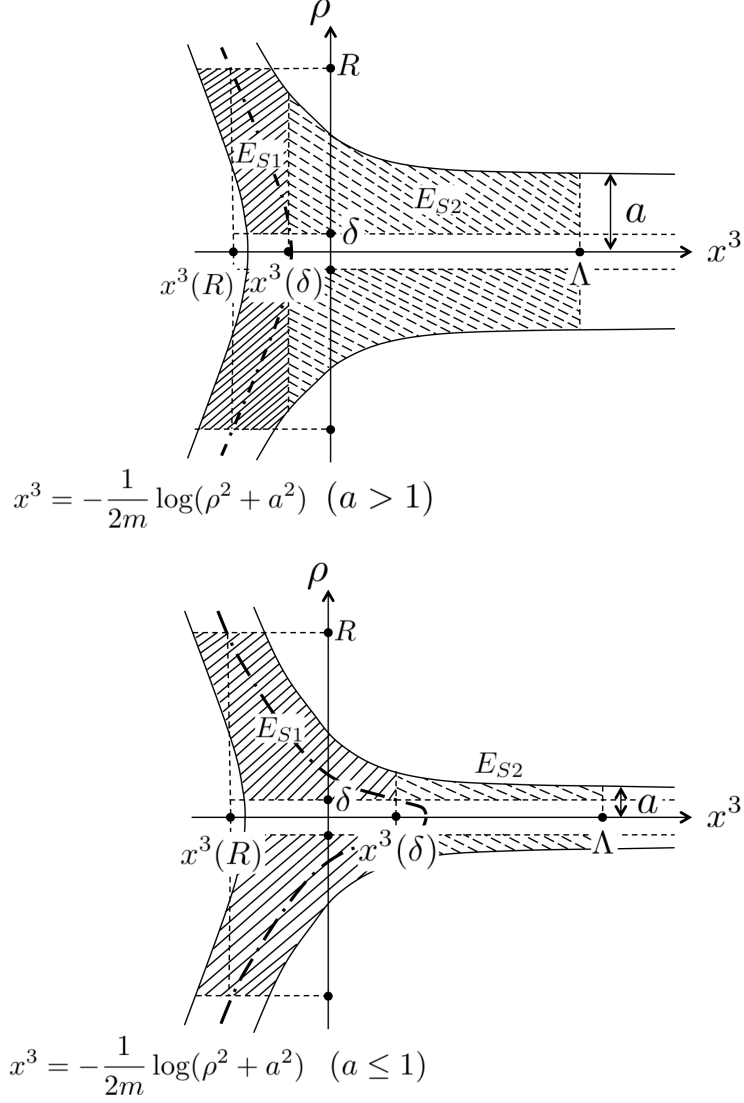


Figure 59: Schematic picture of the semi-local vortex ending on the domain wall for $a > 1$ (upper) and $a \leq 1$ (lower). The dashed-dotted curve shows the position of the domain wall described by $x^3 = -1/(2m) \log(\rho^2 + a^2)$. The solid shaded part of the configuration contributes to the vortex string energy E_{S1} while the dashed shaded part contributes to E_{S2} .

remains unbroken in the model with the partially degenerate masses (9.78). We expect that E_{S2} would be correctly reproduced once we include coupling between the localized zero modes and non-normalizable zero modes. It would be interesting to figure out the interaction, but it is beyond the scope of this paper, so we leave it as a future work.

The last comment is on the dual electric charge. The electric field (9.74) for the

semi-local BIon is given by

$$\hat{E}_i = \frac{1}{\kappa \hat{m}} \frac{x_i}{\rho^2 + a^2}, \quad (9.99)$$

where we recover the dimensional parameter κ . Interestingly, the behavior of \hat{E}_i is similar to one of the magnetic field in the domain wall discussed in subsection 3.3.3. There it was found that the observer in the domain wall sees that the magnetic field of the magnetic point source, which obeys the modified Coulomb's law in a region far from the magnetic source. Similarly, in the DBI theory the observer in the domain wall sees that the electric field obeys the modified Coulomb's law in a region far from the electric point source placed in the domain wall. Recalling the discussion in section 3.5, we see that the electric charge placed on the membrane is given as

$$q_E = \frac{2}{\hat{m}\kappa}. \quad (9.100)$$

10. Outlook

In this paper, we have studied 1/4 BPS equations in the Abelian-Higgs theory. As written at the end of Sec. 8, our solutions also solve non-Abelian BPS equations by trivial embedding. While these embedding solutions are essentially Abelian solutions, genuine non-Abelian objects, like 't Hooft-Polyakov monopoles, may join the game in the non-Abelian theories. We will investigate non-Abelian extensions of 1/4 BPS solutions including monopoles, boojums, domain walls and vortex strings in forthcoming works. It is also interesting to study the 1/4 BPS equations in different spacetime dimensions. For example, the 1/4 BPS equations for vortex sheets and instanton particles in 5 dimensions [22, 52], and those for the domain wall junctions in 3 dimensions [43, 44] are known, but only a little is known about their solutions both in the Abelian and non-Abelian theories for the finite gauge coupling constants. We will also proceed to obtain numerical/analytical solutions for these series of 1/4 BPS equations. Furthermore, the technique developed in this paper may help to solve another type of 1/4 BPS equations or 1/8 BPS equations [69, 54] for which nothing has been known except for the BPS equations.

We obtained the solution of the vortex strings attached to the tilted domain walls on which constant background magnetic field is turned on. This is quite similar to D1-branes suspended between tilted D3-branes. The D1-branes can be seen as the magnetic monopoles in non-commutative spacetime [67, 68]. As a natural analogy, the vortex strings suspended between tilted domain walls in the gauge theory should be seen as electrically charged particles in a low energy effective theory which is a non-commutative theory. If this is the case, the similarity between the solitons in field theories and D-branes in string theories, which is repeated in the literature, is further reinforced.

We have stumbled upon unexpected analytic results, namely exact solutions to 1/2 and 1/4 BPS master equations in models with $N_F \leq 6$ described in Sec. 8. As we stated, we believe that these solutions are just simplest examples of a potentially inexhaustible wealth of exact solutions in models with ever larger number of flavors of fundamental Higgs fields. The indirect evidence for this steams from the fact that our exact composite solitons, denoted as u_{SW}^{4F} and u_{SW}^{6F} , have been ‘build’ from of 1/2 BPS exact solutions for walls and strings. Therefore, it is natural to expect that more complicated combinations should give us another 1/4 BPS solutions in higher flavor models. The exact rules of this ‘solitonic engineering’ are so far unclear. However, the preliminary results shows, that certain restrictions on 1/2 BPS components must be in place, if they are to be used in construction of 1/4 BPS solutions. We have spotted glimpses of this in Sec. 8, namely that domain walls must have sufficiently low tension and cores of semi-local strings must be sufficiently large. The full analysis of this is an essential direction of future research. Furthermore, for parallel 1/2 BPS domain walls, such analysis was done by one of us in the study [79], where it was shown that exact multi-wall solutions can be build up from certain single wall solutions in quite arbitrary fashion, except that the total tension of the final domain wall configuration must be small enough. Effectively, this restriction prevents development of an inner layer inside domain walls, where unbroken phase appears. In fact, no exact solution of domain wall with this inner layer is known at present. Finding such a solution remains as an interesting open problem. The similar study for semi-local vortices is in preparation. By combining the findings for exact 1/2 BPS solitons we may be able to clarify, how their combination can yield exact 1/4 BPS solitons. Naturally, in doing so we may discover similar rules for other composite solitons, such as wall-wall and string-string junctions, which we did not address in this paper. An interesting questions is, whether all exact 1/4 BPS solution can be decomposed as combinations of exact 1/2 BPS solutions, or whether some ‘irreducible’ solutions exist.

A further studies of composite solitons, especially in non-Abelian setting, may be useful for ironing out the phenomenology of dynamically realized brane-world scenarios. In string theory, it is known that intersecting D-branes can generate Standard Model gauge group, chiral fermions and family replication (see [80] and references therein). Similar results were obtained within the field theory as well. Indeed, domain walls and magnetic vortices have been long since used to localize scalar and fermionic fields [81, 82]. The localization of gauge fields is achieved either by Dvali-Shifman mechanism [83], where confining phase in the bulk is assumed, or dynamically using field-dependent gauge coupling constant via Ohta-Sakai mechanism [84]. Using the former, the Standard Model gauge group has been constructed at the junction of perpendicular domain walls in [85], while the later was used to localize large gauge group on coincident domain walls [86, 87]. In the future, using the method developed here, we would like to construct a realistic brane-world scenario on intersecting solitons at finite gauge coupling constant and to clarify the role of negative binding

energy on low-energy effective theory.

We have shown that the spike domain wall configuration in the field theory can be reproduced in the NG action and the DBI action. We have also observed that the DBI action correctly realizes the semi-local boojum as the semi-local BIon. On the other hand, as is addressed in Sec. 9.5, the DBI action cannot reproduce the semi-local lump string itself (E_{S2}) which is perpendicular to the domain wall. A possible reason for this situation is that all the massless modes may not be taken into account in the low energy effective theory. The semi-local boojum is constructed by introducing a partially degenerate masses such as (9.78). If there is a mass splitting in the first two components, there are three discrete vacua and an extra domain wall appears. Associated with this, extra massless modes localize around the extra domain wall. The extra domain wall becomes increasingly broader as the mass splitting disappears. Correspondingly, the extra massless modes spread into the whole half-space and they become non-normalizable. We expect that these non-normalizable modes would be necessary for reproducing E_{S2} in the low energy effective theory. Normally, it is not easy to deal with non-normalizable modes. We may achieve it by considering a small mass splitting which introduces the broad extra domain wall. Further, we may consider a low energy effective action for the two parallel domain walls and investigate the limit when we turn on the mass degeneracy. We leave this problem for a future work.

Acknowledgements

This work is supported by Grant-in Aid for Scientific Research No.25400280 (M. A.) and from the Ministry of Education, Culture, Sports, Science and Technology (MEXT) of Japan. The work of M. E. is supported in part by JSPS Grant-in-Aid for Scientific Research (KAKENHI Grant No. 26800119) and the MEXT-Supported Program for the Strategic Research Foundation at Private Universities “Topological Science” (Grant No. S1511006). F. B. is an international research fellow of the Japan Society for the Promotion of Science. This work was supported by Grant-in-Aid for JSPS Fellows, Grant Number 26004750.

References

- [1] H. B. Nielsen and P. Olesen, *Vortex Line Models for Dual Strings*, *Nucl. Phys.* **B61** (1973) 45–61.
- [2] G. 't Hooft, *Magnetic monopoles in unified gauge theories*, *Nuclear Physics B* **79** (Sept., 1974) 276–284.
- [3] A. M. Polyakov, *Particle Spectrum in the Quantum Field Theory*, *JETP Lett.* **20** (1974) 194–195. [Pisma Zh. Eksp. Teor. Fiz.20,430(1974)].

- [4] J. Polchinski, S. Chaudhuri, and C. V. Johnson, *Notes on D-branes*, [hep-th/9602052](#).
- [5] S. M. Carroll and M. Trodden, *Dirichlet topological defects*, *Phys. Rev.* **D57** (1998) 5189–5194, [[hep-th/9711099](#)].
- [6] M. Bowick, A. De Felice, and M. Trodden, *The Shapes of Dirichlet defects*, *JHEP* **10** (2003) 067, [[hep-th/0306224](#)].
- [7] E. Witten, *Branes and the dynamics of QCD*, *Nucl. Phys.* **B507** (1997) 658–690, [[hep-th/9706109](#)].
- [8] I. I. Kogan, A. Kovner, and M. A. Shifman, *More on supersymmetric domain walls, N counting and glued potentials*, *Phys. Rev.* **D57** (1998) 5195–5213, [[hep-th/9712046](#)].
- [9] A. Campos, K. Holland, and U. J. Wiese, *Complete wetting in supersymmetric QCD or why QCD strings can end on domain walls*, *Phys. Rev. Lett.* **81** (1998) 2420–2423, [[hep-th/9805086](#)].
- [10] G. Dvali and A. Vilenkin, *Solitonic D-branes and brane annihilation*, *Phys. Rev.* **D67** (2003) 046002, [[hep-th/0209217](#)].
- [11] J. P. Gauntlett, R. Portugues, D. Tong, and P. K. Townsend, *D-brane solitons in supersymmetric sigma models*, *Phys. Rev. D* **63** (Apr., 2001) 085002, [[hep-th/0008221](#)].
- [12] M. Shifman and A. Yung, *Domain walls and flux tubes in $N=2$ SQCD: D-brane prototypes*, *Phys. Rev.* **D67** (2003) 125007, [[hep-th/0212293](#)].
- [13] M. Shifman and A. Yung, *Localization of nonAbelian gauge fields on domain walls at weak coupling (D-brane prototypes II)*, *Phys. Rev.* **D70** (2004) 025013, [[hep-th/0312257](#)].
- [14] A. Hanany and D. Tong, *Vortices, instantons and branes*, *JHEP* **07** (2003) 037, [[hep-th/0306150](#)].
- [15] R. Auzzi, S. Bolognesi, J. Evslin, K. Konishi, and A. Yung, *NonAbelian superconductors: Vortices and confinement in $N=2$ SQCD*, *Nucl. Phys.* **B673** (2003) 187–216, [[hep-th/0307287](#)].
- [16] D. Tong, *D-branes in field theory*, *Journal of High Energy Physics* **2** (Feb., 2006) 30, [[hep-th/0512192](#)].
- [17] M. Eto, T. Fujimori, M. Nitta, K. Ohashi, and N. Sakai, *Domain walls with non-Abelian clouds*, *Phys. Rev.* **D77** (2008) 125008, [[arXiv:0802.3135](#)].
- [18] M. Arai, F. Blaschke, M. Eto, and N. Sakai, *Matter Fields and Non-Abelian Gauge Fields Localized on Walls*, *PTEP* **2013** (2013) 013B05, [[arXiv:1208.6219](#)].

- [19] M. Arai, F. Blaschke, M. Eto, and N. Sakai, *Localization of matter fields and non-Abelian gauge fields on domain walls*, [arXiv:1211.1235](#). [*J. Phys. Conf. Ser.* **411**,012001(2013)].
- [20] M. Arai, F. Blaschke, M. Eto, and N. Sakai, *Stabilizing matter and gauge fields localized on walls*, *PTEP* **2013** (2013), no. 9 093B01, [[arXiv:1303.5212](#)].
- [21] D. Tong, *Monopoles in the Higgs phase*, *Phys. Rev. D* **69** (Mar., 2004) 065003, [[hep-th/0307302](#)].
- [22] A. Hanany and D. Tong, *Vortex strings and four-dimensional gauge dynamics*, *JHEP* **04** (2004) 066, [[hep-th/0403158](#)].
- [23] M. Shifman and A. Yung, *NonAbelian string junctions as confined monopoles*, *Phys. Rev. D* **70** (2004) 045004, [[hep-th/0403149](#)].
- [24] A. Gorsky, M. Shifman, and A. Yung, *Non-Abelian meissner effect in Yang-Mills theories at weak coupling*, *Phys. Rev. D* **71** (2005) 045010, [[hep-th/0412082](#)].
- [25] M. Cipriani, D. Dorigoni, S. B. Gudnason, K. Konishi, and A. Michelini, *Non-Abelian monopole-vortex complex*, *Phys. Rev. D* **84** (2011) 045024, [[arXiv:1106.4214](#)].
- [26] M. Eto, T. Fujimori, S. B. Gudnason, Y. Jiang, K. Konishi, M. Nitta, and K. Ohashi, *Vortices and Monopoles in Mass-deformed SO and USp Gauge Theories*, *JHEP* **12** (2011) 017, [[arXiv:1108.6124](#)].
- [27] M. Nitta and W. Vinci, *Non-Abelian Monopoles in the Higgs Phase*, *Nucl. Phys. B* **848** (2011) 121–154, [[arXiv:1012.4057](#)].
- [28] M. Cipriani and T. Fujimori, *Effective Action of Non-Abelian Monopole-Vortex Complex*, [arXiv:1207.2070](#).
- [29] M. Arai, F. Blaschke, M. Eto, and N. Sakai, *Dynamics of slender monopoles and anti-monopoles in non-Abelian superconductor*, *JHEP* **09** (2014) 172, [[arXiv:1407.2332](#)].
- [30] Y. Isozumi, M. Nitta, K. Ohashi, and N. Sakai, *All exact solutions of a 1/4 Bogomol'nyi-Prasad-Sommerfield equation*, *Phys. Rev. D* **71** (Mar., 2005) 065018, [[hep-th/0405129](#)].
- [31] Y. Isozumi, M. Nitta, K. Ohashi, and N. Sakai, *Construction of non-Abelian walls and their complete moduli space*, *Phys. Rev. Lett.* **93** (2004) 161601, [[hep-th/0404198](#)].
- [32] Y. Isozumi, M. Nitta, K. Ohashi, and N. Sakai, *Non-Abelian walls in supersymmetric gauge theories*, *Phys. Rev. D* **70** (2004) 125014, [[hep-th/0405194](#)].
- [33] M. Eto, Y. Isozumi, M. Nitta, K. Ohashi, and N. Sakai, *Moduli space of non-Abelian vortices*, *Phys. Rev. Lett.* **96** (2006) 161601, [[hep-th/0511088](#)].

- [34] M. Eto, Y. Isozumi, M. Nitta, K. Ohashi, and N. Sakai, *TOPICAL REVIEW: Solitons in the Higgs phase: the moduli matrix approach*, *Journal of Physics A Mathematical General* **39** (June, 2006) 315, [[hep-th/0602170](#)].
- [35] D. Tong, *TASI lectures on solitons: Instantons, monopoles, vortices and kinks*, in *Theoretical Advanced Study Institute in Elementary Particle Physics: Many Dimensions of String Theory (TASI 2005) Boulder, Colorado, June 5-July 1, 2005*, 2005. [hep-th/0509216](#).
- [36] D. Tong, *Quantum Vortex Strings: A Review*, *Annals Phys.* **324** (2009) 30–52, [[arXiv:0809.5060](#)].
- [37] K. Konishi, *The Magnetic Monopoles Seventy-Five Years Later*, *Lect. Notes Phys.* **737** (2008) 471–521, [[hep-th/0702102](#)].
- [38] M. Shifman and A. Yung, *Supersymmetric Solitons and How They Help Us Understand Non-Abelian Gauge Theories*, *Rev. Mod. Phys.* **79** (2007) 1139, [[hep-th/0703267](#)].
- [39] H. Oda, K. Ito, M. Naganuma, and N. Sakai, *An Exact solution of BPS domain wall junction*, *Phys. Lett.* **B471** (1999) 140–148, [[hep-th/9910095](#)].
- [40] K. Ito, M. Naganuma, H. Oda, and N. Sakai, *Nonnormalizable zero modes on BPS junctions*, *Nucl. Phys.* **B586** (2000) 231–260, [[hep-th/0004188](#)].
- [41] K. Ito, M. Naganuma, H. Oda, and N. Sakai, *An Exact solution of BPS junctions and its properties*, *Nucl. Phys. Proc. Suppl.* **101** (2001) 304–313, [[hep-th/0012182](#)]. [[,304\(2000\)](#)].
- [42] M. A. Shifman and T. ter Veldhuis, *Calculating the tension of domain wall junctions and vortices in generalized Wess-Zumino models*, *Phys. Rev.* **D62** (2000) 065004, [[hep-th/9912162](#)].
- [43] M. Eto, Y. Isozumi, M. Nitta, K. Ohashi, and N. Sakai, *Webs of walls*, *Phys. Rev.* **D72** (2005) 085004, [[hep-th/0506135](#)].
- [44] M. Eto, Y. Isozumi, M. Nitta, K. Ohashi, and N. Sakai, *Non-Abelian webs of walls*, *Phys. Lett.* **B632** (2006) 384–392, [[hep-th/0508241](#)].
- [45] N. Sakai and D. Tong, *Monopoles, Vortices, Domain Walls and D-Branes: The Rules of Interaction*, *Journal of High Energy Physics* **3** (Mar., 2005) 19, [[hep-th/0501207](#)].
- [46] N. D. Mermin, *Quantum Fluids and Solids*, Plenum, New York (1977).
- [47] G. E. Volovik, *Defects at interface between A and B phases of superfluid ^3He* , *JETP. Lett.* **51** (1990) 449–452.
- [48] K. Kasamatsu, H. Takeuchi, M. Tsubota, and M. Nitta, *Wall-vortex composite solitons in two-component Bose-Einstein condensates*, *ArXiv e-prints* (Mar., 2013) [[arXiv:1303.7052](#)].

- [49] K. Kasamatsu, H. Takeuchi, and M. Nitta, *D-brane solitons and boojums in field theory and Bose-Einstein condensates*, *J. Phys. Condens. Matter* **25** (2013) 404213, [[arXiv:1303.4469](#)].
- [50] M. Cipriani, W. Vinci, and M. Nitta, *Colorful boojums at the interface of a color superconductor*, *Phys. Rev. D* **86** (Dec., 2012) 121704, [[arXiv:1208.5704](#)].
- [51] M. Eto, Y. Hirono, M. Nitta, and S. Yasui, *Vortices and other topological solitons in dense quark matter*, *Progress of Theoretical and Experimental Physics* **2014** (Jan., 2014) 010002, [[arXiv:1308.1535](#)].
- [52] M. Eto, Y. Isozumi, M. Nitta, K. Ohashi, and N. Sakai, *Instantons in the Higgs phase*, *Phys. Rev.* **D72** (2005) 025011, [[hep-th/0412048](#)].
- [53] M. Eto and M. Nitta, *Semilocal Fractional Instantons*, [arXiv:1512.07458](#).
- [54] M. Eto, Y. Isozumi, M. Nitta, and K. Ohashi, *1/2, 1/4 and 1/8 BPS equations in SUSY Yang Mills Higgs systems: Field theoretical brane configurations*, *Nuclear Physics B* **752** (Sept., 2006) 140–172, [[hep-th/0506257](#)].
- [55] C. H. Taubes, *Arbitrary N: Vortex Solutions to the First Order Landau-Ginzburg Equations*, *Commun. Math. Phys.* **72** (1980) 277–292.
- [56] M. F. Atiyah, N. J. Hitchin, V. G. Drinfeld, and Yu. I. Manin, *Construction of Instantons*, *Phys. Lett.* **A65** (1978) 185–187.
- [57] E. Witten, *Some Exact Multi - Instanton Solutions of Classical Yang-Mills Theory*, *Phys. Rev. Lett.* **38** (1977) 121–124.
- [58] A. D. Popov, *Integrability of Vortex Equations on Riemann Surfaces*, *Nucl. Phys.* **B821** (2009) 452–466, [[arXiv:0712.1756](#)].
- [59] A. D. Popov, *Non-Abelian Vortices on Riemann Surfaces: An Integrable Case*, *Lett. Math. Phys.* **84** (2008) 139–148, [[arXiv:0801.0808](#)].
- [60] S. Krusch and J. M. Speight, *Exact moduli space metrics for hyperbolic vortices*, *J. Math. Phys.* **51** (2010) 022304, [[arXiv:0906.2007](#)].
- [61] N. S. Manton and N. A. Rink, *Vortices on Hyperbolic Surfaces*, *J. Phys.* **A43** (2010) 434024, [[arXiv:0912.2058](#)].
- [62] P. Sutcliffe, *Hyperbolic vortices with large magnetic flux*, *Phys. Rev.* **D85** (2012) 125015, [[arXiv:1204.0400](#)].
- [63] N. S. Manton and N. Sakai, *Maximally Non-Abelian Vortices from Self-dual Yang-Mills Fields*, *Phys. Lett.* **B687** (2010) 395–399, [[arXiv:1001.5236](#)].
- [64] M. Eto, T. Fujimori, M. Nitta, and K. Ohashi, *All Exact Solutions of Non-Abelian Vortices from Yang-Mills Instantons*, *JHEP* **07** (2013) 034, [[arXiv:1207.5143](#)].

- [65] N. S. Manton and P. Sutcliffe, *Topological solitons*. Cambridge University Press, 2007.
- [66] R. Auzzi, M. Shifman, and A. Yung, *Studying boojums in $N=2$ theory with walls and vortices*, *Phys. Rev.* **D72** (2005) 025002, [[hep-th/0504148](#)].
- [67] K. Hashimoto, *Born-Infeld dynamics in uniform electric field*, *JHEP* **07** (1999) 016, [[hep-th/9905162](#)].
- [68] A. Hashimoto and K. Hashimoto, *Monopoles and dyons in noncommutative geometry*, *JHEP* **11** (1999) 005, [[hep-th/9909202](#)].
- [69] K.-M. Lee and H.-U. Yee, *New BPS objects in $N=2$ supersymmetric gauge theories*, *Phys. Rev.* **D72** (2005) 065023, [[hep-th/0506256](#)].
- [70] E. R. C. Abraham and P. K. Townsend, *Q kinks*, *Phys. Lett.* **B291** (1992) 85–88.
- [71] E. R. C. Abraham and P. K. Townsend, *More on Q kinks: A $(1+1)$ -dimensional analog of dyons*, *Phys. Lett.* **B295** (1992) 225–232.
- [72] T. Vachaspati and A. Achucarro, *Semilocal cosmic strings*, *Phys. Rev.* **D44** (1991) 3067–3071.
- [73] Y. Isozumi, K. Ohashi, and N. Sakai, *Exact wall solutions in 5-dimensional SUSY QED at finite coupling*, *Journal of High Energy Physics* **11** (Nov., 2003) 60, [[hep-th/0310189](#)].
- [74] M. Eto, Y. Isozumi, M. Nitta, and K. Ohashi, *$1/2$, $1/4$ and $1/8$ BPS equations in SUSY Yang-Mills-Higgs systems: Field theoretical brane configurations*, *Nucl. Phys.* **B752** (2006) 140–172, [[hep-th/0506257](#)].
- [75] K. Ohashi, *Small winding-number expansion: vortex solutions at critical coupling*, *Journal of High Energy Physics* **2015** (2015), no. 11.
- [76] S. Winitzki, *Uniform approximations for transcendental functions*, in *Computational Science and Its Applications – ICCSA 2003* (V. Kumar, M. Gavrilova, C. Tan, and P. L’Ecuyer, eds.), vol. 2667 of *Lecture Notes in Computer Science*, pp. 780–789. Springer Berlin Heidelberg, 2003.
- [77] M. Eto, *J -kink domain walls and the DBI action*, *JHEP* **06** (2015) 160, [[arXiv:1504.00753](#)].
- [78] M. Eto and K. Hashimoto, *Speed limit in internal space of domain walls via all-order effective action of moduli motion*, [arXiv:1508.00433](#).
- [79] F. Blaschke, *Exact BPS domain walls at finite gauge coupling*, to appear (2016).
- [80] R. Blumenhagen, M. Cvetič, P. Langacker, and G. Shiu, *Toward Realistic Intersecting D-Brane Models*, *Annual Review of Nuclear and Particle Science* **55** (Dec., 2005) 71–139, [[hep-th/0502005](#)].

- [81] K. Akama, *An Early Proposal of "Brane World"*, *ArXiv High Energy Physics - Theory e-prints* (Jan., 2000) [[hep-th/0001113](#)].
- [82] V. A. Rubakov and M. E. Shaposhnikov, *Do we live inside a domain wall?*, *Physics Letters B* **125** (May, 1983) 136–138.
- [83] G. Dvali and M. Shifman, *Domain walls in strongly coupled theories*, *Physics Letters B* **396** (Feb., 1997) 64–69, [[hep-th/9612128](#)].
- [84] K. Ohta and N. Sakai, *Non-Abelian Gauge Field Localized on Walls with Four-Dimensional World Volume*, *Progress of Theoretical Physics* **124** (July, 2010) 71–93, [[hep-th/1004.4078](#)].
- [85] B. D. Callen and R. R. Volkas, *Clash-of-symmetries mechanism from intersecting domain-wall branes*, *Phys. Rev. D* **89** (Mar., 2014) 056004, [[arXiv:1310.4097](#)].
- [86] M. Arai, F. Blaschke, M. Eto, and N. Sakai, *Matter fields and non-Abelian gauge fields localized on walls*, *Progress of Theoretical and Experimental Physics* **2013** (Jan., 2013) 010003, [[hep-th/1208.6219](#)].
- [87] M. Arai, F. Blaschke, M. Eto, and N. Sakai, *Stabilizing matter and gauge fields localized on walls*, *Progress of Theoretical and Experimental Physics* **2013** (Sept., 2013) 0903B01, [[arXiv:1303.5212](#)].